Investigation of ageing associated inflammation and genomic instability in zebrafish

By Anne Cathrine Hyde

Submitted for Degree of Doctor of Philosophy (PhD)

March 2025

The University of Sheffield

Faculty of Science

School of Biosciences

Declaration

The research in this thesis was funded by the Dunhill Medical Trust Healthy Lifespan Doctorial training program. Some of the lines in this thesis were not made by me. The *rnaseh2a* line (SH478) was made by Dr Ringailė Zakšauskaitė, characterised by Dr Ruth Thomas and published (Thomas et al., 2024). I did contribute to this publication, among others with the script for the alkaline assay analysis, which is also found in this thesis. Further, the *numa* line (SH678) was made by Dr Ruth Thomas, and the *p21* line was made by Dr Samir Morsli and published (Morsli et al., 2023). The *klotho* line was made and characterised by Dr Oluwaseyi A Pearce. The Mass Spectrometry data for the AMP:ATP, ADP, ATP, NAD/NADH and NADP:NADPH ratios was performed by Dr Kari Fladmark at the University of Bergen. I refer to research on FASTKD2 by Dr Chunyan Liao, as well as research on NuMA by Mathew Daweson and Dr Sarah Antar. All other work was done by me. Part of this projected did include analysis from a human cohort study, the CARE75+. We did obtain ethical approval from the University of Sheffield as well as an agreement from Bradford Teaching Hospital NHS Foundation Trust to use the data and blood samples from this study (REF: 17/YH/0086, Trial registration number: ISRCTN16588124). The data is not presented in the thesis.

Acknowledgements

I would like to first thank my supervisors Dr Freek van Eeden, Professor Sherif El-Khamisy and Professor Maria-Cruz Villa-Uriol. Your guidance and support have greatly benefited me throughout my research. Furthermore, I would like to thank everyone in the van Eeden and the El-Khamisy lab, in particular Dr Eleanor Markham and Dr Chunyan Liao for always being helpful when help was needed. As well as Louise Stephenon and Norah Al-Kandari for constant emotional support and Dr Ruth Thomas and Dr Sameh El-Badry for giving me the warmest welcome to the lab.

I have to thank several people from the Bateson Centre. First Dr Ada Jimenez-Gonzalez for several discussions about ALS fish behaviour and help with swimtunnel and Y-maze assays. Stamatia (Martina) Christaki for her help with adult behaviour analysis. Rachele Bacchetti for teaching me xenografts, even though unrelated to my own thesis. Dr Stone Elworthy for help with generating the mitochondrial reporter line. Lastly, Dr Martin Reijns from the University of Edinburgh whose expertise in studying ribonucleotide incorporation has lead to many great discussions at conferences and helped with several experiments.

I would also like to thank my father Andy Hyde for constant encouragement throughout my higher education career, and for reading through my thesis. As well as my partner James Hill-Cousins for putting up with my weekend work at the end of my PhD and also for reading through my thesis. Coming home to you has calmed me down after stressful days in the lab. I would also like to thank my grandmother Dr Else Grue who as the first PhD in the family inspired me pursue a PhD myself and my mother Kirsten Grue Ullset for support throughout my life.

Abstract

The global population is living longer thanks to advancements in treatments for diseases that previously significantly shortened lifespans. However, these extra years are often accompanied by ill health and frailty, placing a considerable burden on both individuals and society, prompting the requirement into further research. One of the primary hallmarks of ageing is genomic instability, suggesting that increased DNA damage is partly responsible for why we age. One of the most common forms of DNA damage is the incorporation of single ribonucleotides into the DNA. A ribonucleotide is more reactive than a deoxyribonucleotide and if not removed, it can cause replication and transcription stalling as well as DNA breaks.

Here I use zebrafish (*Danio rerio*) as a model to study whether a reduced ribonucleotide removal activity from the genome is related to why someone becomes frail. I have made a frailty index for zebrafish, and I see that the frail fish have a reduced ability to cleave single ribonucleotides in the brain. This suggests that removal of ribonucleotides is important in robust ageing, and a loss of this function might be linked to frailty.

Further, I investigate FASTKD2 as a potential alternative enzyme that can remove single ribonucleotides from the mitochondrial DNA by creating a *fastkd2* homozygous knockout zebrafish mutant. I show that whilst the mutant is viable, it is not efficient in producing energy, and it has no defects in single ribonucleotide removal. I also create a mutant for APRATAXIN, which resolves alternative ligation products, but is hindered by ribonucleotides. I show that the *aprataxin* mutant has reduced movement abilities. Lastly, I attempt to rescue a lethal zebrafish phenotype caused by loss of NuMA in zebrafish larvae by injecting parts of human cDNA NuMA into the genome of the mutant. However, I was unsuccessful in causing a rescue.

Table of Contents

List of Figures

List of Tables

List of abbreviations

53BP1	p53-binding protein 1
γH2AX	phosphorylated Histone2.X
A-T	Ataxia Telangiectasia
aa	amino acid
ADP	Adenosine diphosphate
AGS	Aicardi-Goutières Syndrome
ALS	Amyotrophic lateral sclerosis
AMP	Adenosine monophosphate
AOA-1	Ataxia-Oculomotor Apraxia-1
AP	Abasic site
APTX	Aprataxin
ATM	Ataxia-Telangiectasia-Mutated
ATP	Adenosine triphosphate
BER	Base excision repair
BMI	Body Mass Index
BP	*attB/attP*
bp	base pair
BPM	Beats Per Minute
CARE75+	Community ageing research 75+ study
CFP	Cyan Fluorescent Protein
cGAS	cyclic GMP-AMP synthase
cm	centimetre
COX	Cytochrome c oxidase
CPT	Camptothecin
CRISPR/Cas9	Clustered Regularly Interspaced Short Palindromic Repeats /Cas9
Cy5	Cyanine5
DIF-1	DD1 Interacting Factor-1
DMSO	Dimethyl sulfoxide
dNMP	deoxyribonucleotide monophosphate
dNTP	deoxyribonucleotide triphosphate
dpf	days post fertilization
DSD	Double Stranded Damage
DSB	Double Stranded Break
eFI	electronic Frailty Index
ELSA	English Longitudinal Study of Ageing
ETC	Electron Transport Chain
FASTKD2	FAST kinase domain-containing protein 2
FEN1	Flap Endonuclease 1
FHA	Forkhead-associated domain
GAPDH	Glyceraldehyde-3-phosphate dehydrogenase
GFP	Green Fluorescent Protein
H_2O_2	Hydrogen peroxide
HDAC	Histone deacetylase
HIT	Histidine triad
hpf	hours post fertilisation
INF	Interferon
IR	Ionising Radiation

ISG	Interferon stimulated genes
kDa	Kilo Daltons
KOH	Potassium hydroxide
LB	Lysogeny broth
LB	Lysis Buffer
LR	*attL/attR*
LRLR	Left-Right-Left-Right
LWT	London Wild Type
mdh1b	Putative malate dehydrogenase 1B
MEM	Minimum Essential Media
mm	milimeter
MTS	Mitochondrial Targeting Signal
mtDNA	mitochondrial DNA
NaCl	Sodium Chloride
NAD	Nicotinamide adenine dinucleotide
NADH	Nicotinamide adenine dinucleotide + hydrogen
NADP	Nicotinamide adenine dinucleotide phosphate
NADPH	Nicotinamide adenine dinucleotide phosphate + hydrogen
NAD6	NADH-ubiquinone oxidoreductase chain 6
NaOH	Sodium Hydroxide
NER	Nucleotide Excision repair
NLS	Nuclear Localising Signal
NuMA	Nuclear Mitotic Apparatus
OH	Hydroxide
ONS	Office of National Statistics
OXPHOS	Oxidative Phosphorylation
PARP	Poly (ADP-ribose) Polymerases
PAR	Poly ADP-ribose
PBS	Phosphate-buffered saline
PCNA	Proliferating cell nuclear antigen
PCR	Polymerase Chain Reaction
POL2	DNA Polymerase ε
POLG1	DNA Polymerase γ
PTZ	Pentylenetetrazol
qPCR	quantitative Polymerase Chain Reaction
RER	Ribonucleotide Excision Repair
RLRL	Right-Left-Right-Left
RNaseH	Ribonuclease H
RNaseH2-RED	Ribonucleotide Excision Deficient
rNMP	ribonucleotide monophosphate
rNTP	ribonucleotide triphosphate
rRNA	ribosomal RNA
ROS	Reactive Oxygen Species
s	seconds
SDS	sodium dodecyl sulphate
sGAMP	2’3’ cyclic GMP-AMP
SSD	Single Stranded Damage
SSB	Single Stranded Break

STING	stimulator of interferon genes
TAE	Tris-acetate-EDTA
TBS	Tris-borate-EDTA
TDP1	Tyrosyl-DNA phosphodiesterase 1
TEMED	N,N,N′,N′ -Tetramethylethylenediamine
TOP	Topoisomerase
TOP1-cc	Topoisomerase 1-cleavage complex
tRNA	Transfer RNA
TUNEL	Terminal deoxynucleotidyl transferase dUTP nick end labelling
ubi	Ubiquitin
UV	Ultraviolet
VDAC1	Voltage-Dependent Anion Channels 1
WHO	World Health Organisation
XPF	Xeroderma Pigmentosum
XRCC1	X-ray Repair Cross-Complementing 1

Chapter 1 Introduction

1.1. Ageing and frailty

"At a biological level, ageing results from the impact of the accumulation of a wide variety of molecular and cellular damage over time. This leads to a gradual decrease in physical and mental capacity, a growing risk of disease and ultimately death,"

– World Health Organisation (WHO), October 1st, 2024.

The above statement is how the WHO described ageing in 2024 when talking about ageing and health. In the same statement the WHO emphasised how people worldwide are living longer and by 2030, 1 in 6 people will be 60 years or older. In the UK, the number of aged people has had a rapid increase since 2002, where only 350,700 people were over the age of 90. In 2023, this number had increased to 551,760 people, and there are now almost twice as many women over the age of 90 than men (Figure 1.1). In the UK, 1 in 4, that is 20.7 million people will be aged 65 and over by 2041 (World Health Organisation, 2024, Office for Health Improvement and Disparities, 2023). The challenge with ageing as stated above, is that a person has a growing risk of disease. These diseases include but are not limited to hearing loss, cataracts and refractory errors, back and neck pain and osteoarthritis, chronic obstructive pulmonary disease, diabetes, depression and dementia. Usually at an older age, one can get several of these diseases at the same time, called multimorbidity or comorbidity. This is a problem for the individual, but also very costly and time-consuming for the society (World Health Organisation, 2024). As we extend the lifespan with more medical intervention against some of these diseases, we give people the opportunity to have extra years to spend with family or to pursue activities they did not have the opportunity to do earlier. However, that is the idealised situation, and unfortunately many face these extra years in ill health with frailty and multimorbidity (World Health Organisation, 2024, Office for Health Improvement and Disparities, 2023).

However, when talking about ageing, it is important to speak of it not as a chronological concept, as a person's chronological age might not reflect their biological health. This means that two people of the same age may not have the same health, and one might be very healthy whilst another might be very frail (Gordon and Hubbard, 2022). There is not one definition for

what a frail individual is, whether it is defined as being reliant on services or whether it means that a person has an increased chance of adverse outcomes such as death after disease (Rockwood et al., 1994, Rockwood et al., 2000). Frailty can be a measure of cognitive and physical health as well as physiological function, social environment and medical comorbidity (Howlett et al., 2021, Gordon and Hubbard, 2022). Severe frailty tends to manifest in females more so than males and is observed in 12% of older adults when using a physical frailty scale and 24% when using a deficit accumulation model (O'Caoimh et al., 2021). Females being frailer, and the fact that females live longer than men, is referred to as the “sex-frailty paradox” (Gordon and Hubbard, 2020). Society usually talks about treating ageing, but what they usually refer to is treating frailty, or even preventing it. However, frail people are usually left out of studies due to their adverse outcomes after disease and are not well studied. Therefore, animal models for frailty have been widely used, such as models of rats, mice and dogs (Howlett et al., 2021).

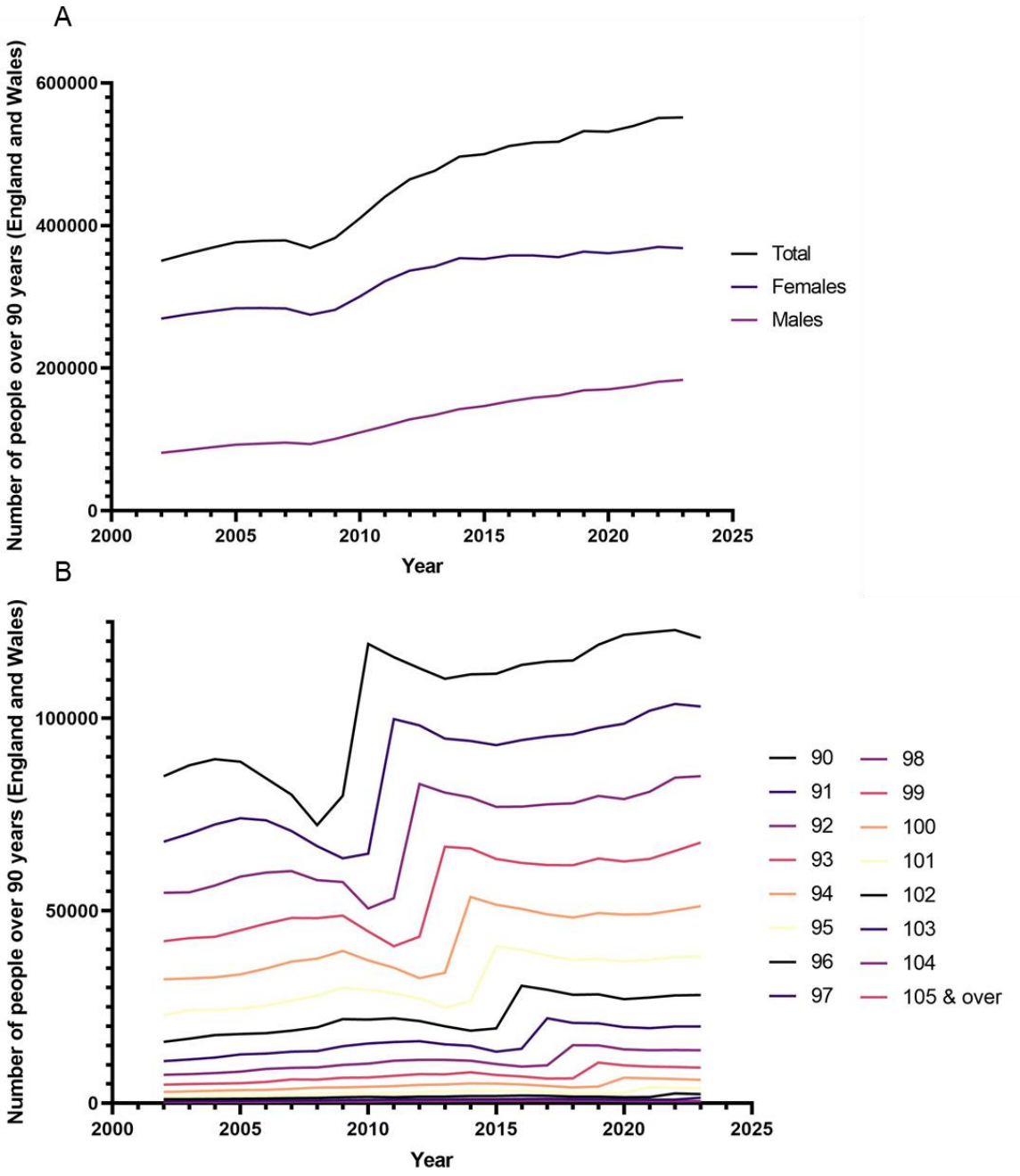

Figure 1.1: Number of people over the age of 90 years in England and Wales from 2002 to 2023. Data from: Office for National Statistics (ONS), released 1 October 2024, ONS website, statistical bulletin, Estimates of the very old, including centenarians, England and Wales: 2002 to 2023. A: Total people, total female and total male over the the age of 90 in England and Wales from 2002 to 2023. B: Total number of people of each age between 90 and 105 and over in England and Wales from 2002 to 2023. The dip in the number of people over the age of 90 around 2008 is due to the low birth numbers after World War One (Office for National Statistics, 2024, Office for National Statistics (ONS), 2019).

1.2. Hallmarks of ageing

In an attempt to define some common denominators of ageing due to a rise in published ageing research Lopez-Otin et al., published a review article in 2013 where the Hallmarks of Aging were defined. The hallmarks had to contribute to the ageing phenotype based on three criteria. 1) The process has to manifest during normal ageing. 2) If you aggravate it, it should accelerate ageing. 3) By improving function, you should obtain normal ageing and an increased healthy lifespan. They decided on nine hallmarks. Primary hallmarks were those that have a negative effect if altered, and included genomic instability, telomere attrition, epigenetic alteration and loss of proteostasis. Antagonistic hallmarks were those that at low levels are beneficial, but if being overactive they could have a deleterious effect. They included deregulated nutrient sensing, mitochondrial dysfunction and cellular senescence. Lastly, integrative hallmarks directly affected cellular homeostasis and function, and they included stem cell exhaustion, and altered intracellular communication. There is a hierarchy between the hallmarks where the primary hallmarks trigger the damage that leads to the antagonistic hallmarks being active which then disturbs the integrative hallmarks which cannot be compensated for by tissue homeostasis mechanisms (Lopez-Otin et al., 2013) (Figure 1.2).

In 2023, they updated the hallmarks of ageing (Lopez-Otin et al., 2023). Using the same criteria, they expanded on a few of the hallmarks including disabled macroautophaghy, which previously was thought of as loss of proteostasis, however, it does not only affect proteins but rather whole organelles and has therefore earned its own hallmark. Chronic inflammation and age-associated dysbiosis were also new additions after being separated from altered intracellular communication. These additions mean there are now twelve hallmarks of ageing, and even though we think of them as separate, it is important to include that affecting one hallmark usually affects several of the others, and that the hallmarks are strongly related (Lopez-Otin et al., 2023) (Figure 1.2). In this thesis, I will focus on two of the hallmarks of ageing: genomic instability and mitochondrial dysfunction.

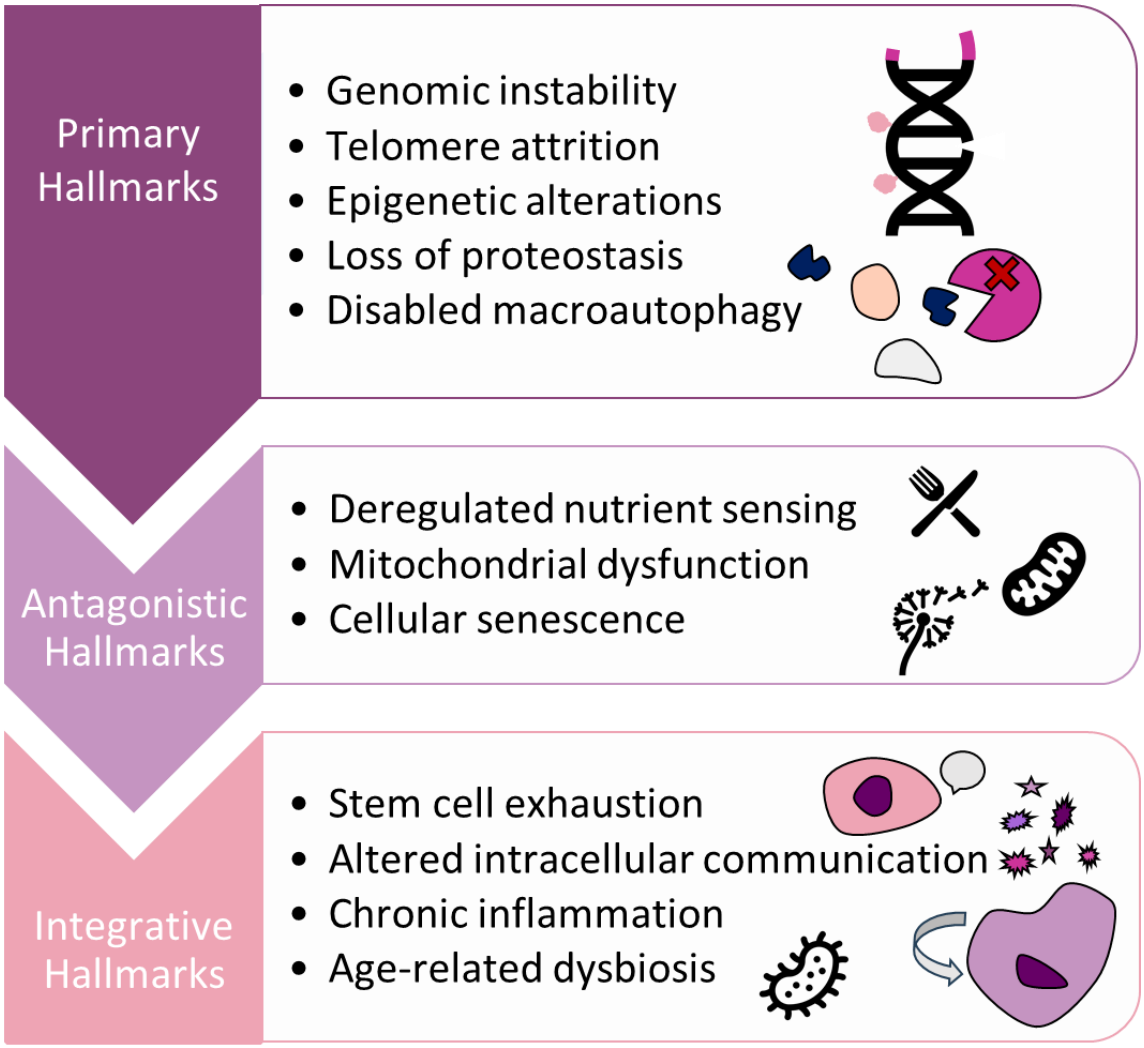

Figure 1.2: Hallmarks of ageing updated by Lopez-Otin in 2023. Figure modified from Lopez-Otin et al, 2023.

1.2.1. Genomic instability

The hallmarks of ageing suggest that not one factor is responsible for ageing. However, one theory is that it is the macromolecular damage that accumulates that drives ageing. Whilst cells with molecular damage in most cases simply degrade and are replaced, the genome, which is the blueprint of our cells, has sophisticated controls and repair mechanisms to correct its damage (Yousefzadeh et al., 2021). These controls are needed as the DNA is constantly under exogenous as well as endogenous stress where each mammalian cell incurs about 10^4-10^5 DNA lesions per day (Marteijn et al., 2014). From the outside, cells can be exposed to ultraviolet (UV) and ionizing radiation as well as alkylating agents which damage the DNA. The last two are used intentionally as cancer treatments. However, the endogenous damage from within the cell is far more persistent and ubiquitous, where molecules and free radicals

might attack the DNA or there might be spontaneous hydrolytic cleavage causing lesions. Further, the DNA is frequently damaged by replication errors and chromosome segregation (Yousefzadeh et al., 2021, Lopez-Otin et al., 2023).

In 2022 Huang et al, showed an increase in single nucleotide variations with an increased age when doing single cell sequencing of human bronchial epithelial cells (Huang et al., 2022). The same results were reported by Martincorena et al in 2018 in oesophagus cells (Martincorena *et al.*, 2018). This suggests that there is an increase in DNA damage accumulation with age, but it is tolerated by the cells, as they are not entering apoptosis. However, this does have the risk of developing deleterious mutations that might affect essential genes and pathways causing dysregulation and compromised homeostasis (Lopez-Otin et al., 2023). Eventually this might lead to poor ageing as seen in prematurely ageing models and progeria diseases with mutations in DNA repair genes. For instance, mice and humans with mutations in the XPF-ERCC1 endonuclease (Explored in section 1.5.2), which is required for repair of helix-distorting DNA lesions and cytotoxic DNA crosslinks, show increased DNA damage and stunted growth and ageing associated phenotypes such as ataxia, sarcopenia and renal insufficiencies (Niedernhofer et al., 2006).

As well as the nuclear DNA being a driver of ageing, mitochondrial DNA instability has also been associated with ageing in several studies discussed by Sanchez-Contreras and Kennedy in 2022. These studies link large deletions in the mitochondrial DNA (mtDNA) to loss of part of the electron transport chain (ETC) whilst other studies suggest that small point mutations in the mtDNA also increase with age (Sanchez-Contreras and Kennedy, 2022). These mutations are not commonly caused by oxidative stress, but rather errors during replication caused by the DNA polymerase γ (POLG1) (Lopez-Otin et al., 2023).

1.2.2. Mitochondrial dysfunction

The mitochondria are usually thought of as the powerhouse of the cell as it produces the energy the cell needs to function. However, with increasing age, there is decreased mitochondrial function due to among other reasons increased genomic instability. Mitochondrial function also decreases due to deficient proteostasis causing the respiratory chain to be dysfunctional. Deficient mitochondria can further cause inflammation through release of reactive oxygen species (ROS) or through the release of mtDNA into the cytoplasm, which triggers anti-viral pathways (Lopez-Otin et al., 2023). Controversially though, decreased

mitochondrial function has on several occasions been shown to improve health span such as by caloric restriction. It is believed that the mitochondria is a key part of this pathway where if calories are in excess, antioxidants and oxidative phosphorylation (OXPHOS) defences are downregulated and the ETC is in a chronic reduced state, favouring a ROS environment which can increase mtDNA mutagenesis. This is among other seen in *Caenorhabditis elegans*, where mutations *neu-6* (complex I) and *isp-1* (complex III) in the ETC causes less energy production and increased lifespan (Lopez-Otin et al., 2023, Lopez-Lluch and Navas, 2016, Amorim et al., 2022, Yang and Hekimi, 2010).

1.2.2.1. Mitochondrial dysfunction and the free radical theory of ageing

The free radical theory of ageing suggests that as the mtDNA is in close proximity to the ETC, it is under great pressure of gaining mutations which will promote mitochondrial dysfunction, and further production of free radicals. These mutations are the driver for the mitochondrial dysfunction in ageing (Amorim et al., 2022, Harman, 1956, Ziada et al., 2020). This theory is partly supported by HIV patients who have undergone a successful treatment with a group of POLG1 inhibitors called nucleoside analogue reverse transcriptase inhibitor anti-retroviral drugs (NRTIs). Due to the POLG1 inhibition in the mitochondria, it causes frequent mutations in the mtDNA. The mitochondria are clonally expanded with pathogenic mutations, causing the HIV patients to experience premature ageing and frailty (Ziada et al., 2020, Payne et al., 2011). Furthermore, in a vicious cycle, once the mtDNA is damaged, it can cause greater damage by not producing the components of the respiratory chain (Guo et al., 2013).

A problem with the free radical theory of ageing is that there is no good evidence that free radicals cause most of the mutations in the ageing mtDNA. The majority of the mutations in an old mtDNA are caused by transition mutations rather than transversion mutations that are caused by oxidative damage. The transition mutations are linked to POLG1 errors (Ziada et al., 2020, Kennedy et al., 2013). This is further emphasised by a POLG1 deficient mice, who had an increase in transition mutations and was prematurely ageing, however it had no increase in oxidative damage. These mice developed normally up to 25 weeks when they developed signs of kyphosis, alopecia and loss of weight. The median lifespan of the mutated mice were 48 weeks (Ziada et al., 2020, Trifunovic et al., 2004). This is not to say that free radicals are not involved in ageing. It probably just plays more of a secondary role potentially as a signalling molecule, and might be a cause of ageing, and not causative to ageing (Lagouge and Larsson, 2013, Ziada et al., 2020). A study with *Drosophila melanogaster* suggests that an increase in free radicals can extend lifespan by acting as a signal to maintain

mitochondrial function (Scialo et al., 2016). There are many theories as to how the mitochondria is affecting ageing, from mutations in the mtDNA being beneficial and to it being detrimental. However, one thing is for sure and that is that the mitochondria are an important hallmark of ageing.

1.3. Types of DNA damage

As mentioned in section 1.2.1 there are between 10^4-10^5 DNA lesions per day in mammalian cells (Marteijn et al., 2014, Yousefzadeh et al., 2021). They can be endogenous, from within the cell, such as ROS or errors in replication, or exogenous, from outside the cell or the outside environment, such as UV irradiation or alkylating agents (Chatterjee and Walker, 2017). In this section, I focus on four types of DNA damage relevant to my project.

1.3.1. Single stranded DNA damage

Single stranded DNA (SSD) lesions are breaks in one of the two strands of the DNA helix. According to Yousefzadeh in 2021, SSD accounts for the majority of the endogenous DNA lesions in the cell, with about 10^4 of the DNA adducts (Yousefzadeh et al., 2021). That is estimated to be about 1 lesion every 1-10 second (Caldecott, 2022). SSD breaks occur as normal parts of the metabolic process or as part of DNA repair, as well as spontaneously. The most common form of single stranded breaks (SSB) result from oxidised deoxyribose caused by a ROS that leads to hydrogen abstractions and 3'deoxyribose fragmentations (Caldecott, 2024). SSB can also form during base excision repair (BER) as well as other excision repair pathways such as ribonucleotide excision repair (RER), nucleotide excision repair (NER) and mismatch repair. Although, these pathways do have intrinsic ways of repairing the breaks (Caldecott, 2022, Abbotts and Wilson, 2017). Lastly, during S phase, Topoisomerase I and II (TOP1 and TOP2) also cause SSB by reducing tension on the DNA supercoil during replication (Abbotts and Wilson, 2017, Caldecott, 2022).

It is important for the cells to recognise and repair SSBs quickly, to avoid disruption to normal cellular processes. Several human diseases have been identified where the SSB machinery does not function including ataxia-oculomotor apraxia-1 (AOA1) caused by mutations in the *aptx* gene coding APRATAXIN. This disease is characterized by early onset cerebellar ataxia, peripheral neuropathy and oculomotor apraxia (O'Driscoll, 2012, Aicardi et al., 1988). As well as the already mentioned prematurely ageing disease progeria caused by the XPF-ERCC1

complex in NER which cause sun sensitivity, increased chance of skin cancer and early death (O'Driscoll, 2012).

1.3.2. Double stranded DNA damage

Breaks in both strands of the DNA are much less common than SSB. Yousefzadeh (2021) predicted only 10^1 endogenous double stranded breaks (DSB) per cell per day (Yousefzadeh et al., 2021). They can be formed by unusual structures of the DNA or chromatin blocking the replication fork or collision with the transcription machinery or other DNA-binding proteins (Mehta and Haber, 2014). Further, some natural processes in the cells require DSBs, such as meiotic recombination by Spo11 (Lam and Keeney, 2014). Potentially, these breaks may also be due to two SSBs being close enough together to form a DSB (Cannan and Pederson, 2016). More commonly talked about might be exogenous DSBs such as those caused by ionising irradiation (IR), where IR splits hydrogen close to the DNA causing free radicals that cause SSBs. In addition, several exogenous cancer drugs have been designed to cause DSBs which are known as *clastogens* (Cannan and Pederson, 2016).

If the mechanisms involved in repairing DSBs are not functioning, several diseases might occur. If Ataxia-Telangiectasia-Mutated (ATM), involved in signalling the presence of a DSB is mutated, it can cause ataxia-telangiectagia (A-T) which is characterised by progressive cerebellar ataxia, oculocutaneous telangiectagia, immune defects and lymphoid tumours (Bohgaki et al., 2010). Further, mouse models of Hutchinson-Gilford Progeria syndrome have increased basal levels of DSB shown by phosphorylated histone2.X (γH2AX), as well as ATM (Liu et al., 2005, Gonzalo and Kreienkamp, 2015).

1.3.3. Ribonucleotide damage

Two crucial processes in the cell are the replication of the genome which is required for cellular division and transcription of the genes in the genome for cellular regulation and for proteins. DNA replication mainly utilises deoxyribonucleotides triphosphates (dNTPs) to produce new strands of deoxyribonucleotide monophosphates (dNMPs), whilst transcription uses ribonucleotide triphosphates (rNTPs). dNTPs and rNTPs are similar molecules, however, the rNTP is characterised by having a hydroxyl group on the C'2 of the ribose ring, where the dNTP only has a hydrogen. There is a large excess of rNTPs in the nucleus compared to dNTPs. In *Saccharomyces cerevisiae* it was shown that there is between 36:1 and 190:1 more rNTPs compared to dNTPs (Nick McElhinny et al., 2010b, Nick McElhinny et al., 2010a). Both

replication and transcription take place regularly in the cell and are tightly regulated. In the eukaryotic nucleus, the DNA polymerases α, δ and ε are responsible for replication of the DNA. The leading strand of the DNA is replicated continually from one place of origin by DNA polymerase ε. On the lagging strand however, replication is initiated from small Okazaki fragments made of about 7-14 rNMPs. These fragments are made by the primase, a heteromeric unit made from RNA polymerase and DNA polymerase α, which synthesises an RNA primer and a small segment of DNA. This segment is then extended by DNA polymerase δ, to replicate a small portion of the genome (Pursell et al., 2007, Nick McElhinny et al., 2008, Brown and Suo, 2011, Zheng and Shen, 2011, Kellner and Luke, 2020). To insert the correct type of nucleotide when the DNA is being replicated the polymerases use a “steric gate” with a tyrosine residue next to the polymerization site which excludes the hydroxyl group of the rNTP (Kellner and Luke, 2020, Brown and Suo, 2011). The process is not perfect however, and a study by McElhinny in 2010 showed that *in vitro*, about 13,000 rNTPs are incorporated into the new strand of the *S. cerevisiae* every replication event. Later, Lujan showed in 2013, that *in vivo* with deficient DNA polymerase ε and the ability to remove singe ribonucleotides in *S. cerevisiae*, the cell incorporates one ribonucleotide per 950bp, and with deficient DNA polymerase δ there is one ribonucleotide per 3400bp (Nick McElhinny et al., 2010b, Lujan et al., 2013). In a mouse study in 2013, they showed that a mouse deficient in RNaseH2 had more than a million single or di-ribonucleotides incorporated in the genome, and it was predicted that for humans this could be closer to 3 million incorporations (Clausen et al., 2013). Further, in mammalian cells there are about 50 million Okazaki fragments made from rNTPs during replication, adding to the ribonucleotide load in the DNA (Zheng and Shen, 2011).

No current research suggests that RNA polymerases incorporate single rNTPs into the genome, as they mostly use one strand of the DNA as a template to make a strand of RNA during transcription. However, by altering the active metal of the DNA polymerase, it can act as a weak RNA polymerase (Williams and Kunkel, 2014). RNA polymerases are however responsible for many R-loops, strands of several rNTPs, at promoter regions in the genome (Crossley et al., 2019).

Once in the DNA, the ribonucleotide is considered a ribonucleoside monophosphate (rNMP). Here they can change the shape of the DNA causing replicative stress and DNA damage (Kellner and Luke, 2020). DeRose showed in 2012, that if a 12bp double stranded DNA helix has a single rNMP in it, the rNMP, and adjacent nucleotide and the transhelical nucleotide adapted a A-shape commonly seen in RNA helices. The other nucleotide remained in a B-

shape (DeRose et al., 2012). However, in 2017, Meroni, proposed a new method to produce DNA helices with several hundred base pairs, where they could randomly integrate rNTPs. This caused a significant shortening of the DNA molecule as well as a significant B to A transition (Meroni et al., 2017) (Figure 1.3). Changes to the shape of the DNA could cause deficiencies in replication, repair, nucleosome assembly as well as protein interactions with the DNA (Kellner and Luke, 2020). Furthermore, Fu et al., saw in 2019, that if the rNMP is on the outside of the histone when the nucleosome forms, the DNA continues to from a B-shape. However, if the rNMP is on the side of the histone, the nucleotides surrounding the rNMP take on an A-from, and the DNA unwinds (Fu et al., 2019). rNMPs may also affect the ability of the DNA polymerase to move along the DNA. Watt suggested in 2011, that the ability of the DNA polymerase to bypass a single ribonucleotide varies from 7.4% to 85% with polymerase α being most efficient and polymerase δ being the least efficient (Watt et al., 2011). Further rNMPs affect the genome stability due to the spontaneous hydrolysis of the 2'OH causing genotoxic breaks in the DNA backbone (Figure 1.3) (Li and Breaker, 1999).

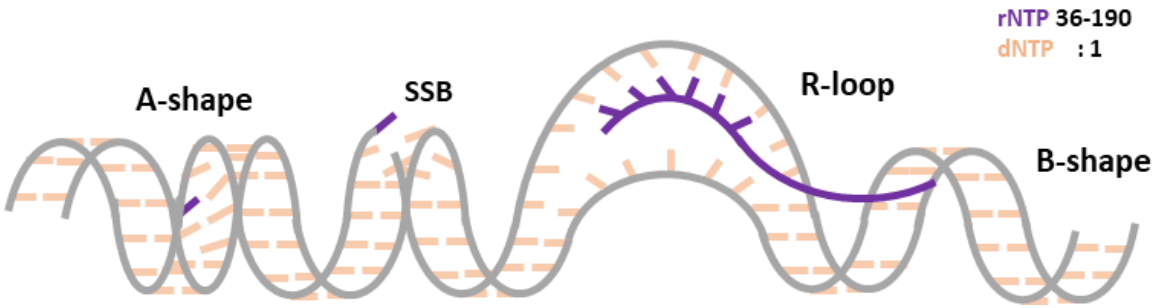

Figure 1.3: Schematic diagram of how rNMPs distort the DNA and can cause DNA damage. rNMPs can cause a change from a B-shape to an A-shape restricting replication, transcription and DNA compression. rNMPs can cause single stranded breaks (SSB), or strands of rNMPs can create R-loops. It is calculated in yeast that there are between 36-190 rNTPs in the nucleus for every 1 dNTP (Nick McElhinny et al., 2010b).

1.3.4. Oxidative DNA damage

Free radicals and oxidants, although beneficial for the cell at a low level as signalling molecules, can also cause damage referred to as oxidative stress. These reactive oxygen species (ROS) include superoxide radicals ($O_2^{\bullet-}$), hydrogen peroxide (H_2O_2) and hydroxyl radicals (•OH). They are metabolic byproducts of normal cellular function and are required to be at an appropriately low level for certain cellular functions such as protein phosphorylation and activation of transcription factors, differentiation, apoptosis, and immunity. Excess ROS

cause oxidative stress, which may affect cellular structure through oxidation of lipids and proteins (Pizzino et al., 2017). However, the highly reactive hydroxyl radical may also affect the DNA and cause strand breakage through attacking the double bonds in the DNA sugar causing abstraction of a deoxyribose hydrogen atom (Cooke et al., 2003, Halliwell et al., 2021, Balasubramanian et al., 1998). There are several ways for free radicals to be released into the cells. Free radicals can be produced by endogenous means such as immune cell activation, inflammation, ischemia, infection, cancer, excessive exercise, mental stress, or ageing. Exogenous sources may also be responsible for free radicals such as environmental pollution of heavy metals, drugs, chemical solvents, cooking, cigarette smoke, alcohol, and radiation. However, most free radicals are produced by the mitochondria during physiological and pathological conditions through cellular respiration (Pizzino et al., 2017).

1.4. DNA damage recognition

In order to repair DNA breaks, they need to be efficiently recognised so repair molecules can be recruited. Recognition of DNA breaks is done by the poly (ADP-ribose) polymerases PARP1, PARP2 and PARP3 (Caldecott, 2024). However, PARP proteins are also involved in chromatin reorganisation, DNA damage response, transcriptional regulation, apoptosis and mitosis (Wei and Yu, 2016). PARP1 can bind nicked or gapped SSBs, as well as overhang and blunt end double stranded breaks (DSBs). Where PARP1 does not have a preference of phosphorylation status of the break, PARP2 and PARP3 prefer breaks with 5'-phosphorylation. When the PARPs bind damaged DNA, it changes confirmation, opening an autoinhibitory helical domain, allowing for activation of PARP1 as NAD+ gains access to the nicotinamide site in the ADP-ribosyl transferase domain, the catalytic domain. ADP-ribose (ADPr) from the NAD+ is then added to the substrate of PARP1 first as a single ADPr on the carboxyl group of the target via an ester link. PAR chain elongation by addition of ADPr happens through 2',1''-O-glycosidic ribose-ribose bonds, and branches of ADPr are created with 2',1'' ribose-ribose bonds. This process can drain the NAD+ levels of the cells. Other proteins important for DNA repair are then recruited to the PARylated sites to initiate repair (Langelier et al., 2018, Pandey and Black, 2021) (Figure 1.4).

In addition to PARylation, DSBs are commonly recognised by the phosphatidylinositol-3 kinase-related kinases (PIKK) family. Notables are ATM, Ataxia-Telangiectasia and Rad3 Related (ATR) and DNA-dependent Protein Kinase catalytic subunit (DNA-PKcs). In resting mammalian cells, ATM and DNA-PKcs is normally bound by Tip60 acetyltransferase and protein phosphatase 2A. MRE11/Rad50/NBS1 (MRN) and KU70/KU80 sense DSBs and bind

the ends of the break to stabilise it close together. Upon DNA damage, MRN recruits Tip60 which in turn causes acetylation of ATM whist KU70/KU80 recruits DNA-PKcs. Conformational changes of ATM cause the release of protein phosphatase 2A causing full activation of ATM. Upon activation by autophosphorylation, ATM phosphorylates potentially 700 other proteins including H2AX, and tumour protein 53 (p53) (Bohgaki et al., 2010, Wang et al., 2017) (Figure 1.4).

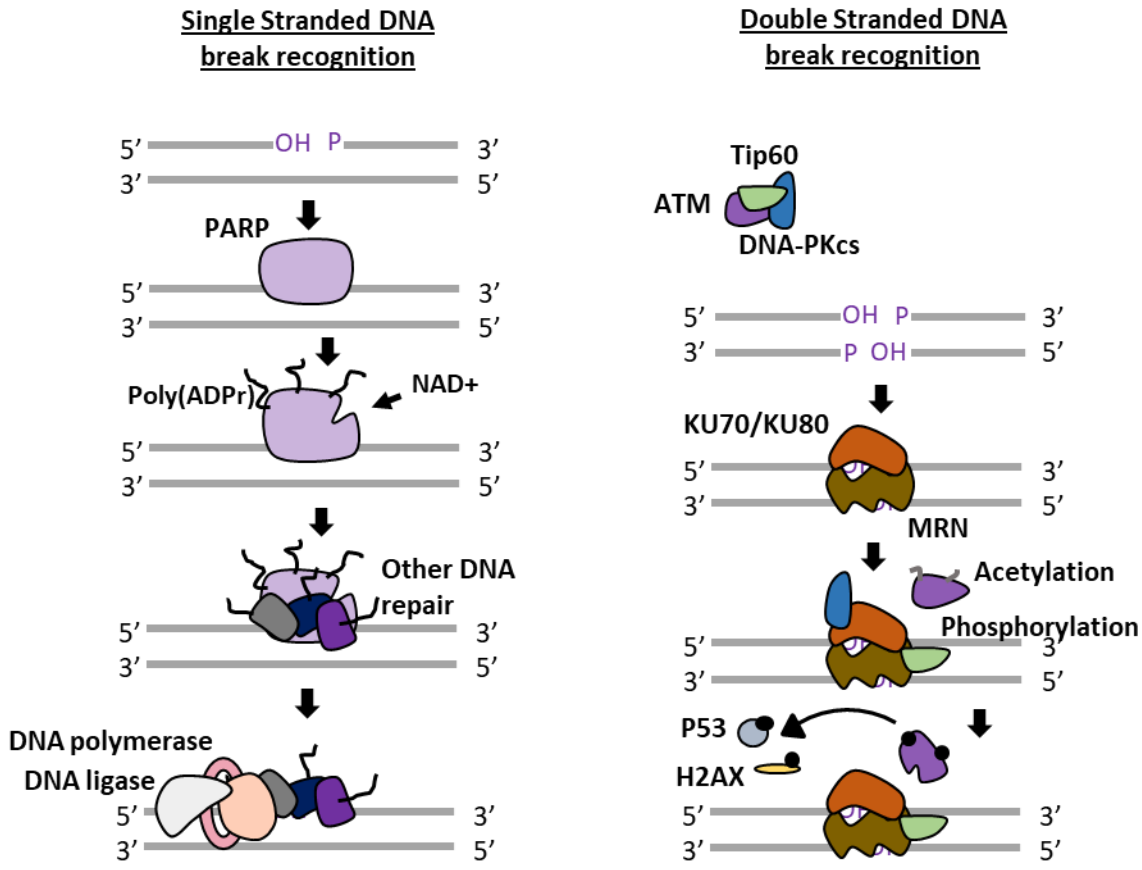

Figure 1.4: DNA damage recognition pathways. Single stranded breaks are commonly recognised by PARP which gets PARylated causing conformational changes and recruitment of other DNA repair proteins including DNA polymerase and DNA ligase. Double stranded breaks are commonly recognised by the MRN complex and KU70/KU80, which cause release of ATM and DNA-PKcs from Tip60. ATM is acetylated causing autophosphorylation and conformational changes allowing it to phosphorylate about 700 other DNA repair proteins including P53 and H2AX.

1.5. Types of DNA excision repair

In this thesis, I focus on the repair processes that resolve single base mistakes in the DNA. Excision repair is also known as the cut-and-paste mechanism. When one base or nucleotide is identified as wrong the identified error is enzymatically cleaved by an endonuclease, then the gap is filled by a DNA polymerase with nucleotides complementary to the undamaged strand, and lastly a DNA ligase will seal the final “nick” (Klug et al., 2016, Dey et al., 2023).

1.5.1. Base excision repair

Base excision repair (BER) is activated if there is a distorted base that does not affect the DNA helix significantly. This primarily happens spontaneously or due to oxidation by ROS but can also happen due to deamination, methylation, spontaneous decay of the DNA or environmental chemicals tobacco smoke, radiation, or treatment with cytostatic drugs (Hegde et al., 2008, Krokan and Bjoras, 2013). Both the nuclear DNA and the mitochondrial DNA can repair lesions by BER using largely similar isoforms of proteins (Krokan and Bjoras, 2013). If the errors are not corrected, they can be replicated causing point or complex mutations, however, BER is one of the few DNA repair pathways that’s functional significance have not been implicated in preventing any diseases. However, nucleotide excision repair and DNA mismatch repair have been linked to cancer and disease (Hegde et al., 2008).

The incision of the flipped-out or damaged base is done by a DNA glycosylase leaving an abasic (AP) site due to cleavage of the N-glycosidic bond of the damaged base. An AP endonuclease then cleaves the AP site creating a 3’OH and a 5’ deoxyribose phosphate terminus. The site is then filled by DNA polymerase-β in the nucleus of mammalian cells and POLG1 in the mitochondria. Flap Endonuclease 1 (FEN1) cleaves the deoxyribose phosphate terminus to generate a 5’ phosphate. The new base is ligated to the nick of the strand on either side by DNA ligase 1 in the nucleus and DNA ligase 3 in the mitochondria (Hegde et al., 2008, Krokan and Bjoras, 2013) (Figure 1.5). BER can also repair single stranded breaks by the same process. Here a single stranded break in the DNA is recognised by X-ray Repair Cross-Complementing 1 (XRCC1) which functions as a scaffolding protein for other BER proteins also activating some of them (Hegde et al., 2008).

1.5.2. Nucleotide excision repair

Nucleotide excision repair (NER) is the main pathway that removes bulky DNA lesions. These can be caused by UV radiation, environmental chemicals, and some chemotherapeutic agents (Scharer, 2013), causing pyrimidine photodimers, platinum adducts, protein-DNA cross-links, as well as DNA modifications caused by the DNA interacting with derivatives of benzo[a]pyrene, benzo[c]anthracene or acetylaminofluorene (Petruseva et al., 2014). In humans, defects in NER have been linked to several autosomal recessive disorders such as xeroderma pigmentosum, Cockayne syndrome, trichothiodystrophy and UV-sensitive syndrome (Kusakabe et al., 2019).

There are two types of NER; global-genomic NER (GG-NER), which usually fixes UV-lesions, and transcription-coupled NER (TC-NER) (Kusakabe et al., 2019, Scharer, 2013). In TC-NER, the damage is recognised during transcription by RNA polymerase II being stopped by the damage (Petruseva et al., 2014). Recognition is however more complicated in GG-NER. A trimer of XPC-RAD23-CETN2 recognises the lesion (Kusakabe et al., 2019). Once bound to the lesion, RAD23 dissociates, indicating that it has a role in stabilizing XPC rather than repairing the lesion (Scharer, 2013). There is one form of common lesion that XPC does not interact with however, and that is the cyclopyrimidine dimers (CPD), a UV induced photoproduct which is believed to be recognised by UV-DDB2 (Scharer, 2013). Once the lesion has been recognised TFIIH which is made up of ten subunits, uses two helicase subunits XPB and XPD to open the DNA around the lesion. Now, RPA bind the lesion to work with XPA as XPC leaves the site, and the endonucleases XPG and ERCC1-XPF enters the open DNA and makes two incisions leaving a gap of about 22-30 nucleotides (Scharer, 2013, Marteijn et al., 2014). The damaged base and surrounding nucleotides bound by TFIIH are released and subsequently degraded. Now DNA polymerase δ and ε, the sliding clamp Proliferating Cell Nuclear Antigen (PCNA), the pentameric clamp loader RFC, RPA, and DNA ligase repair and ligate the gap that has been left by the endonucleases (Scharer, 2013) (Figure 1.5).

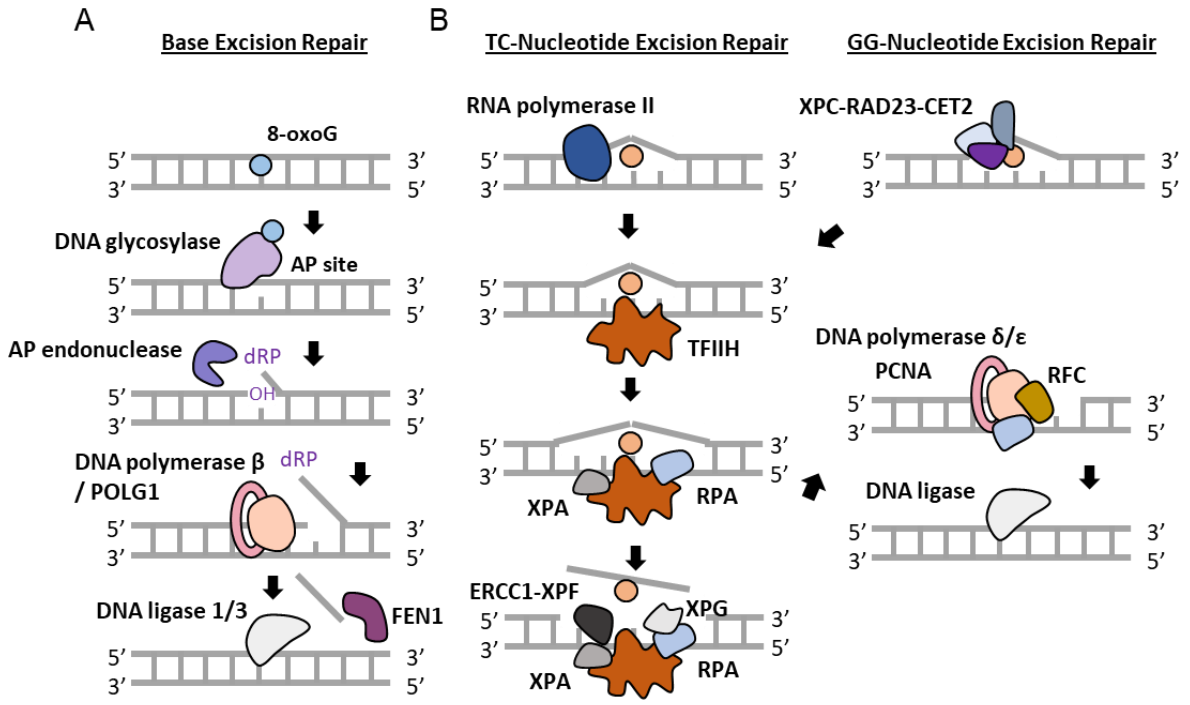

Figure 1.5: Schematic diagram of Base and Nucleotide excision repair. A: Base excision repair of an 8-oxoG lesion. DNA glycosylase removes the damaged base creating an AP site which is cleaved by an AP endonuclease. The gap is filled by either DNA polymerase β or POLG1, and the flap cleaved by FEN1 and gap sealed by DNA ligase 1 or 3. B: TC- and GG- Nucleotide excision repair of bulky lesion. In, TC, RNA polymerase II recognises the lesion, whilst in GG it is recognised by a trimer of XPC, RAD23 and CET2. In both pathways the TFIIH complex recruits XPA and RPA which opens the DNA. ERCC1-XPF and XPG cuts a 20-30bp flap with the lesion from the DNA, which is repaired by DNA polymerase δ/ε with PCNA and the gap is sealed by DNA ligase.

1.5.3. Ribonucleotide excision repair

To avoid the complications associated with single rNMPs in the DNA the cells have sophisticated mechanisms to remove them and repair the nick. Initially, the DNA polymerases have some proofreading abilities themselves. DNA polymerase ε as an example, can remove one third of the rNTPs that it inserts with its 3'-5' exonuclease ability (Williams et al., 2012). However, to remove the remaining rNMPs, the cells use the ribonucleotide excision repair (RER) pathway which primarily involves the enzymes Ribonuclease H2 (RNaseH2), FEN1, DNA polymerase δ and DNA ligase 1. PCNA can act as a scaffolding for the enzymes (Chon et al., 2009, Sparks et al., 2012, Khandagale et al., 2020). Further, exonuclease I, can substitute FEN1, however, it is between 2- to 3- fold less efficient than FEN1. DNA polymerase ε can substitute DNA polymerase δ but is only half efficient (Sparks et al., 2012). The pathway

is initiated by the recognition of the rNMP by RNaseH2. RNaseH2 then cleaves the ribonucleotide at the 5' end and FEN1 cleaves at the 3' end creating a 1 nucleotide gap subsequently filled by DNA polymerase δ and sealed by DNA ligase 1 (Figure 1.6) (Sparks et al., 2012, Rydberg and Game, 2002). In certain circumstances, toxic RER intermediates can be produced through the premature attempts to ligate the nick immediately after RNaseH2 cleavage and before flap processing by FEN1, or at strand breaks when RNaseH2 does not process the rNMP. This attempted ligation can create adenylated 5'-RNA-DNA junctions (Tumbale et al., 2014, Williams and Kunkel, 2014). These junctions may be repaired by APRATAXIN (APTX), whose AMP-hydrolysis activity cleave the AMP, restoring the break for correct repair to occur (Ahel *et al.*, 2006) (Chapter 5).

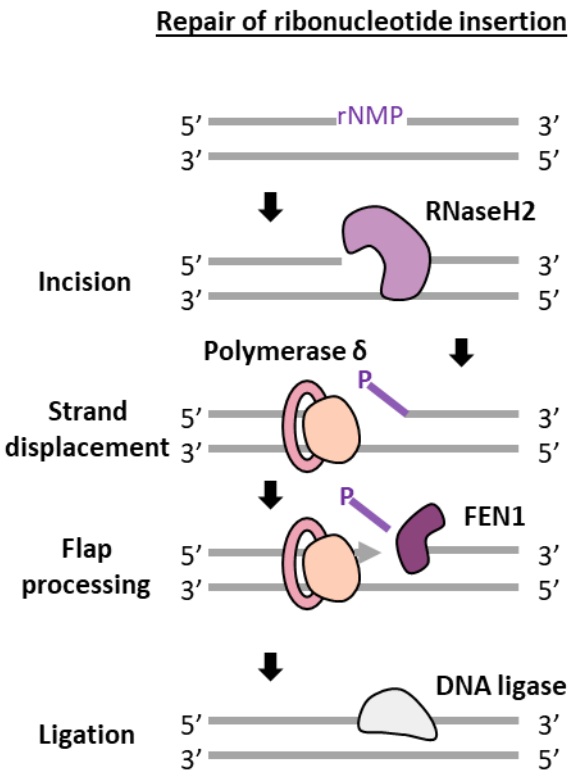

Figure 1.6: Schematic diagram of the ribonucleotide excision repair pathway. RNaseH2 recognise the rNMP and cleave at the 5' end. The rNMP is flipped out by DNA Polymerase δ which repair the nick, and the flap is removed by FEN1. The gap is ligated by DNA ligase.

1.5.3.1. Ribonuclease H

The endonuclease that initiates the RER pathway is RNaseH2. RNaseH2 is part of the RNaseH enzyme family, which also includes of RNaseH1. RNaseH1 is a monomeric protein mainly attributed with resolving R-loops. RNaseH2 is a trimer consisting of RNaseH2A, the

catalytic subunit and two supporting subunits RNaseH2B and RNaseH2C. Whilst subunit A is similar to the monomeric *Escherichia coli* RNaseHII*,* B and C do not have any prokaryotic equivalent, and their function is not fully known. They are believed to be required for assembly of the enzyme, especially B, as it has a PIP-box for PCNA interaction. However, the presence of PCNA is not required for enzyme function (Chon et al., 2009, Reijns et al., 2011, Lockhart et al., 2019). RNaseH2A has also been suggested to interact with RNA polymerase I and II potentially enhancing transcription (Cristini et al., 2022). In 2011, Reijns resolved the human structure of the RNaseH2 enzyme. The three subunits bind linearly and intertwine into a triple β-barrel via the C-terminus of RNaseH2A which protrudes out of its catalytic site (Reijns et al., 2011). Graff (2017) also showed that RNaseH2 did not cross-link to any particular places in the chromatin, except late in S phase where it cross-linked to telomeres (Graf et al., 2017). In 2019, Lockhart suggested that RNaseH2 is expressed in a cell cycle specific manner. By using yeast with RNaseH2 only expressed in certain cell cycles, they saw that when it was only expressed in S-phase, the cells mimicked the phenotype with RNaseH2 deletions. They suggested this was due to RNaseH2 interfering with the replisome causing double stranded breaks which then must be repaired by Rad52. They note that RNaseH2 is expressed during S-phase but suggest it might be negatively regulated. Further, RNaseH2 expression the G2/M phase is required for RER processing (Lockhart et al., 2019).

As well as being a key player in the RER pathway, RNaseH2 is also associated with resolving R-loops (Lockhart et al., 2019). R-loops are three stranded RNA-DNA structures occurring when the RNA displaces the non-hybridised strand. This may happen during transcription, DNA replication and DNA repair causing small hybrids or larger R-loops usually spanning 100-2000 base pairs (Crossley et al., 2019, Petermann et al., 2022). The R-loop resolving function of RNaseH2 can mostly be separated from the single rNMP removal function, known as a RNaseH2-RED (Ribonucleotide Excision Deficient) mutant, which is deficient in RER but not R-loop processing. This mutation is still embryonic lethal in mice, showing the importance of RER in development (Chon et al., 2013, Kellner and Luke, 2020, Cristini et al., 2022).

1.5.3.2. Topoisomerase 1

Topoisomerases resolve topological problems in the DNA. Some topological problems might include opening of the DNA double helix by helicases during replication and transcription, opening of the helix for chromatin remodelling by ATPase translocase ‘motors’ and negative supercoiling around nucleosomes. There are six formal members of the human topoisomerase family. Topoisomerase type IB is divided into TOP1 and mitochondrial TOP1 (TOP1mt). They

specialise in relaxing supercoiling in the nucleus and the mitochondria. Topoisomerase type IIA, consists of TOP2A and TOP2B, and they resolve DNA catenanes. Topoisomerase type IA containing TOP3A, a mitochondrial isoform of TOP3A and TOP3B specialise in processes that require the threading of one strand of nucleotides through another called hemicatenanes (Pommier et al., 2022) (Figure 1.7A). In zebrafish the type IB TOP1 genes have an additional member as there has been a gene duplication event creating a further TOP1 paralogue. There is TOP1a (Formely TOP1 like), which we believe to be the dominant form and TOP1, in addition to TOP1mt.

All Topoisomerases work the same way. The Topoisomerase cleaves a nucleotide and then covalently links itself via a tyrosine nucleophilic residue, creating a TOP covalent complex (TOP-cc). Type IB binds the 3' end of the nick whilst type IIA and IA bind the 5' end. The TOP-cc is normally self-reversible as the cleaved end not conjugated to the TOP1 has a hydroxyl end that act as a nucleophile towards the tyrosyl-DNA phosphodiester bond (Pommier et al., 2022). TOP1 has been suggested to be involved in the removal of single ribonucleotides if RNaseH2 enzyme is not present. TOP1 may prefer to bind the sequence 5'-TGACT-3' to reduce topological tension (Edwards et al., 1982). Whilst there is speculation that TOP1 uses this site to locate rNMPs close to it, other evidence suggests that TOP1 bind next to the rNMP causing cleavage of the hydroxyl by nucleophilic attack of the phosphotyrosyl bond (Huang et al., 2017). There, TOP1 can convert the ribonucleotide to SSB with 3' ends bearing a 2'3'-cyclophosphate which can then be processed by an enzyme called apurinic endonuclease 2 (APE2). Alternatively, a TOP1-cc formed adjacent to the 5' end of the ribonucleotide can create a short 2-5 bp SS DNA fragment, that is released forming a 2-5 bp SSD gap which is often deleted creating a signature deletion for TOP1 attempted ribonucleotide repair. This cleavage is preferably done at a thymine (Figure 1.7B) (Pommier et al., 2022, Reijns et al., 2022).

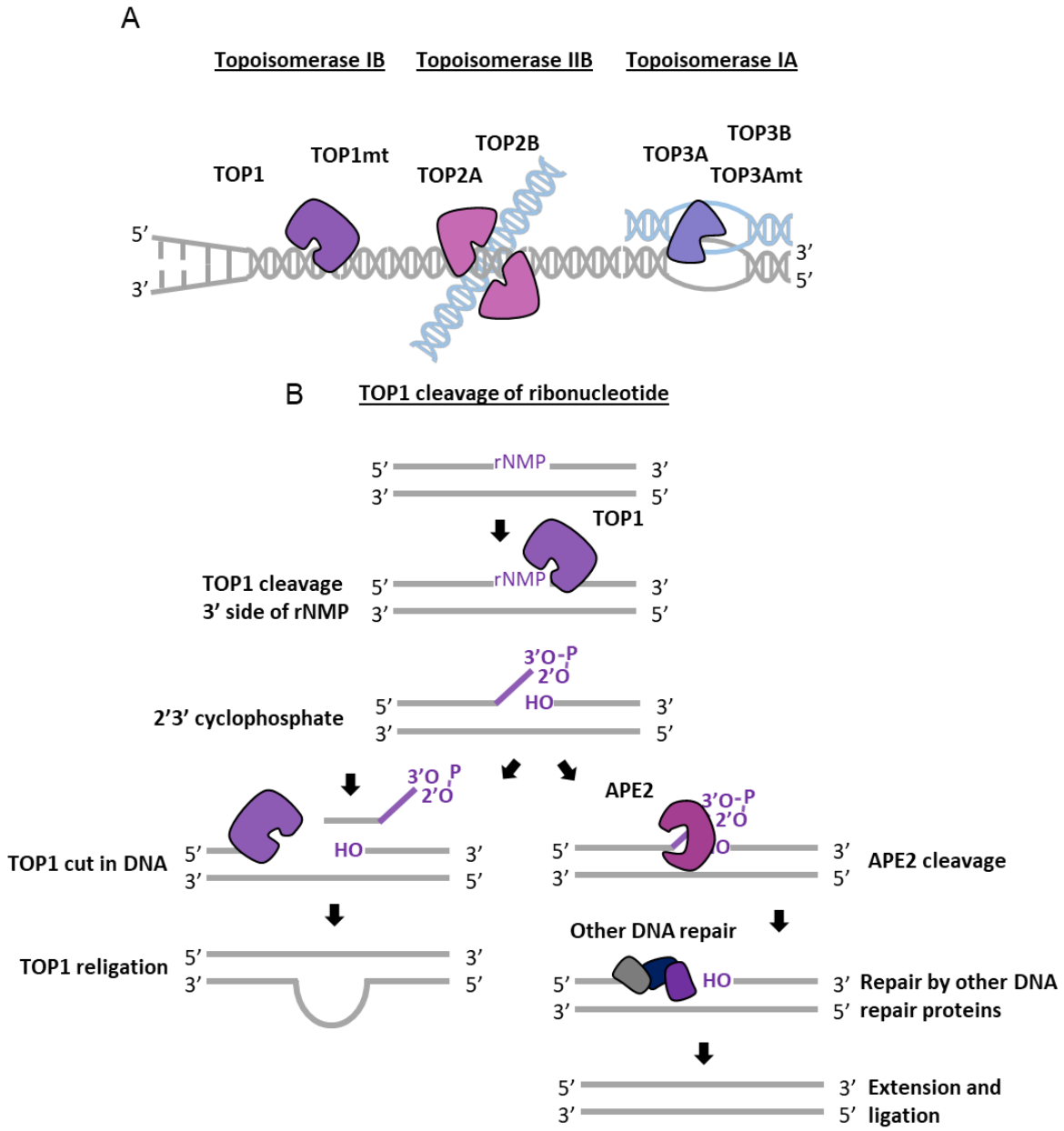

Figure 1.7: Schematic diagram of Topoisomerases in the human cell. A: Topoisomerase IB cause single stranded breaks to relax supercoiling. Topoisomerase IIB resolve catenanes and Topoisomerase IA resolve hemicatenanes. B: Schematic diagram of TOP1 cleavage of a single ribonucleotide (rNMP). TOP1 cleaves at the 3' end of the rNMP creating a 2'3' cyclophosphate and is released. A TOP1-cc is then formed and cuts in the DNA 2-5bp upstream of the ribonucleotide preferably at a thymine. TOP1 then reseals the nick using the 5' OH causing a slippage mutation or misalignment. Alternatively, after 2'3'cyclophosphate formation, APE2 cleaves the rNMP, and the nick is repaired by other DNA repair mechanisms.

TOP1 is vital for embryonic survival, and mouse embryos homozygous for TOP1 die between cell stage 4 and 16 (Morham et al., 1996). Several cancer types including leukaemia, lymphoma and colon cancer have elevated levels of TOP1. As TOP1 is vital for cell survival it is being used as a target for cancer therapy. Camptothecin (CPT), a natural compound derived from the Camptotheca tree native to China, has been used in traditional Chinese medicine for hundreds of years and is the basis of many of these drugs. CPT has high affinity for TOP1 bound to DNA and traps the TOP1 covalently on the DNA. This causes replicative stress, DNA breaks and cell death (Morham et al., 1996, Li and Liu, 2016).

1.6. Genomic instability linked to RNaseH2

Mutations in any of the three subunits of RNaseH2 can cause Aicardi-Goutières Syndrome (AGS), an early-onset autoinflammatory disorder first described in 1984. The disease has similarities with congenital viral infections and lupus erythematosus (Aicardi and Goutieres, 1984, Reijns et al., 2011). AGS primarily affects the brain and is characterized by clinical features such as encephalopathy, basal ganglia calcification, leukoencephalopathy, lymphocytosis and increased interferon-α (INFα) levels in the patient's cerebrospinal fluid and serum. As well as the three subunits of RNaseH2, mutations that cause AGS can be found in Three prime repair exonuclease 1 (TREX1), SAM domain and HD domain-containing protein 1 (SAMHD1), Adenosine deaminase acting on RNA 1 (ADAR1), Interferon Induced With Helicase C Domain 1 (IFIH1), U7 Small Nuclear RNA Associated (LSM11) or RNA, U7 Small Nuclear 1 (RNU7-1). They all cause strands of double stranded nucleic acids to enter the cytoplasm to cause overproduction of type 1 interferons (INFs). Of the nine genes, mutations in *rnaseh2b* are the cause of 36% of AGS cases, with *rnaseh2a* being responsible for only 5% and *rnaseh2c* 12% (Liu and Ying, 2023). Patients with mutations in *rnaseh2b* have a later onset of the disease and less mortality than *rnaseh2a* patients, possibly also reflected in their percentage cases. It was also observed that ASG patients with later onset had lower INF signalling but increase in loss of mental and physical ability (Rice et al., 2007). Rice also observed that some of the patients with *rnaseh2b* mutations had scoliosis (Rice et al., 2007). Further, mutations in *rnaseh2b* have been found in some metastatic prostate cancers and chronic lymphocytic leukaemia (Zimmermann et al., 2018).

1.7. DNA damage-induced inflammation

Increased DNA damage, which is either endogenous through replication stress or faulty DNA repair, or exogenous caused by DNA damaging agents such as CPT or ionising radiation can

cause an inflammatory response through the release of inflammatory cytokines (Ragu et al., 2020). This is done through hijacking a system for identification and processing of viral DNA. DSB or SSB which become DSB during collapse of the replicative fork can cause parts of the dsDNA to break off and move into the cytoplasm (Ragu et al., 2020). Broken DNA can leave the nucleus in micronuclei. Upon micronuclei membrane collapse the DNA can be bound and recognised by cyclic GMP-AMP synthase (cGAS) through a positively charged DNA-binding nucleotidyltransferase domain in the C-terminus (Kranzusch et al., 2013, Mackenzie et al., 2017, Shen et al., 2021). This causes a conformational change in the protein allowing for interaction with the substrates ATP and GTP, converting cGAS to 2'3' cyclic GMP-AMP (sGAMP). In order to reach an appropriate threshold of signalling, several cGAS enzymes need to bind in a ladder along the DNA, therefore short pieces of DNA are insufficient to activate this response. cGAMP is a second messenger and agonist to Stimulator of INterferon Genes (STING) which is a membrane protein which resides on the endoplasmic reticulum (ER). STING acts as a homodimer, and upon cGAMP binding it undergoes extensive conformational changes causing oligomerisation of several STING dimers. As well as oligomerisation, STING dimers will also form disulphide bridges between each other and lead to palmitoylation of certain cystine residues, creating an active STING unit. The active STING unit is then transported to the Golgi via the ER-Golgi intermediate compartment (ERGIC). In the ERGIC and Golgi compartments, STING recruits TANK-binding kinase 1 (TBK1) through its C-terminal tail promoting autophosphorylation of TBK1 once it dimerises which further phosphorylates STING. This activation recruit interferon regulatory factor 3 (INF3) where TBK1 phosphorylates it which enables its dimerization, translocation to the nucleus and target gene induction. INF3 has many targets including type I interferons, interferon stimulated genes (ISGs), inflammatory cytokines such as *il6*, receptors to target natural killer cells for elimination of damaged cells (Pan et al., 2023). TBK1 can also activate nuclear factor κB (NF-κB) signalling. However, STING is also able to do this independently of the C-terminal tail activating TBK1. Some vertebrate fish, such as zebrafish, have developed extra motifs at the STING C-terminal tail promoting NF-κB signalling through TRAF6 (Decout et al., 2021).

1.7.1. Inflammageing and senescence

Inflammation has been recognised as one of the hallmarks of ageing and is often referred to as inflammageing where harmful chronic inflammation weakens the immune system causing ageing related diseases (Li et al., 2023). Senescence, another hallmark of ageing is closely related to inflammation and often referred to as immunosenescence. Senescence is a form of growth arrest where the cells do not repair themselves or go through apoptosis. This might

occur as a response to among others DNA damage, telomere dysfunction, embryogenesis or organismal ageing (Di Micco et al., 2021). Senescent cells are usually characterised by the activation of a chronic DNA damage response seen by markers such as γH2AX and phosphorylated p53 as well as cyclin-dependent kinase inhibitors (CDKi) seen by p21 and p16 expression. Enhanced proinflammatory secretion by IL-6, IL-8 and NF-κB, and tissue-remodelling factors, induction of antiapoptotic genes such as BCL-2, altered metabolic rates such as an increased AMP:ATP or ADP:ATP ratio, and endoplasmic reticulum (ER) stress (Hernandez-Segura et al., 2018).

1.8. Animal models of frailty and ageing

There are many ways to study ageing and frailty; including cells, yeast, invertebrate worms and flies, mice and primates including humans (Lees et al., 2016). *C. elegans* have long been used to study ageing and longevity due to their short lifespan of 2-3 weeks and conserved developmental program (Lapierre and Hansen, 2012). Like mammals*, C. elegans* experience ageing-associated features such as neuromucular degeneration, weakness to stressors, elevated infection levels, decreased physiological activity and increased mortality (Matsunami, 2018). As well as *C. elegans, D. melanogaster* has also been used for ageing research for more than 100 years. *Drosophila* can live for between 70 and 90 days, and towards the end of their lives, they show several age-related phenotypes such as changes to metabolism and behaviour, reduced stress resistance, reduced reproductive capacity, altered neuronal function, modified physical activity, reduced immune capacity, progressive dysplasia and reduced barrier function in the gut, and compromised cardiac function (Piper and Partridge, 2018). Some important research regarding nutrient sensing and ageing has been shown in *C. elegans* and *Drosophila,* such as the involvement of the *C. elegan age-1* and the *daf-2* genes, orthologues of the mammalian phosphoinositide 3-kinase (PI2K) and the insulin/IGF-1 receptor (InR), in longevity. It was found that by modulating these genes by hormonal treatment, you could alter the organisms lifespan (Friedman and Johnson, 1988, Kenyon et al., 1993, Lapierre and Hansen, 2012, Kimura et al., 1997). For the *Drosophila* insulin-like peptides (*ilps 1-8*) and the single insulin receptor and the intracellular components of the canonical PI3K branch showed similar effects on longevety (Piper and Partridge, 2018, Nässel and Broeck, 2016). Further, *C. elegans* were also used to identify mTOR signalling as a longevity factor. mTOR is involved in growth control and reproduction, and if inhibited it extends the lifespan (Lapierre and Hansen, 2012, Kapahi et al., 2010).

Much of the ageing knowledge from non-mammalian organisms have later been tested in mammals, such as the mouse. They too have a short lifespan of 3 years and approximately 99% of human genes have corresponding mouse homologues. Mice have been used in research to extend lifespan by calorie restriction, as well as shorten lifespan (Yuan et al., 2011). However, mice have also been used to understand other aspects of ageing and frailty, such as the shortening of telomeres with age. Mice null for *terc* or *tert* had critically shortened telomeres and chromosomal end-to-end fusions, shortened lifespan, overall frailty, decreased fecundity and tissue atrophy with impaired organ function (Lee et al., 1998, Sahin and Depinho, 2010). However, one limit to using mice is that they are only distantly related to humans and they do not develop several important age-related diseases, such as atherosclerosis and diabetes naturally. Therefore, non-human primates are also being used in ageing and frailty research as they share similar genetics, physiological and behavioural traits, however, unlike humans, non-human primate experiments usually come with complete experimental control (Colman, 2018). Of the non-human primates, the Chimpanzee has been most used in biomedical research, and it has among others been used to study the reduction of grey and white matter in the brain during ageing (Chen et al., 2013). However, the Chimpanzees long lifespan makes it challenging to work with in many ways, and old world monkeys such as Rhesus macaques who has a lifespan of 26 years have been used in among musculoskeletal ageing and frailty to study age related sarcopenia, osteoporosis and osteoarthritis (Colman et al., 1999a, Colman et al., 1999b, Colman et al., 2005, Duncan et al., 2011). As shown in this section, there are several model organisms that can be used to study frailty and ageing, and they all have their own benefits and disadvantages.

1.9. Zebrafish as a model organism

In this project I primarily use zebrafish (*Danio rerio*) as my research model. Zebrafish are members of the Teleostei infraclass. The human genome has 71.4% of gene structures with orthologues in zebrafish, whilst mice have 80%. However, millions of years ago, the ancestor of the zebrafish underwent a genome duplication event. This means that compared to mammals, several of the zebrafish genes have two copies. Zebrafish are commonly used for genetic studies due to the large number of embryos they can produce with external fertilization. This makes them good for large mutagenic screens, as well as one-cell stage genetic manipulations using either Zinc-finger nucleases (ZFNs), Transcription activator-like effector nuclease (TALENs), Clustered Regularly Interspaced Short Palindromic Repeats (CRISPR)/Cas9 and Tol2 transgenic. Embryos hatch within 2 days post fertilization (dpf) from their protective membrane, the chorion, and all major organs start forming and functioning within 5dpf. The embryos are transparent and therefore lend themselves well to fluorescent

imaging and tracking (Kimmel et al., 1995, Veldman and Lin, 2008, Howe et al., 2013, Choi et al., 2021). As well as being great models for early development, zebrafish are good for investigating DNA damage repair pathways as the pathways are conserved from yeast to mammals. Even though the zebrafish did go through a whole genome duplication event, out of 648 DNA repair genes, only 70 are duplicated (Cayuela et al., 2018, Howe et al., 2013). Zebrafish can be used to visualise the first minutes of DNA damage through immunohistochemistry and western blotting, although most antibodies do not recognise zebrafish proteins, meaning these methods are hit and miss. However, qPCR and RNA-seq can be very informative assays for zebrafish (Cayuela et al., 2018). GFP reporter lines and comet assays can also be used to study immediate DNA damage (Jarvis and Knowles, 2003, Santhakumar et al., 2012). The effect of DNA damage can be studied through apoptosis with terminal deoxynucleotidyl transferase dUTP nick end labelling (TUNEL)-assays or acridine orange, or long-term it can be seen through the formation of cancers (Cayuela et al., 2018, Dey et al., 2023).

Furthermore, zebrafish start showing an ageing phenotype by 2 years of age that resembles human ageing and typically live between 3 and 5 years in laboratory settings. These phenotypes include morphological changes in spinal curvature and loss of muscle mass, loss of regenerative ability, reduced reproduction, increase in cancers, cataract, reduced swimming speed, cognitive decline, and cardiovascular dysfunction making them ideal for ageing studies (Gilbert et al., 2014, Khor et al., 2019, Kishi et al., 2009, Abou-Dahech and Williams, 2024). Senescence associated β-galactosidase (SA-β-gal) activity has also been observed in skin of zebrafish as well as oxidised protein accumulation in muscle. (Kishi, 2004, Tsai et al., 2007). Aged zebrafish have also been found with increased accrual of lipofuscin in the liver, which has been associated with ageing min mice and humans previously (Kishi et al., 2008). Further, decreased levels of melatonin were also observed after 2 years of age in zebrafish, something that has been associated with premature ageing in mice and *Drosophila* previously (Zhdanova et al., 2008, Kondratov, 2007). Decreases in neurotransmitter receptors and their downstream signalling molecules were also seen to decline after 4 years in the adult zebrafish brain (Yu et al., 2006). As well as studying the chronological ageing of zebrafish, models to study accelerated ageing have also been made in Zebrafish. Among the genes is *telomerase* which repairs the ends of telomeres. These fish experience an accumulation of DNA damage markers and a p53 response leading to apoptosis and early death (Anchelin et al., 2013, Henriques et al., 2013). Fish with knockouts of *klotho*, a receptor for fibroblast growth factor 23 die at 5 months due to accelerated ageing. They show signs of spinal deformation, loss of fin integrity, and widespread ectopic calcification, especially of the outflow tract of the heart

(Singh et al., 2019, Ogura et al., 2021). *sirt1* is NAD^+ a protein deacetylase. Knockout of sirt1 causes increased inflammation and apoptosis and reduced lifespan in zebrafish as well.

1.10. Summary statements

The role of RNaseH2 in ageing has previously been investigated by one group (Storci et al., 2019) where they suggested that RNaseH2 was increased in centenarians. However, the role of RNaseH2 in normal ageing has not been investigated. In Chapter 3 I aim to study the role of RNaseH2 in the ageing of surplus zebrafish in the aquarium. I see that the aged fish can be divided into three ageing groups, robust, pre-frail and frail. I use these groups to study their RER efficiency and see that there is decreased RER activity in the frail group. To further this research, I aimed to study disease progression amongst an older human population using the Community Ageing Research (CARE75+) study (ISRCTN16588124) (Brown et al., 2021, Heaven et al., 2019). I wanted to identify whether the way in which diseases progressed amongst the population could be linked to DNA damage, and in particular ribonucleotides by also using blood samples available in the study. However, the quality of the dataset and the blood samples available were not justifiable to continue with this study, and therefore, none of the data is presented in the thesis.

Further, in Chapter 4, I investigate FASTKD2, an enzyme that through work by Dr Chunyan Liao was implicated in cleaving ribonucleotides in the mitochondrial DNA. Currently, there is no known enzyme that can remove single ribonucleotides from the mitochondrial DNA. I make a CRISPR/Cas9 knockout zebrafish line of the enzyme and study its mitochondrial defects. In addition, I studied the fish's ability to remove single ribonucleotides, however, I was unable to detect any defects linking it to ribonucleotide removal.

In Chapter 5, I create an APRATAXIN knockout in the background of the RNaseH2A heterozygous zebrafish. Mutations in *aptx* in humans cause the disease Ataxia with oculomotor apraxia type 1 (AOA1), however, mice are viable with no phenotype. Therefore, I create a double knockout to investigate whether it causes a phenotype in zebrafish which later can be used to develop drugs to help the disease.

Lastly, I look at oxidative damage at non-coding promoter and enhancer regions by studying NuMA in Chapter 6. NuMA is a protein with many functions which has been thoroughly studied *in vitro*. However, due to its vital role in development loss of NuMA is lethal. To investigate

NuMA's function on whole organismal level, Dr Ruth Thomas created a NuMA knockout zebrafish line which shows a phenotype at 24hpf and is lethal by 4dpf. To assess what role of NuMA is responsible for the lethality, I aimed to create a rescue of the phenotype by incorporating parts of NuMA into the zebrafish genome. However, I did not see a rescue of the phenotype as the constructs failed to maintain expression of the transgene.

Chapter 2 Methods

2.1. Zebrafish husbandry and maintenance

All zebrafish were kept at the Bateson centre at the University of Sheffield, shoaling in groups of 10-30 adult fish per tank. They were kept in freshwater at 28°C with a 14:10 light:dark cycle and fed according to the feeding schedule seen in table 2.1. The zebrafish lines used in the thesis can be seen in table 2.2. All fish were kept and experiments done under the license PP4947590.

Table 2.1: Zebrafish feeding schedule.

Age (days)	Food schedule
5-10	Zebrafeed <100 (from Sparos) + Rotifers (L-strain rotifers low saline 7ppt from ZM fish food and Equipment) twice daily
10-15	Zebrafeed <100 + Artemia twice daily
15-30	Zebrafeed 100-200 (from Sparos) + Artemia twice daily
31-60	Zebrafeed 200-400 (from Sparos) + Artemia twice daily
60-90	Zebrafeed 400-600 (from Sparos) + Artemia twice daily
90+	Mon, Weds, Fri - Zebrafeed 400-600 AM + PM
	Tue + Thurs - Artemia 2nd Instar AM, Zeb 400-600 PM
	Sat+Sun: Adults single feed of Artemia

Table 2.2: Zebrafish lines used in the thesis.

Name	Mutation	Number

fastkd2_131bp	131bp insertion	SH719
fastkd2_5bp	5 bp deletion	SH720
rnaseh2a	49bp deletion	SH478, (Thomas et al., 2024)
fastkd2 rnaseh2a double homozygous	131bp insertion in *fastkd2*	SH722
	8bp deletion in *rnaseh2a*	
rnaseh2a heterozygous *aptx* homozygous	49bp deletion in *rnaseh2a*	SH723
	40bp insertion in *aptx*	
numa	112bp insertion	SH678
*p21*_GFP	DNA insertion	SH506, (Morsli et al., 2023)
Mit2_neon	DNA insertion	SH721
Nacre	Mutation in mitfa gene	

2.1.1. Caring for zebrafish embryos and larvae

To obtain zebrafish embryos, a male and a female adult zebrafish ~3 months or older were placed on each side of a divider in a pair mating box filled with system water in the afternoon. In the morning, with the light increasing, the divider was removed, and the fish were able to mate. The resulting embryos fell in between a grid at the bottom of the box to protect them from the adult zebrafish. The adult zebrafish were placed back in their aquarium tanks and the embryos were collected using a sieve. Alternatively, a marble box was placed in a tank of adult zebrafish in the afternoon. In the morning, with the light turning on, the adults would mate over the marble and the embryos would fall under a grid under the marbles to be protected from

the adults. Collection of the embryos was done by a sieve. The system water was removed from the embryos and replaced with 1 x E3 media (500μM NaCl, 17μM KCl, 33μM $CaCl_2$ 33 μM $MgSO_4$ with 0.0001% methylene blue) and kept in a 28°C incubator. On very rare occasions embryo development was either slowed down or sped up. For this the Kimmel equation was used to understand what temperature the embryos would need to be at (Kimmel et al., 1995). For a 1.5x delay in development, the embryos were cooled down at 23°C and for a 1.5x acceleration of development the embryos were heated at 32°C. The E3 media would be changed regularly to keep the embryos healthy until 5.2dpf, when if they would not be used for experiments, they would be culled by bleach. No embryos were kept for any longer than 5.2dpf unless they were being raised to adulthood in accordance with the UK Home Office Animals (Scientific Procedures) Act 1986.

2.1.2. Adult zebrafish fin clipping

Adult zebrafish ~3 months old were submerged in ~16.8μg/ml Tricaine (MS-222) (4.2ml 4g/L Tricaine in 100ml system water) for ~1 minute. The fish were lifted out of the anaesthesia with a spoon and the tail fin placed on a cutting board. ⅓ of the fins were cut using a sharp scalpel rinsed in 100% ethanol. The fish was then immediately placed in fresh system water for recovery. The fin was placed in a 200μl PCR tube by tweezers for further genotyping following section 2.6.2.

2.1.3. Zebrafish larvae fin clipping

3–5-day old zebrafish were placed in 30ml E3 media, and 133.3μg/ml Tricaine (1ml in 30ml E3 water) was added to the water to anaesthetise the larvae. Using a pasteur pipette pigmented embryos were placed on autoclave tape taped to the lid of a 10cm petri dish, whilst non-pigmented larvae were placed on the plastic of the same lid. Tissue paper was used to absorb the remaining E3 away from the larvae. A microscalpel was used to cut off the tip of the tail of the larvae, and the larvae was placed in fresh E3 in a 48 well plate to recover. The tail tip was moved using tweezers to a 200μl PCR tube for further genotyping following section 2.6.2.

2.1.4. Culling and dissection of adult zebrafish

Adult zebrafish were submerged in 1.3g/L Tricaine diluted in system water (⅓ 4mg/ml Tricaine ⅔ system water) for ~1 minute as a primary culling method. Using a spoon, the fish was moved

over to a plastic sheet on a scale with a 10 cm ruler. The fish were imaged, and the weight, sex, tumours, and damaged fins were recorded. The fish were moved to the dissection board, and destruction of the brain was used as a secondary method to ensure death as per home office regulations. The tail fin and the pectoral fin were cut off and stored in a microcentrifuge tube on dry ice. The fish was then decapitated, and the brain extracted and placed in a microcentrifuge tube on dry ice. The tissue samples were stored in -70°C.

2.1.5. Camptothecin treatment of larvae

Healthy looking larvae at 4dpf were selected and placed in petri dishes with either 0.1% DMSO (Sigma, D8418) in E3, or 500nM Camptothecin (CPT) (Sigma, C9911) dissolved in DMSO and diluted in E3. At 5dpf, the larvae were imaged according to section 2.9. Alternatively, the larvae were treated with acridine orange according to section 2.5.2 before imaging. Larvae were then used for protein extraction according to section 2.6.5.

2.2. Cell culture maintenance and siRNA knockdown

2.2.1. Recovering cells from liquid nitrogen storage

One vial of HCT 116 cells (p11) stored in liquid nitrogen was recovered by heating in a 37˚C water bath for 30 seconds to 1 minute. The cells were added to 10ml of MEM media (Sigma-Aldrich, M2279; in 500ml MEM: 10% FCS (sigma, F7524-500ml), 1% L-glutamine (Sigma, G7513-100ML), 1% Pen/Strep (Sigma, P0781-100ML)) warmed to 37˚C, then centrifuged at 1000rpm for 5 minutes. The media was removed, and the cells resuspended in 13ml of MEM media. The cells were added to a T75 tissue-culture treated flask (Thermo Scientific 156499) and stored at 37˚C.

2.2.2. Plating cells

Cells were washed in 1x Phosphate buffer saline (PBS) (Sigma, P4417) warmed at 37˚C. 500µl trypsin (1 g trypsin 1:250 powder (Gibco, 27250-018) in 400 ml PBS : 37.5ml PBS, 30ml Trypsin, 7.5ml 4% EDTA) was added and spread over the cells in the flask, then left in the 37˚C incubator for ~1 minute. The cells were shaken and observed under a microscope for detachment. Once the cells had detached 10ml of MEM media warmed at 37˚C was added to the flask, and the cells were collected into a 10ml culture tube. The cells were spun down at

1000rpm for 5 minutes, then resuspended in 10ml MEM media. The cells were counted using a hemocytometer, and the culture diluted in MEM media to allow for 2-3 x 10^5 cells per well on a 6 well plate. 2ml culture was placed in each well, and the plate left at 37˚C until ~80% confluence.

2.2.3. Transfection of cells

For one condition for one well on a 6 well plate (Greing Bio-one, 657160), 40nM scrambled siRNA (5'-AGGUAGUGUAAUCGCCUUG-3') or a *fastkd2* siRNA mix (Dharmacon, 5'-UGGAAAAGAUGCACCGAUU-3', 5'-AAACAAAACCAAACCGUAU-3', 5'-GUUCAGUCUUCACGCCAUA-3', 5'-GCUUAUUGUUUGGGUUCAA-3') was mixed in 100µl Opti:MEM (gibco, 31985-047). 5µl Lipofectamine®RNAiMAX (Invitrogen, 13778075) was also mixed with 100µl Opti:MEM. The tubes were incubated at room temperature for 5 minutes, then the tubes were gently mixed and incubated at room temperature for 15 minutes. 1ml media was removed from the well and the 200µl solution was gently pipetted as droplets into a well. The plate was left at 37˚C for 48 hours.

2.2.4. Collection of transfected cells

Once the cells in the wells were at between 70-80% confluence the media in the wells were removed and the cells washed with PBS warmed at 37˚C. 5 drops of trypsin were added to each well for 15 seconds before being removed. The plate was left at 37˚C for ~1 minute before the plate was shaken and cells floating were observed. 2ml media was added to the wells and the cells resuspended in the media. 1ml of the cells were saved for western blot and 1 ml saved for qPCR. The cells were spun down to pellet the cells, one was snap frozen in liquid nitrogen and storage at -70˚C, and the other was resuspended in 70µl 1 x protein loading buffer (5 x PBL: 10% SDS, 250Mm Tris-HCl pH6.8, 25% Glycerol, 12.5% β-mercaptoethanol, 0.5% Bromophenol blue, H_2O to 50ml). The resuspension was left at room temperature for 5 minutes, then 0.2µl Basemuncher endonuclease (Abcam, AB260049) was added and the cells left at room temperature for 20 minutes. The samples were boiled for 5 minutes at 95˚C and were then used for western blotting following the protocol in section 2.7.6.

2.3. Zebrafish behavioural analysis

2.3.1. Adult tank behavioural analysis

Adult zebrafish were isolated one-day pre-analysis day, and food withheld on the day of analysis. The adult fish were moved into stackable tanks, with system water, and 5 wild type fish were stacked on the left against a white background plate with light, and 5 homozygous fish were stacked on the right. Using Ethovision version 17 by Noldus, a box was drawn around the full individual tanks for the arena, and a box was drawn at the top of the tank for the top (see schematic in Figure 2.1). After disturbing the fish by waving, the fish were filmed for 5 hours. Distance was recorded for each hour.

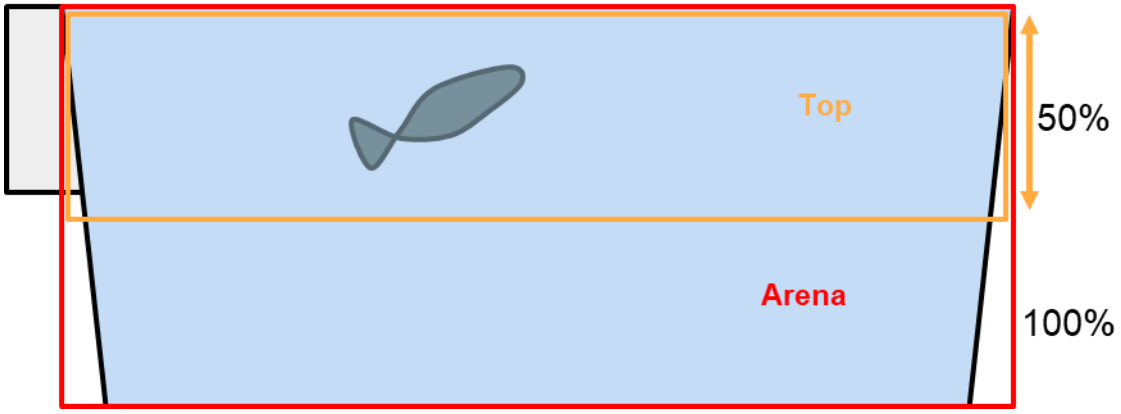

Figure 2.1: Schematic of adult zebrafish behavioural assay arena set up. The box for the arena covers the whole area the single adult fish can swim. A second box is drawn at the top 50% of the tank to capture the swimming of the single adult fish at the top half of the tank.

2.3.2. Adult swim tunnel assay

Adult zebrafish were moved to the assay room the day before the experiment to acclimatise. On the day, one fish at the time was placed in a swim tunnel with system water and then left to swim again a current with an initial flow rate of 6.57 cm/s which was increased every 5 minutes in 6.57 cm/s increments until the fish was no longer able to swim. The fish were then given a 30 second break before the flow rate was increased to the speed the fish was at initially until the fish was no longer able to swim. The total time the fish was swimming for and what flow rate the fish reached was recorded. The fish was anaesthetised with ~16.8µg/ml Tricaine (4.2ml 4g/L tricaine in 100ml system water) and measured from the tip of the lip to the start of the tail. The critical swimming velocity (Ucrit)/ body length was calculated using the equation in figure 2.2.

$$Ucrit = \frac{Ui + \left(\frac{UiiTi}{Tii}\right)}{B}$$

Figure 2.2: Equation for critical swimming velocity. Ucrit = critical swimming velocity (body lengths/s), Ui = the highest velocity maintained for a full 5-minute period (cm/s), Uii = the velocity increment (6.57 cm/s), Ti = tie time to exhaustion (s), Tii = the time interval, B = body length (cm).

2.3.3. Adult Y maze assay

Adult fish were acclimatised to the behavioural room for 30 minutes. They were then placed in a Y shaped tank produced by Zantiks, and their movement was recorded and followed for 1h. The threshold was set to 15 and 6. Fish that were miss tracked were removed by looking at the tracking video (Figure 2.3). Furthermore, fish that did less than 100 turns were also removed from the analysis. The number of tetragram turns were recorded and plotted.

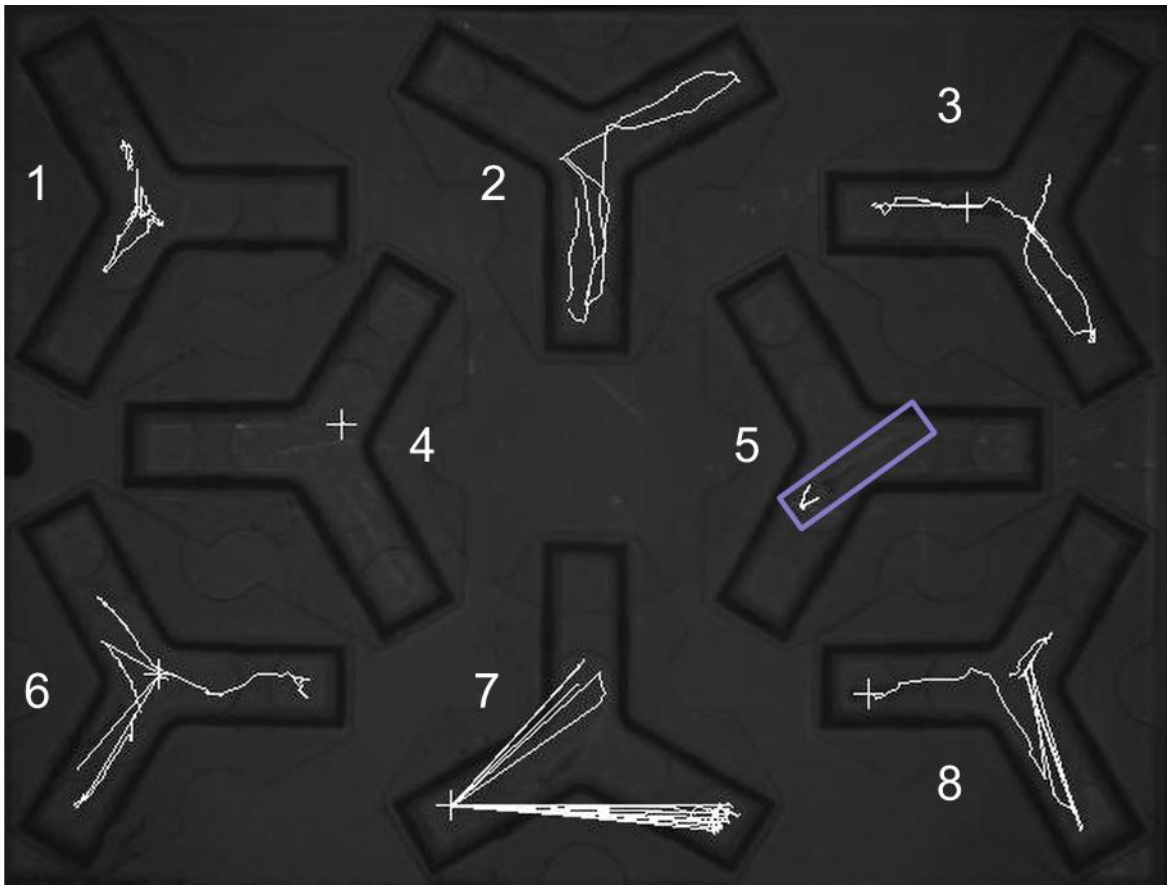

Figure 2.3: Image from Zantiks video of Y-maze. Image shows, Y-box 2 and 3 are tracking the fish well, whilst Y-box 6, 7 and 8 has miss tracking of the fish. The fish in Y-boxes 1, 4 and 5

are not moving much. The Purple box shows the size of a fish to indicate that the fish is the same as the length of one Y-arm.

2.3.4. Larval behavioural analysis

Early in the morning, 5dpf embryos with an inflated swim bladder were pipetted with a p1000 (with a truncated tip) together with 400µl E3 into wells of a 96 well plate (Corning® 3595). The plate was placed in a ZebraBox Viewpoint system (Viewpoint Behaviour Technology) and the embryos were left to acclimatise for 30 minutes. With the thresholds at 3 for small movement and 9 for large movement, a light-dark cycle of 5 minutes of 100% light and 5 minutes of 0% dark was run for 4 cycles. The total distance moved, and time spent moving at no, small and large movements were recorded.

2.3.4.1. Larval behaviour after PTZ treatment

Healthy looking 4dpf larvae were selected before swim bladder development and placed individually in wells on a 48 well plate (VMR, 734-2326). A 160mM stock solution of pentylenetetrazol (PTZ) (Sigma, P6500) was made in E3 media and diluted in E3 media to the desirable concentrations (80mM, 40mM, 20mM, 10mM, 5mM, 2.5mM, 1.25mM), E3 media was used as a control. The existing media on the larvae was removed and quickly replaced by the dilutions. The larvae were left in the solution for 10 minutes before their movement was measured in a ZebraBox Viewpoint system (Viewpoint Behaviour Technology) for another 10 minutes with 2 minutes of light and dark. The thresholds for small movement were 3 and for large movement 9. Analysis was done on total movement during the 10 minutes. This was performed with five embryos at each concentration on three different occasions.

2.3.4.2. Larval touch assay

Dechorionated larvae at 48hpf were placed in the centre of a 10 cm petri dish with 30 ml E3 media with circles increasing in diameter by 1 cm increments. The distance the larvae moved after being touched by a seeker was recorded (Wei et al., 2020). Alternatively, 5dpf embryos with swim bladders were placed in a 10 cm petri dish with 30ml E3 media. The time it took the larvae to stop moving after being touched by a seeker was recorded.

2.3.5. Counting larval heart rate

5dpf larvae were placed in 50µg/ml Tricaine in E3 media and left to settle for ~1 minute. Using a cell counter, the heart rate of the larvae was counted for 20 seconds 3 times per larvae. Wild type and homozygous embryos were mixed, and heart beats were counted blindly. Genotyping then followed section 2.6.2.

2.4. Zebrafish genome editing

2.4.1. Microinjections into one-cell stage embryos

Embryos were injected using thin-wall single-barrel borosilicate glass capillaries (World Precision Instruments, TW120-4) that were pulled into needles using a micropipette puller (P-97, Sutter Instrument Co., Novato, USA). The needles were filled with 3µl of the injection solution by microloader pipette tips (Eppendorf, 930001007) and inserted in a PV820 Pneumatic Pico-Pump injector (World Precision Instruments). The needle tip was broken using a tweezer and calibrated in immersion mineral oil covering a 10mm graticule. The needle was calibrated to expel 0.1mm in diameter solution equivalent to 0.5nl. One-cell stage embryos were placed along a microscope slide in the lid of a 10 cm petri dish, and excess aquarium water was removed. 0.5, 1 or 2nl of the injection solution was injected directly into the yolk of the embryos. The embryos were then gently transferred into a petri dish with E3 media.

2.4.2. gRNA design and CRISPR injections

Genes for CRISPR editing were identified from the ensembl gene browser (https://www.ensembl.org/), and CRISPR guides for gene knockout were made using CHOPCHOP (https://chopchop.cbu.uib.no/) (Table 2.3) and ordered through IDT. Early in the morning of injections, 20µM gRNA (IDT) was mixed with 20µM tracrRNA (IDT), 2µM Cas9 protein (NEB, M0386), 1x phenol red and dH_2O to make up 5µl. The enzyme was activated by incubation at 37°C for 1 minute. Injections followed the protocol in section 2.4.1. At ~3 months old, the injected fish were fin clipped following section 2.1.2, and genotyped following section 2.6.2 using the primers in table 2.3. The DNA was sent for sequencing (genewiz), and frameshift mutants were outcrossed to Nacre (wild type) to raise an F1 generation.

Table 2.3: Guides and corresponding primers used in this thesis for CRISPR/Cas9 knockout.

Gene	gRNA	Location	F/R	Primers
fastkd2	CCTGGGAGTTTC GCAACACACGC	Exon 1	F	TGAGGTGTGATGATTTGGCTTA
			R	AAAAACAATTCTCGCACAGCTT
rnaseh2a	CGGACTGTGACC TCCACACCGGG	Exon 6	F	GTTTGTGGACACTGTGGGTC
			R	CTCCCGTTTTCTCCACCTCT
rnaseh2a – for crispant	GATGAGGCCAAA AGTTTCGTAGG	Exon 4	F	TTTAGACTCAAAGACGCTGACG
			R	GGTACCTTTGTAGCATGCTGGT
rnaseh2a – for crispant	AATCCAGAGCATA CTGCACCAGG	Exon 5	F	GCAAAATACAATCTGAATGCCC
			R	CAGGTTTGCTTTGTCTCAATCA
aptx	AAGCAGGTGAGC ATAAAGCCGGG	Exon 4	F	TGGTCTGCTTAACATCACACAA
			R	TCTTTTGGAGGGTTTGGATCT

2.4.3. Injection of Tol2 reactions

A 5µl reaction of 25ng/µl plasmid and 25ng/µl Tol2 mRNA was mixed with 0.5µl phenol red. The reaction was kept on ice until injection. Injections into one-cell stage embryos followed the protocol in section 2.4.1.

2.5. Staining of larvae and tissue

2.5.1. γH2AX staining

5dpf larvae with inflated swim bladders were culled with an overdose of Tricaine before being fixed in cold 50% methanol:50% acetone in -20°C for 5 days. The larvae were washed with 50% methanol in PBS for 5 minutes before a brief wash in PBS, and 3 times 5-minute washes in 0.5% triton in PBS. The larvae were then placed in individual tubes and blocked for 3 hours in 2% block (Roche, 13085100), 5% FCS, 1% DMSO in PBS. 1:1000 primary γH2AX antibody (Sigma-Aldrich, Anti-phospho-Histone H2a.x (Ser139) Antibody, clone JBW301, 05-636-I, same as WB, Table 2.7) was diluted in 2% block and the larvae was incubated in the antibody overnight at 4°C. The primary antibody was washed of 8 times for 15 minutes with PBST (PBS + 1% Tween), before a secondary anti-goat alexa 488 antibody was diluted to 1:2000 in 2% block and the larvae were incubated in it for 2 hours in the dark. The secondary antibody was washed off with 4 times 15-minute washes in PBST before being mounted following section 2.9.1, and imaged following section 2.9.

2.5.2. Acridine orange staining

A 1x dilution of a 1mg/ml (100x) Acridine Orange (Sigma Aldrich, 494-38-2) stock stored in -20°C protected from the light was made in E3 by mixing 30ml E3 with 300µl acridine orange stock. 5dpf larvae were transferred into a clean 10ml petri dish with as little E3 as possible and the diluted acridine orange was poured over them. The larvae were incubated for 30 minutes at room temperature in the dark before the acridine orange was washed off with methylene blue free E3 by moving the larvae to a new petri dish with as little liquid as possible. The wash was repeated 3 times for 10 minutes each. The larvae were anaesthetised in Tricaine and imaged following section 2.9.

2.5.3. Whole mount *in situ* hybridisation

2.5.3.1. Making whole-mount in situ hybridisation probes

Primers making a 1001bp product 3' to the mutation in *fastkd2* were designed to include a T7 transcription site for the antisense probe and T3 transcription site for the sense probe (Table 2.4). The primers were used in a PCR reaction with genomic DNA from wild type 5dpf zebrafish larvae, and the product was run on a gel to test for specificity of the primer. The remaining PCR product was PCR purified using a Qiagen QIAquick PCR Purification Kit. The purified product was used in two transcription reaction with 2µl T7 or T3 polymerase (Roche), 4µl

transcription buffer (Roche), 1x DIG RNA labelling mix (Roche), 0.5µl RNase inhibitor (Recombinant RNasin®, N251B), between 100-350 ng/µl PCR product and dH_2O to make up 20µl. The transcription took place at 37°C for 2 hours, before removing the excess DNA by Turbo DNase (from Invitrogen mMASSAGE mMACHINE kit, AM1346) at 37°C for 30 minutes. A gel with pre and post turbo DNase was run. The probe was then precipitated with 80µl dH_2O, 33µl 10mM NH_4Ac and 350µl ethanol at -80°C overnight. The probe was cleaned by centrifugation at 4°C at 13,300rpm, the supernatant removed, and 70% ethanol added before a second spin for 5 minutes. The ethanol was removed and the probe pellet air dried for 5 minutes before being resuspended in RNase-free H_2O and stored at -70°C.

Table 2.4: Primers for whole mount in situ probe for *fastkd2*.

fastkd2 T3 sense af_mut _Fv	CATTAACCCTCACTAAAGGGAAAACGGCAATA ATGTTCAAGCCC
fastkd2 T7 antisense af_mut_Rev	TAATACGACTCACTATAGGGTCTCCAGGCAGC GTAATAACAC

*Red = T3 or T7 sites.

2.5.3.2. Whole mount in situ hybridisation staining

Embryos at 2dpf were fixed in 4% PFA (28794.295, VMR Chemicals) in 1xPBS overnight at 4°C with rocking. The next day the PFA was removed and the embryos washed for 5 minutes 3 times with PBST (1xPBS, 0.1% Tween), before being gradually dehydrated with 30%, 60%, 100% MeOH diluted in PBST for 10 minutes at room temperature on a rocker. The embryos were then stored in 100% MeOH at -20°C until further usage. On the first day for the procedure, stored embryos were removed from the -20°C and gradually rehydrated in 60% and 30% MeOH diluted in PBST for 10 minutes at room temperature on a rocker, then 100% PBST on a rocker at room temperature for 5 minutes 4 times. The embryos were then digested with proteinase K (Sigma, P6556) diluted in PBST at room temperature, not on the rocker. For 2dpf embryos they were left in 10µg/ml proteinase K for 30 minutes, then washed with PBST for 5 minutes. They were then refixed in 4% PFA diluted in PBS for 20 minutes at room temperature on a rocker and washed with PBST for 5 minutes 3 times.

The embryos were then pre-hybridized in 500µl hybridization mix (HM^+) (50% formamide, 5x SSC, 0.1% Tween20, 9.2mM Citric Acid, 50µg/ml Heparin, 500µg/ml tRNA and dH_2O to make up the final volume), for at least 1 hour at 70°C. The hybridization mix (HM^+) was then replaced with hybridization mix (HM^+) with 500ng of the probe preheated for 10 minutes at 70°C. The embryos were then left to hybridize overnight at 70°C. The next day the probe was saved and washed off by decreasing concentrations of hybridization mix (HM^-) (50% formamide, 5x SSC, 0.1% Tween20, 9.2mM Citric Acid and dH_2O to make up the final volume) in SSC. First a brief wash in 100% (HM^-) at 70°C, then 70% (HM^-)/25% 2x SSC, 50% (HM^-)/50% 2x SSC, 25% (HM^-)/75% 2x SSC, 100% 2x SSC at 70°C for 15 minutes each with rocking. The embryos were then washed in 0.2 x SSC at 70°C for 30 minutes twice at room temperature, then a decreasing concentration of SSC in PBST; 75% 0.2x SSC/25% PBST, 50% 0.2x SSC/50% PBST, 25% 0.2x SSC/75% PBST, 100% PBST for 10 minutes each at room temperature with rocking. The embryos were then blocked in 1ml 2% blocking buffer (Roche, 1305100) in malate buffer (Maleic Acid, 0.2M NaCl, dH_2O, pH 7.4) for several hours at room temperature on a rocker. The primary anti-DIG antibody (Roche, 11266027) was then diluted 1:5000 in 2% blocking reagent and the embryos were incubated in 500µl antibody solution overnight at 4°C in the dark in a rocker.

The next day the embryos were briefly washed in PBST in the dark at room temperature on a rocker before being washed with PBST for 30 minutes 4 times in the dark on a rocker at RT. The embryos were then washed with AP^- buffer (0.1M Tris-HCL at pH 9.5, 0.5M NaCl, 0.1% Tween20, and dH_2O to make up the volume) for 15 minutes in the dark on a rocker. They were then washed for 10 minutes 2 times in AP^+ buffer (0.1M Tris-HCL at pH 9.5, 0.2M $MgCl_2$, 0.5M NaCl, 0.1% Tween20, and dH_2O to make up the volume). Colour development was done with a 1:1 ratio of AP^+ and BM purple solution (Roche, 59673100) in the dark on a rocker. Overnight the solution was changed with AP^- and the embryos were stored at 4°C, before continuing colour development the next day. For the *fastkd2* probe, colour development took between two and three weeks.

2.6. Small molecule extractions

2.6.1. Zebrafish whole genomic DNA extraction

Brains from various ages were thawed on ice and homogenised with a micropestel in a 100µl warm total nucleic acid extraction buffer (100mM Tris-HCL pH 8.0, 100 mM EDTA, 250 mM

NaCl, 1% SDS). A further 300µl buffer was added to the homogenisation before 80 ng/µl Proteinase K was added. The solution was left in a 55°C heat block. After 3 hours, 200µl phenyl:chloroform:isoamyl:alcohol was added and the solution was centrifuged at room temperature for 5 minutes at 13,300 rpm. The upper clear aqueous liquid was transferred to a clean 1.5ml microcentrifuge tube, and 200µl chloroform was added to the clear solution. The microcentrifuge tube was again centrifuged at room temperature for 5 minutes at 13,300 rpm, and the clear upper aqueous liquid was transferred into a new 1.5ml microcentrifuge tube. The DNA was precipitated with 100µl 3M NaAc and 800µl 100% ethanol, and the solution was centrifuged at 4°C at 13,300 rpm for 30 minutes. The supernatant was removed, and the pellet resuspended in 20µl dH_2O. To remove single stranded RNA 0.5µl 10mg/ml RNaseA was mixed in and the solution was left in a 37°C heat bath for 30 minutes. The DNA was then precipitated with 51.25µl (2.5x volume) 100% cold ethanol and 2.05µl (0.1x volume) 3M NaAc, and the solution was left at -70°C overnight. The next day the precipitated DNA was centrifuged at 13,300 rpm at 4°C for 30 minutes to pellet the DNA and the supernatant was removed. The DNA pellet was washed with 500µl 70% ethanol at 4°C at 13,300 rpm for 1 minute. The supernatant was removed and a 30 second spin at 4°C ensured all the supernatant was removed. The pellet was air dried for 10 minutes and resuspended in 35µl sterile water. The concentration of the genomic DNA was determined by Nanodrop (ND-100 v3.8.1). 1µl of the DNA was also mixed with 10µl dH_2O and 2µl loading dye to check the concentration on a 1% agarose gel.

2.6.2. Zebrafish HOTSHOT DNA extraction

DNA used for genotyping was acquired using the HOT SHOT DNA extraction method. For adult fin clips and for whole embryos 25µl 1x base solution (50x stock: 0.7015g KOH crystals, 299µL 0.5mM EDTA, 10ml dH2O) was added to dry samples in 200µl PCR tubes, and the samples were heated to 95°C for 30 minutes in a thermal cycler to lyse the embryos. The reaction was terminated by 25µl neutralisation solution (50x stock: 3.152g Tris-HCL, 10ml dH2O) and kept on ice. For larval fin clips, 10µl of base and neutralisation buffer was used. DNA was further analysed by PCR following section 2.7.1.

2.6.3. Zebrafish larva and tissue total RNA extraction

Fin clips or brains from -70°C were defrosted on ice and quickly washed in PBS, or 20 zebrafish larvae were placed in a 1.5ml microcentrifuge tube and all E3 was removed. The samples were broken down with a micro rotor or by hand using a pestle. The samples were homogenised with 500µl Trizol using the pestle and left at room temperature with occasional

shaking of the tubes. After 5 minutes 100µl chloroform was added, and the samples vigorously shaken for 15 seconds, then left at room temperature for 3 minutes with occasional shaking before they were centrifuged at 12,000xg for 15 minutes at 4°C. The clear upper aqueous phase was moved into a new 1.5ml microcentrifuge tube and mixed with 250µl isopropanol, vigorously shaken and left at room temperature for 10 minutes with occasional shaking. The samples were then centrifuged at 12,000xg for 10 minutes at 4°C. The supernatant was removed and the pellet washed with 1ml 75% ethanol at 7,500xg for 5 minutes at 4°C. The supernatant was removed, then the tubes spun for another 30 seconds at 12,000xg at 4°C to remove the remaining supernatant. The pellets were then air dried for 2 minutes before being dissolved in 15µl dH_2O for larva or 7µl for fin clips or brains. The RNA was stored in -70°C.

2.6.4. Human cell total RNA extraction

Snap frozen cell pellets were collected from -70˚C and thawed on ice before being washed with ice cold 1 x PBS. The pellets were then resuspended in 1ml trizol and left at room temperature for 5 minutes. 250µl chloroform was mixed into the trizol by shaking, and the mix was left at room temperature for 5 minutes before being centrifuged at 4˚C at 10 000rpm for 5 minutes. The clear upper solution was moved into a new tube, and 550µl isopropanol was mixed in. The mix was left at room temperature for 5 minutes before being centrifuged at 4˚C at 13 300rpm for 20 minutes. The supernatant was removed, and the pellet was washed with 1ml 75% ethanol at 9500rpm for 5 minutes. The ethanol was removed, and the tube spun again for 30 seconds at 9500rpm to remove any leftover ethanol. The pellet was then air-dried for 3 minutes before being dissolved in 15µl dH_2O. The RNA was stored in -70˚C.

2.6.5. Zebrafish larva and tissue protein extraction

Fin clips or brains from the -70°C were defrosted on ice and washed in PBS, or 20 zebrafish larvae were placed in a 1.5ml microcentrifuge tube and all E3 was removed. The tissue or larvae were lysed using a micro rotor or a micropestle dry, before the pestle was rinsed in 25µl lysis buffer (200mM Hepes, 40 mM NaCl, 2mM MgCl2, 0.5 % Triton X-100), with 1x phosphostop phosphatase inhibitor cocktail (Roche, 4906837001) and 1x protease inhibitor cocktail (Roche, 4693159001) added on the day. The protein lysate was left on ice for 1 hour, before being centrifuged at 13,300 rpm at 4°C for 15 minutes to pellet the remaining tissue. The supernatant containing the protein was moved to a clean microcentrifuge tube and protein concentration in 1µl was measured on a spectrophotometer at 595nm using 999µl Coomassie PlusTM Protein Assay Reagent (Thermo Scientific, 23200).

2.6.6. Mitochondrial extraction of zebrafish larvae

To extract the mitochondria from zebrafish 60 dechorionated 24hpf or 50 5dpf embryos were crushed dry with a micropestle. To isolate the mitochondrial and cytosolic fractions a mitochondrial isolation kit for mammalian cells (Thermo Science Scientific, 89874) was used and the protocol for the reagent-based method was followed. As I was only interested in proteins within the mitochondria, I removed any proteins on the outside of the mitochondria by following a protocol by Shih-Chieh Chiang from her thesis submitted in 2019. The mitochondrial pellet was washed with 50ul homogenisation buffer 1 (0.6M Mannitol, 10mM Tris pH 7.4m 1mM EGTA, 1mM PMSF, 0.2% BSA in H_2O), and a Bradford assay was used to confirm that the samples were clean, and no proteins were found on the outside of the mitochondrial membrane. Based on the Bradford assay, the pellets were digested with a 1:1 ratio of RNase-free proteinase K on ice for 30 minutes to remove any outside protein. If no protein was identified 0.4ng of protein was assumed and used to calculate the proteinase K concentration used. The reaction was stopped with 100uM PMSF and centrifuged at 12 000g for 10 minutes. The pellet was washed with 500ul homogenisation buffer 2 (0.6M Mannitol, 10mM Tris pH 7.4m 1mM EGTA, 100µM PMSF, 0.2% BSA in H_2O) then centrifuged at 12 000g for 10 minutes. The mitochondrial pellet was then lysed with 10µl human cell lysis buffer with 1x protease inhibitor and 1x phosphostop buffer. Mitochondrial protein and cytosolic protein concentration in 1µl was measured on a spectrophotometer at 595nm using 999µl Coomassie PlusTM Protein Assay Reagent. A western blot for HDAC1, β-tubulin, GAPDH, VDAC1, COX-IV and γH2AX was used to confirm the purity of the fractions (Section 2.7.6).

2.7. Molecular visualisation

2.7.1. Genotyping PCR and agarose gel visualisation

For DNA collected using the HOT SHOT method (Section 2.6.2) a PCR reaction of 20µl was made up with 1x Firepol (FIREPol® Master Mix Ready to Load (7.5 mM MgCl2), Solis Biodyne), 0.5µM forwards and reverse primers (Table 2.3), 1.5µl HOT SHOT template and dH_2O. PCR cycles for each gene can be seen in table 2.5. The PCRs were run in a BioRad T100TM thermal cycler. A 3% agarose gel with 1x TAE (245g Tris, 57.1ml Acetic Acid, 100ml 0.5M EDTA pH 8, H_2O up to 1L) and ethidium bromide was made for genotyping, and 10µl of the PCR reaction was loaded onto the gel with 3µl 100bp DNA ladder. For genotyping the gel was run at 120V for 40 minutes, but for checking CRISPR/Cas9 efficiency it was run for 90

minutes. If PCR samples were sent for sequencing, 5µl of the PCR was treated with 0.05µl exonuclease 1 (Exo1) (Thermo Fisher Scientific, 15513677) and 4.95µl shrimp alkaline phosphatase (SAP) purification (NEB, M0371S). 100ng/µl was sent for sequencing with 10µM forwards primers to Genewiz.

Table 2.5: PCR cycles for genotyping.

<table>
<tr><td>Cycle step</td><td colspan="2">fastkd2/aptx</td><td colspan="2">rnaseh2a</td></tr>
<tr><td>Initial denaturation</td><td colspan="2">95°C 3 min</td><td colspan="2">95°C 3 min</td></tr>
<tr><td>Denaturation</td><td>95°C 30 sec</td><td rowspan="3">34 x</td><td>95°C 30 sec</td><td rowspan="3">34 x</td></tr>
<tr><td>Elongation</td><td>60°C 30 sec</td><td>53°C 30 sec</td></tr>
<tr><td>Annealing</td><td>72°C 30 sec</td><td>72°C 1 min</td></tr>
<tr><td></td><td colspan="2">72°C 5 min</td><td colspan="2">72°C 7 min</td></tr>
<tr><td>Storage</td><td colspan="2">12°C ∞</td><td colspan="2">12°C ∞</td></tr>
</table>

2.7.2. Alkaline assay

DNA extracted using the whole genome extraction method in section 2.6.1 were incubated with either sodium hydroxide (NaOH) or sodium chloride (NaCl) for 45 minutes to 3 hours at 55°C. The amount of DNA used for the assay was judged by the intensity of the test gel, as the nanodrop tended to be less accurate, and diluted in 7µl dH_2O with 3µl 1M NaOH or NaCl. After the incubation, the 10µl reaction was mixed with 2µl 50% glycerol and 2µl 6x loading dye. The 14µl reaction was loaded onto a 15 cm 1% agarose gel made with 1x TAE and ran at 65V for 5 minutes to get the samples out of the wells. The gel was then run at 15V for 22 hours after which the gel was incubated in Sybr safe (STBR® Safe DNA gel stain, Invitrogen) for 1 hour before imaging on UV. Plotting of the smearing was done by a python and R script written by myself which can be seen in Appendix 9.1.

2.7.3. cDNA and quantitative PCR

Following RNA extraction in section 2.6.3 and 2.6.4, 470ng/µl of the template RNA was mixed in a 10µl reaction with 1µl d(T)23 VN primers, 5µl ProtoScript II Reaction Mix (2x), 1µl ProtoScript II Enzyme Mix (10x) and nuclease-free-H_2O following the ProtoScript kit (ProteoScript® I, NEB). The reaction was incubated at 42°C for 1 hour and the enzyme inactivated at 80°C for 5 minutes. Alternatively, 470ng/µl were mixed with 8µl $dH2_2O$ and 2µl LunaScript (LunaScript® RT SuperMix, NEB). Primer annealing occurred for 2 minutes at 25˚C, cDNA synthesis for 10 minutes at 55˚C and heat inactivation for 1 minute at 95˚C.

A qPCR was set up by making master mixes for 20µl reactions with 1x Firepol Mix (HOT FIREPol® EvaGreen® qPCR Mix Plus (no ROX), Solis Biodyne (08-25-00001-10)), 0.5µM Forward and Reverse primers (Table 2.6) and dH_2O. After aliquoting 19µl of the master mix into the qPCR plate (Biorad, HSP9601), 1µl of 1/10 diluted cDNA was mixed by pipetting. Three technical repeats of each cDNA were used, as well as rsp29 as a control housekeeping gene on each plate. Three technical repeats of 1µl dH_2O were also run for each primer set. To assess primer efficiency, a protocol from BioRad's Application guide for Real-Time qPCR (2006) was used. A serial dilution of wild type cDNA was used to generate a standard cure with triplicates of 100%, 10%, 1% and 0.1% cDNA. The average ct value of each triplicate was used to construct a standard curve by plotting the log of the starting quantity of the template (0, -1, -2, -3) against the average ct. The slope value was used in the equation seen in figure 2.4 to calculate the Amplification efficiency (E), then to calculate the percentage efficiency of the primers by subtracting 1 and displaying it as a percentage by timesing it by 100 %. Ideal reactions will have a percentage efficiency of 100%. Primers with amplification efficiencies of about 90-110% were chosen as efficient primers.

$$\left(\left(10^{\left(\frac{-1}{Slope}\right)}\right)-1\right)\times 100\%$$

Figure 2.4: Equation to calculate the percentage efficiency of the primers based on standard curve.

The qPCR plate was spun down at 4200 rpm at room temperature for 2 minutes. Using a BioRad qPCR machine (Biorad, CFX96^{TM}Real time system), the samples were denatured at

95°C for 15 minutes, before 40 cycles of 95°C denaturation for 5 seconds, 60°C elongation for 15 seconds, and 72°C annealing for 10 seconds, and a melt curve from 70-95°C at 0.2°C increments at 10 seconds per step.

Table 2.6: qPCR primers used in this thesis.

Target gene	F/R	Primer sequence 5'-3'	Source
actin - human	F	GACCTGTACGCCAACACAGT	Dr Chunyan Lio
	R	AGTACTTGCGCTCAGGAGGA	
aptx	F	CAC TGG AGC CAA GGA CTT AAA	This thesis
	R	GAT AAC GAG CCT TCG GGT ATT T	
mt-cox1	F	GGA ATA GTA GGG ACC GCA TTA AG	This thesis
	R	GCC TGC AAG AGG TGG ATA AA	
mt-cox4i1	F	GGTCGGAGACGCTAGAATGT	This thesis
	R	AGTAGTCCTCGACCTTCGCA	
fastk	F	CTTCAGCTCACACCTGTTCTAC	This thesis
	R	TGTCAACCTTCTTAGGCAACTC	
fastkd1	F	CGCTAGTGTGACCGTTGAAA	This thesis
	R	CCATTGGTGGGTCGTAGTTTAG	

fastkd2	F	CTCTTTCGGTTTTGGCTGCTG	(Wei et al., 2020)
	R	TCTCAGGAACACGGTCCTTC	
fastkd3	F	CCGAAAGGTGGAGTCTGTATTG	This thesis
	R	GAAGAGTGCAGGCATGAAGTAG	
fastkd4	F	CTACAGTTGGCTGGGTTCATAG	This thesis
	R	CAGCAACTGCCTTCCCTAAT	
fen1	F	CTATAAAGGGAATCGGACCCAAG	This thesis
	R	CTGGAGCAGGGTGCTTATTT	
il-6	F	TCAACTTCTCCAGCGTGATG	(Safari et al., 2016)
	R	TCTTTCCCTCTTTTCCTCCTG	
isg15	F	AACTCGGTGACGATGCAGC	(Hamilton et al., 2020)
	R	TGGGCACGTTGAAGTACTGA	
mt-nd1	F	AGCCTACGCCGTACCAGTATT	(Artuso et al., 2012)
	R	GTTTCACGCCATCAGCTACTG	
mt-nd6	F	TTT AGG TGG GAT GCT TGT AGT G	This thesis
	R	CCG CTT ACA TCA GCT CGA ATA	

numa	F	CAAGTAGAGCAGGCGATGATTA	This thesis
	R	CAGGGTCTCTTGATGGGAAAG	
p16	F	ATGATGAACGTCGAGGATGAACTG	(Morsli et al., 2023)
	R	ATTGGCATTCACTCCGTTAGAAAGT	
p21	F	AGGAAAAGCAGCAGAAACG	(Morsli et al., 2023)
	R	TGTTGGTCTGTTTGCGCTT	
p53	F	GCTTGTCACAGGGGTCATTT	(Morsli et al., 2023)
	R	ACAAAGGTCCCAGTGGAGTG	
parp1	F	CAGACCCAAGAGCTACAGTATC	(Zhang et al., 2021)
	R	GGATCTTCAGCAGGTATTTCAGG	
polg1	F	GGTGACCAGTGAAGACCGATA	(Artuso et al., 2012)
	R	GTCCACTGCGCTAAAGAAGG	
rad51b	F	TCTTCAACCTTCCTCAGGCT	(Honjo and Ichinohe, 2019)
	R	TGAGCGTTTAGCTGACATCC	
rad51c	F	TTCAACACTGCACCCTCCTA	(Honjo and Ichinohe, 2019)
	R	GGTAAACCTCCGCTAACAGC	

rnaseh1	F	AGA CCA ACC AAA GAG CAG AAT	This thesis
	R	TGA ACT TGC TGT CCG TGT ATA G	
rnaseh2a zebafish	F	GGTGCAGTATGCTCTGGATT	Dr Ruth Thomas's thesis
	R	CGACAGCTTGTCCTGATACTT	
rnaseh2a human	F	AATGGAGGACACGGACTTTG	(Sugawara et al., 2022)
	R	CCCAGTGGCTGTATCATGTG	
rnaseh2b	F	CCAGAGATTTCCAGCCCTAAA	This thesis
	R	TGTAGTCTTCTCCAGCCTCTAC	
rnaseh2c	F	TCTCGTGTTCACCAAGGTTAC	This thesis
	R	GTCAAATAGGTGCCCTCTACTG	
mt-rnr2 (16s rrna)	F	CGT TGA ACA AAC GAA CCC TTA AT	This thesis
	R	GAA CGG GCA CAG CTC TAA A	
rsp29 (house-keeping)	F	TTTGCTCAAACCGTCACGGA	(Bower et al., 2017)
	R	ACTCGTTTAATCCAGCTTGACG	
tnfa	F	GCGCTTTTCTGAATCCTACG	(Dorsemans et al., 2017)
	R	TGCCCAGTCTGTCTCCTTCT	

xrcc1	F	GAGGATAAACCCATCCCTGAAC	(Honjo and Ichinohe, 2019)
	R	CGATGATGTAGCGCAGAAGTAG	

The Maestro® Analysis Software (Biorad) was used to calculate the quantification cycle (Ct) values. These were then used to calculate the average fold change by the ΔΔCt method presented (Livak and Schmittgen, 2001). The Ct values were used to subtract the *rsp29* (housekeeping) Δct from each target gene replicate Δct. The average Δct for each sample was then subtracted from the individual Δcts for controls making a ΔΔct before the fold change was calculated by taking the power of 2^- ΔΔct as qPCRs are exponential. Average fold change was calculated by averaging the fold change of the three replicates.

2.7.4. Ribonucleotide cleavage activity assay

Protein samples were diluted in 5µl to 25ng/µl, 50ng/µl and 100ng/µl for adult tissue or 100ng/µl, 200ng/µl and 400ng/µl for embryos in reaction buffer (225µl dH_2O 25µl ThermoPol®Reaction Buffer, 0.5µl 1M DTT, 0.5µl 2mg BSA). A final concentration 0.05µl 5' Cy5 tagged double stranded substrate with a ribonucleotide as the 21st base (5' Cy5-GGTAACGCCAGGGTTTTCTCrGTTCACGACGTTGTAAAACGA 3') was added together with 3µl of 100µM competitor DNA (5' GGTAACGCCAGGGTTTTCTC 3') for a final volume of 16µl. 2µl RNaseH2 enzyme (NEB) and Lysis buffer were used as positive and negative controls. The digestion was left at 37˚C in a thermal cycler for between 1-2 hours. The reaction was terminated at 65°C for 20 minutes in the dark with 16µl 2x termination buffer (10mM EDTA, 80% formamide, 1 drop bromophenol blue). A 20% polyacrylamide 12 M urea gel was set in a 1mm glass cassette by combining 8ml concentrate (UreaGel system concentrate, national diagnostics), 1ml diluent (UreaGel system diluent, national diagnostics), 1ml complete (UreaGel system buffer, national diagnostics) Ultrapure Urea Gel components, 40µl 10% APS and 4µl TEMED (UltraPure™ TEMED, invitrogen) for 1 hour at room temperature. The gel was prerun with 65°C 1xTBE (108g Tris, 55g Boric acid, 40ml 0.5M EDTA pH8, H_2O up to 1L) buffer for 1 hour at 180V. The samples were boiled at 95°C for 5 minutes before 12µl was loaded onto the urea gel and run for 1 hour 15 minutes in 65°C 1xTBE buffer at 180V. The gel was imaged on a BioRad Chemidoc for Cy5. Band intensity was measured using BioRad Image Lab 6.0. Four bands are created during cleavage. Full length at 41bp and cleaved at 21bp, as

well as a middle band at about 30bp and a band just above the 21bp band. These are believed to be non-specific cleavage by endonucleases, and are not related to the rNMP as when the position of the rNMP is moved, the middle band does not change (Figure 2.5).

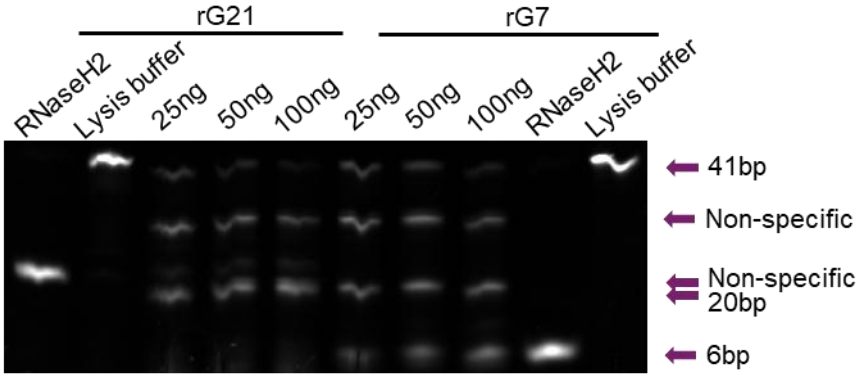

Figure 2.5: Ribonucleotide cleavage assay urea gel to explain bands. The rNMP is at position 21bp (rG21) or 7bp (rG7) and shows that the non-specific bands are independent of the rNMP position.

2.7.5. TDP1 activity assay

The TDP1 assay was conducted as described in Zaksauskaite et al., (2021). Protein was extracted from adult brains as in section 2.6.5. A master mix of 1µl 10x TDP1 assay buffer (25 mM HEPES, pH 8.0, 130 mM KCl, 1 mM DTT), 0.25µl 2µM TDP1 substrate (5' (Cy5.5)GATCTAAAAGACT(pY)-3') (Midland Certified Reagent Company Texas, USA) and 1µl 10mM DTT was made up for the assay and 2.25µl of the master max was added to a PCR tube with the protein diluted into 25ng, 50ng, and 100ng in 5µl dH_2O. A final 2.75µl dH2O was then added to the tubes to make a final volume of 10µl. Controls of 3µl with 100ng/µl recombinant TDP1 protein or 3µl lysis buffer were used with 4.75µl dH2O and 2.25µl of the master mix. The solutions were incubated for 1 hour at 37°C and the digestions were terminated by 10µl 2x termination buffer (44% deionized formamide, 2.25 mM tris-borate, 0.05 mM EDTA, 0.01% xylene cyanol and 1% bromophenol blue) for 10 minutes at 90°C. A urea gel was made as in section 2.7.4, and run at 180V for 1 hour before imaging on a BioRad Chemidoc for Cy5. Band intensity was measured using BioRad Image Lab 6.0.

2.7.6. Western blots

Protein samples as extracted in section 2.6.5 and 2.6.6 were diluted with dH_2O to between 5-30µg/µl in 12µl and mixed with 3µl 5x protein loading buffer and ~0.03µl basemuncher before they were boiled at 95°C for 5 minutes before they were loaded onto a homemade 4-20% or 4-15% gradient gel (Miller et al., 2016). The 4% gel was made with 1.8ml dH_2O, 390µl 30% acrylamide, the 15% gel was made with 840µl dH_2O and 1.5ml 30% acrylamide, and the 20% gel was made with 192µl dH_2O and 2ml 30% acrylamide. All three gels also used 750µl 1.5M Tris at pH8.8, 30µl 10% SDS, 30µl 10% APS and the 4% gel used 2.4µl TEMED whilst the 15 and 20% gels used 1.2µl TEMED. The individual gel mixtures were gently inverted 3 times, before 2.5ml of the 4% gel was taken up in a 5ml pipet. In the same pipet, with the 4% gel mix still in the pipet, 2.5ml of either 15% or 20% gel mixture was taken up to make a total of 5ml. Two air bubbles were then taken up to allow the two gels to mix, before the gel was released into a 1mm glass cassette. The top of the gel was levelled out with 100% isopropanol and left to set for 15 minutes. A 4% stacking gel was made with 1.867ml dH_2O, 340µl 30% acrylamide, 250µl 1M Tris at pH6.8, 20µl 10% SDS, 20µl 10% APS and 5µl TEMED. The isopropanol was poured off the gel and dried up with tissue, before the stacking gel was poured over the separating gel, and the appropriate comb was placed, and the gel was set for another 15 minutes at room temperature. The gel was placed in a Bio-Rad Mini-PROTEAN Tetra electrophoresis cell (BioRad, 1658004) and filled with SDS running buffer (25 mM Tris, pH 8.3, 192 mM glycine, 0.1 % w/v SDS). The boiled protein samples were loaded onto the gel with 3µl Precision Plus Protein Dual Colour Standard protein ladder (Biorad, 1610374). The gel was run at 120V for 15 minutes, before it was run at 180V for ~50 minutes, until the ladder reached the bottom of the gel. The blot was transferred onto a 0.45µm nitrocellulose membrane (BioRad, 170-4271) by semidry transfer in a Biorad Trans-Blot Turbo® transferTM system (BioRad, 17001915) at 1.3A-25V for 10 minutes, then blocked in 5% milk in 1x TBST (200 mM Tris,140 mM NaCl, 0.1 % Tween-20, pH 7.9) for 1 hour. The blot was then left in primary antibody (Table 2.7) shaking overnight in a cold room at 4°C or in room temperature for 1-2 hours. The blot was washed 3 x 5 minutes in 1x TBST then transferred over to the secondary antibody in 5% milk for 1 hour. Imaging the blot was washed 3 x 5 minutes in 1x TBST and covered in Clarity Western ECL blotting substrate (BioRad, 1705060), then imaged using a ChemiDoc MP imaging system (BioRad, 1708280). The band intensity was measured using Fiji ImageJ imager, inverting the band intensities, and subtracting the background.

Table 2.7: Primary antibodies used in this thesis.

Primary antibody target	Molecular weight (kDa)	Identification code	Dilution	Secondary antibody	Method used in
β-actin	42	ab8226	1:1000	Mouse	WB
β-tubulin	50	ab7792	1:1000	Mouse	WB
γH2AX	15	GTX127342	1:1000	Rabbit	WB and IF
Cox IV	16	ab140643	1:1000	Rabbit	WB
FASTKD2	50-81	ab479	1:1000	Rabbit	WB
FASTKD2	50-81	17464-1-AP	1:1000	Ravvit	WB
GAPDH	36	Genetex (GTX100118)	1:1000	Rabbit	WB
GFP	27	ab1218	1:1000	Mouse	WB
HDAC1	55	ab7028	1:2000	Rabbit	WB
NuMA	210	a301-510A	1:1000	Rabbit	WB
PAR	Modification	Tulip Biolabs (1020)	1:1000	Mouse	WB

RNaseH2A	33	A304-149A	1:2000 or 1:5000	Rabbit	WB
RNaseH2A	33	AV40647	1:2000	Rabbit	WB
RNaseH2A	33	16132-1-AP,	1:2000	Rabbit	WB
RNaseH2A	33	sc-515475	1:2000	Rabbit	WB
VDAC1	30	ab15898	1:1000	Rabbit	WB

2.7.7. Mass spectrometry for mitochondrial function

Adult brains were dissected as described in 2.1.5, and stored in -70˚C, whilst 5dpf larvae were snap frozen in liquid nitrogen and stored in -70˚C. The samples were then transported in a liquid nitrogen container to the University of Bergen. There they were processed by Mass spectrometry by Dr Kari Fladmark to identify the level of ADP/AMT/ATP, NAD^+/NADH and $NADP^+$/NADPH (Chavali et al., 2023).

2.8. Plasmid preparation

2.8.1. Transformations

Competent bacteria (10-beta Competent *Escherichia coli* (*E.coli*) (High Efficiency) NEB) were taken out of the -70°C freezer and thawed on ice for 5 minutes. 1-5µl of plasmids containing 1pg-100ng were mixed into the cells carefully by flicking, and the cells were left on ice for 30 minutes. The cells were heat shocked for 30 seconds at 42°C then immediately placed back on ice for 5 minutes, and 950µl of autoclaved LB (Sigma, L3022) was added and the cells were placed in a 37°C water bath for 60 minutes. Transformation plates were made by melting autoclaved LB agar (Sigma, L2897) and cooling it down to room temperature before adding the wanted antibiotics. For ampicillin I used 100µl (100mg/ml in ethanol) in 400ml LB, and for kanamycin (Sigma, K0254, 500mg/mL) I used 400µl in 400ml LB. The agar was poured

halfway to the top in 10 cm petri dishes, and the plates left to cool next to a Bunsen burner. After the incubation, the cells were inverted, and 10-100µl were spread next in sterile conditions next to a Bunsen burner onto the transformation plates. The plates were incubated at 37°C overnight. The next morning, one colony was picked using a sterile 200µl pipet tip, and the pipet tip was dropped into 5ml of LB with the desired antibiotics under sterile conditions. The colony was grown at 37°C overnight and purified using a Qiagen QIAprep Spin Miniprep kit.

2.8.2. Digestion reactions and visualisation

Digestion reactions for plasmids were performed in 50µl reactions, with ~1µg plasmid (1µl miniprep) as measured by the nanodrop, 1µl of each enzyme, 1x appropriate buffer and dH_2O. Table 2.8 summarises all the restriction enzymes used in this thesis and what buffers were used with them. All the buffers used were from New England Biolabs (NEB). The reactions were left at 37°C for 1 hour, unless stated otherwise. To visualise the digest, 5µl of the reaction was mixed with 1µl 6x loading dye (NEB), and 1µl undigested plasmid was mixed with 4µl dH2O and 1µl 6x loading dye and loaded onto a 1% agarose gel with ethidium bromide together with 3µl 1kbp DNA ladder (Thermo Scientific, SM0311). The gel was run at 120V for 40 minutes, and the bands visualised under a UV light.

Table 2.8: Restriction enzymes and buffers used in plasmid digestion reactions.

Enzyme	Producer	Buffer
AccI	NEB	r2.1/Cutsmart
BamHI	NEB	r3.1
BglII	NEB	r3.1
BtgI	NEB	Cutsmart
EcoRI	NEB	Cutsmart/r3.1

EcoRV	NEB	r3.1
HindIII	NEB	r2.1
NdeI	NEB	Cutsmart
NheI	NEB	r2.1
NotI	NEB	r3.1
PvuI	NEB	r2.1/r3.1
SpeI	NEB	r2.1
SspI	NEB	Cutsmart
XhoI	NEB	r3.1

2.8.3. Generation of the Mit2_mneon line

A mitochondrial localisation signal (mls) from zmLOC100282174 fused to mneon from Dr Stone Elworthy was used in a LR reaction using Gateway™ LR Clonase™ II Enzyme mix with a ubi promoter vector ((pENTR5'_ubi was a gift from Leonard Zon (Addgene plasmid # 27320 ; http://n2t.net/addgene:27320 ; RRID:Addgene_27320)) from Dr Henry Roel), a p3e-Sv40polyA, and pdegt tet2pA2 empty vector following the equation in figure 2.5 to obtain the concentration needed for each vector. 2µl LR clonase was added to a 8µl reaction of vectors and TE buffer (1mM EDTA, 10mM Tris-HCl pH8) and left at 25°C overnight. The reaction was terminated with 1µl proteinase K at 37°C for 10 minutes in the morning. The expression vector was transformed and grown (section 2.8.1), using ampicillin selection. The purified plasmids were digested with HindIII and SpeI (Table 2.8) to identify correct plasmids.

2.8.4. Generation of the NuMA plasmids

2.8.4.1. BP reaction for C-terminal NuMA

BP reactions use a system developed by the lambda phage when it infects bacteria. The phage has a site called *attP*, and the bacteria has a site called *attB* causing recombination of the lambda phage into the bacterial genome. The sites *attB* and *attP* give rise to the name BP. The recombination between the *attP* and *attB* sites causes the integrated lambda phage to be flanked by two new sites, the *attL* (left) and the *attR* (right) sites. The sites attL and *attR* give rise to the name LR. This system is utilised in research by flanking a PCR product with attB sites and integrating them into a plasmid with *attP* sites creating attL sites flanking the PCR product. A destination vector with *attR* sites is then used to integrate the *attL* flanked PCR product into an expression clone (Reece-Hoyes and Walhout, 2018).

Primers containing *attB1* and *attB2* sites were used in a 20µl PCR reaction with 1x Phusion buffer, 200µM dNTPs, 0.05µM forwards and reverse primer, Phusion polymerase, 1pg-10ng plasmid, and dH_2O. (NuMA_1700-2115_BP_Fw: 5' GGGGACAAGTTTCTACAAAAAAGCAGGCTGGATGGTGAGCAAGGGCGAG 3'; NuMA_1700-2115_BP_Rv: 5' GGGGACAACTTTGTATAAAGTTGGCCTTTAGTGCTTTGCCTTGCC 3'). An initial denaturation at 98°C for 30 seconds was followed by 34 cycles of 98°C for 10 seconds, 61°C for 30 seconds and 72°C for 4 minutes. The cycles were finished off with 72°C for 5 minutes. The PCR product was purified using a Qiagen QIAquick PCR Purification Kit, then run on a 1% agarose gel. The 2044bp product was cut out of the gel using blue light and gel purified using a Qiagen QIAquick Gel Extraction Kit. A BP clonase reaction ran overnight with 10µl 20-50fmoles PCR product, 150ng/ml supercoiled p221 donor vector containing *attP* sites, 2µl BP enzyme following the Gateway®BP Clonase™ II Enzyme Mix from Invitrogen, and TE buffer. In the morning the reaction was stopped with 2µg/µl proteinase K, then transformed and grown (section 2.8.1) using Kanamycin selection. Successful BP reactions were identified by digestion with XhoI, PvuI and BamHI (Table 2.8).

2.8.4.2. Generation of plasmids for tol2 integration of C-terminal NuMA

pEGFP and pNuMA_1700-2115 were digested with BtgI and EcoRI (Table 2.8). Bands of 2591bp for pEGFP and 2641bp for pNuMA_1700-2115 were cut out of the gel and gel purified using Qiagen QIAquick Gel Extraction Kit. The pEGFP vector and pNuMA_1700-2115 insert

were ligated in a 1:3 ratio in a 20µl reaction with 1x T4 ligation buffer (NEB), 1µl T4 ligase (NEB) and dH_2O at room temperature for 1 hour. The reaction was terminated at 65°C for 10 minutes, then transformed and grown (section 2.8.1) using Kanamycin for selection. XhoI and PuvI (Table 2.8) were used to check for correct plasmid size.

The plasmid was then used in an LR reaction using Gateway™ LR Clonase™ II Enzyme mix together with a ubi promoter ((pENTR5'_ubi was a gift from Leonard Zon (Addgene plasmid # 27320 ; http://n2t.net/addgene:27320 ; RRID:Addgene_27320)) from Dr Henry Roel), p3e-Sv40polyA, and pdegt tet2pA2 empty vector or an empty vector with CFP directed by a *cry* promoter using the equation in figure 2.6 for the concentration of each vector in the reaction, 2µl of LR enzyme and TE buffer to make a 10µl reaction. The reaction was left at 37°C overnight before being transformed and grown (section 2.8.1) using Ampicillin as a selection marker. Correct plasmids were identified by digestion with SpeI, AccI and NheI (Table 2.8) for plasmids with no *cry*-CFP, and digestion with SpeI and NheI for the plasmid with *cry*-CFP.

$$ng = \frac{(Size(bp) * 20fmol * 660)}{10^6}$$

Figure 2.6: Equation for concentration of vectors in LR reactions.

2.8.4.3. Generation of plasmids for tol2 integration of full length NuMA

pEGFP and pNuMA_FL were digested with EcoRI for 2 hours then with BglII (Table 2.8) for 2 hours. This sequential digest was due to the short distance between the digestion sites in pEGFP. There was a worry that the two restriction enzymes would not have enough space next to each other if the digestion occurred at the same time. A digestion product of 11693bp from pNuMA_FL and 3327bp from pEGFP were gel extracted using a Qiagen QIAquick Gel Extraction Kit. The ends of the digestion product of pEGFP were then rSAP dephosphorylated with 1µg DNA, 1x Cutsmart buffer (NEB), 1µl rSAP, and dH_2O in a 20µl reaction. pEGFP and pNuMA_1700-2115 were then ligated in a 20µl reaction in a 1:3 ratio with 1x T4 ligation buffer (NEB), 1µl T4 ligase (NEB) and dH_2O for 1 hour at room temperature. The 20µl reaction was digested with NdeI to eliminate any re-ligated pNuMA_FL for 30 minutes, before the whole reaction was terminated at 65°C for 5 minutes. The plasmid was then transformed and grown

(section 2.8.1) with Kanamycin selection. The plasmid was checked with SspI and AccI (Table 2.8).

The plasmid was then used in an LR reaction together with the ubi promoter, p3e-Sv40polyA, and pdegt tet2pA2 empty vector or an empty vector with CFP directed by a *cry* promoter using the equation in figure 1 for the concentration of each vector in the reaction, 2µl of LR enzyme and TE buffer to make a 10µl reaction. The reaction was left at 37°C overnight before being transformed and grown (section 2.8.1) using Ampicillin as a selection marker. Correct plasmids were identified by digestion with PvuI and EcoRV (Table 2.8) for plasmids with no *cry*-CFP, and for the plasmid with *cry*-CFP.

2.8.5. Making Tol2 mRNA

Tol2 mRNA is used to integrate DNA from a plasmid into the genome of zebrafish. 10,000ng of a plasmid containing the Tol2 gene was digested with NotI (Table 2.8) overnight. The digest was then phenol cleaned using equal amounts of digest to Phenol:Chloroform:isoamyl alcohol mixed well and centrifuged at 13,000 rpm at room temperature for 5 minutes. The clear upper liquid was moved into a clean tube and the process was repeated for chloroform. The linearised plasmid was precipitated overnight at -80°C with 30µl 3M NaAc at pH5.2 and 750µl 100% ethanol. The precipitation was centrifuged at 13,000 rpm at 4°C for 30 minutes. The supernatant was removed and the pellet washed with 500µl 70% ethanol in a centrifuge at 13,000 rpm for 5 minutes at room temperature. The supernatant was again removed and the pellet air dried for 5 minutes before it was resuspended in 20µl dH_2O. A mMESSAGE mMACHINE™ T7 Transcription Kit from invitrogen was used to transcribe the Tol2 from the linearised plasmid.

2.9. Microscopy

Embryos were taken out of their chorions, and larvae were anaesthetised with Tricaine prior to imaging. Whole zebrafish embryos and larvae were imaged with either bright field or with fluorescence by using a Leica M165FC fluorescent stereoscope with a digital colour camera (DFC310FX) and a Leica external fluorescent light source (EL6000). All GPF used a GFP2 filter with 460-500 excitation and 510LP emission. The images were taken using the Leica Application Suite v.4.3.0. For images of cells for γH2AX or mitochondria in whole larvae, the larvae were mounted following section 2.9.1, then imaged using a Nikon W1 Spinning Disk confocal using a x100 silicon lens.

2.9.1. Mounting

5dpf embryos with swim bladders were culled by a tricaine overdose and fixed in 5% PFA overnight at 4°C with rocking. The PFA was removed, and the embryo washed in 1 x PBST. Whole larvae were placed on a microscope slide (Sigma-Aldrich, CLS294875X25-72EA) using tweezers within a square cut out in a piece of diamond tape on the slide, six embryos in a square, three on the left and three on the right. Alternatively, using a pasteur pipette pigmented embryos were placed on autoclave tape taped to the lid of a 10 cm petri dish, whilst non-pigmented larvae were placed on the plastic of the same lid. Tissue paper was used to absorb the remaining E3 with the larvae. The tail was cut off by the yolk and using tweezers the tail was moved to the square cut out in the tape on the microscope slide. The heads were placed in 200µl PCR tubes for genotyping. One drop of Vectashield mounting media (Vector Labs, H-1200-10) with DAPI was placed in the square, and a 25x25mm coverslip (Sigma-Aldrich, BR470045) was gently lowered over the tape square using tweezers. Clear nail polish was used on the edge of the cover slip to keep it in place. The mounted larvae on microscope slides were placed in the dark at 4°C for storage.

2.10. Image analysis

2.10.1. Image J

Fiji ImageJ v.2.0 was used to analyse the length of larvae, the number of foci in ɣH2AX stained fins, the number of foci in acridine orange-stained embryos, the intensity of p21 expression in larvae, and it was used for quantification of band intensity of western blots and for alkaline assays. For the ɣH2AX, a protocol by Dr Ruth Thomas was followed. A mask and outline map were created around the DAPI stained nuclei. On the GFP images, in find maxima, all single points were selected. On the nuclei outline, under set measurements for analyse particles, the integrated density was selected and redirected to the maxima of the single point GFP image. The nuclei outline showed which GFP points were in the nucleus and the integrated density was measured and divided by 255 to find the number of foci per nucleus. The number of apoptotic cells were counted by identifying the number of single points in the whole treated larvae, and the level of p21 expression was measured by obtaining the fluorescent intensity of the whole embryo.

2.10.2. Image analysis using Arivis vision4D x 64 for mitochondrial size

Images from the spinning disk were transformed into sis files and uploaded onto Arivis vision4D x 64. An area of about 48,000 pixels of fin muscle over the anus was chosen for analysis through all planes. Only the green channel for the mitochondria was selected. A background correction for the green channel was used conserving brightness. The blob finder was used to identify the mitochondria marked by the GFP seen in the green channel. The diameter was set to 2.47µm, the probability threshold was at 5.21% and the split sensitivity at 65.4%. Any blob detected that was smaller than 6969690020.141601nm3 were excluded from the analysis (Figure 2.7). Volume and sphericity of the mitochondria was chosen for further analysis.

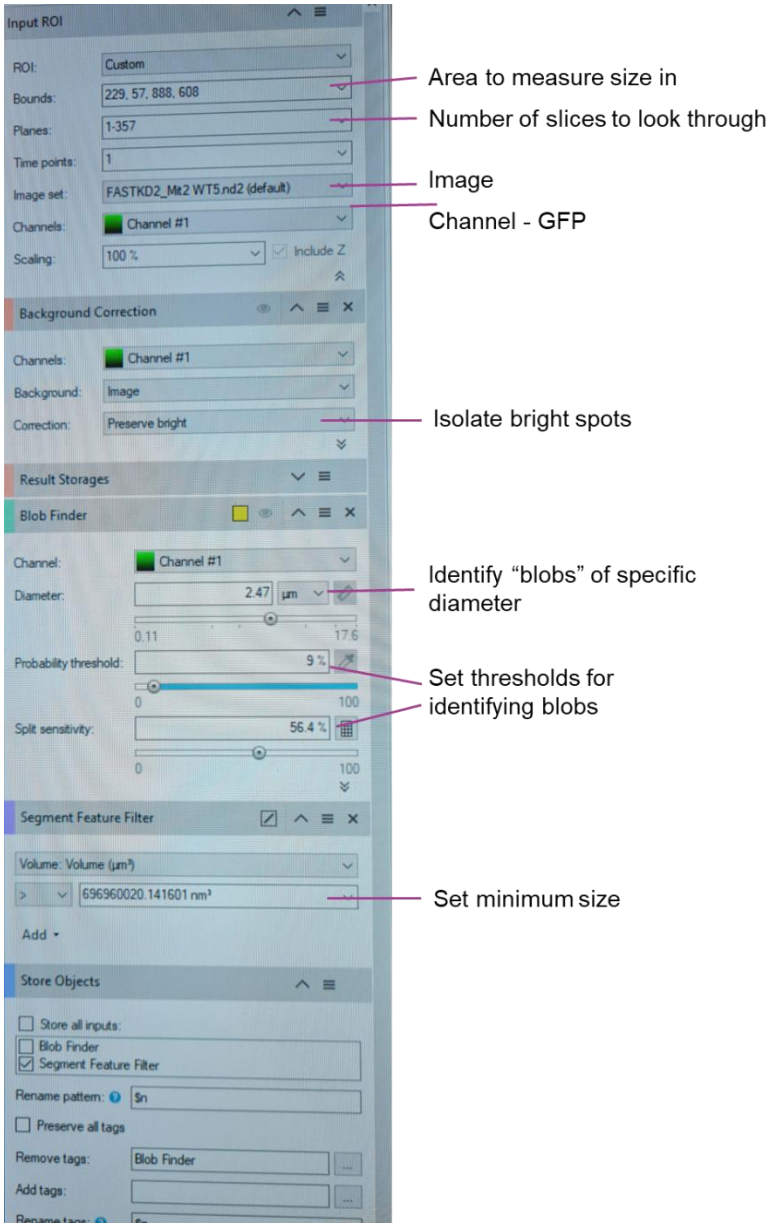

Figure 2.7: Arivis vision 4D x 64 protocol for measuring mitochondrial size. Note the probability threshold and split sensitivity in the figure is different from what was used in the analysis.

2.11. Statistical analysis

Statistical analysis was performed using GraphPad Prism version 9.3.1 for Windows 10 (GraphPad Software, La Jolla, California, USA, www.graphpad.com). All stat tests are mentioned in the figure legends. A Kolmogorov-Smirnov Test of Normality was used to determine normal distribution. Unpaired t-tests were used to check the significance between two normally distributed sample groups. When comparing the means of more than two sample groups one- or two- way ANOVAs were performed with the recommended Tukey post hoc test. Alternatively, R and R-Studio version 4.1.1 were used to create some figures. $P<0.05$ was considered statistically significant for all statistics tests and data is presented as with standard error of the mean.

2.12. Graphical figures

All graphical figures were made using Power Point from Microsoft office 360, version 2501. All statistical figures were made in GraphPad Prism mentioned in 2.11 and formatted in Power Point.

Chapter 3 Ribonucleotide excision repair in aged zebrafish

3.1. Introduction

RNaseH2, introduced in Chapter 1.5.3 is the main enzyme in the ribonucleotide excision repair (RER) pathway. It can cleave at the 5' end of a single ribonucleotide (rNMP) that has been incorporated into the genome to initiate the RER pathway and remove the rNMP. If the rNMP is not removed, it can cause distortion of the DNA double helix as well as spontaneous cleavage of the rNMP causing strand breakage. RNaseH2 is a trimeric enzyme consisting of the catalytic RNaseH2A subunit and two supportive subunits RNaseH2B and RNaseH2C. Mutations in any of the three subunits can cause the neuro-inflammatory disease Aicardi-Goutières syndrome (Reijns et al., 2011, Lockhart et al., 2019).

There are several models for loss of RNaseH2 function. Yeast with a lack of RNaseH2, have increased rNMP incorporation as well as increased sensitivity to hydroxyurea which is used to increase the rNTP pool in nucleus (Arudchandran et al., 2000, Nick McElhinny et al., 2010b). Yeast was also used to unlink two different roles of RNaseH2, when the Ribonucleotide Excision Deficient (RED) mutant was created. This mutant was deficient in RER, but efficient in R-loop processing (Chon et al., 2013, Cerritelli and Crouch, 2019). In contrast to yeast, mice with complete loss of RNaseH2 function or mice with the RED mutation are embryonic lethal due to activation of p53-dependent DNA damage responses. However, mice with no R-loop processing ability but functioning RER are viable, as well as mice with partial loss of RNaseH2 activity (Reijns et al., 2012, Uehara et al., 2018). This shows that in vertebrates, the RER ability of RNaseH2 is vital for survival, however, simpler organisms such as yeast have other mechanisms to work around it.

A viable multicellular organism with the lack of RNaseH2A function has however been missing. Recently, Dr Ruth Thomas showed that a null mutant for RNaseH2A in zebrafish is second-generation lethal (Thomas et al., 2024). Surprisingly, a first generation *rnaseh2a* homozygous zebrafish showed no external embryonic phenotype, survived through adulthood and could produce embryos. At 5dpf, the homozygous embryos from a heterozygous cross had no decrease in the activity to remove a single rNMPs form double-stranded DNA, they did not have an increase in rNMPs in the genome, and they had no change in movement compared to their siblings. However, at 6 months, the adults did have an increase in rNMPs in the brain,

although they did not have an increase in double stranded breaks or increase in inflammation. At 15 months, the homozygous adults had reduced movement compared to their wild type siblings. The embryos from the first-generation homozygous fish undergo normal early cleavages and start gastrulation and epiboly. However, by 24hpf they show severe developmental delay, small head, reduced tail length and apoptosis throughout the body (Figure 5.22). Second-generation homozygous embryos have a reduced ability to cleave single rNMPs as well as an increase in rNMPs in the genome. Further, they have an increase in double stranded DNA breaks as seen by an increase in γH2AX as well as *isg15*, *mxa*, and *infΦ* interferon expression and senescence as seen by *p21*. They do not have a significant increase in expression of inflammatory markers *tnfα*, *il-1β* or *il-6* (Thomas et al., 2024).

One theory for why the first generation of *rnaseh2a* homozygous zebrafish survive is that Topoisomerase 1 (TOP1) can compensate for the lack of RNaseH2 activity during the vital replicative events during early development. However, there was no change in phenotypes when making top1 crispants in an RNaseH2 heterozygous cross. Furthermore, there were no detectable 2-5 TOP1 signature deletions in the genome of the *rnaseh2a* homozygous embryos (Thomas et al., 2024). The theory therefore stands that the maternal mRNA deposited into the first-generation embryos is enough to get the embryo through the crucial early hours. The larvae then reach adulthood where the lack of RNaseH2A gradually causes an increase in rNMPs in the non-replicative DNA in the brain which causes some effect during adulthood that does not affect their reproductive ability. The second-generation embryos have a great number of rNMPs in the genome. By some unknown mechanism, the embryos manage to overlook the rNMPs, or the level of fragmentation due to rNMPs do not reach the correct threshold for cell death, and they therefore manage replicate the genome for the first few hours, until the rNMP load gets too high and the DNA is fragmented causing developmental delay and apoptosis.

Whilst RNaseH2 is mostly associated with embryonic lethality or childhood onset disease, one paper has explored the role of RNaseH2 in ageing. In 2019 Storci showed that centenarians (>99 years) have the same amount of RNaseH2A and RNaseH2B as young individuals (18-40 years) which is significantly more than in old, non-centenarian (58-98 years) primary dermal fibroblasts. The centenarians had significantly more RNaseH2C than both old and young. They also showed a decrease in basal inflammation (*il-6*) and DNA damage by comet tail length and γH2AX, as well as decreased inflammation and DNA damage by either radiation

or doxorubicin in centenarians compared to old (Storci et al., 2019). This publication suggests that having well functioning RNaseH2 might be important for healthy ageing.

Genomic instability is one of the primary hallmarks of ageing (Chapter 1.2.1) and many important factors in maintaining genomic instability have already been linked to poor ageing or age-related diseases. It therefore stands to reason that RNaseH2, which was identified as a factor in robust ageing by Storci in 2019 might be responsible for parts of the ageing process. Zebrafish are good model organisms regularly used to study development. However, they have a relatively short lifespan of about 3 years and gain several ageing phenotypes in their last year. Here I use aged surplus zebrafish, as well as aged RNaseH2 homozygous adult zebrafish to identify whether a reduction in RNaseH2 activity may be partially responsible for their ageing.

Hypothesis: When we age, the ribonucleotide repair pathway declines, causing an increase in rNMP in the DNA. This leads to activation of an antiviral immune response, which causes inflammation, and promotes frailty.

Aims:

- Classify young, healthy old and frail old adult zebrafish.
- Assess the state of the RER pathway in young and healthy old zebrafish, and healthy old and frail old zebrafish.
- Assess the level of DNA damage in young, healthy old and frail old zebrafish.
- Assess the level of inflammation in young, healthy old and frail old zebrafish.

3.2. Results

3.2.1. Young and old adult zebrafish show no difference in ribonucleotide burden

In this thesis, I was interested in the difference in RER between young and old zebrafish. Therefore, my first question was whether the rNMP burden was heavier in old fish compared to young. Initially I chose any zebrafish between 3 and 6 months as young, and any zebrafish between 2.5 and 3 years old as old. I first looked at whether there was a decline in single

ribonucleotide cleavage from young to old by using a ribonucleotide activity assay, which has a double stranded DNA with a single rNMP in the middle. The rNMP is cleaved and visualised on a urea separating gel by a Cy5 tag on the 5' end of the strand with the rNMP (Figure 3.1A). I used protein from the fin of the fish due to the easy access to fin tissue. I took fin tissue from female and male zebrafish and saw no significant difference in ribonucleotide cleavage between young and old in any sexes (Figure 3.1B-E). I also wanted to know if there was an increase in rNMPs in the genome of the aged zebrafish. I used an alkaline assay to evaluate the cleavage of rNMPs by sodium hydroxide and saw that even with only four samples per age group, there was great variation between the samples of the same age groups, and I could not make out a definitive answer to this question (Figure 3.1F and G).

Further, I wanted to investigate whether there was any difference in DNA damage or inflammation between the young and old groups. I performed western blotting for γH2AX but saw no significant increase in DNA damage between the groups or the sexes (Figure 3.2A-C), although there was a trend, particularly in the male group. Further qPCR of RNA from fins for *il-6* and *isg15*, two inflammatory markers that were significantly increased in second-generation *rnaseh2a* homozygous embryos (Thomas et al., 2024), also showed great variation. There were no significant differences in expression for females, however, for the males there was a significant increase in both markers. When male and female data points were combined, there was still a significant increase in *il-6*, but not for *isg15* (Figure 3.2D and E). Further, qPCR for *rnaseh2a*, the catalytic unit of RNaseH2, showed a significant increase for males but not the females, and a non-significant increase when all data points were combined (Figure 3.2F). Lastly, when comparing young and old males, I also saw no difference in expression of *fastkd2*, a potential novel protein in the RER pathway (Chapter 4) (Figure 3.2G). Whilst there did not appear to be any change in rNMP cleavage or damage between young and old, there did appear to be a non-significant trend towards increase in general double stranded DNA damage and inflammation in the older animals.

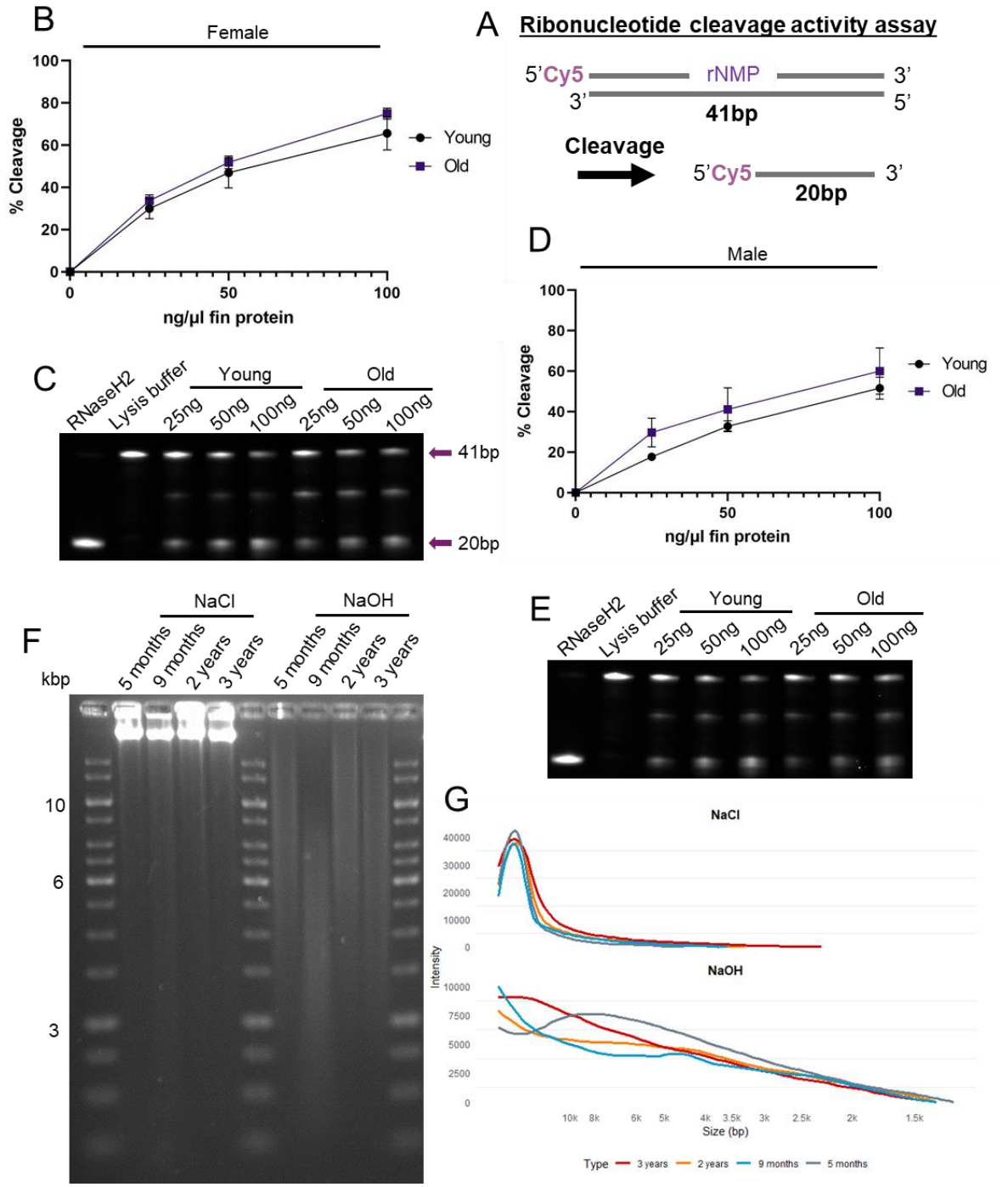

Figure 3.1: Assessment of rNMP load in young and aged zebrafish. A: Schematic of ribonucleotide cleavage activity assay. The substrate is a double stranded piece of DNA, 41bp in length with a ribonucleotide at base 21 of the sense strand. The 5' end of the sense strand is tagged with Cy5. When the substrate is mixed with protein, cleavage of the rNMP by enzymes that can cleave it occurs, and once the digestion is run on a gel you get a 41bp full length uncleaved band and a 20bp cleaved band. B: Female young (3-6 months) and old (2.5-3 years) fin tissue showing no difference between young and old rNMP cleavage. Unpaired t-test, n=4. C: Representative urea cleavage gel for female fish. D: Male young (3-6 months)

and old (2.5-3 years) fin tissue showing no difference between young and old rNMP cleavage. Unpaired t-test, n=3. E: Representative urea cleavage gel for male fish. F: Alkaline digest on TAE gel with non-alkaline (NaCl) control. Showing, male young (5 months), adult (9 months), aged (2 years) and old (3 year) brain genomic DNA. G: Visualisation of intensity of smear from alkaline digest, n=4.

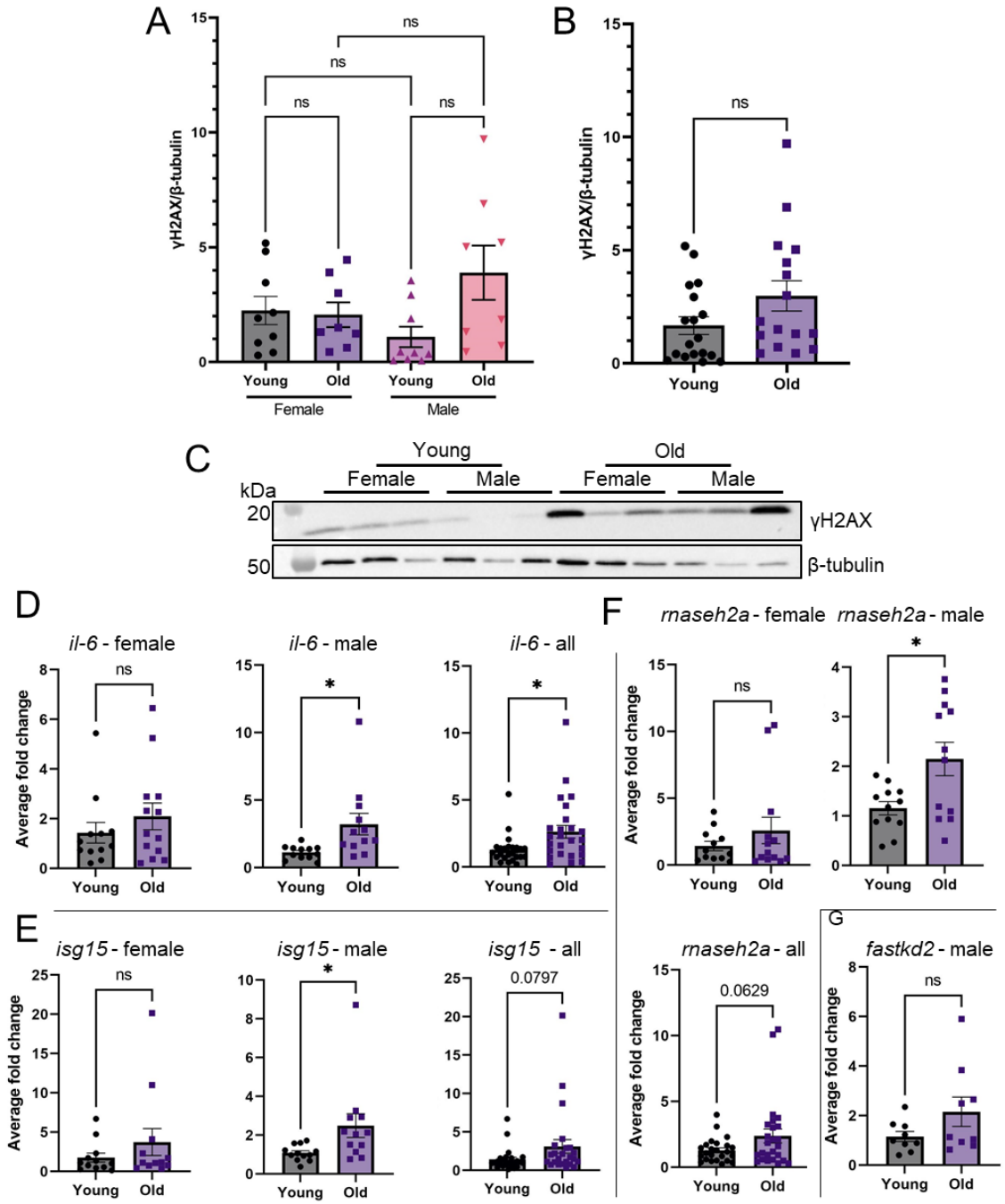

Figure 3.2: DNA damage and inflammation in young and old zebrafish. A: DNA damage levels in young and old, female and male adult zebrafish tail fins as seen by western blotting for

γH2AX. B: Total γH2AX in young and old adult zebrafish tail fins. C: Example western blot for γH2AX for young and old, female and male adult zebrafish. D: qPCR for *il-6* in young and old female, male and total adult zebrafish tail fin. E: qPCR for *isg15* in young and old female, male and total adult zebrafish tail fin. F: qPCR for *rnaseh2a* in young and old female, male and total adult zebrafish tail fin. G: qPCR for *fastkd2* in male young and old male zebrafish. Western blot: One-Way ANOVA, young n=18, old n=16, qPCR: Unpaired t-test, n=24.

3.2.2. Characterisation of zebrafish young, old *robust,* old *pre-frail* and old *frail* status

When considering the results in figure 3.2.1, I concluded that the results were very variable. I considered whether the large differences in expression within the old group was due to dominant or subordinate status in the fish tank. However, this was excluded as a possibility. A second possibility was the idea that ageing is not chronological. Some individuals will age well, whilst others will age poorly, have multimorbidity and be frail. Therefore, I considered whether the reason for the variation was due to some fish being frail and others being robust and just as healthy as a young fish. For the remainder of this thesis, I decided to adopt four classifications for the adult fish: young, old *robust*, old *pre-frail* and old *frail*. Figure 3.3A shows images of the four classifications for both female and male fish. The four classifications come from five criteria I used to create a frailty index. The index uses width/length ratio, as this significantly changes with age in mutant *tert* zebrafish (Henriques et al., 2013). Loss of BMI (g/cm^2) as this decreases with frailty in humans (Fried et al., 2001, Crow et al., 2020). BMI is also a measure that has been used on zebrafish in other research especially to study obesity (Smolińska et al., 2024, Oka et al., 2010). Spinal height, as zebrafish show gross morphological changes in their spinal curvature and muscle mass with age (Gerhard and Cheng, 2002, Hayes et al., 2013). Cancer occurrence, as this increases with age in zebrafish as well as in humans (Kishi et al., 2003, Cayuela et al., 2018, Laconi et al., 2020), and whether the fish might have any fin damage that has not been regenerated as the ability to regenerate their fins diminish as they age (Gilbert et al., 2014). If a fish scores yes or above or below a threshold (Table 3.1) on any of these criteria, they receive a value of 1. If they do not score, they receive a value of 0. The additive score was divided over 5 to get an index of frailty. The cut offs for each criterion were based on 12 initial old fish that I had visually identified as robust or frail (Figure 3.3B-G). Based on the lower value of the robust and the higher values of the frail, a value was set for width/length ratio, BMI and spinal height. Cancer and fin regeneration was a yes or no question. The frail females were easier to identify than frail males at the age of 3, meaning there were significantly more frail females than males (Figure 3.3H). This might

also be because male fish become frail earlier than females around 2 years of age instead of 3, meaning they were mostly outside of the age window I was using. The frailty phenotype can occur throughout the lifespan of the fish; however, it was mostly found in older fish as seen in figure 3.4, which shows the density of fish at each age in the aquarium compared to the density of fish with a frailty phenotype at each age. Whilst there are fewer old fish in the aquarium, there was a larger density of fish with a frailty phenotype at old age.

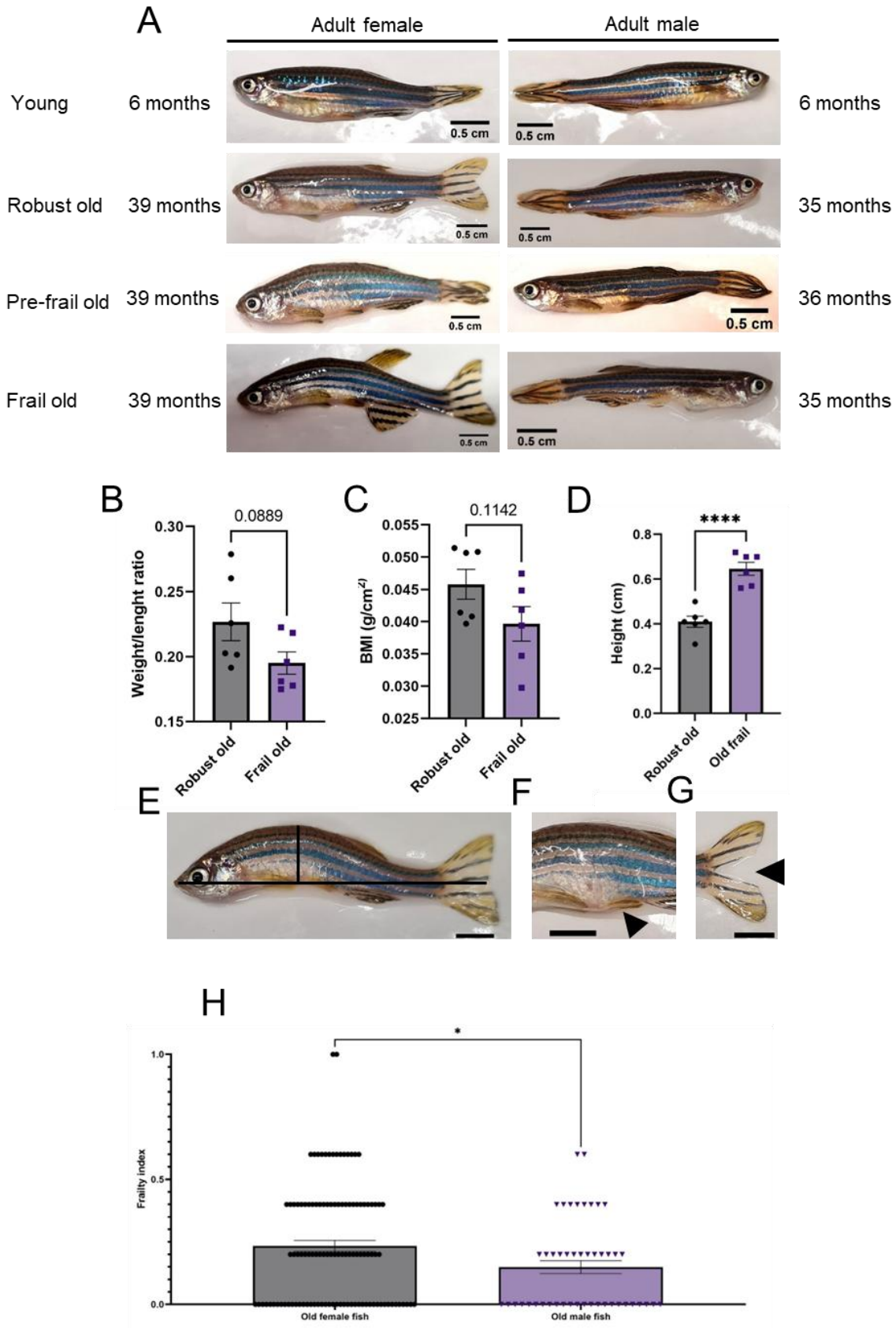

Figure 3.3: Classification of aged fish used in thesis. A: Representative pictures of adult zebrafish of both sexes. The top fish are 6-month young siblings. The female robust and frail

old fish are siblings, and the male robust and frail old fish are siblings. Old fish are divided into robust old, pre-frail old and frail old. B: Weight/length ratio trends to decreases in frail old female fish. C: The BMI (g/mm^2) trends to decreases in old frail female fish. D: The spinal curvature increases in frail old female fish. Unpaired t-test, n= 6. E: Way used to measure spinal curvature in adult fish. A line was drawn from the mouth to the middle of the tail. Another line was drawn from that line to the top of the spine and its length was measured. F: Example of tumour in adult fish. G: Example of loss of regenerative ability of the fin as seen by a split fin. H: Frailty index distribution within female and male old fish (30 months +). Unpaired t-test, n= 56 (female), n=29 (male).

Table 3.1: Criteria for frailty index used in this thesis.

Criteria	Female threshold	Male threshold	Scoring
Width/length ratio	0.19	0.18	< = 1 > = 0
BMI (g/cm^2)	0.0395	0.029	< = 1 > = 0
Spinal curvature	0.55	0.4	> = 1 < = 0
Fin degeneration	Yes/No	Yes/No	Yes = 1 No = 0
Tumour	Yes/No	Yes/No	Yes = 1 No = 0

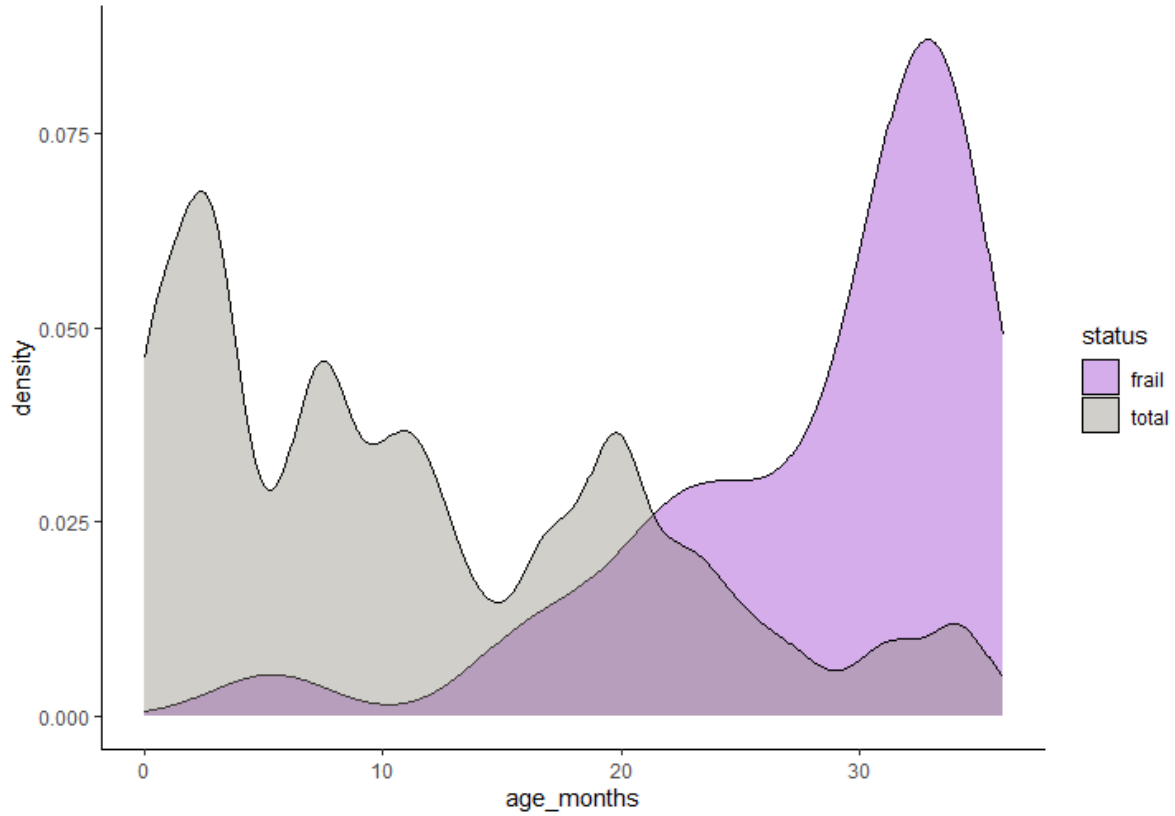

Figure 3.4: Density plot showing an increase in frail fish in the aquarium with age. This was not due to an increase in old fish in the aquarium.

After this, with the new classification of the old fish, I went back to the data in figure 3.2.2 and separated out the old into robust, pre-frail and frail. I looked back at *il-6*, which is a well-known frailty marker (Puts et al., 2005, Marcozzi et al., 2023). For the female group where there were no significant differences between young and old fish, all but one old fish fell into the robust old category, with the one fish being pre-frail (Figure 3.5A). For the male fish, there was at least three fish in each category, and there was a significant increase in *il-6* with increasing frailty (Figure 3.5B). With the lack of pre-frail and frail female fin samples, I performed a new qPCRs on fin clips with pre-identified fish and saw a significant increase of *il-6* and *p21*, another frailty marker, with increasing frailty status for the female fish (Figure 3.5C and D).

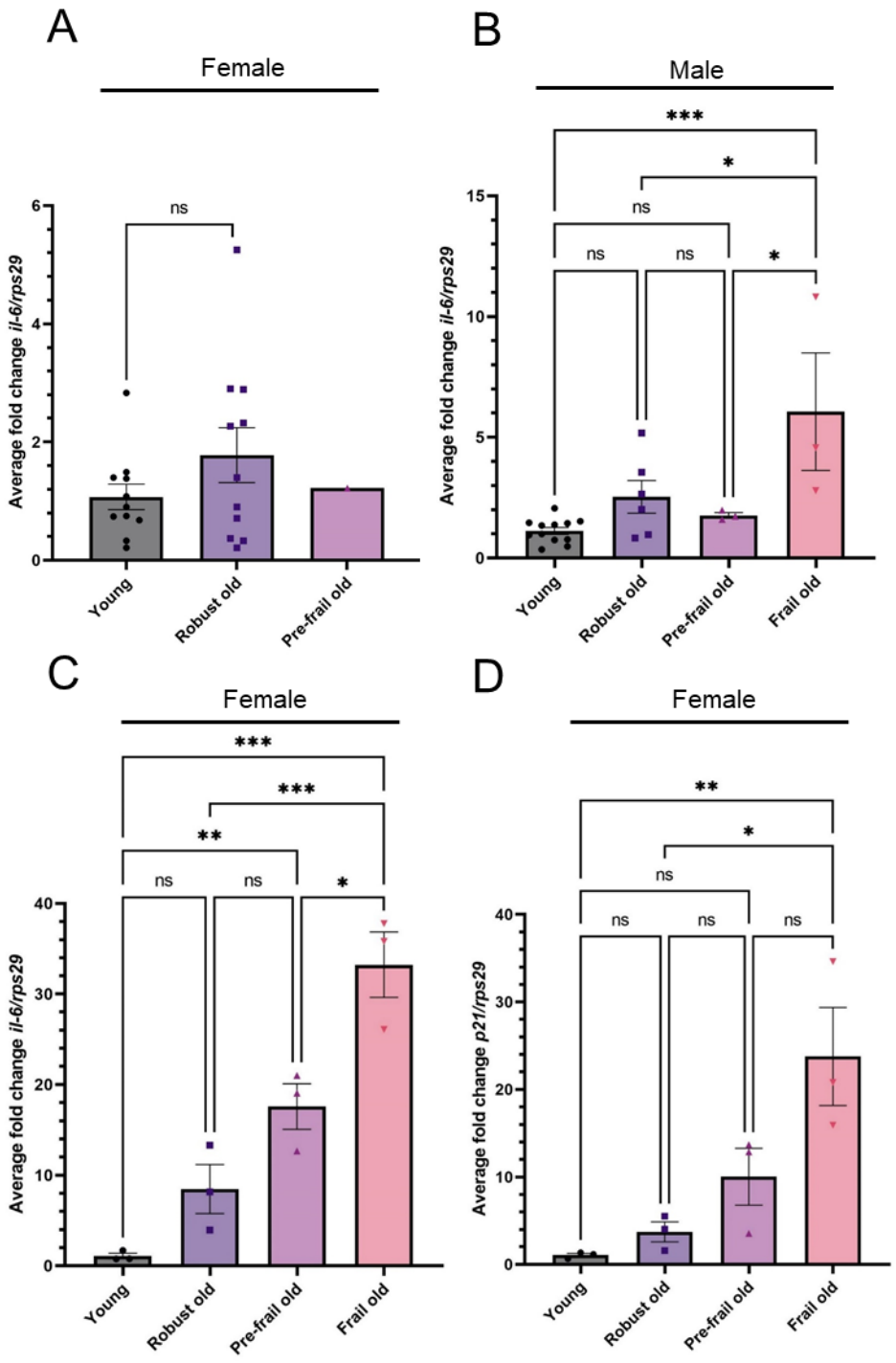

Figure 3.5: Expression of frailty markers with increasing frailty status. A: Data from figure 3.2D *il-6* females arranged as young, robust old and pre-frail old. B: Data from figure 3.2D *il-6* males arranged as young, robust old, pre-frail old and frail old. C: New qPCR on fin RNA from young, robust old, pre-frail old and frail old females for *il-6* and D: *p21*. One way ANOVA, n=3.

3.2.3. Expert frailty scoring of zebrafish

There is no one way to define frailty, however, it is commonly described as a loss of physiological function making an individual more reliant on services and they often have a higher chance of adverse outcomes such as death after disease. However, when working with animals, having death as an endpoint is not commonly accepted. Therefore, to further verify the frailty index created in 3.2.2, I asked 7 Named Aquarium Care and Welfare Officer (NACWO)-trained aquarium staff and other zebrafish ageing researchers to visually score the frailty of 10 of each robust young, robust old, pre-frail old and frail old male and female zebrafish, a total of 80 fish. I then plotted the average score of each fish against my frailty index (Figure 3.6A). I also plotted the average score given to each fish against the fish's BMI, width/length ratio and spinal height (Figure 3.6B-D). With a regression analysis, I saw that the experts' scores increased as my frailty index increased suggesting that my frailty scoring system was in concordance with the experts. Further, I saw that the experts viewed BMI and width/length ratio more important than spinal height as both significantly increased with the expert's frailty score whilst spinal height did not. Spinal height trended to increase with expert opinion for the females, however it was not significant. I also saw that the fish that had cancer or fin damage scored average or higher on the experts' scores, which could suggest that they are partly associated with frailty (Figure 3.6F and G).

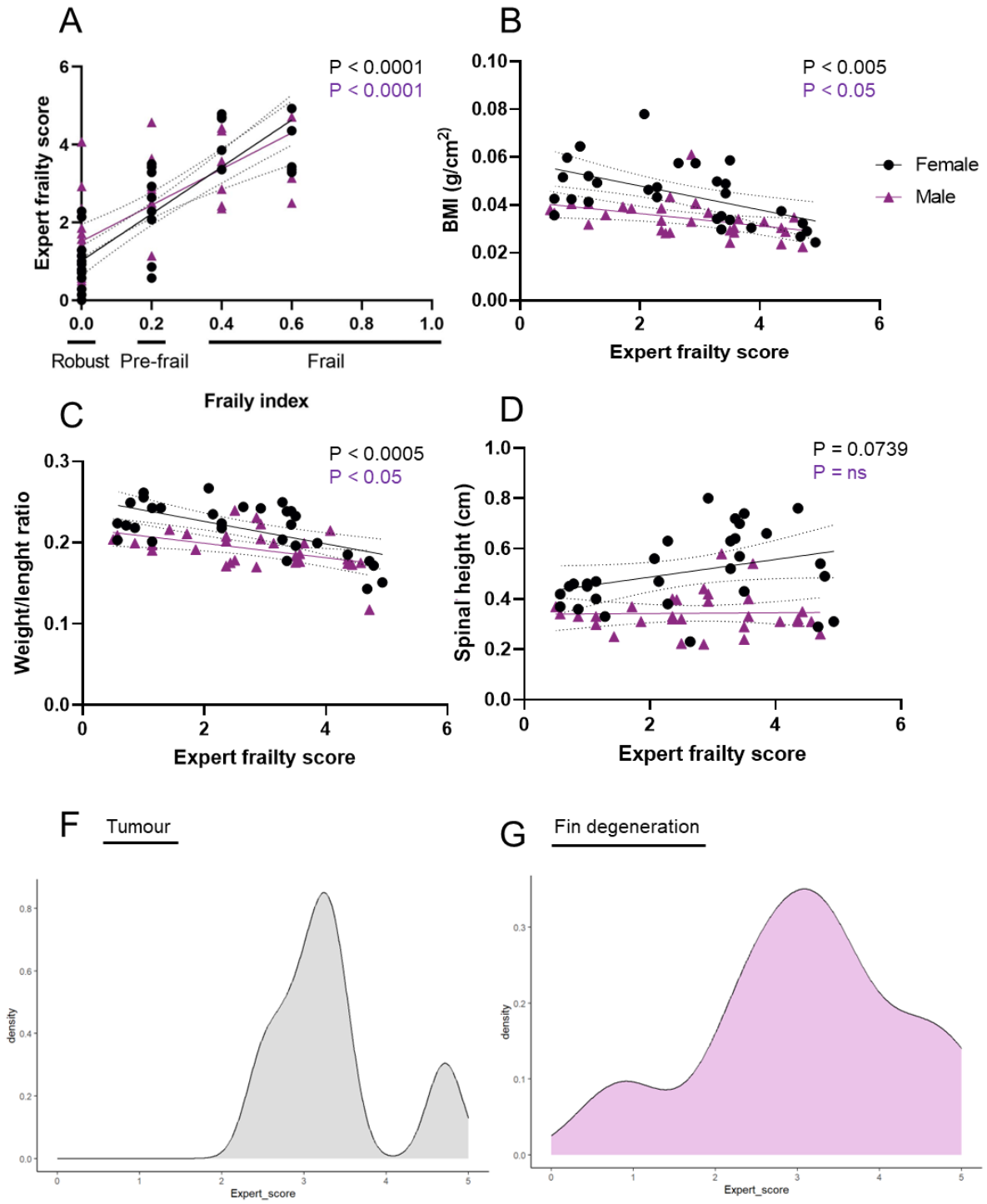

Figure 3.6: Frailty scoring of young, old robust, pre-frail and frail old female and male zebrafish by zebrafish NACWOs and ageing research experts. A: The average score per fish by the experts plotted against the frailty index. B: Significant decrease in BMI with increasing expert frailty score. C: Significant decrease in width/length ratio with increasing expert frailty score. D: No significant increase in spinal height with higher frailty scores given by experts. Simple linear regression. A, n=40. B-D n=30. F: Density plot of tumour occurrance amongst the 60

old fish against the experts' scores. n=6. G: Density plot of fin degeneration amongst the 60 old fish against the experts' scores. n=8.

3.2.4. Frail old female zebrafish have a higher ribonucleotide burden in the brain

With the new classifications of old fish, I then wanted to evaluate the rNMP burden between robust and frail old zebrafish. Considering that AGS is a neurological disorder affecting the brain (Cristini et al., 2022), I decided to use the brain for my experiments. When assessing the ability of robust and frail old female and male zebrafish to cleave single rNMPs in the brain, I saw that the frail fish were not able to cleave the rNMP as effectively as the robust (Figure 3.7A-D). This was statistically significant for the female brains but only trended in the males without reaching statistical significance. This might be because I found identifying male fish that are frail more difficult than the females as they show less of a frailty phenotype. This might have meant that some of the fish I chose for the assay might not have been as frail as the female fish were. It can also be seen that the frail old male fish do cleave the rNMP better than the frail old female too, again potentially due to the different frailty between the sexes. Due to the difficulty with the old male fish, my data for the remainder of this chapter is mainly for female fish. The reduced cleavage activity of the frail old female fish, however, does not appear to be due to a general decrease in enzyme activity as there was no change in the activity of TDP1, another DNA repair enzyme (Zaksauskaite et al., 2021) (Figure 3.7E and F). I also determined that robust old zebrafish brain extracts were better at cleaving the rNMP than young female brains (Figure 3.7G and H), but this was observed only after one hour of digestion. The assay had been optimised for a two-hour digestion. However, after two hours the products in both the young and the robust old samples were completely cleaved at all protein concentrations, and therefore it was determined to keep the concentration the same for all categories but shorten the time of the digestion to be able to observe the cleavage happening.

Next, I wanted to assess whether a lack of cleavage activity resulted in an increase of rNMPs in the genome of the frail old female brains. By alkaline treatment of genomic DNA extracted from the brains of robust and frail sibling female fish, and running the DNA on a TAE gel, I saw that the frail old fish had more DNA smearing after treatment than their robust siblings. This indicates that they might have more rNMPs in their genome that are attacked by the hydroxyl and cleaved from the neighbouring dNMP causing shredding of the DNA and smaller DNA fragments (Figure 3.8A and B). Although the change in ratio of small to large between the

robust and frail old fish was not significant after the alkaline conditions, the p value was 0.0549 suggesting there was a trend. Further, whilst there was no significant increase in smearing between the NaCl and the NaOH for the robust old brains, there was a significant increase in the frail old brains (Figure 3.8C). Altogether, this suggests a trend towards an increase in rNMPs in the frail old brains compared to the robust.

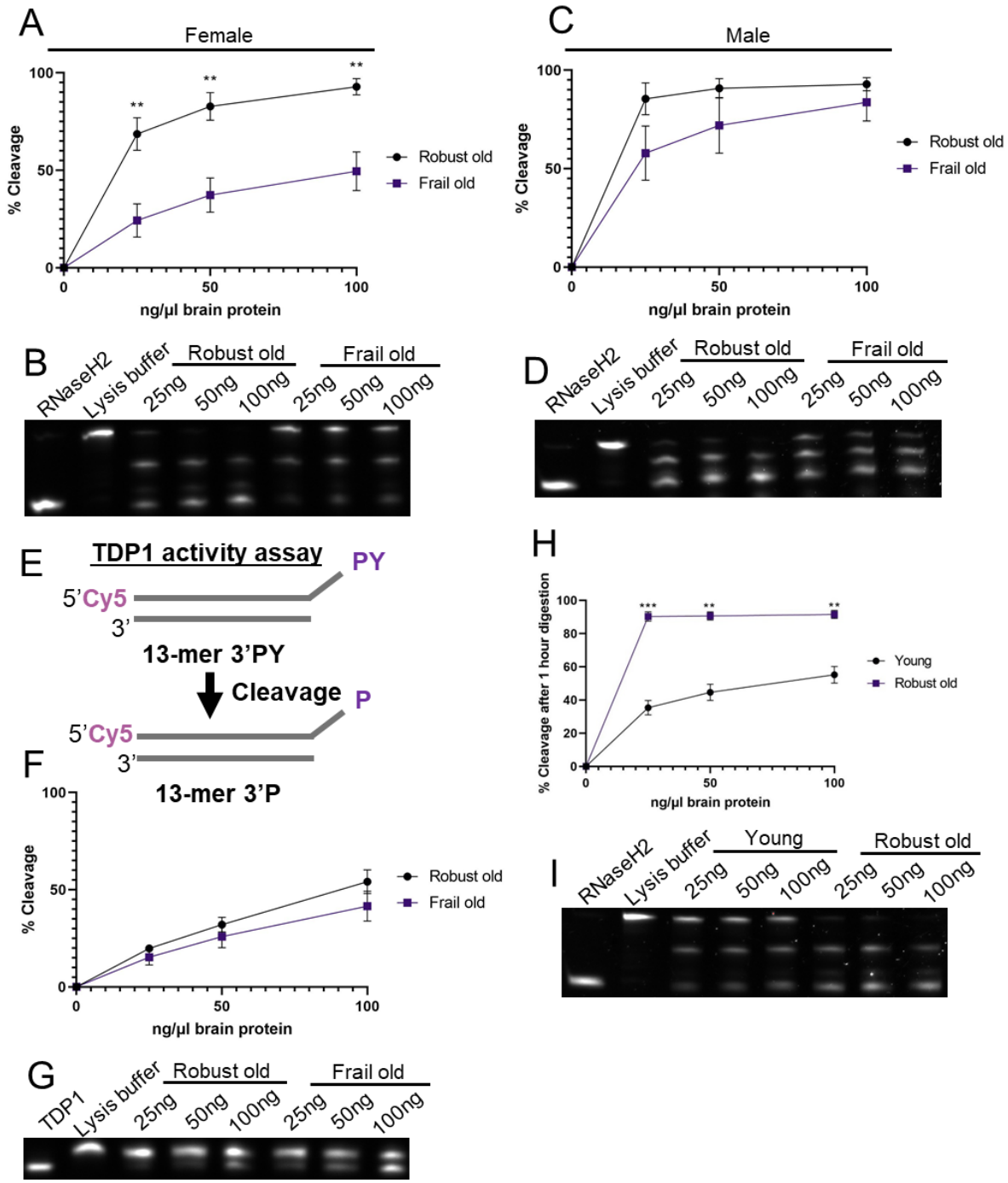

Figure 3.7: Ribonucleotide cleavage assays for young, robust, old frail female and male brains. A: Percentage cleavage of the rNMPs by robust old and frail old female brain protein. Unpaired

t-test, n=7. B: Example image of rNMP cleavage by old female brains on a urea gel. C: Percentage cleavage of the rNMPs by robust old and frail old male brain protein. Unpaired t-test, n=3, p-value at 25ng = 0.160. D: Example image of rNMP cleavage by old male brains on a urea gel. E: Schematic diagram of TDP1 activity assay. A double stranded 13bp DNA is Cy5 tagged on the 5' end of the sense strand. The 3' end of the sense strand has a phosphotyrosyl (PY) molecule. Once protein is added, TDP1 cleaves the phosphodiester bond at the DNA 3'end linked to a tyrosyl moiety, making the double stranded DNA lighter, and it travels faster on a urea gel (Zaksauskaite et al., 2021). F: Percentage cleavage of phosphate on the end of a 13'mer double stranded DNA by robust old and frail old female brain protein. Unpaired t-test, n=3. G: Example image of phosphate cleavage by old female brains on a urea gel. H: Percentage cleavage of the rNMP by young and robust old female brain protein. Unpaired t-test, n=3. I: Example image of rNMP cleavage by female brains on a urea gel.

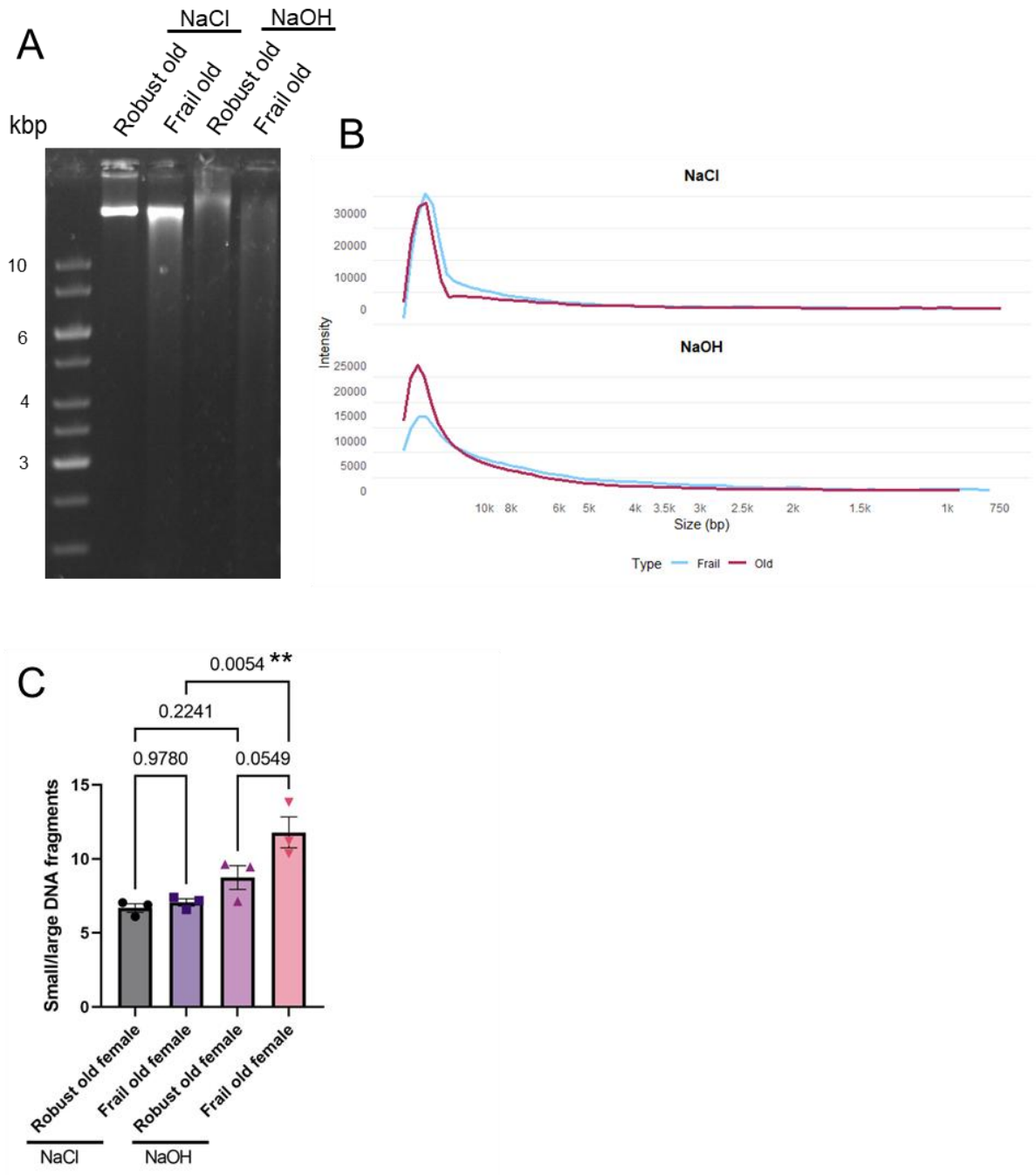

Figure 3.8: Alkaline treated robust and frail old female brain genomic DNA. A: Example of non-alkaline and alkaline treated genomic DNA run on a TAE gel. B: Intensity plot of alkaline treated samples. Labels explained: Type: Frail = Frail old. Type: Old = Robust old. C: Small/large fragments for robust and frail old non-alkaline and alkaline treated samples. One-way ANOVA, n=3.

3.2.5. Frail old female brains have more single stranded DNA damage but no increase in inflammation

When seeing this decrease in rNMP removal in the frail old female brains I questioned whether this was due to a decrease in the expression of any of the three subunits of RNaseH2. However, the expression of *rnaseh2a*, *rnaseh2b* or *rnaseh2c* did not change in between the two groups (Figure 3.9A). I further looked at the RNA expression of other enzymes that can remove rNMPs. RNaseH1 removes strands of several ribonucleotides; however, its expression did not change. FASTKD2 is an enzyme that potentially removes single rNMPs in the mitochondrial DNA (Chapter 4), however, that did not change in RNA expression either. TOP1 removes rNMPs in the absence of RNaseH2, although there was no change in expression of *top1a*, the dominant TOP1 in zebrafish. Lastly, I looked at the expression of NuMA, a protein that protects non-coding regions from oxidative DNA damage (Chapter 6) which has been proposed to be involved in poor ageing. However, there was no significant change in its expression there either. Although there was a trend for increased *numa* expression in the frail old brains (Figure 3.9B). If a decrease in *rnaseh2* expression was not the reason for the loss of RER function, I decided to look at the expression of other genes involved in RER and single stranded break repair. I looked at the expression level of *aptx* (Chapter 5), *fen1*, *rad51b* and *rad51c,* but saw no change in expression. I also saw no change in expression of *xrcc1*, which is involved in single stranded DNA break repair or *p53*, which is involved in apoptosis and highly expressed in *rnaseh2a* homozygous embryos (Figure 3.9C) (Thomas et al., 2024).

For second-generation *rnaseh2a* knockout larvae, the consequences of reduced RNaseH2 is an increase in double stranded breakage as seen by an increase in γH2AX (Thomas et al., 2024). However, in section 3.2.1 I saw no change in γH2AX between young and old. I further saw no change in γH2AX levels between robust old and frail old female brain protein (Figure 3.9D and E). However, I saw an increase in PARylation in the frail old samples which could suggest increased single-stranded DNA damage (Figure 3.9D and F). This was not due to an increase in *parp1* expression, as it did not change (Figure 3.9G). An increase in PARylation was also seen in second-generation *rnaseh2a* homozygous embryos (Figure 3.9H and 5.27). Further, AGS is an auto inflammatory disease, and several inflammatory markers are highly expressed in second-generation *rnaseh2a* homozygous embryos. I saw no change in expression level of *il-6* or *isg15,* which were upregulated in the mutants. I also saw no change in expression of *il-1b* and *tnfα,* which are upregulated in some ASG patients (Takanohashi et al., 2013) (Figure 3.10A). Lastly, looking at expression levels of *p21* and *p16* two known

senescence markers, I did not see any change in their expression between robust and frail old brain groups (Figure 3.10B).

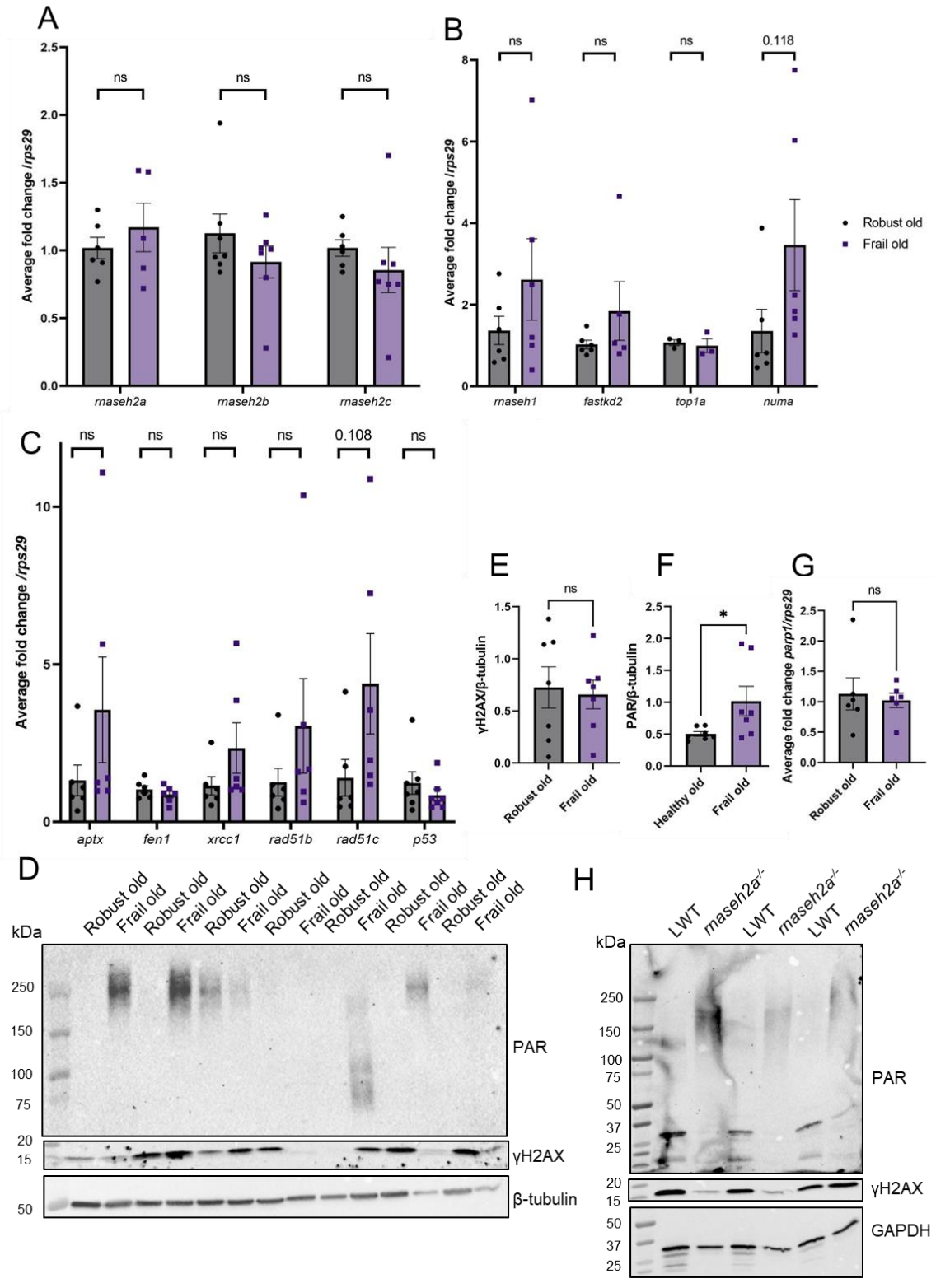

Figure 3.9: rNMP related DNA damage in frail old female brains. A: Expression of RNaseH2 subunits *rnaseh2a*, *rnaseh2b* and *rnaseh2c*. B: Expression of *rnaseh1, fastkd2*, *top1a* and *numa*. C: Expression of *aptx*, *fen1*, *xrcc1*, *rad51b*, *rad51c*, and *p53*. Unpaired t-test, n=6. D: Western blot showing PARylation, γH2AX and β-tubulin for robust and frail old female brains. Each robust old and frail old sample are siblings. E: Quantification of γH2AX between robust and frail old female brains. F: Quantification of PARylation between robust and frail old female brains. Unpaired t-test, n=7. G: Expression levels of *parp1*. Unpaired t-test n=6. H: Western blot showing PARylation, γH2AX and GAPDH for 24hpf LWT (London wild type) and second-generation *rnaseh2a* homozygous embryos. n=3.

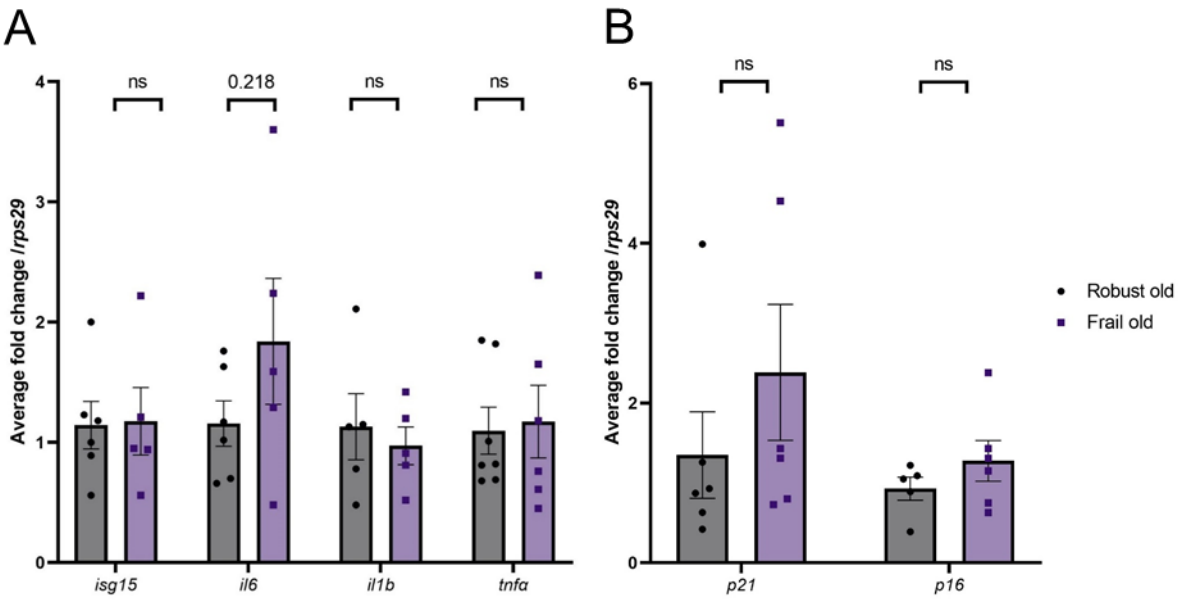

Figure 3.10: Inflammation and senescence in robust and frail old female brains. A: Expression of *isg15*, *il-6*, *il1-b*, *tnfα*. B: Expression of senescence markers *p21* and *p16* in robust and frail old female brains. Unpaired t-test, n=6.

3.2.6. The fin protein of frail old females cleaves ribonucleotides at the same rate as fin protein from robust old females

Most analysis for this project has been done in brains, as AGS is a neurological disease affecting the brain. However, the most common time for ribonucleotides to be misincorporated into the genome is during replication. The brain does not replicate its cells often (Frade and Ovejero-Benito, 2015, Kase et al., 2020). Therefore, I decided to extend my analysis to more replicative tissue such as the tail fin, which was also used in investigations early in the project

in sections 3.2.1. When looking at the ribonucleotide cleavage assay for young and old fin clips, there were no differences (Figure 3.1A-D). When looking at activity assays for fin clips from robust old and frail old protein, I again saw no differences in activity (Figure 3.11A and B). However, when looking at the expression levels of the RNaseH2 subunits, I saw a significant increase in *rnaseh2a* and *rnaseh2c*, with *rnaseh2b* being almost significantly upregulated (Figure 3.11C). Further, I saw significant increases in *rnaseh1*, *fastkd2* and *top1a* (Figure 3.11D). As there was a potential increase in single stranded DNA repair in the brains as seen by PAR but not double stranded as seen by γH2AX, I looked at PARylation and γH2AX in the fin clips. Whilst there was some PARylation in the robust old fins, there was none in the frail old fins, and the PARylation pattern was at a different size than in the brains. As before, I saw no increase in γH2AX between robust and frail fin clips either (Figure 3.11E). Contradictory to these findings however was in the *klotho* mutant fish. *klotho* mutants are prematurely ageing fish that have an endpoint at 6 months when they develop many ageing diseases (Kuro-o et al., 1997). The line used in these experiments was made by Dr Oluwaseyi A Pearce (Seyi), and together we saw a significant decrease in rNMP cleavage in the tail fins of *klotho* homozygous mutants compared to their wild type siblings (Figure 3.11F and G).

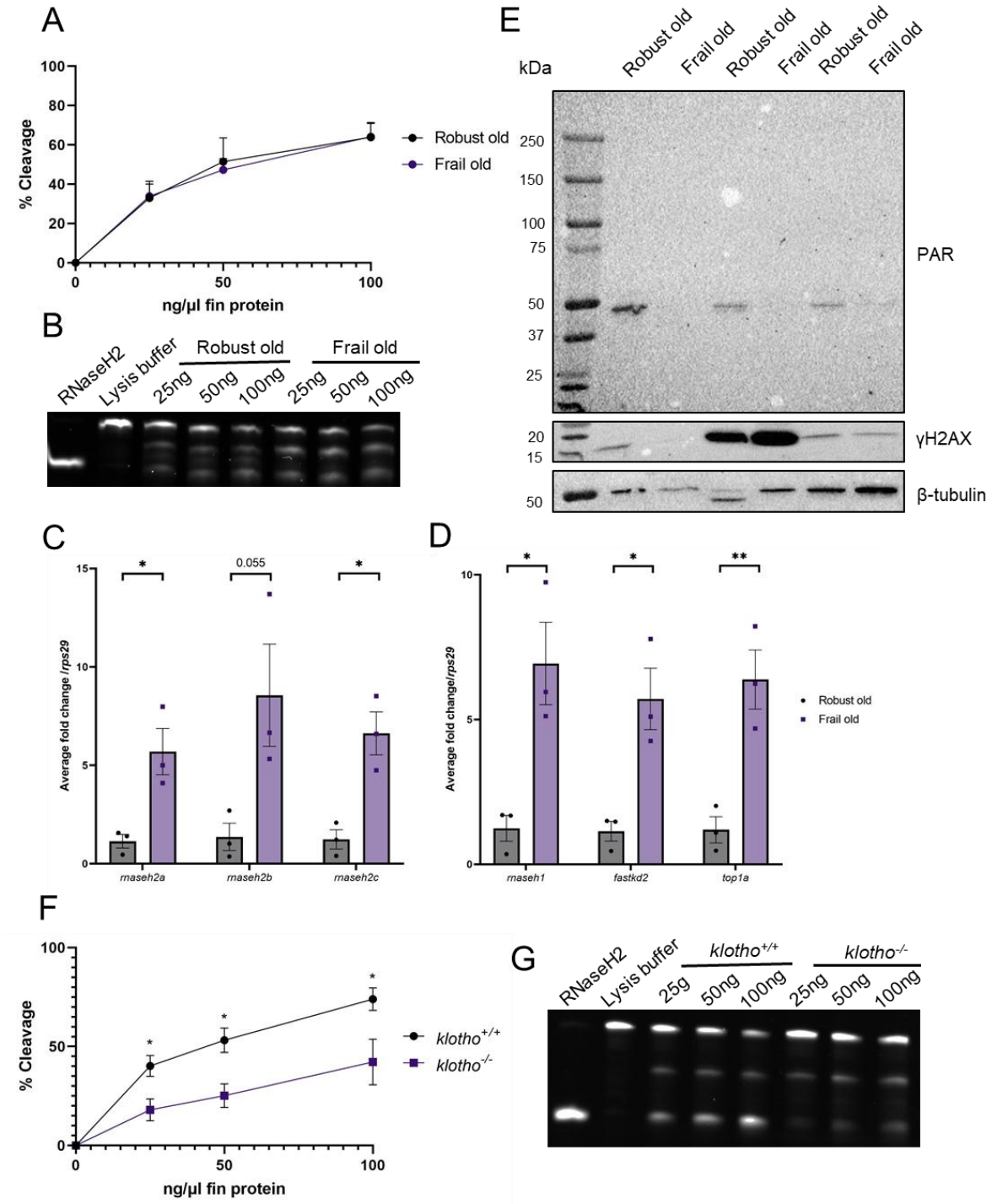

Figure 3.11: Ribonucleotide burden in robust and frail old female fin clips. A: Percentage cleave of rNMP in fin clips from robust and frail old females. Unpaired t-test, n=3. B: Representative cleavage urea gel or rNMP cleavage in robust and frail old female fin clips. C: Expression of subunits of RNaseH2, *rnaseh2a*, *rnaseh2b* and *rnaseh2c*. Unpaired t-test, n=3. D: Expression of other potential proteins in the ribonucleotide repair pathway, *rnaseh1*, *fastkd2* and *top1a*. Unpaired t-test, n=3. F: Percentage cleavage of rNMP in *klotho* wild type and

mutant fin clips at 6 months old. G: Representative cleavage urea gel or rNMP cleavage in *klotho* wild type and mutant fin clips.

3.2.7. *rnaseh2a* homozygous old adults are frailer than their wild type siblings

Human *rnaseh2a* is located on chromosome 19 and is 1164bp long making a 299aa protein (ENST00000221486.6). The protein is 62.1% similar to the zebrafish version of *rnaseh2a*, which is located on chromosome 1, and is 1302bp long making a 307aa protein (ENSDART00000045894.7) (Figure 3.12). Figure 3.12, also show that RNaseH2A share similarities with mouse (ENSMUST00000109736.9), tropical clawed frog (ENSXETT00000010319.5), coelacanth (ENSLACT00000008885.1) and spotted gar (ENSLOCT00000009593.1) RNaseH2A, showing that the protein is well conserved. When studying TDP1 function during her PhD, Dr Ringailė Zakšauskaitė made a CRISPR/Cas9 knockout line for *rnaseh2a* in zebrafish with a 49bp frameshift deletion in exon 6, creating an early stop codon and a truncation of the protein. The line is second-generation lethal, meaning the first-generation embryos are viable and will grow until adulthood. This is probably because they have mRNA of *rnaseh2a* from their mother during the crucial replicative steps in early development, and functional RNaseH2 is not as vital in later life. These fish survive until they are 3 years old, however, they appear to show more frailty phenotypes than their wild type siblings. In figure 3.13A, images of female and male *rnaseh2a* homozygous adults at 3 years of age show spinal curvature in the female homozygous fish, and loss of weight in the male homozygous fish. The male wild type fish has cataract. However, even though they show some phenotypes there was no significant difference in BMI or the width/length ratio between the sexes and the genotypes. The homozygous female has a significantly higher spine than the wild type siblings, although, this was an n of 1 (Figure 3.13B-D). When applying the frailty index from chapter 3.2.2 to the *rnaseh2a* wild type and homozygous fish I saw that the homozygous fish had a significantly higher frailty index value than the wild type siblings, with most homozygous being pre-frail and two being frail, whilst in the wild type most were robust with one fish being pre-frail. The number of fish in each tank was very low between 2 and 3 years of age, suggesting that several of the fish that might have been sicker and frailer might have been removed from the tanks by the aquarium staff or died earlier (Figure 3.13E).

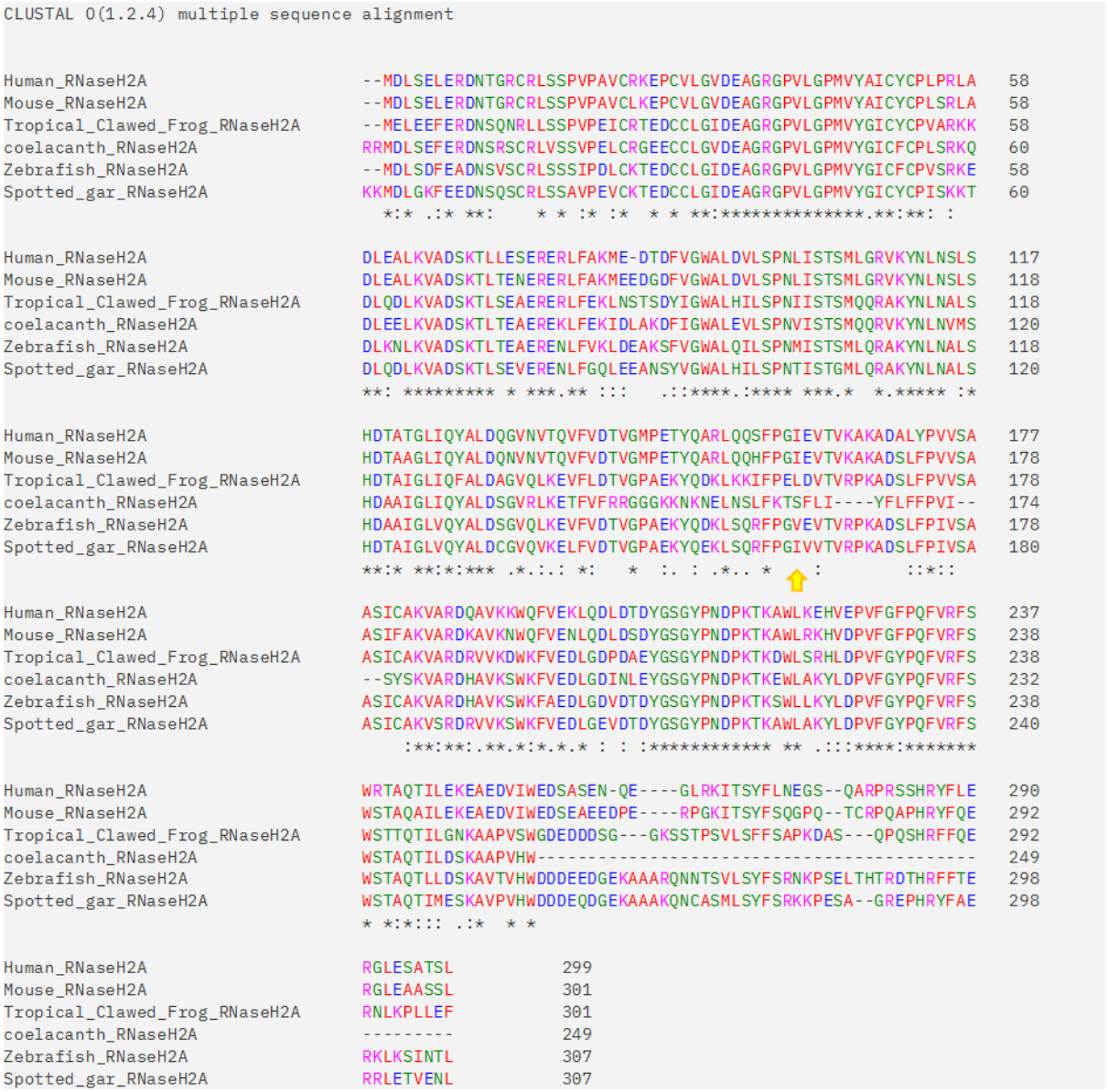

Figure 3.12: Comparison of human, mouse, tropical clawed frog, zebrafish, coelacanth and spotted gar RNaseH2A protein. Comparison performed using EMBL-EBI clustal omega multiple sequence alignment. Stars indicate same amino acid. Two dots and one dot indicate similar amino acids. Red amino are small hydrophobic amino acids, blue are acidic amino acids, magenta are basic amino acids and green are hydroxyls, sulfhydryl and amine amino acids (Madeira et al., 2024). Yellow arrow indicate the site of the mutation in the zebrafish genome.

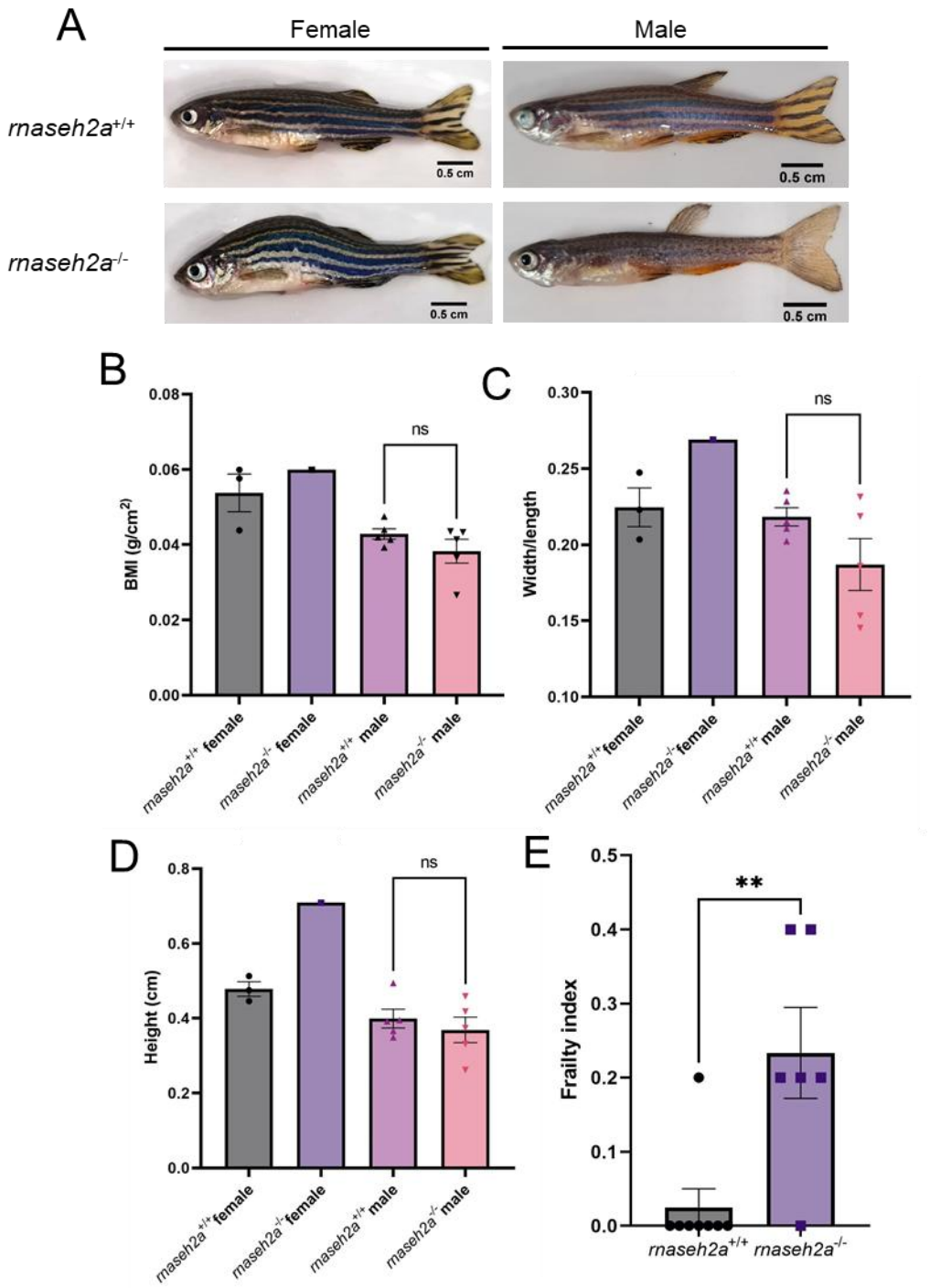

Figure 3.13: Frailty status of old *rnaseh2a* homozygous adults. A: Images of 3-year-old female and male *rnaseh2a* wild type and homozygous siblings. B: BMI (g/cm^2). C: Width/length ratio. D: Spinal height (cm). E: Frailty index for *rnaseh2a* wild type and homozygous adults. Unpaired t-test, wild type n=8, homozygous n=6.

First-generation *rnaseh2a* adult homozygous embryos that are 6 months of age do not have a defect in rNMP removal from a double stranded DNA as shown by Dr Ruth Thomas. Based

on this I asked whether the protein from the brains of 3-year-old wild type and homozygous first-generation fish were able to cleave the rNMP and I saw no difference in cleavage ability (Figure 3.14A and B). When looking at the expression level of the RNaseH2 subunits, *rnaseh2a*, *rnaseh2b* and *rnaseh2c*, I also saw no significant decrease in expression (Figure 3.14C). I further saw no change in expression of *rnaseh1* or *top1a* (Figure 3.14D) as potential compensatory enzymes for the loss of RNaseH2. However, I did see a significant increase of *fastkd2* in the *rnaseh2a* homozygous adults (Figure 3.14D). FASTKD2 may be able to cleave single rNMPs as is explored in Chapter 4, and this might suggest that FASTKD2 is compensating for the lack of RNaseH2. In addition, I looked at the consequence of loss of RNaseH2 at old age by looking for DNA damage signalling. I saw a trend of increased signalling in the wild type adults as seen by γH2AX, which was not significant, and possibly an increase in PAR in the wild type too, however, this signal was very weak (Figure 3.14E and F). Lastly, I saw a trend of increasing inflammation and senescence using *il-6*, *isg15* and *p21* in the homozygous adult brains. However, this was again not significant (Figure 3.14G). Taking these results together, it appears that the *rnaseh2a* homozygous adult fish are frailer than their wildtype siblings. However, whilst this might be due to the loss of RNaseH2A function, I could not confirm a loss of rNMP cleavage activity, although we are confident in the knockout of the line. This could be due to the increased expression of *fastkd2*, which could be compensation for the loss of RNaseH2A function.

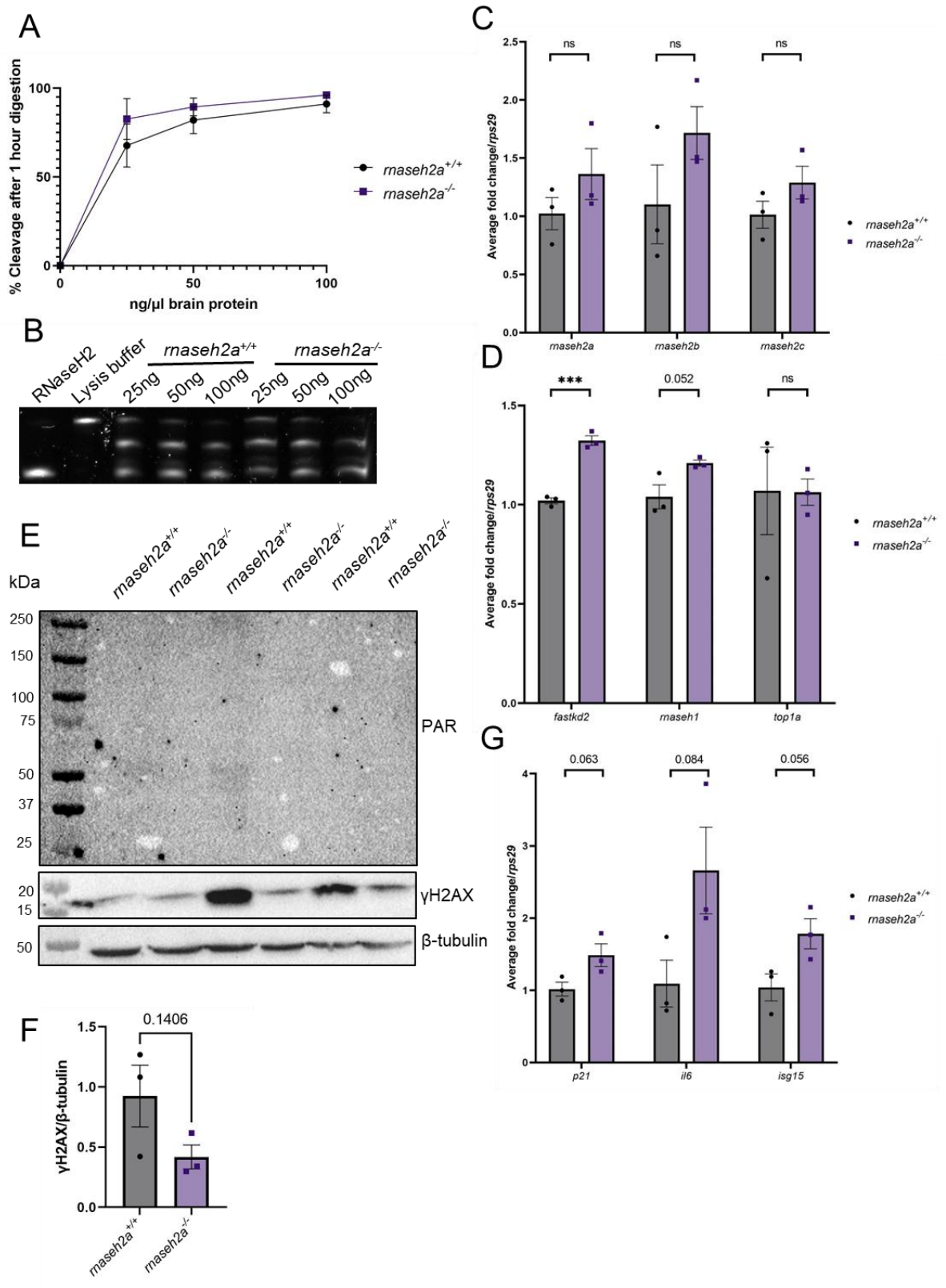

Figure 3.14: Ribonucleotide, inflammatory and DNA damage burden in *rnaseh2a* wild type and homozygous 3-year-old adults. A: Percentage cleavage for wild type and homozygous brain protein. Unpaired t-test, n=3. B: Representative urea cleavage gel for wild type and homozygous brains. C: Expression of the subunits in RNaseH2, *rnaseh2a*, *rnaseh2b* and

rnaseh2c. Unpaired t-test, n=3. D: Expression of *fastkd2*, *rnaseh1* and *top1a*. Unpaired t-test, n=3. E: Western blot for PAR, γH2AX and β-tubulin between wild type and homozygous brains. F: Quantification of γH2AX over β-tubulin. Unpaired t-test, n=3. G: Expression of senescence marker *p21*, and the inflammatory markers *il-6* and *isg15*. Unpaired t-test, n=3.

3.3. Discussion

Incorporation of ribonucleotides (rNMPs) into the genome either by purpose or by accident is one of the most common forms of DNA damage in the cell and if they are not removed they can cause single- or double-stranded breaks in the DNA leading to mutations and disease (Kellner and Luke, 2020, Li and Breaker, 1999). The removal of rNMPs is initiated by the trimeric enzyme RNaseH2, and mutations in RNaseH2 causing reduced function causes the neuro-inflammatory disease Aicardi-Goutières syndrome in humans and a loss of function is lethal in mice (Reijns et al., 2012). Because of this, there has been a lack of a model to study loss of function of RNaseH2 in a whole organism. Recently, Dr Ruth Thomas published that second-generation *rnaseh2* homozygous zebrafish embryos are lethal; however, the first-generation is not, leaving us with a viable lack-of-function whole organism (Thomas et al., 2024). Many premature ageing diseases are linked to faults in DNA repair enzymes, and Storci published in 2019, that RNaseH2 expression was significantly higher in centenarians than old people suggesting that RNaseH2 is important for healthy ageing (Storci et al., 2019). However, no further published reports have investigated the role of RNaseH2 in ageing. Therefore, in this chapter I asked whether a reduced rNMP removal activity can be related to ageing in zebrafish. I used zebrafish because they have a relatively short lifespan of 3 years and show many ageing phenotypes in their last year.

3.3.1. Chronological age is not the same as biological age for zebrafish

A turning point in this thesis was incorporating the idea that not everyone ages in the same way. Initially, when investigating the change in rNMP removal, DNA damage load and inflammation between young and old, I saw some large variation in the results (Figure 3.1, 3.2). I concluded that these variations could be due to the way in which individual zebrafish had aged. Some of the fish had aged well, whilst other had aged poorly (Figure 3.3). I termed this *robust* ageing, *pre-frail* ageing and *frail* ageing. Frailty was first described by Fried and colleagues, who hypothesised that it related to a cycle of negative energy balance, sarcopenia, and diminished strength, and tolerance for exertion. They then made a frailty index, the Fried

index, which considered unintentional weight loss, weakened grip strength, poor endurance and energy, slow walking speed and low physical activity (Fried et al., 2001). Later, frailty has been described as a state in which people are reliant on services due to a change in physiological healthy which increases a persons chance of adverse effects such as death after disease (Rockwood et al., 1994, Rockwood et al., 2000, Kane and Howlett, 2021).

Because of this description, I refer to our index as a pseudo descriptor, as I was not allowed to let the fish die, and therefore cannot confirm frailty, as the endpoint of frailty is death. My index takes inspiration from Fried where I have five criteria, loss of weight (BMI), decrease in width/length ratio, increase in spinal curvature (spinal deformation), cancer occurrence and fin degradation (Figure 3.3). These phenotypes increase with age in the aquarium (Figure 3.4) and it correlates with increase in expression of frailty markers (Figure 3.5). However, as I cannot use death as an endpoint, I also asked seven zebrafish experts with expertise in ageing to assess the frailty visually of fish that already had been scored according to my index. Their scores do significantly align with my index giving me more confidence that the index is appropriate (Figure 3.6). Further, their scores showed me that for the index, loss of BMI and a decrease in width/length ratio are the most important factors when assessing the frailty of the fish. The fish with spinal curvature did not consistently score the same, suggesting that for the experts spinal curvature might not be an important factor in poor ageing. Some experts would score them high and other low meaning that the spinal height did not significantly align with their scores. Although, the p value for female fish was 0.0739, showing a trend that for the females' spinal curvature could be important. Although fish spinal curvature might not be directly comparable to humans, an interesting study has found that sarcopenia, which can be involved in the pathogenesis of scoliosis, is more common in women compared to men in community dwelling people (Hwang and Park, 2022). This index uses a step-function rather than a continuous system for scoring of zebrafish frailty which I decided on as I used the Fried index as a guide for my index. The Fried index is also a step-function (Fried et al., 2001). It is possible that a continuous system would capture a greater range of frailty, however, it would become a more laboursome system to use. Further, I opted for a step-system with several factors to measure frailty instead of a singular measure such as width and length but do that continuously.

I also saw that more female fish scored as frail in the index than the male fish. This might be as identifying potential frail male fish in the aquarium was difficult. My theory is that the male fish go frail earlier than the female fish, around 2 years rather than 3 years. Therefore, they

were removed from the aquarium for ethical reasons before I could identify them as I initially looked at fish that were 3 years of age. This is also seen in the human population and is referred to as the “sex-frailty-paradox”. It says that females live longer than men, however, they become frailer (Gordon and Hubbard, 2020).

3.3.2. Frail old female fish have a higher ribonucleotide burden than robust old female fish in the brain

With a classification system for the aged fish, I could investigate whether a reduction in RNaseH2 activity correlated with why some fish age poorly and others not. First, I showed that both female and male frail old fish had a reduced ability to cleave rNMPs in the brain, although this was only significant for the females (Figure 3.7A and B). I believe this again to be because of the difficulty in identifying frail male fish, as their phenotype is not as prominent as the frail old female fish. This meant that potentially the male fish I used were not as frail as the females. Because of this, my research in this chapter has focused on females. I also saw that the old robust female fish were better at cleaving the rNMP than the young female fish (Figure 3.7D). This could be because the DNA damage burden in the old fish was higher than the young fish due to their age, meaning they might have been more prepared for damage. Alternatively, one could look at the robust old fish as centenarian fish. Storci (2019), did suggest that dermal fibroblasts from centenarians had more *rnaseh2c* than young, and better recovery after damage (Storci et al., 2019). This might explain the efficiency of the robust old samples to cleave the substrate. For the young and the old fish, one problem is that they are different genotypes as the fish used were surplus fish from the aquarium. This could also have introduced some variation into the experiment which was not seen between the robust and the frail old as those fish were siblings, making those results more convincing.

With a decreased ability to remove rNMPs, there should be more rNMPs in the genome. Through an alkaline assay, I showed that frail old female fish may have more rNMPs in their brain genome (Figure 3.8). This result was not significant and would require more repeats. Although, for the frail fish there was a significant increase after treatment with NaOH, which is not seen in the robust old samples. This result indicates that in a non-replicative tissue such as the brain, were there are less rNMPs being misincorporated through the primary mechanism of rNMP insertion, replication, rNMPs must still be incorporated through inadequate repair (Williams and Kunkel, 2014, Williams et al., 2016, Sassa et al., 2019). The reduced rNMP removal and therefore increased rNMP load in the genome may correlate with the frailty seen in the frail samples. The rNMPs that are left in the genome may cause cellular

stress during transcription or increased mutation due to the spontaneous cleavage of the hydroxyl group or the potential 2-5bp mutation signature of TOP1 cleavage (Williams and Kunkel, 2014). Although, Dr Ruth Thomas showed that there was no TOP1 signature cleavage in the *rnaseh2a* homozygous genome, suggesting that TOP1 does not have the same ability to cleave rNMPs in zebrafish as it has in other organisms (Thomas et al., 2024).

Knowing that the frail old fish might have a higher rNMP burden, I wanted to investigate why the rNMPs were not removed efficiently. Expression analysis of *rnaseh2a* showed that there was no reduced expression of any of the three subunits (Figure 3.9A), suggesting that if reduced RNaseH2 activity is the reason for the rNMP load, it could be due to the protein not functioning after translation. However, I was not able to find an antibody that would recognise zebrafish RNaseH2A, and therefore could not confirm this. I also investigated whether there was a change in any other enzymes suggested to be able to remove rNMPs, however, I saw no change in expression of *rnaseh1* or *top1a* (Figure 3.9B).

This thesis is also exploring whether FASTKD2 can remove single rNMPs (Chapter 4), however, I saw no change in *fastkd2* levels either (Figure 3.9B). Further, Matthew Dawson in Professor Sherif El-Khamisy's lab has shown that a lack of NuMA causes an increase in R-loops (unpublished observation). NuMA, which is introduced in Chapter 6, is a mitotic protein that recently has been shown to cause protection from oxidative damage in non-coding promotor and enhancer regions. Therefore, I also looked at whether NuMA could be involved in the lack of rNMP removal or poor ageing, however, although there is a trend towards an increase in *numa* expression in frail old fish brains, this was not significant (Figure 3.9B). There was no change in expression in *aptx*, which is responsible for fixing abortive ligations after a ligase attempts to ligate a RNA-DNA hybrid after spontaneous cleavage (Chapter 5) (Williams and Kunkel, 2014), or *fen1* which is responsible for removing the rNMP after RNaseH2A has cleaved it. There was no increase in the single stranded break repair enzyme *xrcc1* (Brem and Hall, 2005), or in the DNA damage marker *rad51b* or *rad51c* either which Storci (2019) saw a decrease of in centenarians compared to old human fibroblasts (Storci et al., 2019). Together this suggests that even though there is an increased rNMP burden due to the rNMPs not being efficiently removed, this is not due to a change in expression of genes in the RER pathway and it does not seem to trigger any alternative repair pathways.

However, the consequence of an increase in rNMPs in the brain genome and them not being efficiently removed is genomic instability (Williams, Lujan and Kunkel, 2016). When looking at

the protein level for markers of genomic instability I saw an increase in general PARylation in the frail old brains compared to the robust old (Figure 3.9D). There are many reasons for PARylation to occur, one of them being single stranded DNA damage repair signalling (Wei and Yu, 2016). I also saw an increase in PARylation in *rnaseh2a* second-generation homozygous embryos (Figure 3.9H). Reijns (2012) saw that in RNaseH2 null mice and Zimmermann (2018) saw that in RNaseH2 knockout cells there was also an increase in PARylation. However, they believe that this is due to TOP1 mediated rNMP removal causing PARP trapping DNA lesions which further cause genomic instability and cell death (Reijns et al., 2012, Zimmermann et al., 2018). In the frail fish, the loss of rNMP removal ability did not cause fragmentation of the DNA as seen in RNaseH2 deficient organism such as mice (Bartsch et al., 2017), as I saw no increase in γH2AX which is a signalling molecule for double stranded brakes. I only saw PARylation, suggesting that the rNMPs in the genome is not enough to cause double stranded breaks and therefore cell death. Mice lacking functional RNaseH2A are lethal due to the increase in double stranded breaks causing apoptosis signalling by p53 (Reijns et al., 2012). However, I saw no change in *p53* expression, further emphasising that there is no clear increase in double stranded breakages (Figure 3.9C).

Lastly, I looked at inflammatory markers as AGS is a neuro-inflammatory disease. *isg15* was significantly increased in second-generation *rnaseh2a* homozygous embryos (Thomas et al., 2024), however, I saw no changes in *isg15* expression in robust and frail old female brains (Figure 3.10A). No change in *isg15* was seen in 19-month-old first generation *rnaseh2a* homozygous either (Thomas et al., 2024). Other inflammatory markers were also investigated in Thomas's paper; however, they were all non-significant in second- and first-generation fish, except for *il-6* which had a slight decrease in 19-month-old brains. *Il-6* is a well-known inflammatory marker that has been seen to increase with age (Puts et al., 2005, Marcozzi et al., 2023), however, I saw no significant changes in its expression. Further, *il-1b* and *tnfα* are two markers seen to increase as protein in AGS patient's cerebrospinal fluid (CSF) or their plasma (Takanohashi et al., 2013), and I saw no changes in these markers in the frail samples either. I also saw no changes in senescence markers in the brain (Figure 3.10C). However, this is not unexpected as the brain is a non-proliferative tissue, and even though it can go through senescence, it is not as high as other tissues (Yousefzadeh et al., 2020). Further, it might be that both robust and frail brain samples are experiencing senescence and therefore there is not much change. These results suggest that the frail old fish may only be experiencing single stranded breaks due to the rNMPs not being efficiently removed, which is not enough to trigger inflammation or senescence.

The cells in the brain are usually referred to as postmitotic, meaning they do not replicate in adult tissues. Cells might attempt to re-enter the cell cycle upon DNA damage; however, they usually go through cell death at the G1/S checkpoint before any DNA can be synthesised (Frade and Ovejero-Benito, 2015). This means that the cells of the brain do not get the majority of their incorporated rNMPs from DNA replication. Because of this, I decided to investigate a tissue that does replicate its DNA, and I decided on the tail fin due to its easy accessibility. The fin clips from robust and frail of females were equally able to remove the rNMP (Figure 3.11A and B), and I saw a five-to-tenfold increase in the expression of all three subunits of RNaseH2, as well as *rnaseh1*, *fastkd2* and *top1a* (Figure 3.11C and D). I further saw only some PARylation in the robust samples, and no change in double stranded DNA damage signalling by γH2AX (Figure 3.11E). Lastly, potentially contradictory to these findings was some research on 6-month-old klotho wild type and homozygous mutants. KLOTHO is a membrane bound protein that interact with fibroblast growth factor (FGF) receptors and is involved in phosphate metabolism. Lack of KLOTHO causes premature ageing (Kuro-o, 2010, Kuro-o et al., 1997). The fin clips of the *klotho* fish had a reduced ability to cleave the rNMP compared to its sibling (Figure 3.11F and G). This could be due to their accelerated ageing disorder making the ageing phenotype more severe compared to the fish that have lived 3 years (Kuro-o et al., 1997). These findings might suggest that there are still more rNMPs being inserted into the genome, however, the frail cells can remove them efficiently due to an increased expression of the enzymes involved in the process. This might also suggest that the challenge in removing rNMPs in the old frail fish might be either tissue specific or due to the way in which the rNMPs are incorporated, either through DNA repair or DNA replication.

3.3.3. *rnaseh2a* homozygous zebrafish show a frailty phenotype

The aged female zebrafish that had no manipulations done to them regarding the RER pathway, had a decrease in RER pathway activity and potential increase in single stranded DNA damage. Therefore, I wanted to assess how the first-generation *rnaseh2a* homozygous fish aged. Thomas et al., (2024) showed that adult first-generation *rnaseh2a* zebrafish had increased rNMPs in their genome, and they had decreased movement (Thomas et al., 2024). To extend these results, I observed that at two and a half years old there was an increased frailty phenotype in both female and male fish (Figure 3.13). I saw that whilst the wild type siblings were mostly seen as robust, most of the homozygous adults showed at least one of the frailty criteria used in this thesis classifying them as pre-frail. One of the homozygous showed no phenotype, whilst two showed two classifying them as frail. Thomas had reported that at a young adult age, the homozygous fish were equally good at removing rNMPs as their siblings suggesting and alternative mechanism for removing rNMPs. I equally saw that at 3

years, the first-generation homozygous were still able to cleave the rNMP as well as their siblings (Figure 3.14A and B). In addition, I observed no decrease in the expression of the RNaseH2 subunits (Figure 3.14C). I also saw no changes in *rnaseh1* or *top1a* expression as alternative methods to remove these rNMPs (Figure 3.14D). What I did observe however, was a significant increase in *fastkd2* expression. This could suggest that FASTKD2, although considered a mitochondrial protein, might function in the nucleus to remove the rNMPs when RNaseH2 is not functional (Figure 3.14D). This theory is explored further in Chapter 4.

I further saw no significant changes in DNA damage in the old brains, although there was a trend of decreased DNA damage signalling in the homozygous brains (Figure 3.14E). For the frail wild type brains in 3.3.2, there was no difference in DNA damage signalling between robust and frail similar to these findings. This was also seen in a cohort study of adults living in urban area, where they saw no difference in baseline DNA damage between non-frail and frail adults. Although it is contradicted by another cohort study where they saw a study increase of γH2AX with frailty (Valdiglesias et al., 2019, Smith et al., 2023). I also saw an increase in the inflammatory markers *il-6* and *isg15* as well as the senescence marker *p21.* Although this was not significant this could suggest that even though the removal of the rNMPs is efficient, the cells are still struggling with the lack of RNaseH2, causing some inflammation. I have shown that the *rnaseh2a* adult homozygous fish experience more frailty phenotypes and possibly more inflammation that their wild type siblings. However, they do not have a decrease in rNMP removal, suggesting a yet unknown compensatory mechanism or that FASTKD2 is compensating for the lack of RNaseH2 function.

3.3.4. Conclusion

In this Chapter, I have created a frailty scoring index for aged zebrafish which considers BMI, width/length ratio, spinal curvature, cancers and fin regeneration. A conclusion figure showing images of fish that scored robust, pre-frail and frail can be seen in figure 3.15. By using this scoring system, I have shown that old frail females have a potential increase in ribonucleotides in their genome in their brain compared to their robust siblings. This might be due to them having a significant reduction in removal activity of ribonucleotides from double stranded DNA. Potentially because of this, they have in increased occurrence of single stranded but not double stranded DNA brakes which is insufficient to cause an increase in inflammation or senescence. In a proliferative tissue that replicates its DNA such as the tail fin of the fish however, there is a significant increase in expression the subunits of RNaseH2, and the cells are not challenged in removing ribonucleotides, suggesting that the issue might be due to

ribonucleotides incorporated during DNA repair rather than replication. Further, aged first generation *rnaseh2a* homozygous fish show an increased frailty phenotype compared to their wild type siblings, suggesting that the lack of RNaseH2 activity does affect frailty.

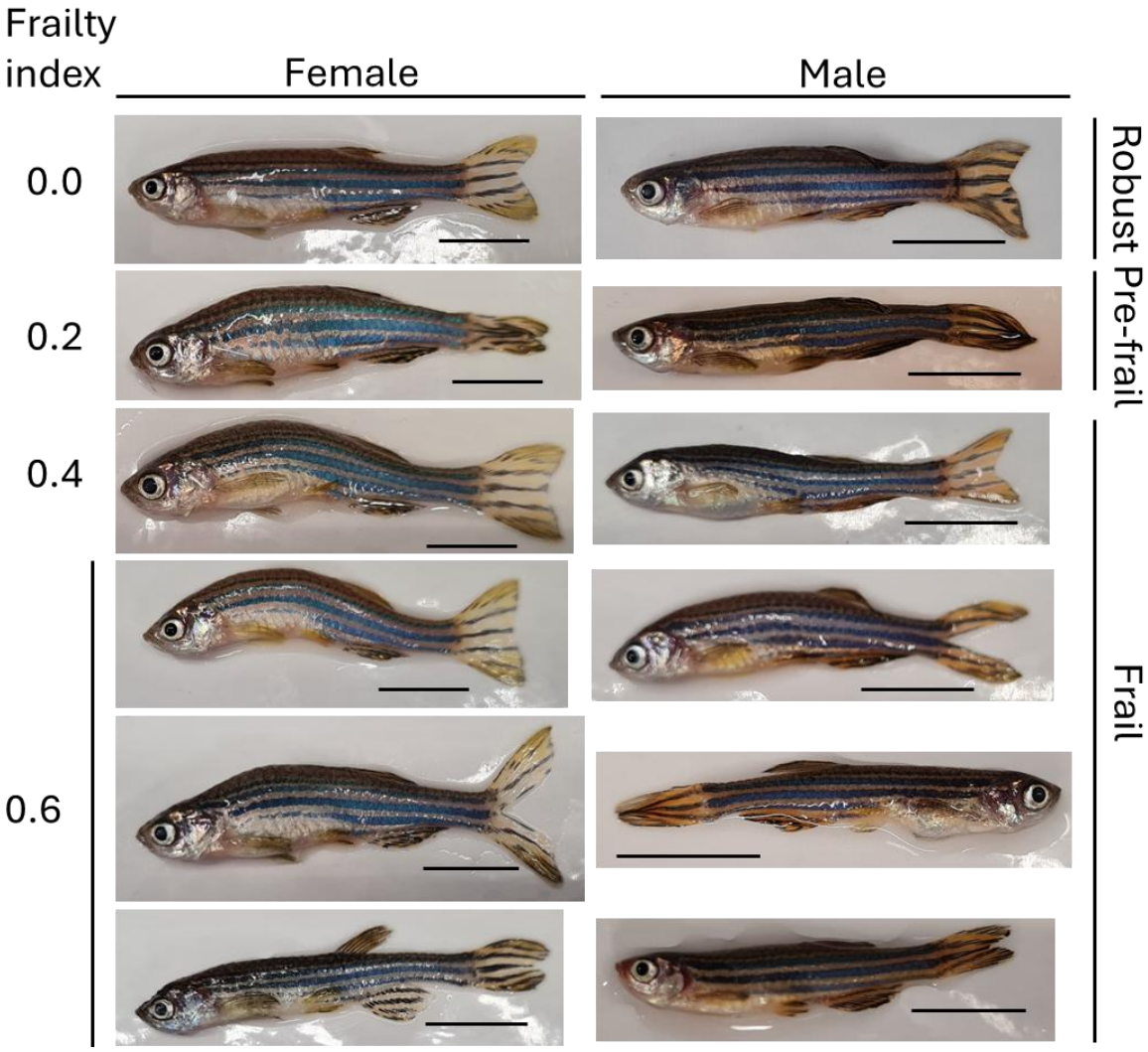

Figure 3.15: Example images of female and male fish that scored robust, pre-frail and frail using the frailty index presented in this thesis.

Chapter 4 Creating a *fastkd2* homozygous mutant to study FASTKD2 involvement in DNA repair and ageing

4.1. Introduction

The mitochondria have several roles in the cell, including regulating cellular stress, and they are central in cellular metabolism and homeostasis. One cell may have many mitochondria, with tissues that require more energy having more (Fernandez-Vizarra et al., 2011). The mitochondria are enclosed by two membranes creating an intermembrane space and a mitochondrial matrix. The outer membrane acts as a barrier towards the cytoplasm whilst the inner membrane contains the protein structures required for oxidative phosphorylation (OXPHOS). The mitochondrial matrix contains the mitochondrial DNA (mtDNA) as well as metabolic products, enzymes, ribosomes and proteins, and is the place of protein biosynthesis, lipid biosynthesis, Krebs cycle, OXPHOS for ATP production and mtDNA replication (Chen et al., 2023). The mtDNA shows a resemblance to its proteobacterial ancestors, where although the majority of the genes have been lost or transferred to the nuclear genome, there is still a 16.5kb circular genome containing the code for 11 mRNAs essential for complex I, III, IV and V of OXPHOS, 22 tRNAs and 2 rRNAs in humans (Kim et al., 2022). Like the nuclear DNA, the mtDNA is subject to damage from endogenous and exogenous factors, and like the nuclear DNA, the mtDNA is hypothesised to have single rNMPs misincorporated by DNA polymerase γ (POLG1). In contrast to the nuclear DNA however, the literature suggests that there is no way to remove these single rNMPs. As a result of these POLG1 errors, there may be as many as 30-60 rNMPs in a mtDNA at any time. In contrast, long stretches of RNA used as primers for replications can be removed by RNaseH1 (Nava et al., 2020). As single rNMPs may be quite damaging to the function of the mitochondria, there are doubts as to whether these rNMPs are in fact “unremovable” or whether they can be removed by a currently unknown mechanism.

The mitochondrial protein Fas-activated serine-threonine kinase domain 2 (FASTKD2) is part of a family of architecturally similar protein in the FAST family coded for in the nuclear DNA. The founder of the family, FAST, was first identified in 1995, where they suggested that FAST is consecutively phosphorylated, then dephosphorylated when Fas, a death receptor from the tumour necrosis factor receptor (TNF-R) superfamily, was ligated to it, activating FAST. They suggested that FAST activation triggered the downstream events in the apoptosis program, thereby linking the FAST family to apoptosis (Tian et al., 1995, Kaufmann et al., 2012).

However, the activation by Fas ligation has since been questioned. It is now believed that in cells experiencing Fas ligation or UV-induced apoptosis, FAST is released from the outer mitochondrial membrane, and it inhibits apoptosis as a survival strategy (Li et al., 2004, Simarro et al., 2010). After Tian's initial discovery it was identified that FAST had a mitochondrial targeting signal (MTS) which was also shared with the other 5 members of the family FASTKD1-5. The members also share three other domains FAST_1, FAST_2 and RAP (Jourdain et al., 2017, Simarro et al., 2010). Whilst the shared FAST_1 and FAST_2 domains' function remain unknown; the RAP domain is predicted to bind RNA (Jourdain et al., 2017). In this thesis, I am interested in FASTKD2, and the location of the domains of FASTKD2 can be seen in figure 4.1.

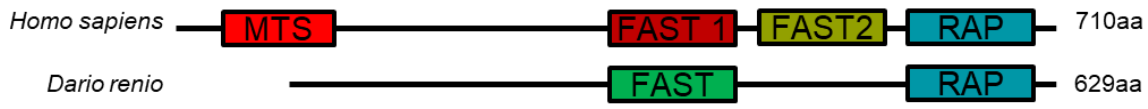

Figure 4.1: Domains of FASTKD2 in humans and zebrafish. The human FASTKD2 has an annotated mitochondrial targeting signal (MTS). The MTS has not been identified in zebrafish, and there is poor sequence homology at the start of the protein. The human protein has annotated FAST_1, FAST_2 and RAP domains, whilst the zebrafish only has an annotated FAST and RAP domain.

FASTKD2 is the only family member that has been linked to a pathology. In 2008, Ghezzi et al, reported on two siblings with a mitochondrial encephalopathy. They were characterized by developmental delay, hemiplegia, convulsions, asymmetrical brain atrophy and low cytochrome c oxidase (COX) activity in the skeletal muscles (Ghezzi et al., 2008). By 2022, there were seven reported cases of patients with gene variations of FASTKD2 (Wu et al., 2022). FASTKD2 has a strong affinity to 16S ribosomal RNA (RNR2) and NADH dehydrogenase subunit 6 (NAD6) messenger RNA transcribed from the mtDNA (Antonicka and Shoubridge, 2015, Popow et al., 2015), as shown by a knockdown and a knockout of FASTKD2 in cells cause a significant reduction in both the 16S ribosome and NAD6 as well as the 7S ribosome. It further showed a reduction in global mitochondrial translation, greater in the knockout than the knockdown. This then leads to a reduction in cellular respiration, in particular a reduction in activity of complex I of which ND6 is a part of. In contrast, complex II is not affected as all its subunits are transcribed by nuclear genes (Popow et al., 2015). Further, Antonicka and Shoubridge showed by mass spectrometry analysis of mitochondrial RNA granules that FASTKD2 was one of the top scoring proteins. By knocking down FASTKD2

in fibroblasts cells, they identified a 45-75% decrease in mitochondrial protein synthesis (Antonicka and Shoubridge, 2015).

Of the FASTKD proteins in the FAST family only FASTKD2 has been associated with pro-apoptotic properties, as FAST itself was first suggested to be. In 2011, Yeung et al, suggested that *fastkd2* can be bound by Death domain 1 interacting factor 1 (DIF-1) at the 5' first exon repressing apoptosis in breast and pancreatic cancer cells. This does not happen in HeLa cells, however. If *fastkd2* is overexpressed in HeLa, the cells go through apoptosis. The apoptotic function of FASTKD2 was also seen to be independent of its mitochondrial localisation (Yeung et al., 2011). This was followed up by testing the other FASTKD family members for apoptotic properties, however, only FASTKD2 was able to cause apoptosis (Das et al., 2014, Wu et al., 2022).

My interest in FASTKD2 stems from preliminary data from Professor Sherif El-Khamisy's lab. In a functional complementation experiment with a human cDNA library, they screened a yeast double mutant for RNaseH1 and RNaseH2 to identify factors that could rescue the mutant. The yeast double mutants are viable, but sensitive to hydroxyurea (HU) which decreases the dNTP pool in the cell, therefore increasing rNTP incorporation (Arudchandran et al., 2000). *fastkd2* was identified as able to rescue this phenotype. Further, Dr Chunyan Liao, a postdoctoral fellow in the El-Khamisy lab, found that cells with a knockdown of *fastkd2* had severe mitochondrial phenotypes, and human FASTKD2 protein purified using *E.coli* were able to cleave rNMPs in vitro (manuscript in preparation). This led to the proposal that FASTKD2 may be a factor that can remove single rNMPs from the mtDNA.

However, the situation appears to be complex, as FASTKD2 has many proposed roles such as RNA processing, apoptosis and DNA repair. Some of these functions are mitochondrial whilst others have been proposed to be independent of its mitochondrial role. Whilst several papers have been published investigating patients with mitochondrial encephalopathy with mutations in *fastkd2,* no published papers describe a mouse model with a knockout mutation in *fastkd2* even though it seems to be viable with a severe phenotype according to the Mouse Genome Informatics (MGI). One paper has been published describing a knockdown of *fastkd2* using morpholinos in zebrafish, where they saw defects in the COX proteins, heart rate and movement. They also saw increased death with increased morpholino, suggesting that a knockout of the gene is lethal (Wei et al., 2020). A potential DNA repair function of FASTKD2 has not been explored in patients or in the zebrafish model. Therefore, despite Wei's

suggestions of lethality with complete knockout, I made a CRISPR/Cas9 knockout model of *fastkd2* to study the whole organism's ability to cleave single rNMPs if FASTKD2 was not functional.

Hypothesis: FASTKD2 can remove single ribonucleotides from the mitochondrial DNA, like RNaseH2 can in the nucleus. Knocking out *fastkd2* from the zebrafish genome, will result in embryos with sickness similar to human patients with *fastkd2* mutations, with a reduced mitochondrial function and a reduced ability to remove single ribonucleotides from the mitochondrial genome.

Aims:

- Create a CRISPR knockout line for *fastkd2* in zebrafish
- Characterise mitochondrial function
- Evaluate the ribonucleotide removal ability of the *fastkd2* homozygous zebrafish

4.2. Results

4.2.1. Creating a *fastkd2* homozygous knockout

Zebrafish, like humans, have one gene for *fastkd2,* which encodes for a 629 amino acid (aa) protein (ENSDART00000108816.4). This is shorter than the 710 aa protein found in humans (ENST00000402774.8), but they still share 35% sequence identity according to a Clustal W alignment on Uniprot.org. The zebrafish FASTKD2 is less annotated than the human protein, and where the human protein has a defined mitochondrial targeting signal (MTS), a FAST 1 and FAST 2 domain and a RAP domain, the zebrafish protein only has a FAST kinase leucine-rich domain and the RAP (Figure 4.2). A comparison between human, mouse (ENSMUST00000027103.7), chicken (ENSGALT00010063051.1), tropical clawed frog (ENSXETT00000061728.3), zebrafish, coelacanth (ENSLACT00000005965.1) and spotted gar (ENSLOCT00000012761.1) FASTKD2 protein sequences can be seen in figure 4.2. There is very low sequence homology at the human MTS for the zebrafish, however, when predicting whether the zebrafish FASTKD2 do localise to the mitochondria with TargetP-2.0, it shows an 81.7% likelihood that the zebrafish FASTKD2 has a mitochondrial transfer peptide (Almagro Armenteros et al., 2019). It is possible that the MTS for FASTKD2 had developed after fish, as there is morehomology with mice and chicken. Although, the spotted gar also seems to

have some homology with humans in the MTS. Using the CRISPR/Cas9 knockout system, I made RNA guides using CHOPCHOP (https://chopchop.cbu.uib.no/) specific for *fastkd2* to cause a nick in exon one of the gene.

None of the injected embryos showed any signs of disease, and a G0 generation of nacre-injected zebrafish was raised. A fish with a 132bp insertion and a 1bp deletion, referred to as a 131bp insertion was chosen as a founder. This line had an early stop codon at one base into the insertion (Figure 4.3A). By comparing the 131bp insertion to the whole genome of the zebrafish, part of the insertion shared a sequence similarity to an intron in *mdh1b* about 1500bp downstream of *fastkd2* (Figure 4.3B and C). It was therefore likely that there was an attempt at alternative end-joining (alt-EJ) or microhomology-mediated end-joining (MMEJ) (Thyme and Schier, 2016) with a different part of the chromosome. After raising an F1 homozygous generation and inbreeding them, the embryos showed no phenotype and were viable. To further verify that the knockout did not cause a morphological phenotype, a second mutant line with a 5bp deletion was raised which also did not show a morphological phenotype. This mutant had an early stop codon 64bp after the deletion (Figure 4.3D). The 5dpf larvae of the 131bp insertion and the 5bp deletion is shown in figure 4.4A and B, which shows that the larvae look similar to their wild type cousins. A qPCR showed that both lines had a reduced expression of *fastkd2* (Figure 4.4C). Adult *fastkd2* homozygous zebrafish did not show any viasual phenotypes either (Figure 4.30). A whole mount in situ hybridisation (WISH) of a heterozygous *fastkd2* cross showed that *fastkd2* was highly expressed in the brain, such as at the midbrain-hindbrain boundary and in the hindbrain, as well as in the notochord, the pronephros and weakly in the muscles (Figure 4.4D). The WISH also suggests that there was reduced expression of *fastkd2* according to a Mendelian ratio (Figure 4.4E). However, I was not able to genotype these embryos due to the colour development procedure.

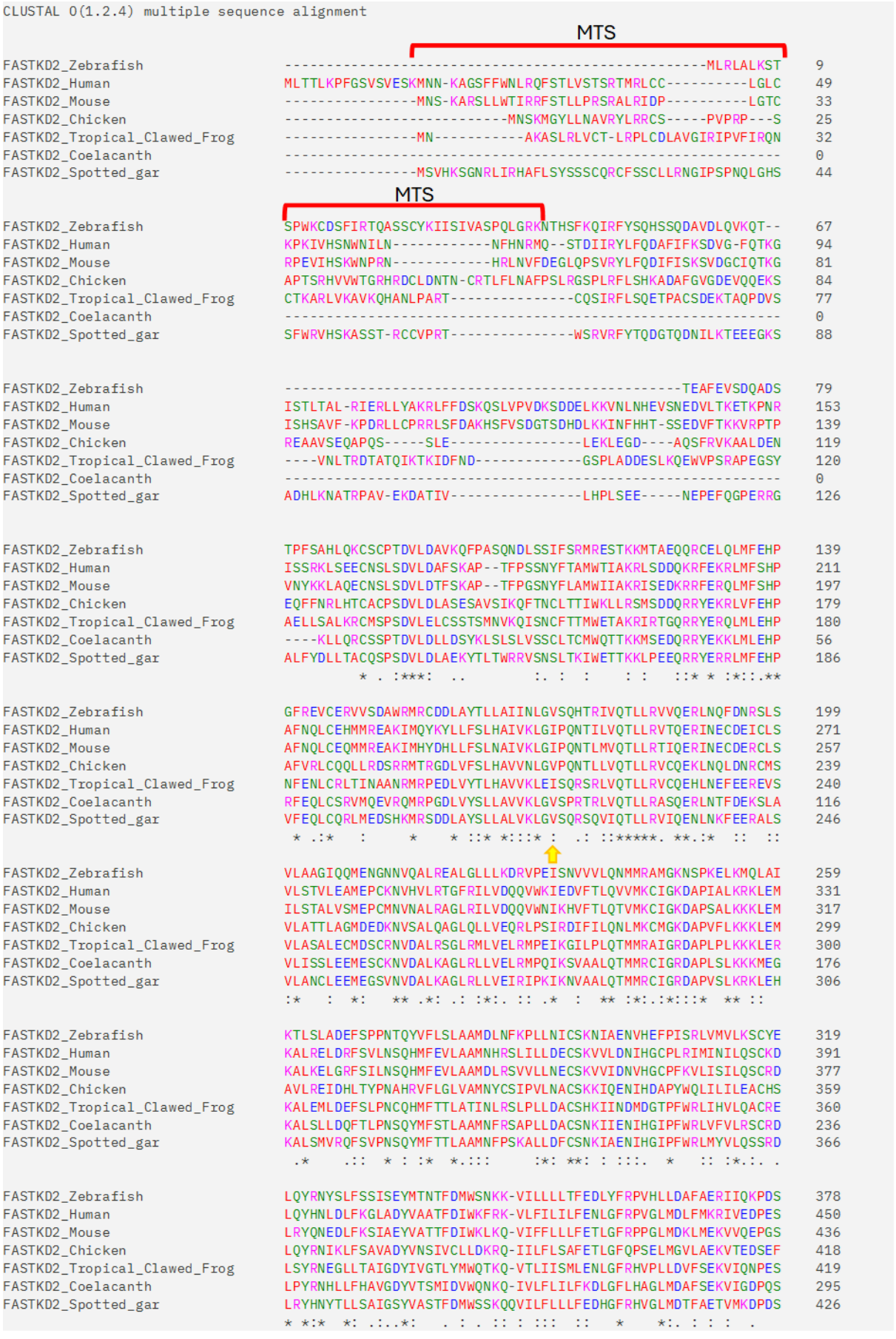
CLUSTAL O(1.2.4) multiple sequence alignment
MTS
MTS
FASTKD2_Zebrafish ----------MLRLALKST 9
FASTKD2_Human MLTTLKPFGSVSVESKMNN-KAGSFFWNLRQFSTLVSTSRTMRLCC----------LGLC 49
FASTKD2_Mouse ----------MNS-KARSLLWTIRRFSTLLPRSRALRIDP----------LGTC 33
FASTKD2_Chicken ----------MNSKMGYLLNAVRYLRRCS-----PVPRP---S 25
FASTKD2_Tropical_Clawed_Frog ----------MN----------AKASLRLVCT-LRPLCDLAVGIRIPVFIRQN 32
FASTKD2_Coelacanth ---------- 0
FASTKD2_Spotted_gar ----------MSVHKSGNRLIRHAFLSYSSSCQRCFSSCLLRNGIPSPNQLGHS 44
FASTKD2_Zebrafish SPWKCDSFIRTQASSCYKIISIVASPQLGRKNTHSFKQIRFYSQHSSQDAVDLQVKQT-- 67
FASTKD2_Human KPKIVHSNWNILN----------NFHNRMQ--STDIIRYLFQDAFIFKSDVG-FQTKG 94
FASTKD2_Mouse RPEVIHSKWNPRN----------HRLNVFDEGLQPSVRYLFQDIFISKSVDGCIQTKG 81
FASTKD2_Chicken APTSRHVVWTGRHRDCLDNTN-CRTLFLNAFPSLRGSPLRFLSHKADAFGVGDEVQQEKS 84
FASTKD2_Tropical_Clawed_Frog CTKARLVKAVKQHANLPART----------CQSIRFLSQETPACSDEKTAQPDVS 77
FASTKD2_Coelacanth ---------- 0
FASTKD2_Spotted_gar SFWRVHSKASST-RCCVPRT----------WSRVRFYTQDGTQDNILKTEEEGKS 88
FASTKD2_Zebrafish ----------TEAFEVSDQADS 79
FASTKD2_Human ISTLTAL-RIERLLYAKRLFFDSKQSLVPVDKSDDELKKVNLNHEVSNEDVLTKETKPNR 153
FASTKD2_Mouse ISHSAVF-KPDRLLCPRRLSFDAKHSFVSDGTSDHDLKKINFHHT-SSEDVFTKKVRPTP 139
FASTKD2_Chicken REAAVSEQAPQS-----SLE----------LEKLEGD----AQSFRVKAALDEN 119
FASTKD2_Tropical_Clawed_Frog ----VNLTRDTATQIKTKIDFND----------GSPLADDESLKQEWVPSRAPEGSY 120
FASTKD2_Coelacanth ---------- 0
FASTKD2_Spotted_gar ADHLKNATRPAV-EKDATIV----------LHPLSEE-----NEPEFQGPERRG 126
FASTKD2_Zebrafish TPFSAHLQKCSCPTDVLDAVKQFPASQNDLSSIFSRMRESTKKMTAEQQRCELQLMFEHP 139
FASTKD2_Human ISSRKLSEECNSLSDVLDAFSKAP--TFPSSNYFTAMWTIAKRLSDDQKRFEKRLMFSHP 211
FASTKD2_Mouse VNYKKLAQECNSLSDVLDTFSKAP--TFPGSNYFLAMWIIAKRISEDKRRFERQLMFSHP 197
FASTKD2_Chicken EQFFNRLHTCACPSDVLDLASESAVSIKQFTNCLTTIWKLLRSMSDDQRRYEKRLVFEHP 179
FASTKD2_Tropical_Clawed_Frog AELLSALKRCMSPSDVLELCSSTSMNVKQISNCFTTMWETAKRIRTGQRRYERQLMLEHP 180
FASTKD2_Coelacanth ----KLLQRCSSPTDVLDLLDSYKLSLSLVSSCLTCMWQTTKKMSEDQRRYEKKLMLEHP 56
FASTKD2_Spotted_gar ALFYDLLTACQSPSDVLDLAEKYTLTWRRVSNSLTKIWETTKKLPEEQRRYERRLMFEHP 186
FASTKD2_Zebrafish GFREVCERVVSDAWRMRCDDLAYTLLAIINLGVSQHTRIVQTLLRVVQERLNQFDNRSLS 199
FASTKD2_Human AFNQLCEHMMREAKIMQYKYLLFSLHAIVKLGIPQNTILVQTLLRVTQERINECDEICLS 271
FASTKD2_Mouse AFNQLCEQMMREAKIMHYDHLLFSLNAIVKLGIPQNTLMVQTLLRTIQERINECDERCLS 257
FASTKD2_Chicken AFVRLCQQLLRDSRRMTRGDLVFSLHAVVNLGVPQNTLLVQTLLRVCQEKLNQLDNRCMS 239
FASTKD2_Tropical_Clawed_Frog NFENLCRLTINAANRMRPEDLVYTLHAVVKLEISQRSRLVQTLLRVCQEHLNEFEEREVS 240
FASTKD2_Coelacanth RFEQLCSRVMQEVRQMRPGDLVYSLLAVVKLGVSPRTRLVQTLLRASQERLNTFDEKSLA 116
FASTKD2_Spotted_gar VFEQLCQRLMEDSHKMRSDDLAYSLLALVKLGVSQRSQVIQTLLRVIQENLNKFEERALS 246
FASTKD2_Zebrafish VLAAGIQQMENGNNVQALREALGLLLKDRVPEISNVVVLQNMMRAMGKNSPKELKMQLAI 259
FASTKD2_Human VLSTVLEAMEPCKNVHVLRTGFRILVDQQVWKIEDVFTLQVVMKCIGKDAPIALKRKLEM 331
FASTKD2_Mouse ILSTALVSMEPCMNVNALRAGLRILVDQQVWNIKHVFTLQTVMKCIGKDAPSALKKKLEM 317
FASTKD2_Chicken VLATTLAGMDEDKNVSALQAGLQLLVEQRLPSIRDIFILQNLMKCMGKDAPVFLKKKLEM 299
FASTKD2_Tropical_Clawed_Frog VLASALECMDSCRNVDALRSGLRMLVELRMPEIKGILPLQTMMRAIGRDAPLPLKKKLER 300
FASTKD2_Coelacanth VLISSLEEMESCKNVDALKAGLRLLVELRMPQIKSVAALQTMMRCIGRDAPLSLKKKMEG 176
FASTKD2_Spotted_gar VLANCLEEMEGSVNVDALKAGLRLLVEIRIPKIKNVAALQTMMRCIGRDAPVSLKRKLEH 306
FASTKD2_Zebrafish KTLSLADEFSPPNTQYVFLSLAAMDLNFKPLLNICSKNIAENVHEFPISRLVMVLKSCYE 319
FASTKD2_Human KALRELDRFSVLNSQHMFEVLAAMNHRSLILLDECSKVVLDNIHGCPLRIMINILQSCKD 391
FASTKD2_Mouse KALKELGRFSILNSQHMFEVLAAMDLRSVVLLNECSKVVIDNVHGCPFKVLISILQSCRD 377
FASTKD2_Chicken AVLREIDHLTYPNAHRVFLGLVAMNYCSIPVLNACSKKIQENIHDAPYWQLILILEACHS 359
FASTKD2_Tropical_Clawed_Frog KALEMLDEFSLPNCQHMFTTLATINLRSLPLLDACSHKIINDMDGTPFWRLIHVLQACRE 360
FASTKD2_Coelacanth KALSLLDQFTLPNSQYMFSTLAAMNFRSAPLLDACSNKIIENIHGIPFWRLVFVLRSCRD 236
FASTKD2_Spotted_gar KALSMVRQFSVPNSQYMFTTLAAMNFPSKALLDFCSNKIAENIHGIPFWRLMYVLQSSRD 366
FASTKD2_Zebrafish LQYRNYSLFSSISEYMTNTFDMWSNKK-VILLLLTFEDLYFRPVHLLDAFAERIIQKPDS 378
FASTKD2_Human LQYHNLDLFKGLADYVAATFDIWKFRK-VLFILILFENLGFRPVGLMDLFMKRIVEDPES 450
FASTKD2_Mouse LRYQNEDLFKSIAEYVATTFDIWKLKQ-VIFFLLLFETLGFRPPGLMDKLMEKVVQEPGS 436
FASTKD2_Chicken LQYRNIKLFSAVADYVNSIVCLLDKRQ-IILFLSAFETLGFQPSELMGVLAEKVTEDSEF 418
FASTKD2_Tropical_Clawed_Frog LSYRNEGLLTAIGDYIVGTLYMWQTKQ-VTLIISMLENLGFRHVPLLDVFSEKVIQNPES 419
FASTKD2_Coelacanth LPYRNHLLFHAVGDYVTSMIDVWQNKQ-IVLFLILFKDLGFLHAGLMDAFSEKVIGDPQS 295
FASTKD2_Spotted_gar LRYHNYTLLSAIGSYVASTFDMWSSKQQVILFLLLFEDHGFRHVGLMDTFAETVMKDPDS 426

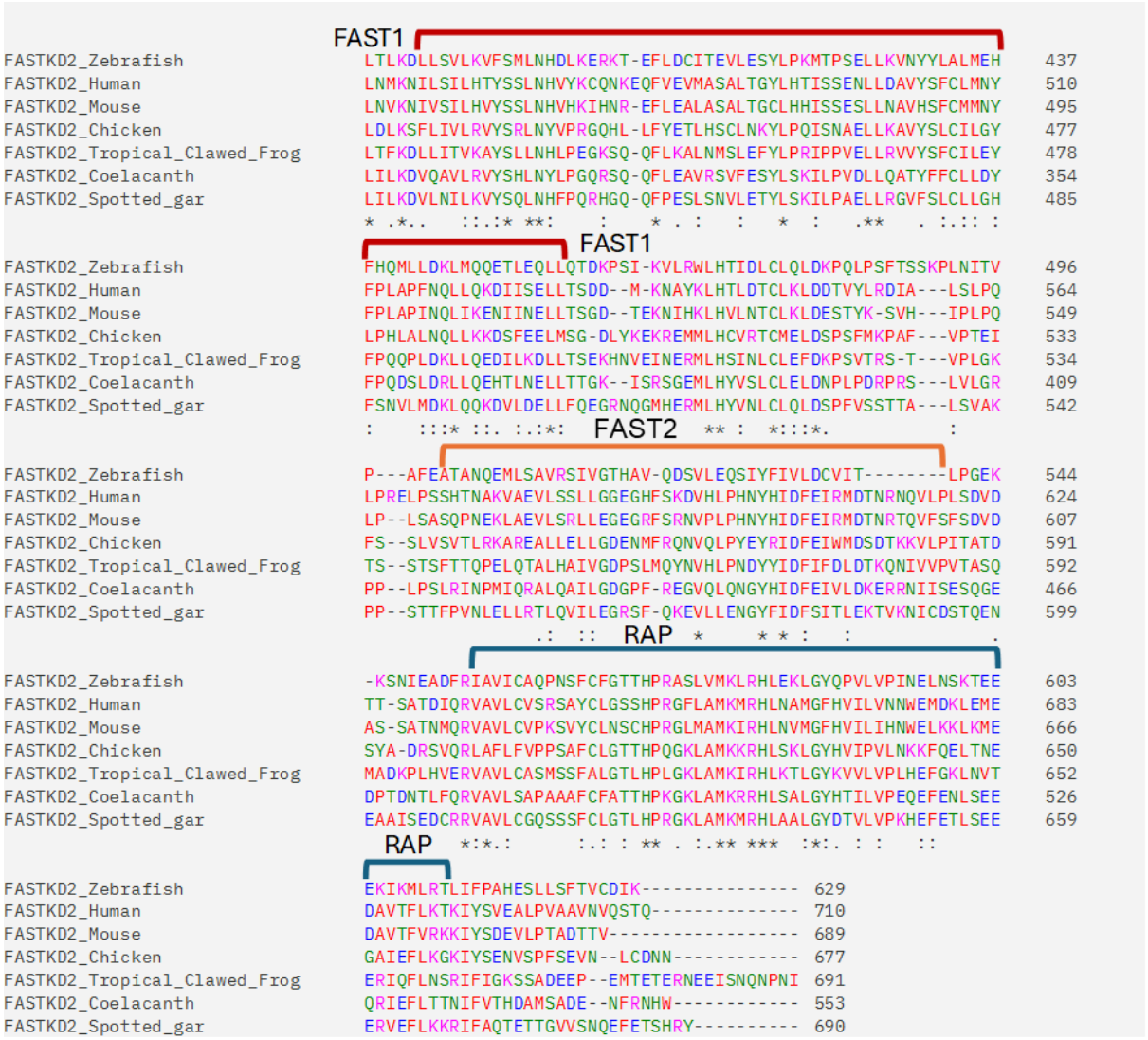

Figure 4.2: Comparison of human, chicken, mouse, tropical clawed frog, zebrafish, coelacanth and spotted gar FASTKD2 protein. Comparison performed using EMBL-EBI clustal omega multiple sequence alignment. Stars indicate same amino acid. Two dots and one dot indicate similar amino acids. Red amino are small hydrophobic amino acids, blue are acidic amino acids, magenta are basic amino acids and green are hydroxyls, sulfhydryl and amine amino acids (Madeira et al., 2024). Yellow arrow indicates the site of the mutation in the zebrafish genome. Highlighted are the human mitochondrial targeting signal (MTS) in red, human FAST1 domain in dark read, human FAST2 domain in orange and the RAP domain in blue. The mutation site in the 131bp and the 5bp zebrafish lines is marked with a yellow arrow.

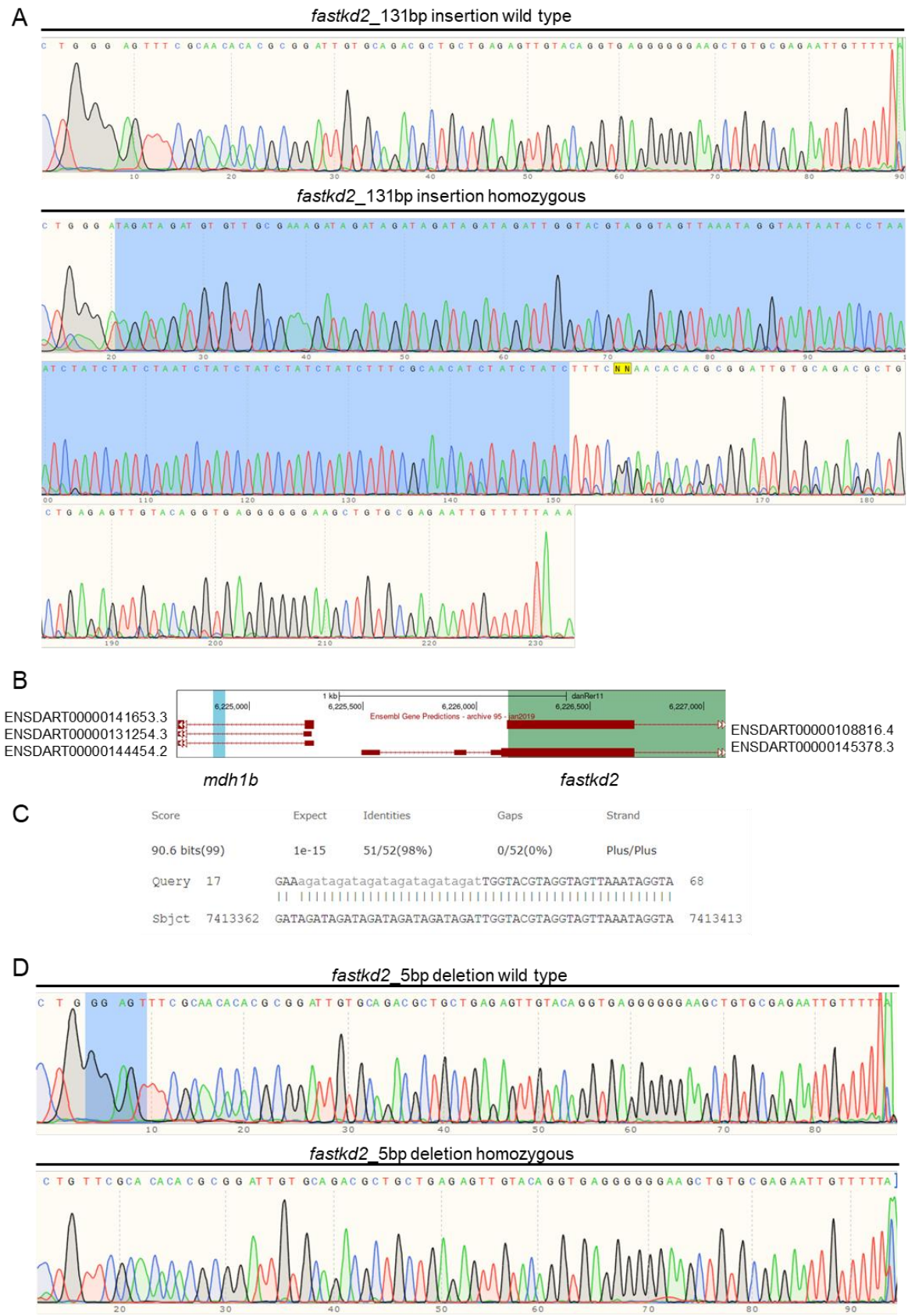

Figure 4.3: Sequence comparison between wild type and mutant siblings *fastkd2* lines. A: 131bp insertion line comparison showing wild type sequence at top and the 131bp insertion highlighted in blue in the homozygous at the bottom. B: Genome browser image showing

proximity of *mdh1b* to *fastkd2*. Potential insertion sequence is highlighted in blue. C: Sequence comparison between parts of 131bp insertion and *mdh1b*. D: 5 bp deletion line comparison showing wild type sequence at top and 5bp deletion highlighted in blue in the wild type sequence compared to the homozygous at the bottom.

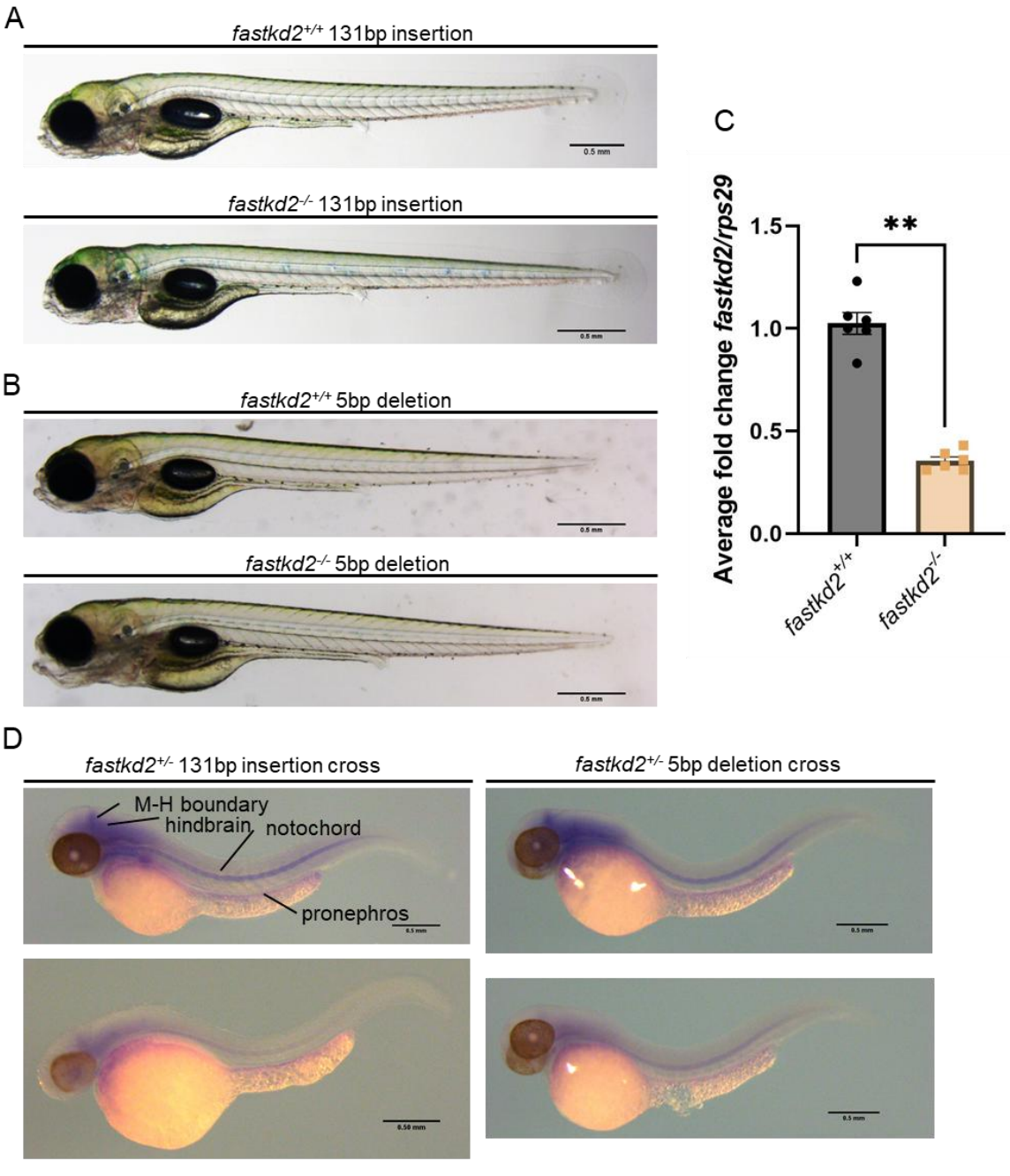

E

	Nr of 131bp insertion	Nr of 5bp deletion
Colour development	16	13
No colour development	4	2

Figure 4.4: *fastkd2* homozygous larvae do not show a morphological phenotype up to 5dpf. A: Wild type and homozygous cousins from the *fastkd2* 131bp insertion line. B: Wild type and homozygous cousins from the *fastkd2* 5bp deletion line. C: Combined qPCR from 131bp insertion and 5bp deletion line showing a significant reduction in *fastkd2* mRNA in 5dpf homozygous larvae. Unpaired t-test, n=6. D: Whole in situ hybridization for *fastkd2* expression in 2dpf embryo. Expression shown at the midbrain-hindbrain (M-H) boundary, in the hindbrain, notochord and pronephros. Weak expression along muscles. The WISH probe is after the mutation site, done on heterozygous crosses. Example images from same plates of colour development for 131bp insertion heterozygous larvae and 5dp deletion heterozygous larvae. E: Table showing the number of larvae with and without colour after 18 days of colour development.

4.2.2. *fastkd2* mutants have decreased expression of several *fastk* members

As the *faskd2* larvae and adult fish do not have any morphological defects, I considered whether any of the other FASTK family members were compensating for the lack of FASTKD2. When using uniprot's BLAST align tool, it suggested that zebrafish *fastkd2* and *fastkd1* specifically were related (Figure 4.5A). However, a qPCR for expression of the four *fastk* members found in zebrafish showed that there was no compensation, rather that a knockout of *fastkd2* results in a significant reduction in *fastkd1*, *fastkd3* and *fastkd4*. No difference was seen in *fastk* (Figure 4.5B). I was not able to identify *fastkd5* in the zebrafish genome.

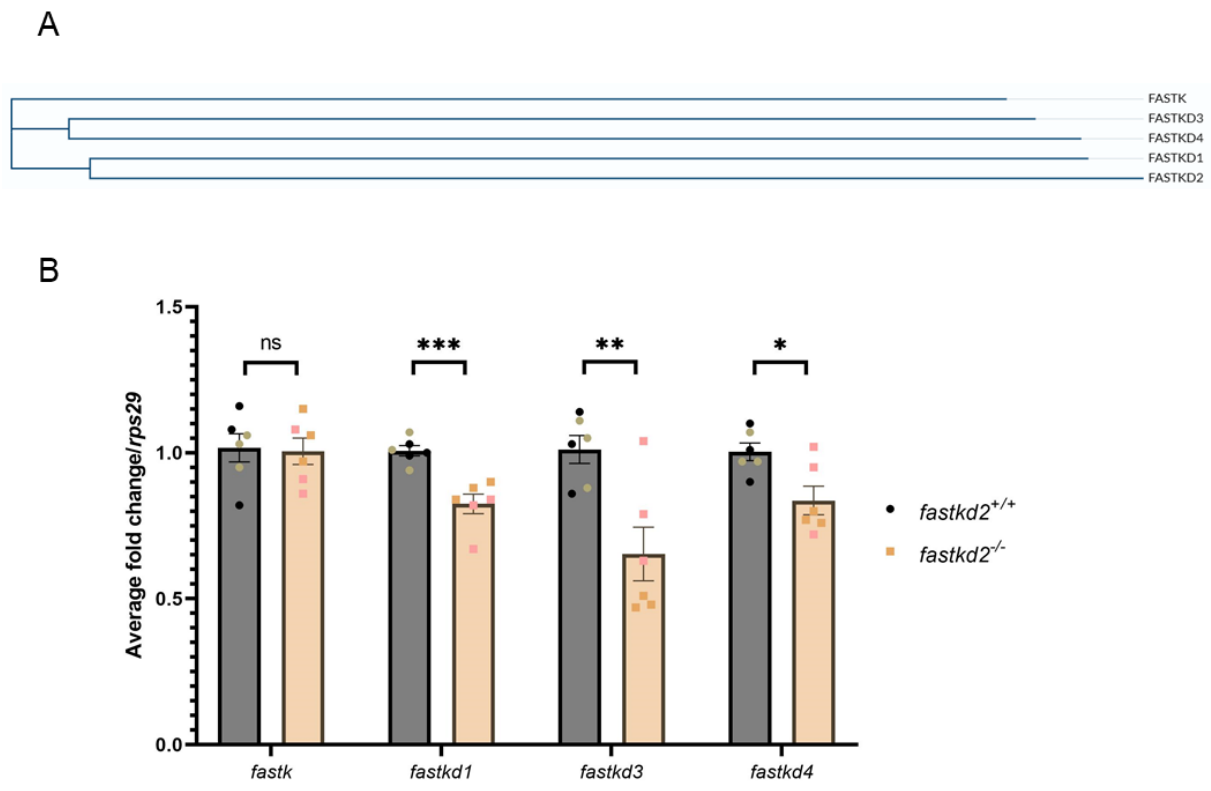

Figure 4.5: FASK family members do not compensate for the lack of *fastkd2*. A: Phylogenetic tree showing that the FASK family members found in zebrafish are related, with high relation between *fastkd2* and *fastkd1*. Uniport BLAST align. Protein sequence from ensamble.org. B: qPCR for *fastk* (ENSDART00000134125.2), *fastkd1* (ENSDART00000141405.2), *fastkd3* (ENSDART00000168888.2) and *fastkd4 (tbrg4)* (ENSDART00000180804.1). Unpaired t-test, n=6. Black = Wild type 131bp insertion. Green = Wild type 5bp deletion. Yellow = Homozygous 131bp insertion. Pink = Homozygous 5bp deletion.

4.2.3. *fastkd2* knockouts larvae do not change their behaviour

As a *fastkd2* morpholino mutant had been made before by Wei (Wei et al., 2020), it was appropriate to evaluate the observations made in their paper. They observed no changes in movement in response to light and dark stimuli at 48hpf. My mutants survive past day 5, therefore, I looked at movement in response to light and dark stimuli at day 5. Like Wei, I observed no difference between wild type *fastkd2* and homozygous *fastkd2* larvae in the time or the distance they moved (Figure 4.6A-C). Further, Wei looked at the response the embryos had to a touch stimulus. At 48hpf, they saw a decrease in the distance the embryos would move after being touched. Here, I observed no difference at 48hpf in how far the embryos moved (Figure 4.6D). I also wanted to see what the older larvae at 5dpf would do when touched, however, due to them being more mobile, I decided to look at how long it would take

the larvae to rest after being disturbed. Here I observed no difference in the time it took for the wild type and the homozygous larvae to stop moving either (Figure 4.6E). Wei also reported a decrease in heart rate at 48hpf. I looked at the heart rate at 5dpf and saw no difference in the beats per minute (BPM) (Figure 4.6F).

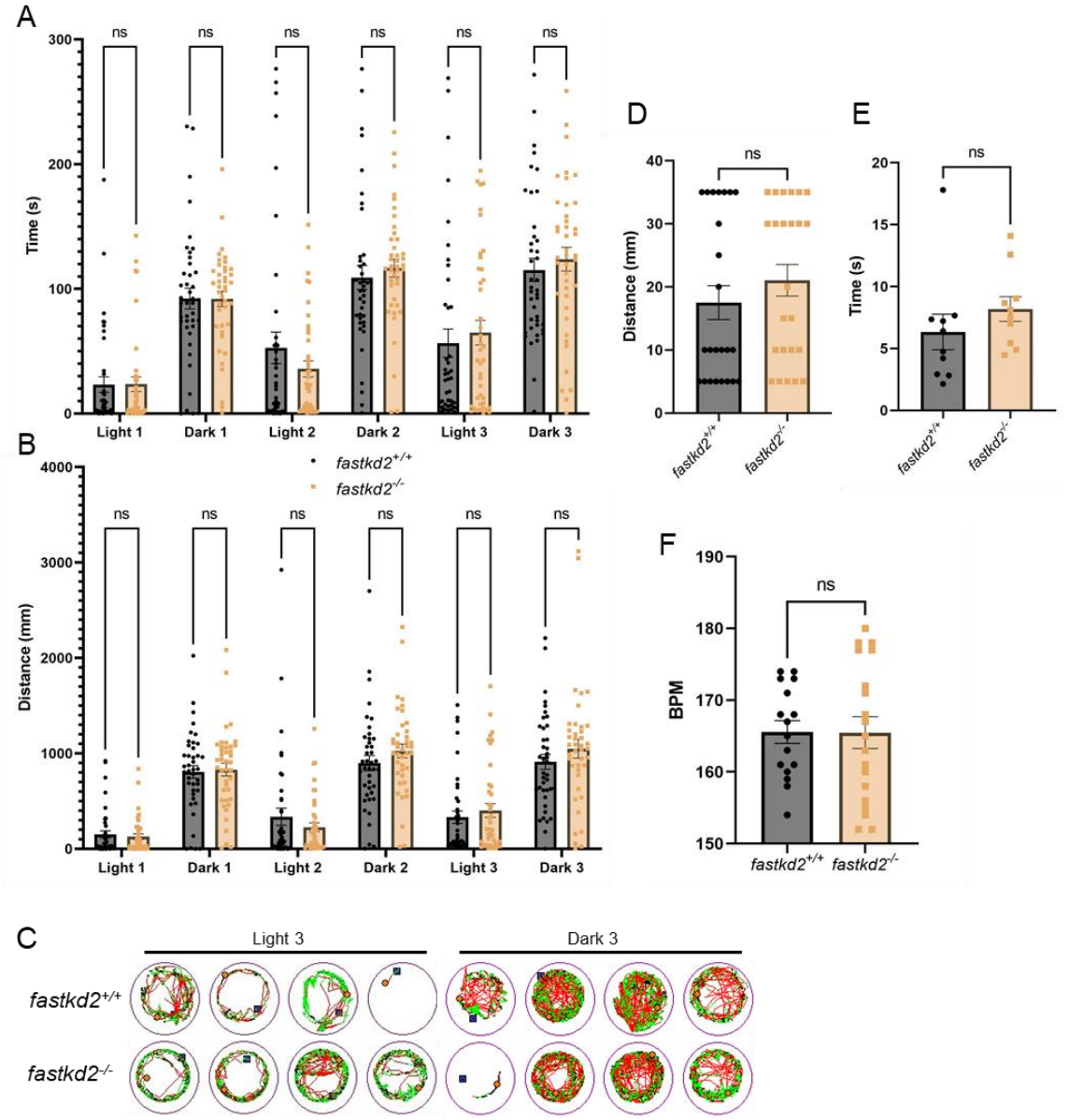

Figure 4.6: Various movement analysis and heart rate analysis on the 131bp insertion mutant as performed in Wei et al., 2019. A: Amount of time (s) 5dpf wild type and homozygous larvae spent moving in 3 cycles of 5 minutes light or dark, n=41. B: Distance (mm) moved by 5dpf wild type and homozygous larvae in 3 cycles of 5 minutes light or dark, n=41. C: Examples of movement by four wild type and four homozygous 5dpf larvae in the final cycle of light and dark. Green represents small movement, and red represents large movement. The yellow

circle is the larvae. D: Distance (mm) 48hpf wild type and homozygous larvae moved after being touched by a seeker, n=24. E: Time (s) it took for wild type and homozygous 5dpf larvae to settle down after being touched by a seeker, n=10. F: Average beats per minutes (BPM) in wild type and homozygous 5dpf larvae, n=16 wild type, n=19 homozygous. Unpaired t-test.

4.2.4. *fastkd2* knockouts are sensitive to PTZ

A known characteristic of the patients with *fastkd2* mutations is an increased tendency of epileptic seizures (Wu et al., 2022). Pentylenetetrazol (PTZ) has been shown to cause epileptic seizures in zebrafish larvae (Baxendale et al., 2012), with the greatest effect of the drug at 40mM, 20mM and 10mM. Here I used the same concentrations of PTZ, 1.25mM, 2.5mM, 5mM, 10mM, 20mM, 40mM and 80mM, however, I did not see any significant differences in movement between wild type and homozygous *fastkd2* larvae (Figure 4.7). In Baxendales's paper they show the average movement over the 10 minutes, 5-10 minutes after the addition of the PTZ.

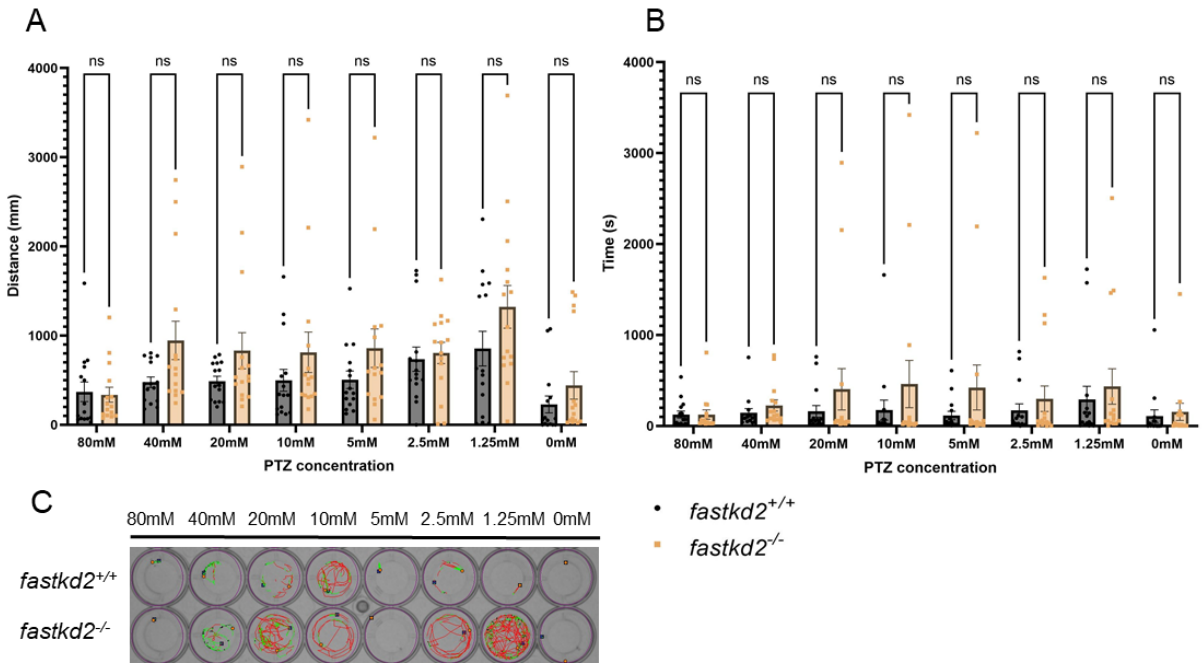

Figure 4.7: Movement analysis on 4dpf larvae treated with increasing concentrations of PTZ. A: Total distance (mm) moved during 10 minutes of 2-minute light dark cycles by larvae 10 minutes after treatment with PTZ from 1.25mM to 80mM. B: Total time (s) spent moving during 10 minutes of 2-minute light dark cycles moving by the larvae 10 minutes after treatment with PTZ from 1.25mM to 80mM. C: Example of larvae movement. Green represents small movement and red represents large movement. Yellow dot is the larvae. 2-way ANOVA, n=15.

4.2.5. *fastkd2* knockouts have a reduced mitochondrial volume and function

fastkd2 is transcribed in the nucleus and transported to the inner mitochondrial membrane where it is important for normal mitochondrial function. Therefore, I wanted to assess what a lack of *fastkd2* would do to the shape and number of mitochondria. I made a mitochondrial zebrafish reporter line which marks all mitochondria with neon fluoresces. A LR reaction was performed with the *ubiquitin* promoter (*ub*i), a polyadenylation signal in the 3'UTR for stabilisation, a tet2pA2 empty vector and a zmLOC100282174 fused to mNeon middle entry clone from Dr Stone Elworthy. A digest with HindII and SpeI confirmed the LR reaction had worked (Figure 4.8A). Figure 4.8B shows the predicted expression clone plasmid map (Snapgene). Injected larvae that showed any neon expression were raised and outcrossed to AB wild types. Figure 4.8C shows uniform neon expression in the F1 larvae. The Mit_2_neon larvae were outcrossed to *fastkd2* homozygous adults to create heterozygous adults for *fastkd2* with a mitochondrial neon expression.

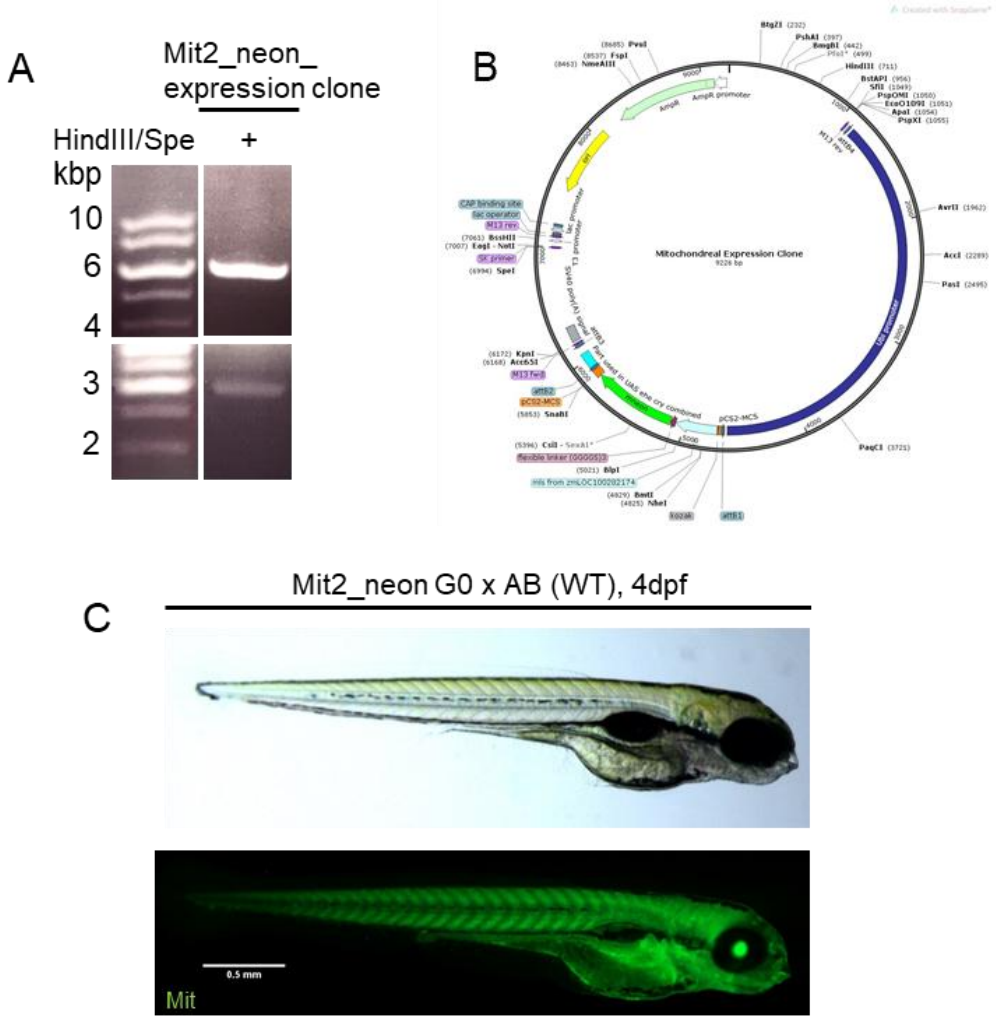

Figure 4.8: Mit2_Neon_expression clone and embryo injections. A: Digestion with HindIII and SpeI after LR reaction with zmLOC100282174 fused to mNeon from Dr Stone Elworthy, *ubi* promoter, a polyadenylation signal in the 3'UTR for stabilisation, and empty vector tet2pA2 (9226bp). B: Predicted plasmid map of Mit2_neon_expression clone. C: Mit2_neon_expression clone injected embryos outcrossed with AB (wild type) transmit the plasmid into the F1 generation. Mit=mitochondria.

Heterozygous adults for *fastkd2* who transmitted the Neon-tagged mitochondria were outcrossed to *fastkd2* wild types or homozygous adults. The tails of the 5dpf larvae were mounted and the heads genotyped to identify which were wild type, heterozygous and homozygous. Wild type and homozygous tails were imaged on a spinning disk microscope using a 100x silicon lens, and the image stacks analysed in Arivis. Figure 4.9A and B show 3D and 2D images of the mitochondria in green and the nucleus in blue for wild type and homozygous *fastkd2*. All images were taken over the anus. The images propose that there was a small but significant decrease in the volume of the mitochondria of the homozygous larvae (Figure 4.9C). The shape of the homozygous mitochondria did not change when compared to the wild type (Figure 4.9D). Neither did the number of mitochondria (Figure 4.9E).

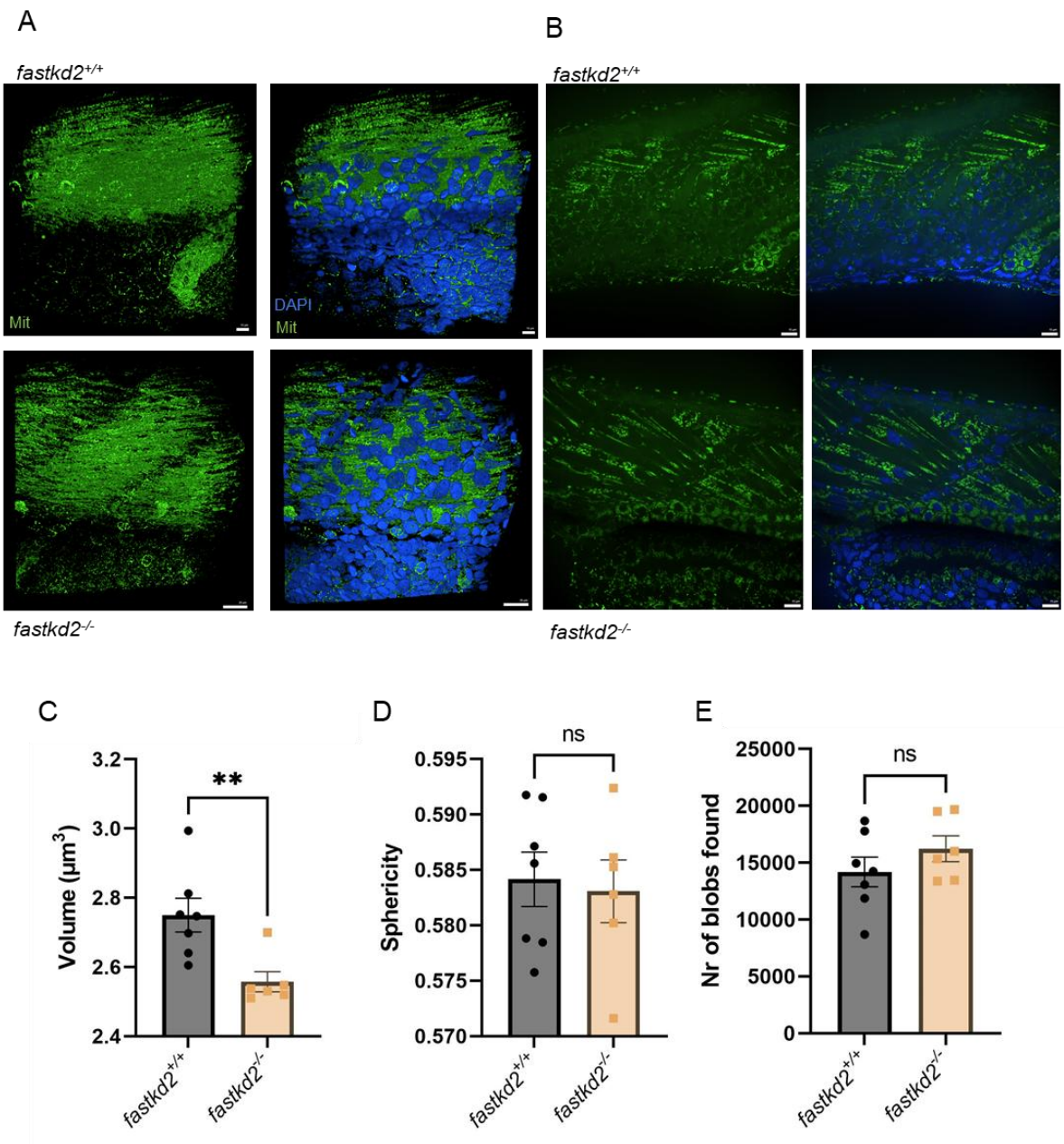

Figure 4.9: Mitochondrial phenotype of *fastkd2* homozygous larvae. A: 3D images of wild type and homozygous larvae mitochondria in green and nucleus in blue. B: 2D images of wild type and homozygous larvae mitochondria. C: Volume of the mitochondria of wild type and homozygous larvae. D: Sphericity of the mitochondria of wild type and homozygous larvae. E: Number of mitochondria (blobs) found by the Arivis program for wild type and homozygous larvae. Unpaired t-test, n=7 wild type, n=6 homozygous, scale bar = standard error. Mit = mitochondria. DAPI = nucleus.

With the reduced size of the mitochondria of the larvae, I also saw a reduced mitochondrial function when looking at mass spectrometry data performed by Dr Kari Fladmark, a

collaborator at the University of Bergen, on my wild type and homozygous *fastkd2* larvae and adult brains (Figure 4.10A-D). For the 5dpf larvae, there was an increased NAD+/NADH, NADP+/NADPH, AMP/ATP and ADP/ATP ratio in the homozygotes, indicating that the mitochondria might be challenged in converting the NAD+ and NADP+ to NADH and NADPH respectively, as well as converting AMP and ADP to ATP. For the adult homozygous zebrafish, I did not see the same significance. However, there may be a trend of a reduced NAD+/NADH and NADP+/NADPH ratio. The adult did also follow a trend similar to the significance of the larvae for the AMP/ATP and ADP/ATP ratio, where they did have an increased ratio. However, this was not significant with the p-value for the AMP/ATP ratio being 0.1535, and for the ADP/ATP ratio being 0.0779. Further, several proteins in the mitochondria required for energy production have been reported in patients with *fastkd2* mutations to be reduced. I looked at the expression of some of those genes via qPCR, and only saw a significant reduction in *polg1*, and no change in *mt-nd1, mt-nd6, cox1, cox4* and *rnr2* (16S rRNA) (Figure 4.11A). However, when I looked at the protein expression of COX IV in the 5dpf larvae and brains of 29-month-old adult wild types and homozygous *fastkd2* 131bp fish I did see a reduction in the protein, although not significant (Figure 4.11B and C).

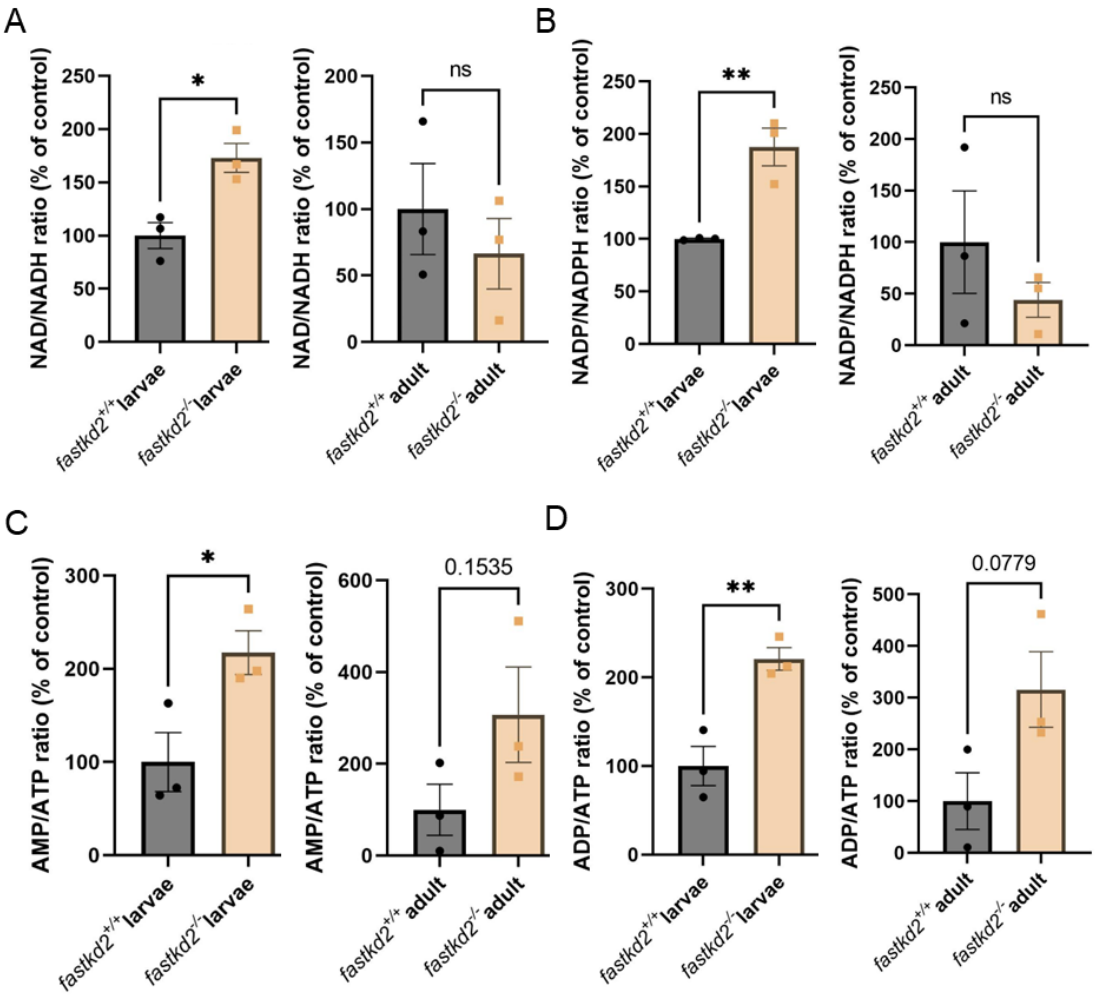

Figure 4.10: Reduced energy production in *fastkd2* homozygous larvae. A: NAD+/NADH ratio for 5dpf larvae and brain of 7-month-old adults. B: NADP+/NADPH ratio for 5dpf larvae and brain of 7-month-old adults. C: AMP/ATP ratio for 5dpf larvae and brain of 7-month-old adults. D: ADP/ATP ratio for 5dpf larvae and brain of 7-month-old adults. Unpaired t-test, n=3.

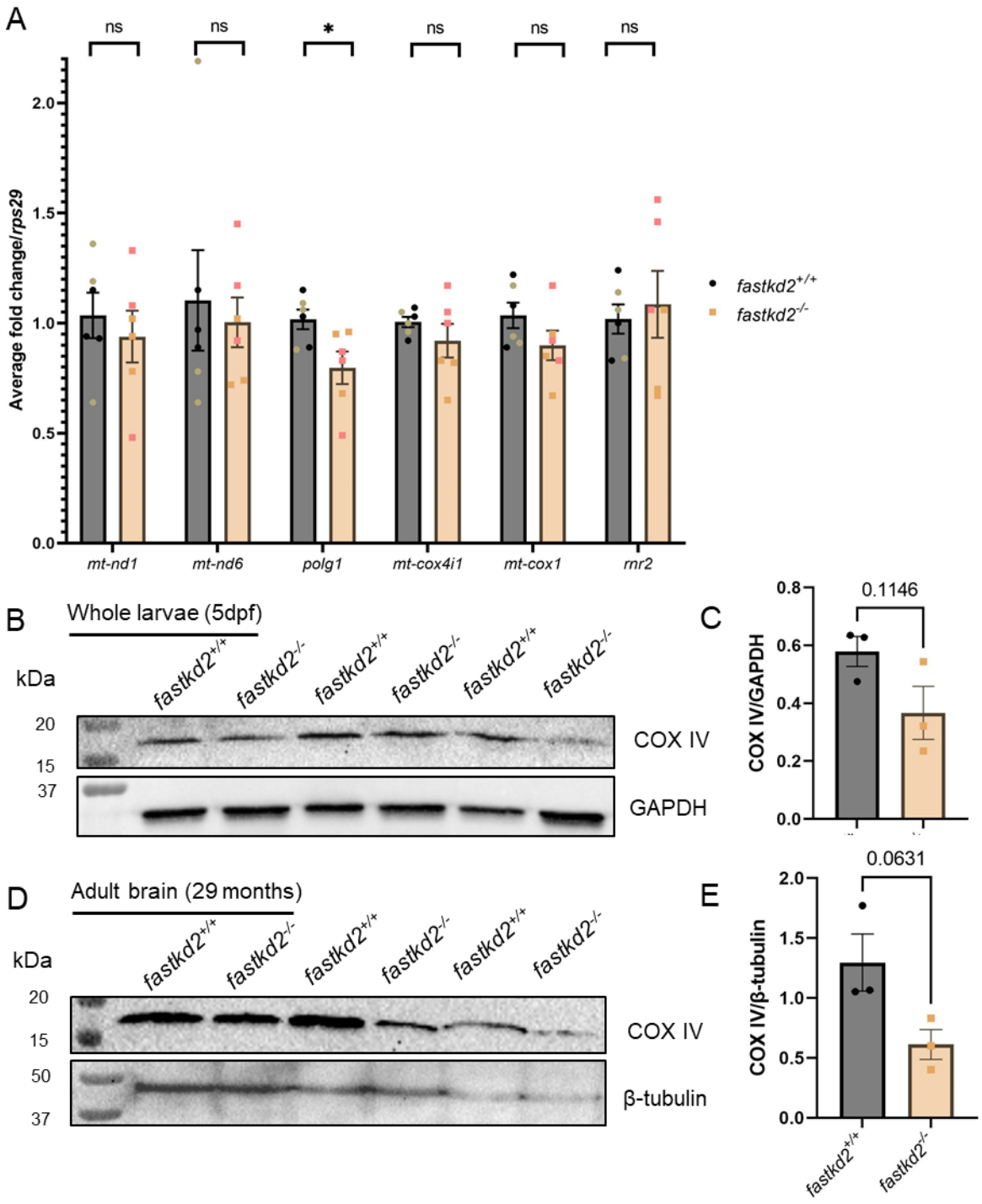

Figure 4.11: Expression of some nuclear genes for mitochondrial proteins and mitochondrial genes in wild type and homozygous larvae and adult 29-month-old brains protein. A: qPCR of mitochondrial proteins *mt-nd1*, *mt-nd6*, *polg1*, *mt-cox4i1* and *RNR2* (16S rRNA) for *fastkd2* wild type and homozygous. Unpaired t-test, n=6. Black = Wild type 131bp insertion. Green = Wild type 5bp deletion. Yellow = Homozygous 131bp insertion. Pink = Homozygous 5bp deletion. B: Western blot for whole protein of wild type and homozygous 5dpf larvae for COX

IV and GAPDH. C: Quantification of larval COX IV. D: Western blot of adult brains for COX IV and β-tubulin. E: Quantification of adult brain COX IV. Unpaired t-test, n=3.

4.2.6. Adult *fastkd2* homozygous zebrafish swim at the top of the tank

When moving the tanks with the *fastkd2* homozygous adults for pair mating, I observed that the fish preferred to swim at the top of the water in the tank compared to the wild type adults who would swim through all the water (Figure 4.12A). They also had an increased tendency to jump out of the tank when on the bench compared to the wild type. It is important to note that this was only seen with one tank of fish there was only one tank of homozygous *fastkd2* adults. Therefore, it is possible that something else could have been wrong with the tank, such as oxygen level. Although, the fish were swapped to new tanks throughout their lifespan and the behaviour did not change. To investigate this behaviour further, I did an adult movement analysis looking at their swimming in the whole tank versus the top of the tank for 5 hours. The first hour of the analysis was immediately after disturbance such as walking in front of the fish and closing the door to the videoing room. Whilst all the adults moved an equal amount in the whole tank (arena) (Figure 4.12B and C), the adult female homozygous fish had significantly increased movement in the top part of the tank compared to the wild type females (Figure 4.12D). This behaviour was not observed in the homozygous adult male fish who moved the same distance as the wild type males in the top of the tank (Figure 4.12E). When combining all the female and the male fish, there was no significant increase in the distance the fish move at the top of the tank, however, there was still a trend in the homozygous fish moving more at the top (Figure 12F).

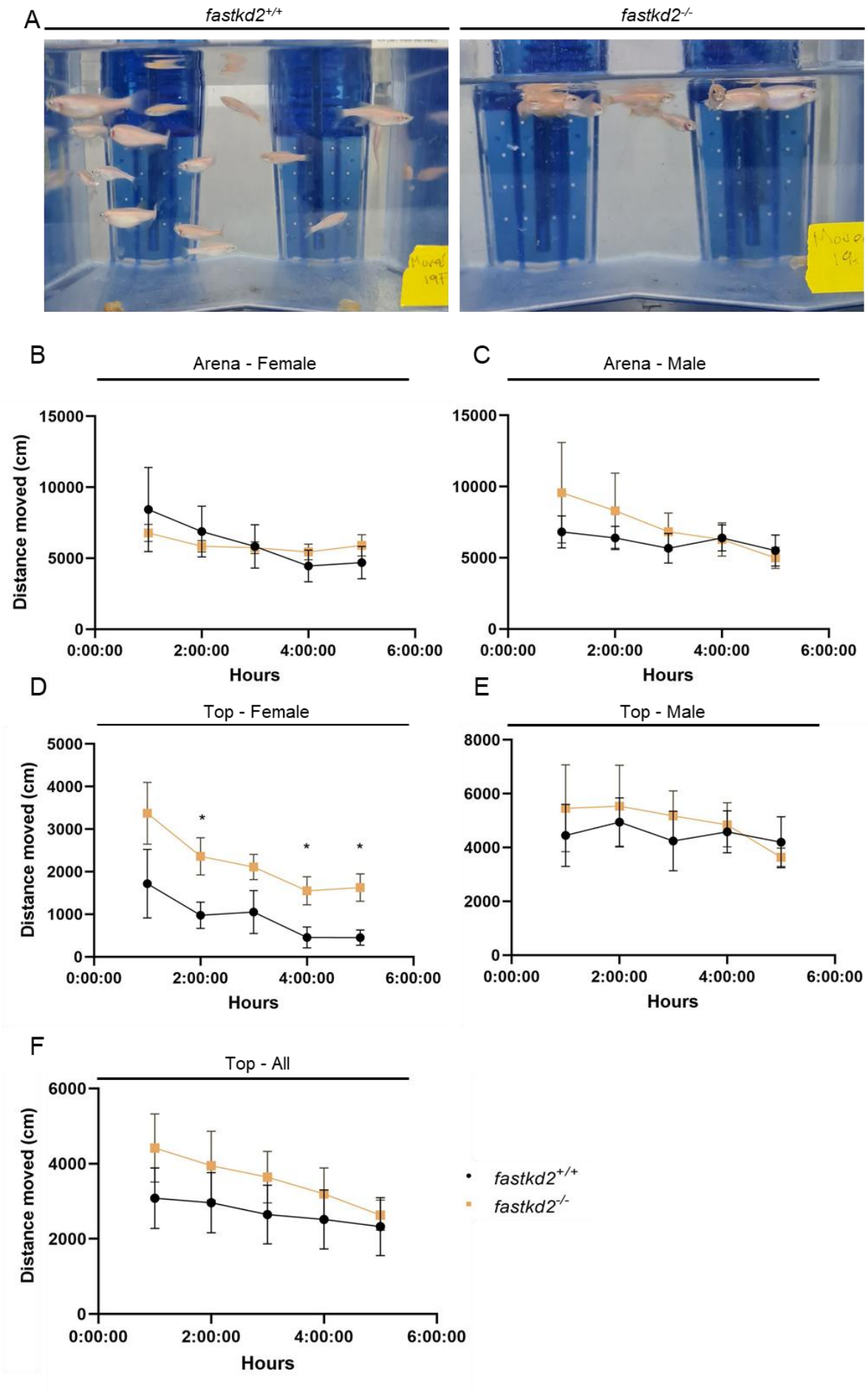
A
fastkd2+/+
fastkd2-/-
B
Arena - Female
C
Arena - Male
Distance moved (cm)
15000
10000
5000
0
0:00:00
2:00:00
4:00:00
6:00:00
Hours
D
Top - Female
E
Top - Male
8000
6000
4000
2000
F
Top - All
fastkd2+/+
fastkd2-/-

Figure 4.12: Tank behaviour by *fastkd2* wild type and homozygous adult fish. A: Pictures of observed behaviour of *fastkd2* 131bp insertion adult homozygous fish. When the tanks of the *fastkd2* homozygous were handled, the homozygous adults swam at the top of the tank compared to the wild types who would swim throughout the whole tank. Their water levels were also kept lower than usual when handled due to an increase in jumping out of the tank compared to wild type. B-D: Distance (cm) moved by adult *fastkd2* wild type and homozygous (20 months) in the arena and at the top for 5 hours. The first hour is acclimation after a disturbance. B: Distance (cm) moved in the arena by female adults, n=5. C: Distance (cm) moved in the arena by male adults, n=5. D: Distance (cm) moved at the top by female adults, n=5. E: Distance (cm) moved at the top by male adults, n=5. F: Movement by all adults at the top of the tank. Unpaired t-test at time points.

To attempt to identify why the female fish swam at the top of the tank I did a cognitive memory test of the fish using a Free-movement pattern (FMP) Y-maze. The FMP Y-maze is an effective tool to study executive function such as working memory and behavioural plasticity. It is an alternative to a blocked arm Y-mazes and T-mazes which require a period of learning or habituation before the experiment, which could mean that organisms with increased anxiety or locomotion difficulties could be heard to interpret (Cleal et al., 2021). Using the FMP Y-maze for the *fastkd2* adults was explored after a discussion with Dr Ada Jimenez-Gonzalez who studies amyotrophic lateral sclerosis (ALS) in Dr Andrew Grierson's lab at the University of Sheffield. Her adult fish have a reduced swim capacity, as well as a preference to swim at the top of the tank potentially due to a lack of remembering that swimming at the top of the tank is dangerous. By using a FMP Y-maze, she has shown a reduced cognitive memory in their ALS fish by showing a reduced level of non-random left-right-left-right (LRLR) or right-left-right-left (RLRL) maze choices. The *fastkd2* homozygous and wild type sibling fish however, due to their age of 28 months, were considerably larger than the ALS fish. The length of the fish was therefore the same length of the Y-arm of the Y-maze. This did lead to a considerable number of fish being miss tracked and having to be excluded from the study leaving an n-number of 4 for the wild types and 3 for the homozygous *fastkd2* fish. There was no significant reduction in LRLR or RLRL choices amongst the fish. However, a trend with a decreased LRLR or RLRL choices amongst the homozygous fish was observed particularly amongst the LRLR choices (Figure 4.13A). The total number of decisions and the total distance the homozygous and wild type fish made was equal (Figure 4.13B and C).

Further, considering the decrease in energy conversion in the larvae and potential reduction the adults, I also wanted to assess whether this had an impact on their swimming capacity. I used male and female wild type and homozygous *fastkd2* adults at 26 months in a swim tunnel that showed a decreased swimming capacity of the homozygous fish compared to their wild type siblings (Figure 4.13D). Male wild type and homozygous fish had a significantly greater swim capacity than the female fish, and the decrease in swim capacity was greater amongst the female fish.

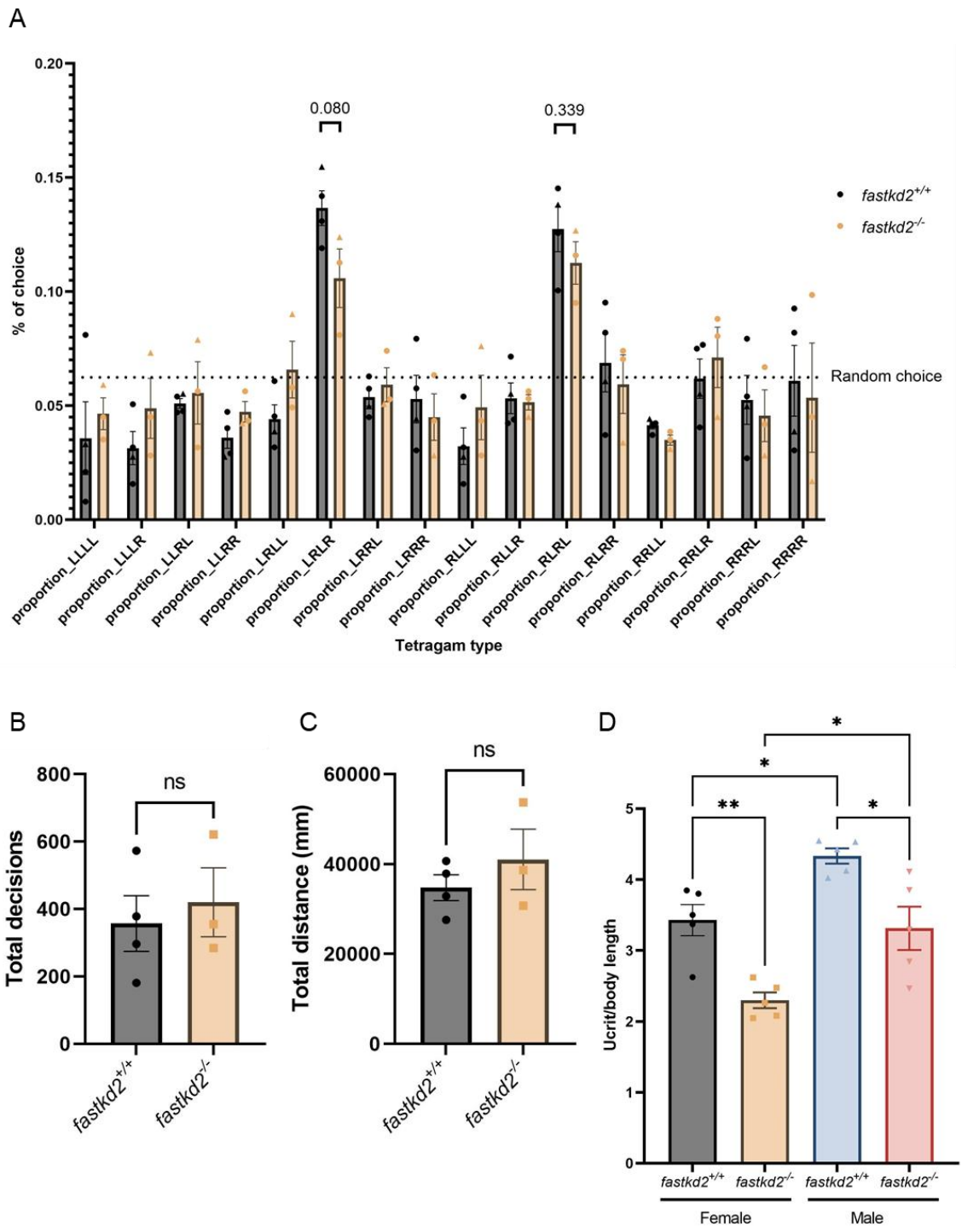

Figure 4.13: Cognitive and motor tests of aged adult *fastkd2* knockout and wild type zebrafish. A: Percentage occurrence of tetragram choices during a Y-maze recording of 1 hour. Filled circle = male fish, filled triangle = female fish. B: Total decisions made by fish during Y-maze. C: Total distance swam by fish during Y-maze. Unpaired t-test, n=4 wild type, n=3 homozygous. D: Swim tunnel assay showing the Ucrit/body length of female and male *fastkd2* wild type and homozygous adults. One-way ANOVA, n=5 female and 5 male.

4.2.7. *fastkd2* homozygous larvae has no baseline increased DNA damage

rnaseh2 second-generation homozygous embryos have increased baseline DNA damage due to the incorporated rNMPs not being removed, the rNMPs are cleaved by other molecules in the nucleus or by TOP1 and cause a strand breakage (Thomas et al., 2024). As I am investigating whether FASTKD2 performs the role of RNaseH2 but in the mitochondria, I wondered what the baseline DNA damage load was in the *fastkd2* larvae. Immunofluorescence for γH2AX on the tails of 5dpf larvae showed no difference in the number of γH2AX foci in the nucleus of the wild type and homozygous *fastkd2* (Figure 4.14A and B). Further, a western blot for γH2AX on 5dpf lysate from whole larvae showed a decrease in γH2AX in the mutant, although not significant (Figure 4.14C and D). Whilst a western blot on 29-month aged adult brains showed no increase in γH2AX (Figure 4.14E and F). There was also no PARylation as seen in the larvae or the adult *fastkd2* fish as has been seen in frail old fish and second-generation *rnaseh2a* homozygotes embryos (Chapter 3.2.5). As there was no baseline damage in the *fastkd2* line, I tested if the larvae would have increased DNA damage if I challenged them with the DNA damaging agent Camptothecin (CPT). 4dpf larvae were treated with either 0.1% DMSO or 500nM CMP overnight before being lysed. Whilst there was a significant increase in γH2AX after CPT treatment in both wild type and homozygous larvae, there was no difference in double stranded damage between the two (Figure 4.15). Increased PARylation at high kDa could be seen in two of the three wild type CPT treated larvae, but not in the homozygous. Whilst some PARylation at 50kDa could be seen in all CPT treated samples (Figure 4.15A).

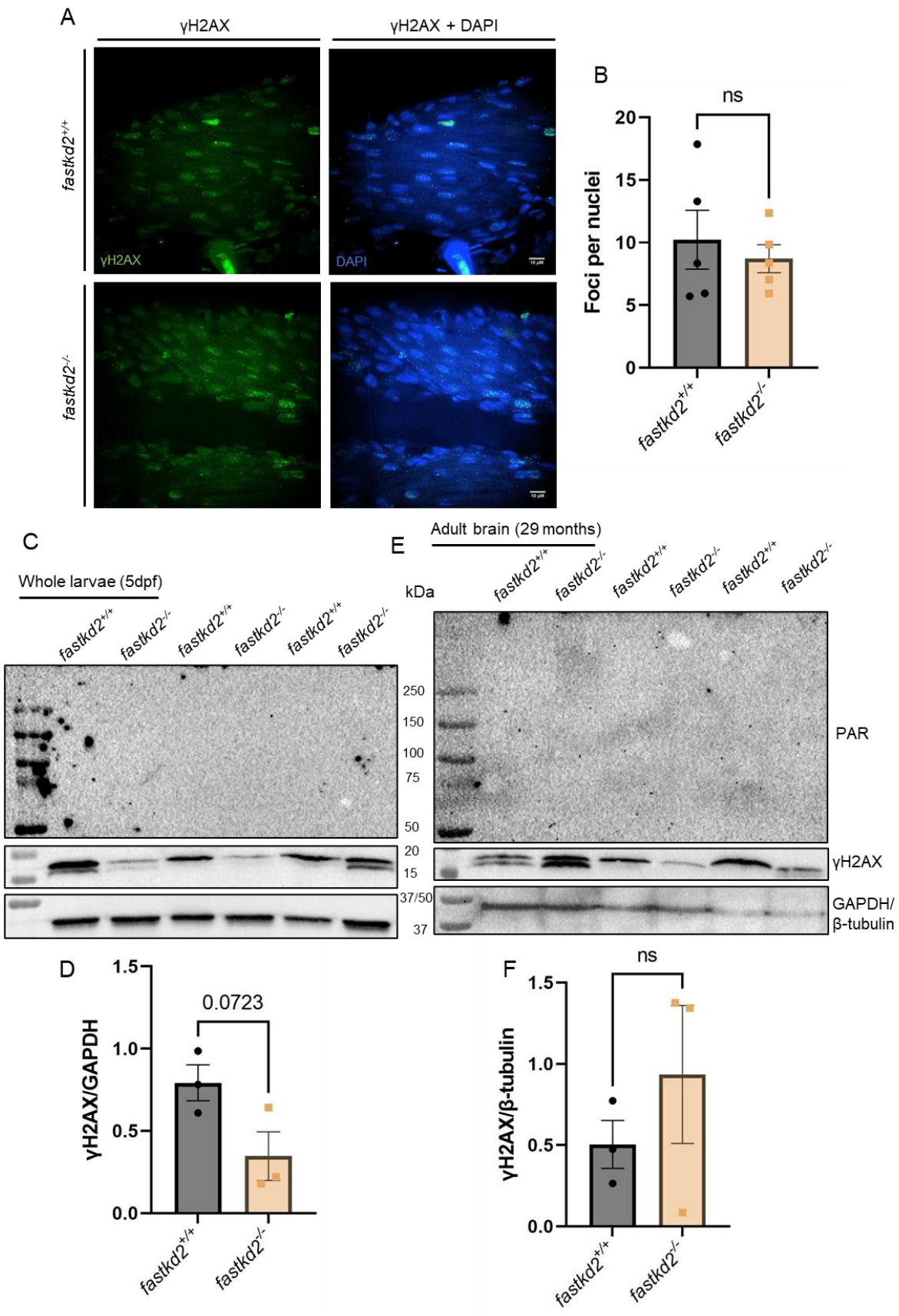

Figure 4.14: Baseline DNA damage in *fastkd2* wild type and homozygous larvae and adult brains. A: γH2AX immunofluorescence in tail muscle of 5dpf wild type and homozygous

larvae. Nuclei are stained blue with DAPI and the γH2AX is shown with GFP. B: Quantification of the number of γH2AX foci per nuclei in wild type and homozygous. Unpaired t-test, n=5. C: Western blot for PAR, γH2AX and GAPDH in whole 5dpf larvae lysate. D: Quantification of γH2AX in larvae. E: Western blot for PAR, γH2AX and β-tubulin in 29-month-old adult wild type and homozygous brains. F: Quantification of γH2AX in adult brains. Unpaired t-test, n=3.

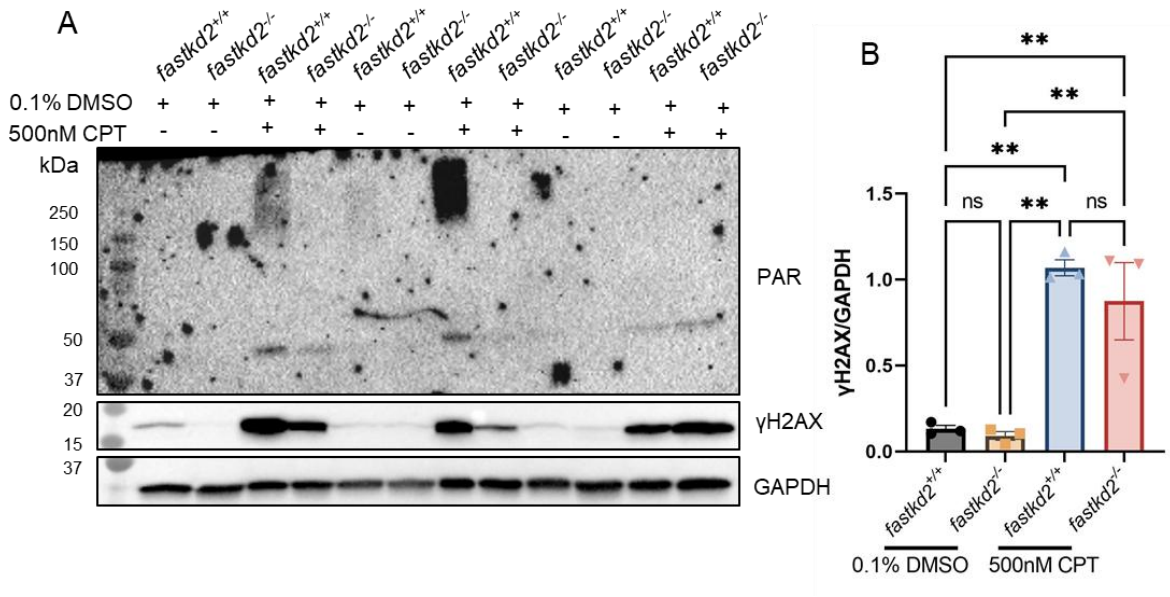

Figure 4.15: DNA damage in 5dpf larvae after 0.1% DMSO or 500nM CPT treatment for 24h at 4dpf wild type and homozygous larvae. A: Western blot for PAR, γH2AX and GAPDH for wild type and homozygous larvae. B: Quantification of γH2AX. One-way ANOVA, n=3.

The *rnaseh2a* second-generation homozygous embryos also show an increase in apoptosis through acridine orange staining (Thomas et al., 2024). Further, FASTKD2 has been implicated in apoptosis. Therefore, I decided to look at apoptosis of 5dpf *fastkd2* homozygous larvae. Considering there was no change in baseline DNA damage when looking at western blots, I decided to treat the larvae with CPT to induce DNA damage and potentially apoptosis. 4dpf larvae were treated with 0.1% DMSO or 500nM CPT overnight and then treated with acridine orange. Whilst there was no difference in apoptotic cells between the wild type and the homozygous larvae when treated with DMSO, there was a significant increase in apoptotic cells in both wild type and homozygous larvae after treatment. However, there were significantly less apoptotic cells in the treated homozygous larvae compared to the wild type treated larvae (Figure 4.16). There are a few problems with using acridine orange with zebrafish. Zebrafish often autofluores, meaning there might be some non-specific readings. There can also be significant differences in staining between embryos treated in the same

way, making quantification challenging, and it would therefore require a large sample size. Further, one can question whether what you see is actually single cells that are going through apoptosis. It is also therefore important to keep the measurements consistent between groups that you are comparing.

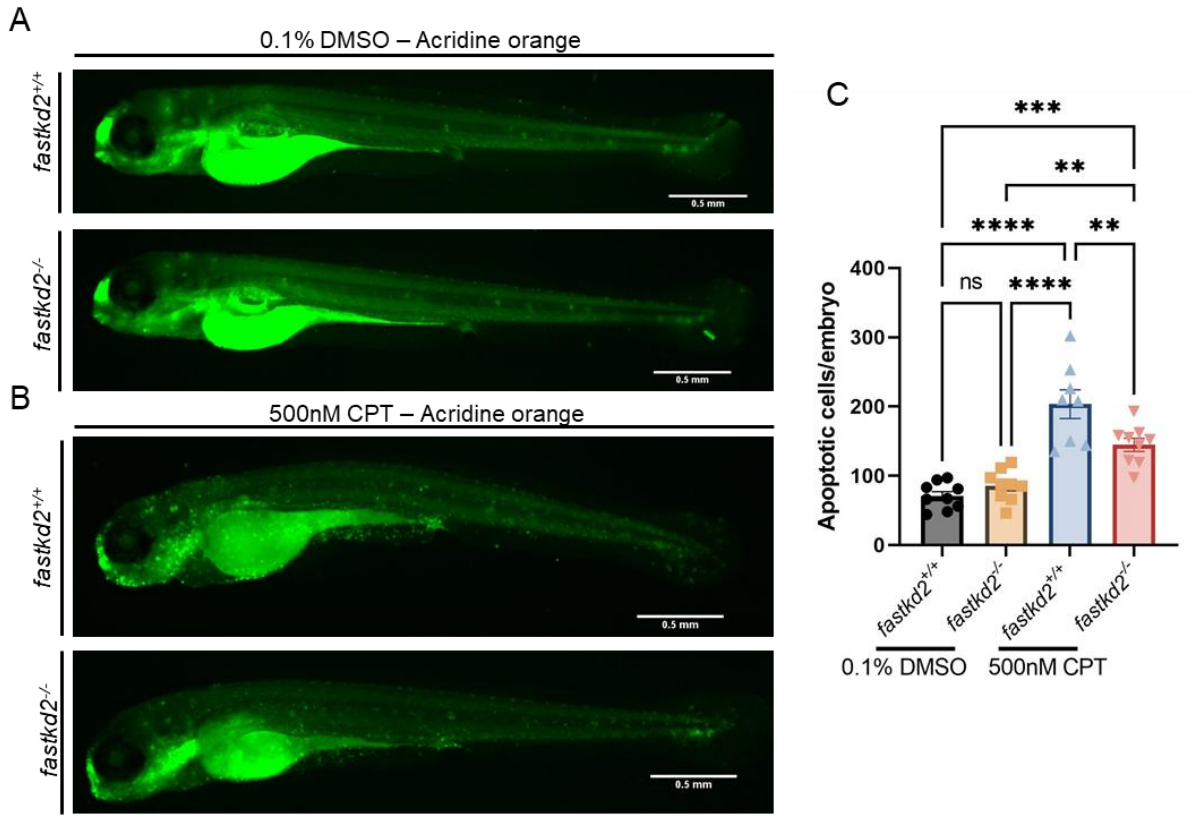

Figure 4.16: Acridine orange staining to identify apoptotic cells in 5dpf *fastkd2* wild type and homozygous larvae treated with 0.1% DMSO or 500nM CPT. A: 5dpf 0.1% DMSO treated larvae for 24h at 4dpf stained with acridine orange at 5dpf. B: 5dpf 500nM CPT treated larvae for 24h at 4dpf stained with acridine orange at 5dpf. C: Increase in GFP foci is seen in wild type larvae treated with CPT but not in homozygous larvae. Normalised to wild type DMSO, One-way ANOVA, n= 9, *fastkd2* wild type 500nM CPT n=8.

4.2.8. Homozygous *fastkd2* larvae do not show any change in inflammation or senescence

When there is no RNaseH2, rNMPs are not removed from DNA, causing strand breakage. In some cases, these breaks can be close enough together to cause double stranded breakages, and it is thought that DNA fragments float into the cytoplasm or enter the cytoplasm through micronuclei activating an anti-viral pathway and causing inflammation (Li and Chen, 2018). In

fastkd2 larvae I did not see any increase in DNA damage at baseline, however, I did decide to investigate the same inflammatory pathways as in the *rnaseh2a* homozygous mutants for the *fastkd2* mutants (Thomas et al., 2024). *isg15* in particular has a 40x fold change increase in the *rnaseh2a* mutants. In the *fastkd2* mutants, there was no change in *isg15*, or for *il-6* and *tnfα*. Although there was no significant change in the homozygous compared to the wild type, there was a trend where both genes did decrease compared in the homozygous, where the p-value for *il6* was 0.167 and for *tnfα* 0.093 (Figure 4.17A). Further, DNA damage can cause senescence and ageing. However, I saw no change in *p21* expression by qPCR on untreated larvae (Figure 4.17A). Therefore, I crossed the 5bp *fastkd2* mutant to a *p21* senescence reporter (Morsli et al., 2023). I saw the reported *p21* expression pattern in the head and along the midbrain-hindbrain barrier in all the larvae, and when I treated the larvae with CPT, I saw a significant decrease in *p21* expression in the homozygous (Figure 4.17B-D).

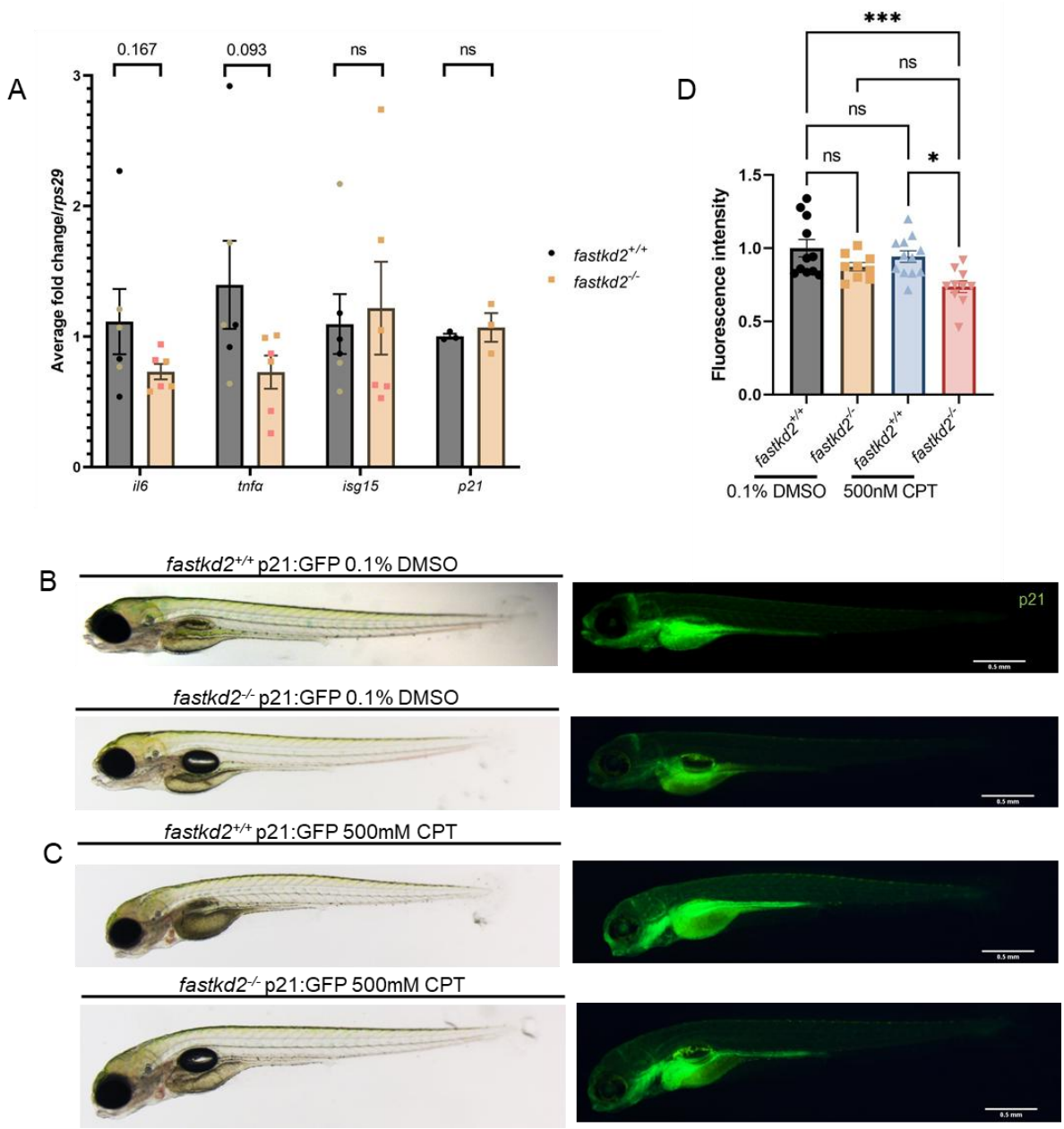

Figure 4.17: Inflammation and senescence in *fastkd2* homozygous larvae. A: qPCR for inflammatory gens *il-6*, *tnfα*, *isg15,* n=6, and senescence marker *p21*, n=3, Unpaired t-test. Black = Wild type 131bp insertion. Green = Wild type 5bp deletion. Yellow = Homozygous 131bp insertion. Pink = Homozygous 5bp deletion. B: Bright field and GFP images of wild type and homozygous *fastkd2* larvae treated with either 0.1% DMSO or C: 500mM CPT for 24h at 4dpf. Imaged at 5dpf. GFP indicates p21 expression. D: Whole embryo florescence normalised to wild type DMSO. One-way ANOVA, n= 11 (wild type DMSO), 12 (homozygous DMSO), 9 (wild type CPT), 10 (homozygous CPT).

4.2.9. *fastkd2* homozygotes do not have a decreased ability to cleave ribonucleotides

Previous research in Professor Sherif El-Khamisy's lab by Dr Chunyan Liao and others, has shown that *faskd2* can rescue a *rnaseh2* and *rnaseh1* double knockout phenotype in yeast. Yeast, which would be sensitive to hydroxyurea, survived when human *fastkd2* cDNA was added. Further, human FASTKD2, purified in *E.coli* had the ability to cleave single rNMPs embedded in a double stranded DNA (Manuscript in preparation, unpublished). However, protein lysate from whole *fastkd2* wild type and homozygous zebrafish larvae and 29-month-old adult brains showed no difference in the ability to cleave rNMPs (Figure 4.18A and B, F and G). In addition, when extracting the whole genomic DNA from the *fastkd2* wild type and homozygotes larvae and treating it with NaOH which cleaves rNMPs, there was no difference in the smearing of the DNA which was also seen in the intensity graph (Figure 4.18C and D). When quantified, there was no difference in the number of small DNA fragments compared to the wild type larvae after NaOH treatment (Figure 4.18E).

Although it did not appear that *fastkd2* was involved in cleaving rNMPs in zebrafish there was an increase in the expression of *rnaseh2a*, the catalytic subunit of RNaseH2, in the 5dpf larvae. There was no change in the expression of the other subunits *rnaseh2b* and *rnaseh2c*, however, a decrease in *rnaseh1* was observed (Figure 4.19). This decrease was less reliable though as the RNA from the 5bp deletion line and the 131bp insertion line cluster together, with the 5bp deletion line showing no difference to the wild type.

Considering that FASTKD2 is a mitochondrial protein that is transcribed in the nucleus, I decided to assess the *fastkd2* homozygote's ability to cleave rNMPs in the mitochondria. There is no RNaseH2 in the mitochondria as it is a nuclear protein. I extracted the mitochondria of 5dpf larvae and performed a ribonucleotide activity assay on protein extracts from the extraction. Figure 4.20A shows the purity of the mitochondrial protein extracted. However, there was still no difference in the wild type and the *fastkd2* homozygous larvae's ability to cleave ribonucleotides (Figure 4.20B and C).

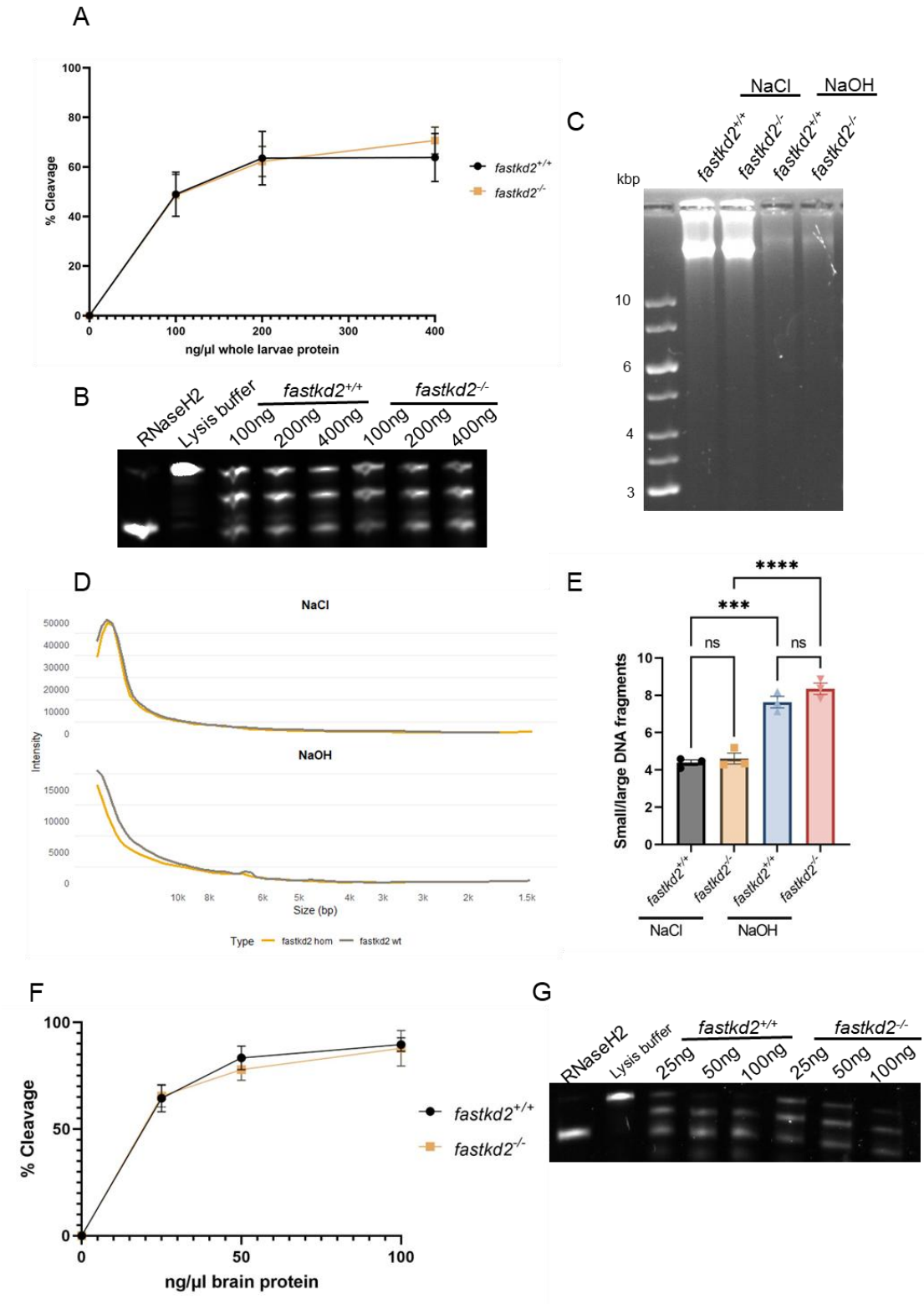

Figure 4.18: Cleavage of single rNMPs by 5dpf *fastkd2* homozygous larvae. A: Ribonucleotide cleavage assay between wild type and homozygous *fastkd2* larvae. Unpaired t-test at protein concentration, n=3. B: Representative urea cleavage gel between wild type and homozygous larvae. C: Representative image of an alkaline treated genomic DNA from wild type and homozygous *fastkd2* larvae run on a TAE gel. D: Intensity plot of non-alkaline and alkaline

treated genomic DNA. E: Quantification of small DNA fragments over large DNA fragments for non-alkaline and alkaline treated samples. One-way ANOVA, n=3. F: Ribonucleotide cleavage assay between wild type and homozygous *fastkd2* adult brains. Unpaired t-test at protein concentration, n=3. B: Representative urea cleavage gel between wild type and homozygous adult brains.

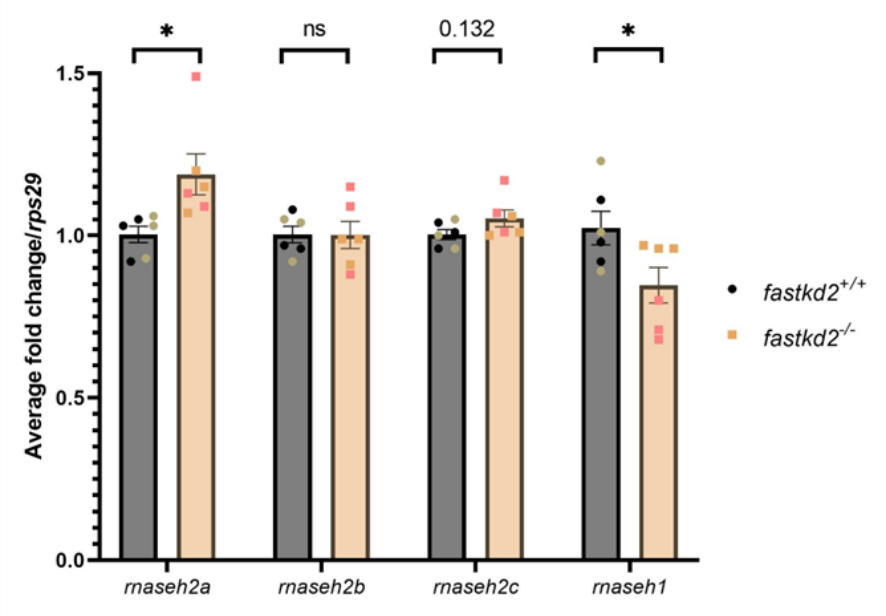

Figure 4.19: mRNA expression for the three subunits of RNaseH2, *rnaseh2a*, *rnaseh2b*, *rnaseh2c*, and *rnaseh1* in *fastkd2* wild type and homozygous 5dpf larvae. Unpaired t-test, n=6. Black = Wild type 131bp insertion. Green = Wild type 5bp deletion. Yellow = Homozygous 131bp insertion. Pink = Homozygous 5bp deletion.

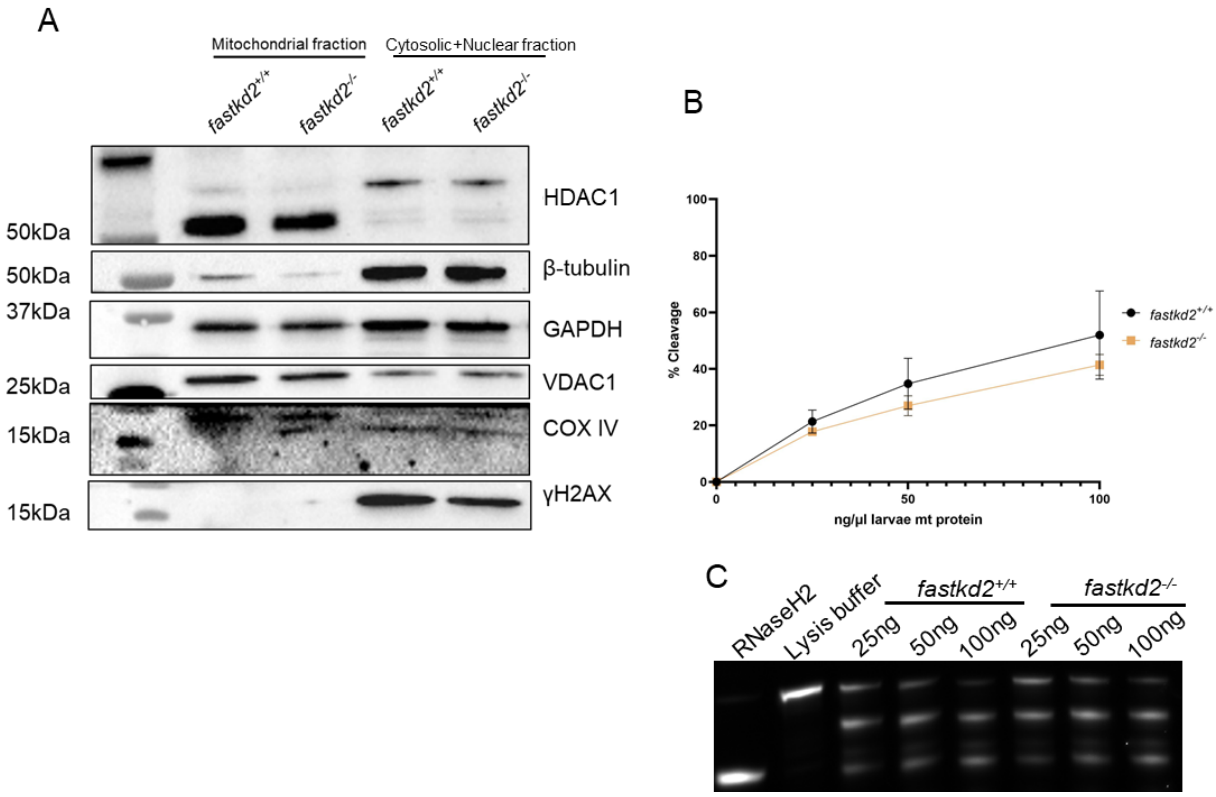

Figure 4.20: Cleavage of rNMP by mitochondrial proteins from *fastkd2* wild type and homozygous 5dpf larvae. A: Western blot showing the purity of the mitochondrial fraction compared to the cytosolic and nuclear fraction using HDAC1, β-tubulin, GAPDH, VDAC1, COX IV and γH2AX. B: Ribonucleotide activity assay on protein from the mitochondrial extraction of wild type and homozygous embryos. C: Representative urea cleavage gel between wild type and homozygous larvae. Unpaired t-test, n=3.

4.2.10. Knockdown of *faskd2* in HCT116 cells does not cause an increase in *rnaseh2a* expression

To examine if an increase in *rnahse2a* could also be seen in human cells, I used siRNA to knockdown *fastkd2* in HCT116 cells. This colorectal cancer cell line was chosen as other FASTKD2 research in cells in the lab used this cell line due to its large flat surface and cytoplasm, with easy visualisation of mitochondria. Whilst there was a decrease in FASTKD2 protein, the level of RNaseH2A protein did not change (Figure 4.21A-C). Further, a qPCR for *rnaseh2a* did not show a change in mRNA expression (Figure 4.21D).

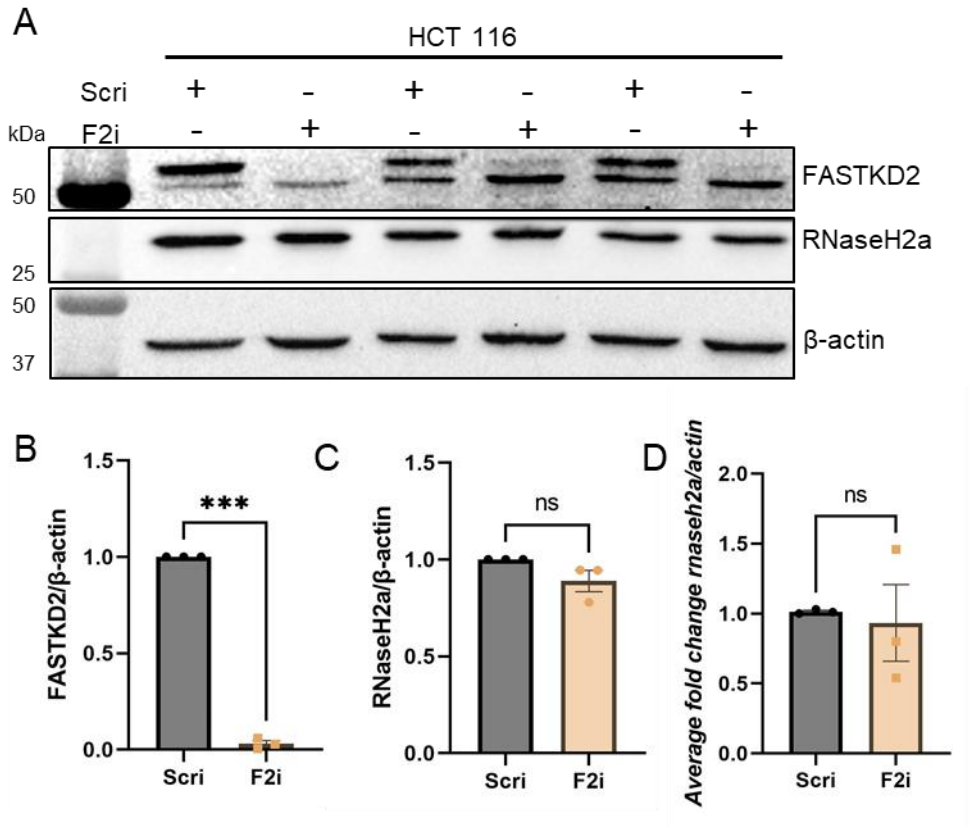

Figure 4.21: Knockdown of *fastkd2* in HCT 116 cells. A: Western blot to show knockdown of FASTKD2 and RNaseH2A expression. B: Quantification of top band of FASTKD2. C: Quantification of RNaseH2A. D: qPCR for *rnaseh2a* expression. Unpaired t-tests, n=3.

4.2.11. Creating and characterising a double homozygous *fastkd2* and *rnaseh2a* line

Due to the increase in *rnaseh2a* expression in the *fastkd2* knockout zebrafish line but no decrease in ribonucleotide cleavage activity, I speculated that the higher *rnaseh2a* expression might be compensating for the lack of FASTKD2, masking the effect of the *fastkd2* knockout. Therefore, I created a double knockout zebrafish line for *fastkd2* and *rnaseh2a*. Initially, I attempted to make this line by crossing the *fastkd2* homozygous line, which was viable with the *rnaseh2a* heterozygous line, which produce viable offspring. Once I obtained double heterozygous fish from this however, the occurrence of a double homozygous larva was much lower than 1:16. I saw 6 double wild type and 3 double homozygous larvae out of 336 larvae. This was because *fastkd2* and *rnaseh2a* are both found on chromosome 1 (Figure 4.22A). This makes a chromosomal crossover event the only way to get a double homozygous larva. However, this showed that a first-generation double mutant for *fastkd2* and *rnaseh2a* was viable. To be able to work with the double homozygous embryos, I had to make a new

CRISPR/Cas9 knockout line of *rnaseh2a* in the *fastkd2* homozygous background. The CRISPR cleavage site was the same as the SH478 line (Thomas et al., 2024), but I created an 8bp deletion, causing a frameshift and an early stop codon 21bp after the cleavage site (Figure 4.22B).

A

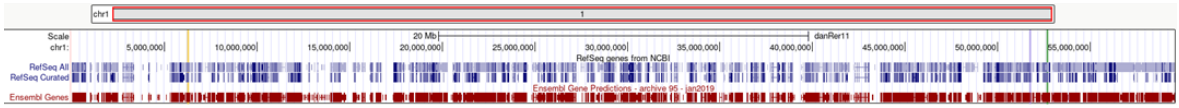

Yellow *fastkd2* - Chromosome 1: 6,225,493-6,243,978
Purple *rnaseh2a* - Chromosome 1: 51,712,869-51,720,633
Green *aptx* - Chromosome 1: 52,653,626-52,659,711

B

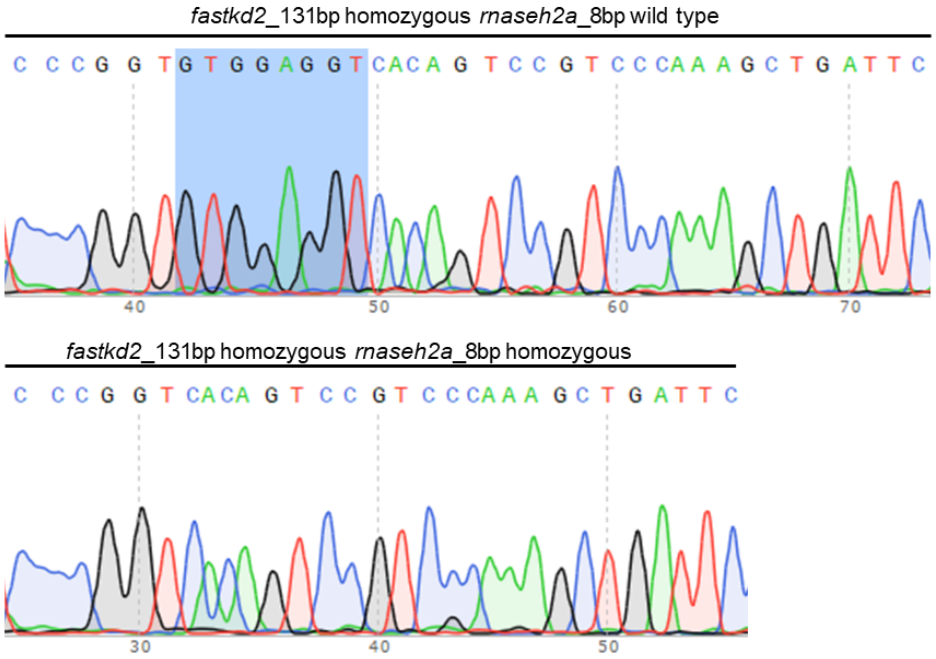

Figure 4.22: Location of *fastkd2* in relation of *rnaseh2a* and *aptx* on chromosome 1. A: *fastkd2* (yellow): Chromosome 1: 6,225,493-6,243,978. *rnaseh2a* (purple): Chromosome 1: 51,712,869-51,720,633. *aptx* (green): Chromosome 1: 52,653,626-52,659,711. B: *fastkd2*_131bp homozygous background showing sequencing for *rnaseh2a* wild type at the top, blue shows 8bp deletion in homozygous sequence at the bottom.

4.2.12. *fastkd2 rnaseh2a* second generation double homozygotes are lethal at 24hpf

Whilst double mutants from a *fastkd2* homozygous *rnaseh2a* heterozygous parent was viable, the embryos resulting from a double homozygous parent showed a lethal phenotype at 24hpf. Figure 4.23 show images of the embryos at 24hpf, where the wild type and the *fastkd2* single mutant showed an unaffected phenotype. The double mutants and the *rnaseh2a* single mutants however showed a variety of severe phenotypes with delayed development, small heads, and short, necrotic tails. The phenotypes were segregated into mild, moderate, severe and dead depending on the tail length and level of necrosis. When counting the number of embryos per phenotype out of 60 embryos from different crosses, it appeared that there were more severe phenotypes seen in the single *rnaseh2a* mutant compared to the double mutant. Further, the single mutant experienced more deaths out of the 60 embryos (Figure 4.23B).

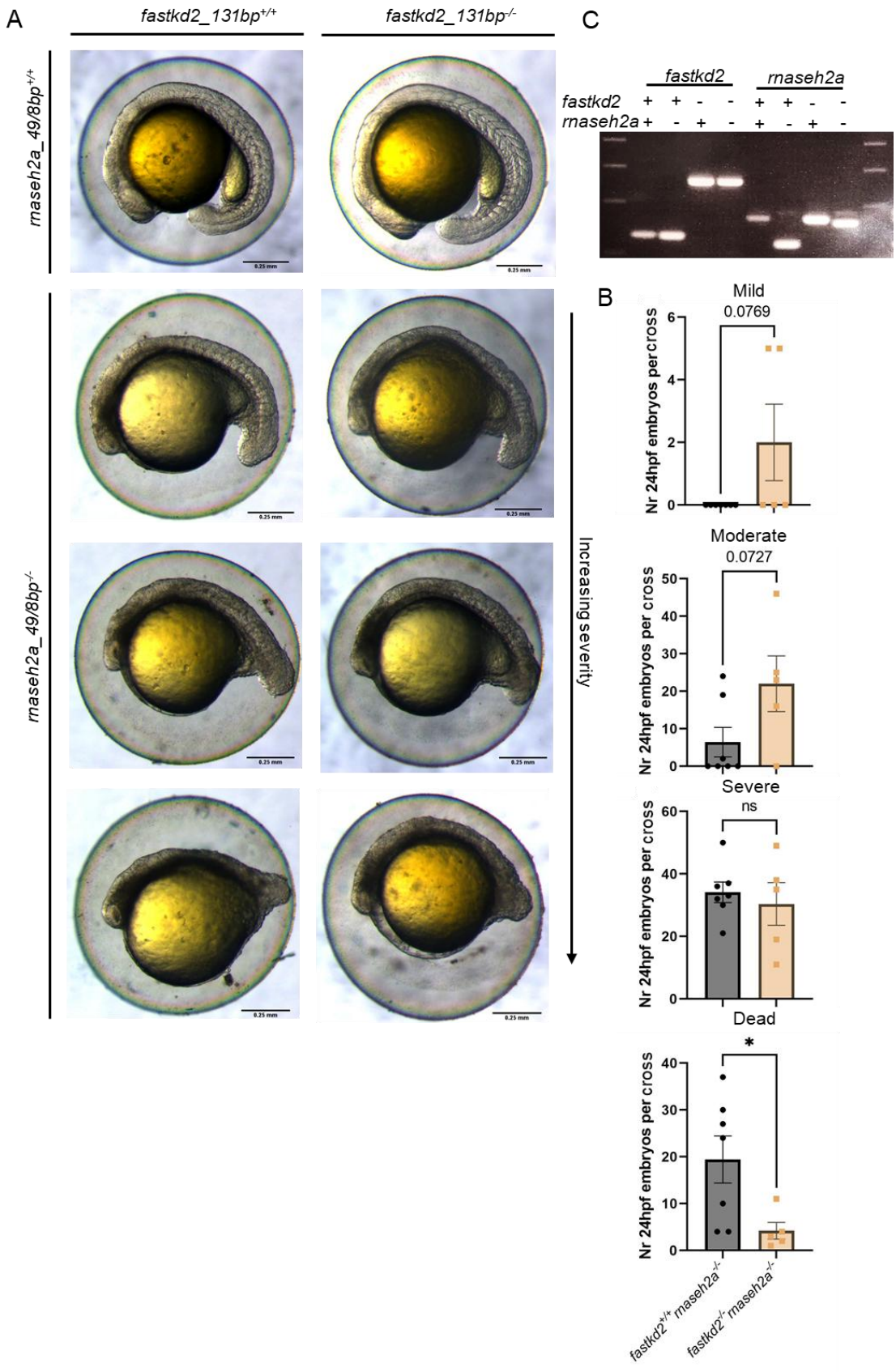

Figure 4.23: Phenotype of double *fastkd2 rnaseh2a* second-generation homozygotes. A: Brightfield images of wild type, *fastkd2* single mutant, *rnaseh2a* single mutant and *fastkd2*

rnaseh2a double mutant embryos at 24hpf. B: Phenotype severity counts for *rnaseh2a* single and double mutants out of 60 embryos selected on day 0. Phenotype counted at 24hpf. Unpaired t-test, n=7. C: Gel image of *fastkd2* and *rnaseh2a* genotypes for each line.

As the double homozygous embryos were healthier than the single *rnaseh2a* homozygous embryo I wanted to assess their survival ability past 24hpf. Fertilized wild type, *fastkd2* single mutants, *rnaseh2a* single mutants, and *fastkd2 rnaseh2a* double mutants were selected on day 0 and monitored until day 5. At each 24 hour point the number of dead embryos were counted and removed. This showed that there were significantly more early deaths in the *rnaseh2a* single mutants compared to the double mutants. There were no deaths in the wild type and the *fastkd2* single mutants (Figure 4.24A). However, the embryos that survived until day 5 for the *rnaseh2a* single mutants and the double mutants showed similar phenotypes of bent tails, small heads, oedema and necrosis (Figure 4.24B).

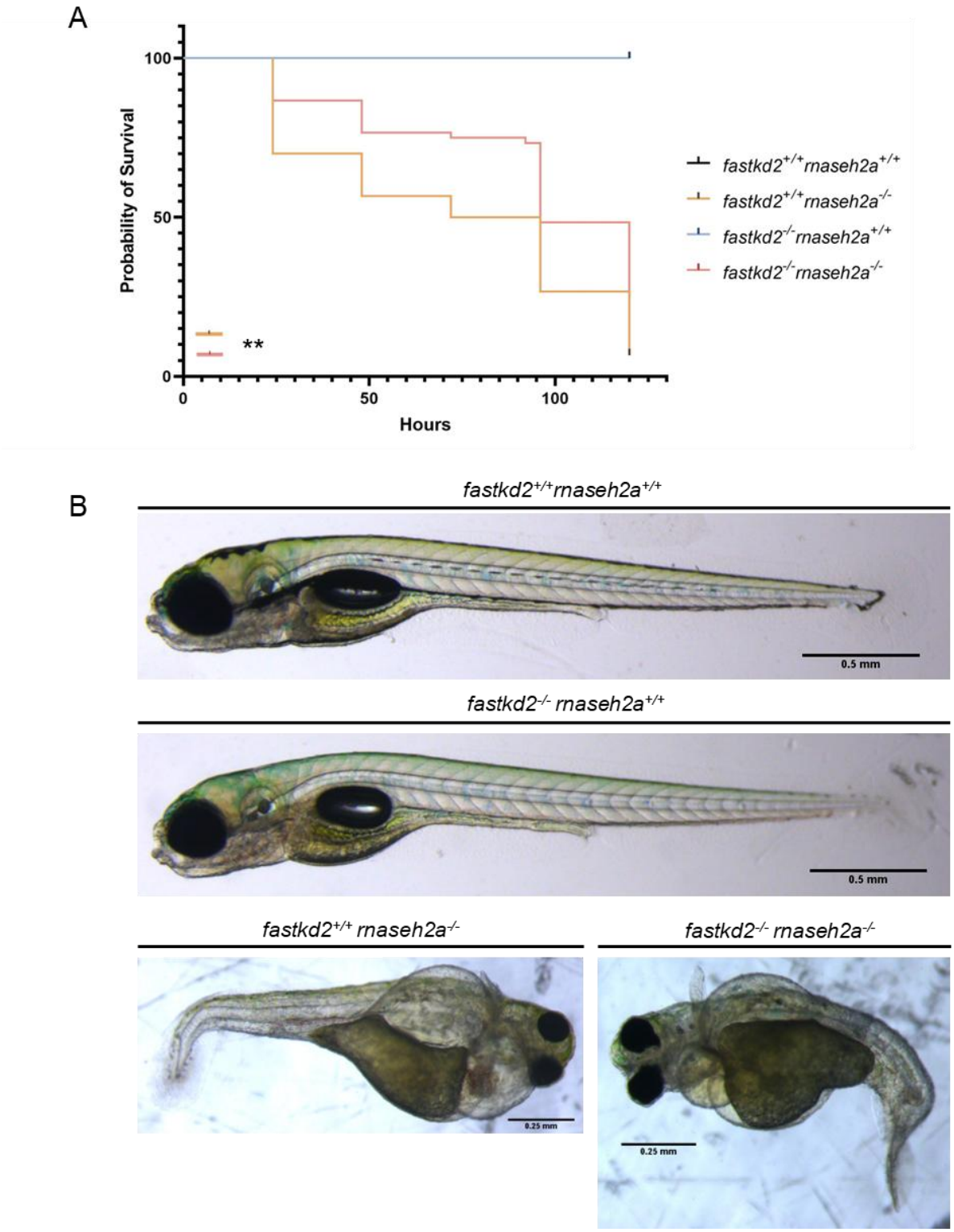

Figure 4.24: Survival assay for wild type, *fastkd2* single mutant, *rnaseh2a* single mutant and *fastkd2 rnaseh2a* double mutants. A: Survival graph. Deaths counted each 24 hours until 120 hours. Stats = survival, n=60. B: Brightfield images of wild type, *fastkd2*, *rnaseh2a* and double mutants at 5dpf.

4.2.13. Double mutants are as efficient as *rnaseh2a* single mutants to cleave ribonucleotides

Now that I had a line with no rNMP cleavage by RNaseH2, I could assess whether a lack of FASTKD2 would affect the cleavage of rNMPs any more than the lack of RNaseH2A alone. Initially, the ribonucleotide activity assay was performed with protein from whole lysates from CRISPR injected *fastkd2* homozygous larvae. This showed no difference in cleavage activity between wild type, *fastkd2* single mutants, *rnaseh2a* crispants and *fastkd2 rnaseh2a* crispants (Figure 4.25A and B). With a CRISPR/Cas9 line, the activity assay was performed on the embryos from the double homozygous adults when the embryos were 24hpf. Whilst there was a significant decrease in cleavage activity for the *rnaseh2a* single mutant and the double mutant, the difference between the two lines was not significant (Figure 4.25C and D).

Further, I also observed that the band from the *rnaseh2a* single mutant and the double mutant ran quicker on the urea gel compared to the wild type and the *fastkd2* single mutant. Therefore, based on the research by Dr Chunyan Liao, who had seen that purified human FASTKD2 could cleave single rNMPs on the 3' of the rNMP similar to cleavage by KOH, I decided to assess the size of the cleavage bands in my activity assay. If FASTKD2 cleaved rNMPs in the absece of RNaseH2, I would expect the cleavage band for the *rnaseh2a* single mutant and double mutant to be the same size as bands cleaved by KOH, whilst the wild type and the *fastkd2* single mutant would be the same size as the RNaseH2 cleavage band. However, I saw that all the cleavage bands were significantly smaller than the cleavage band by KOH. Whilst the cleavage bands by the wild types and the *fastkd2* single mutants were roughly the same as the cleavage band by RNaseH2, the cleavage bands by the *rnaseh2a* single mutant and the double mutant were smaller than the cleavage band by RNaseH2 (Figure 4.26). This was not significant in most cases, however, there was a trend suggesting it might be one base smaller than the cleavage band by RNaseH2.

I further wanted to look at the cleavage ability of the mitochondrial proteins without the possibility of contamination in the protein lysate from RNaseH2. The mitochondria from the four lines were extracted at 24hpf, and the protein used in further activity assays. The western blots showed reasonable extraction of the mitochondria (Figure 4.27A), although I did see γH2AX in the mitochondrial lysate which was unexpected. However, there was no difference in cleavage activity between any of the lines in the mitochondria either (Figure 4.27B and C). I did not measure the size of the cleavage bands, as there were visually no differences.

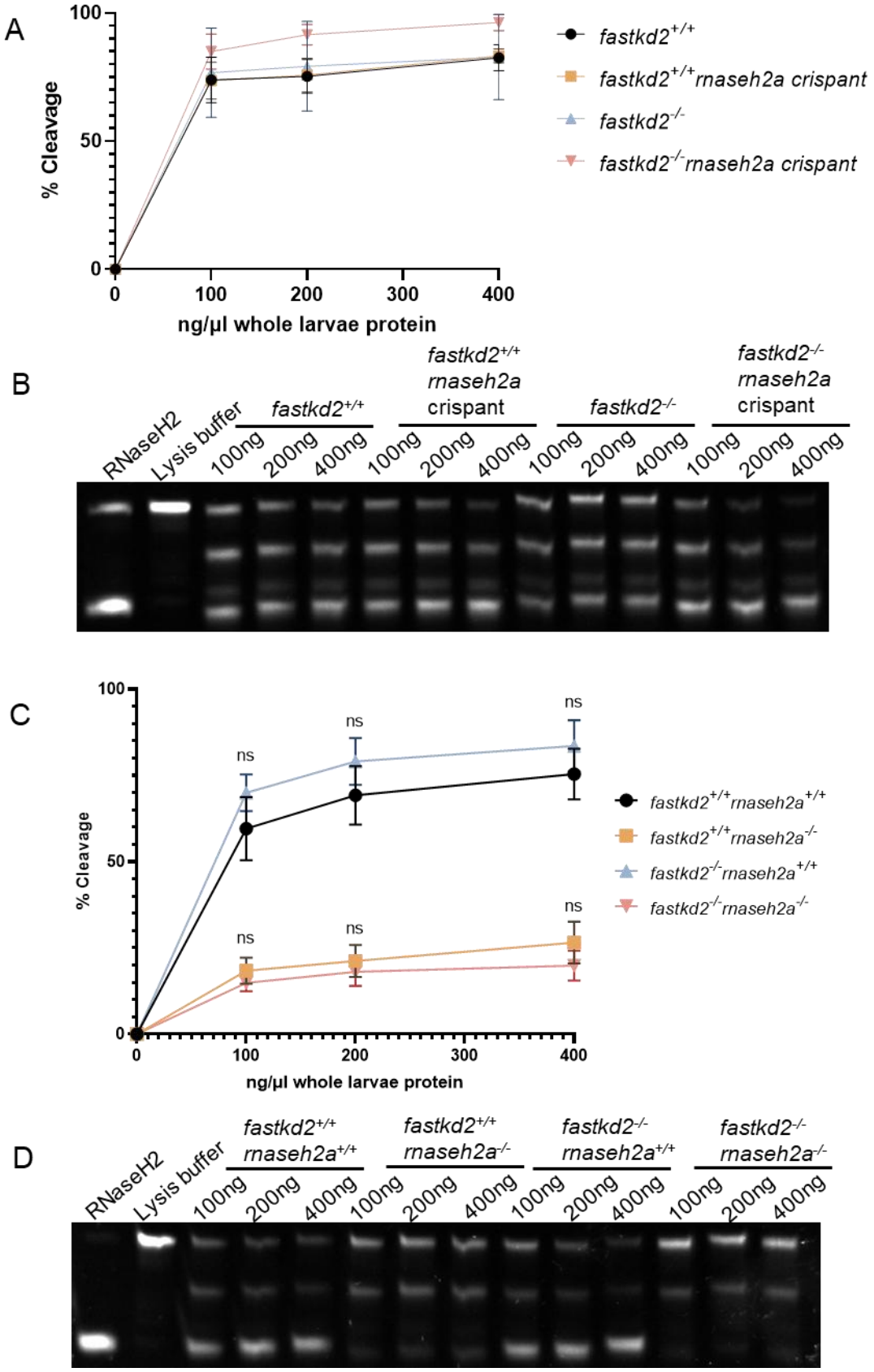

Figure 4.25: Ribonucleotide cleavage activity on crispants and CRISPR/Cas9 double mutant embryos. A: Quantification of cleavage for wild type, *fastkd2* single mutant, *rnaseh2a* crispant, *fastkd2_rnahseh2a* crispant at 5dpf. Unpaired t-test, n=3. B: Representative image of urea

cleavage activity gel of crispants. C: Quantification of cleavage for wild type, *fastkd2* single mutant, *rnaseh2a* single mutant, *fastkd2_rnahseh2a* double mutant at 24hpft. Unpaired t-test, n=5. D: Representative image of urea cleavage activity gel for CRISPR/Cas9 knockout lines.

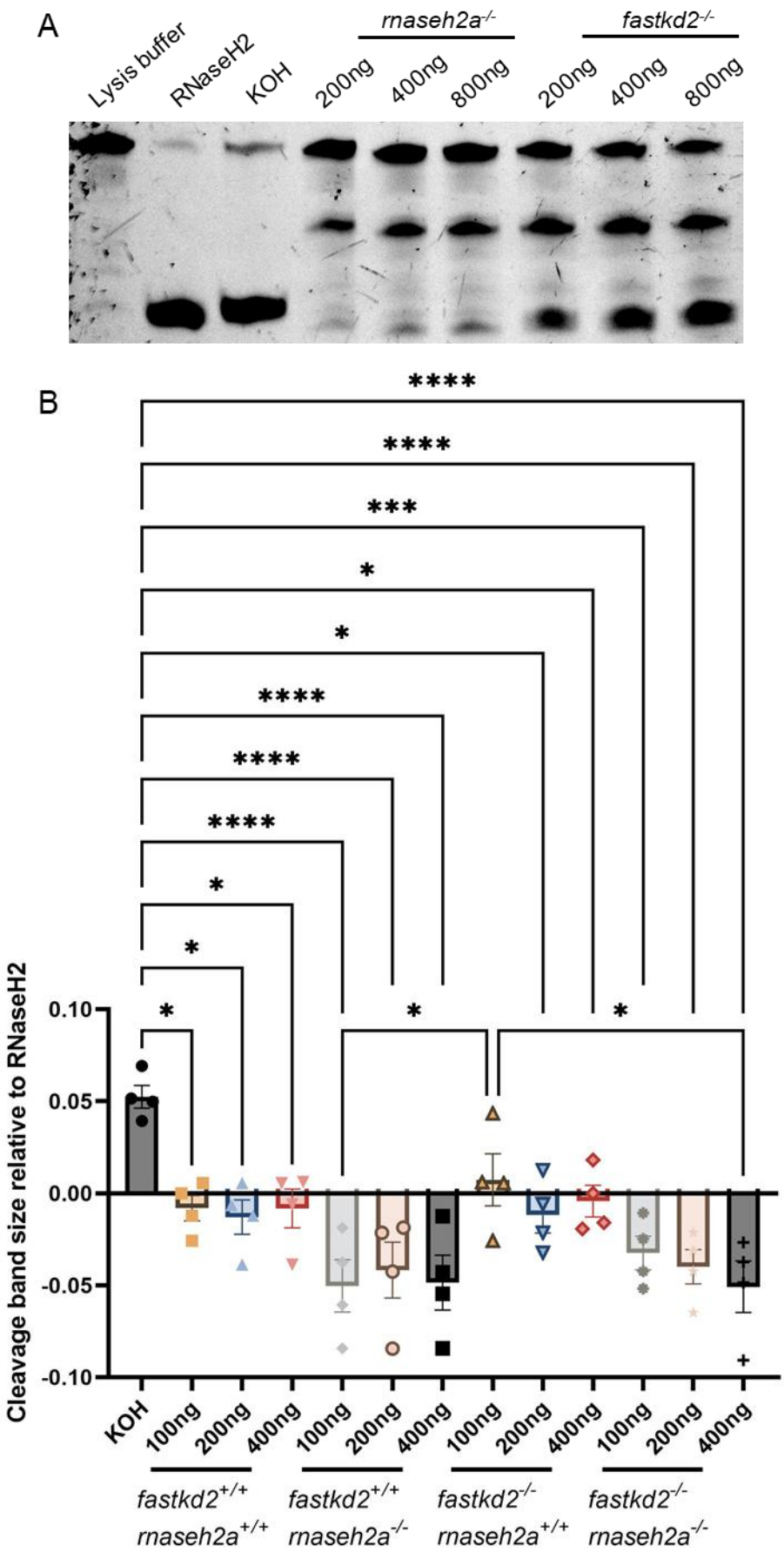
A
Lysis buffer
RNaseH2
KOH
rnaseh2a-/-
200ng
400ng
800ng
fastkd2-/-
200ng
400ng
800ng
B
****
****
***
*
*
****
****
****
*
*
*
*
*
*
Cleavage band size relative to RNaseH2
0.10
0.05
0.00
-0.05
-0.10
KOH
100ng
200ng
400ng
100ng
200ng
400ng
100ng
200ng
400ng
100ng
200ng
400ng
fastkd2+/+
rnaseh2a+/+
fastkd2+/+
rnaseh2a-/-
fastkd2-/-
rnaseh2a+/+
fastkd2-/-
rnaseh2a-/-

Figure 4.26: Analysis of cleavage band size of wild type, *rnaseh2a* single mutant, *fastkd2* single mutant and double mutant relative to cleavage by RNaseH2. A: Ribonucleotide cleavage assay with KOH and RNaseH2 controls with *rnaseh2a* and *fastkd2* single mutant protein lysate to show size of cleavage band. B: Analysis of cleavage band relative to RNaseH2 cleavage band size for urea gels in figure 4.25D with KOH controls run on separate gels. One-way ANOVA, n=4.

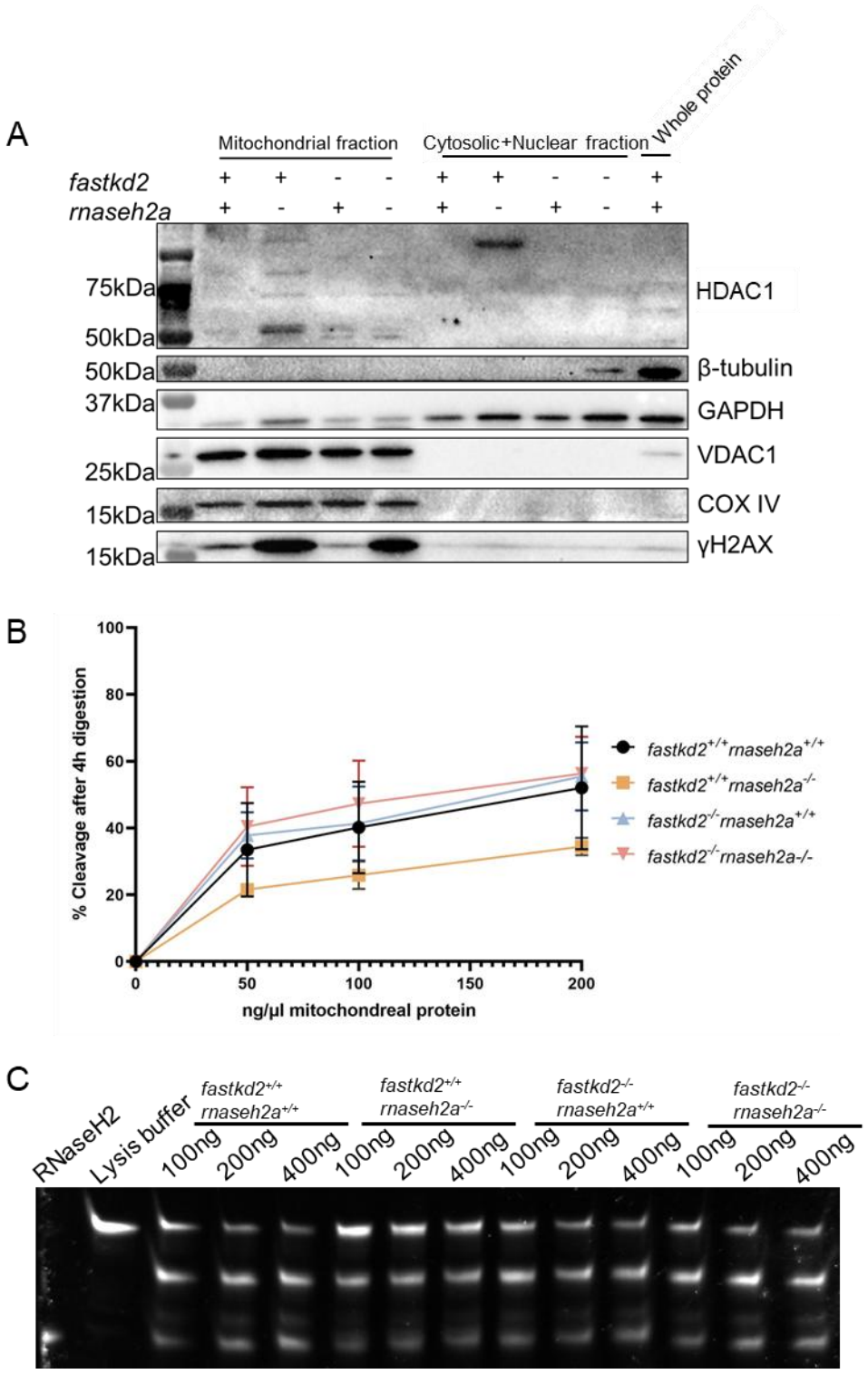

Figure 4.27: Activity assay on 24hpf larvae mitochondrial protein. A: Western blot showing purity of the mitochondrial protein compared to the cytosolic and nuclear fraction as well as whole larval protein, using HDAC1, β-tubulin, GAPDH, VADC1, COX IV and γH2AX as markers for either mitochondria or cytoplasm/nucleus. B: Quantification of cleavage for wild type, *fastkd2* single mutant, *rnaseh2a* single mutant, *fastkd2_rnaseh2a* double mutant. Unpaired t-test, n=3. C: Representative image of urea activity gel.

4.2.14. *fastkd2 rnaseh2a* double mutants have high levels of inflammation, DNA damage and apoptosis

The *rnaseh2a* single mutant and the double mutant have severe phenotypes at 24hpf, and both have a decreased ability to cleave rNMPs in the nucleus, but not the mitochondria. With this lack of rNMP ability in the nucleus, I would expect that the double mutants had high levels of inflammation, DNA damage and apoptosis such as the *rnaseh2a* single mutant. qPCRs for *fastkd2* and *rnaseh2a* showed a significant decrease in expression of both proteins in the corresponding lines (Figure 4.28A and B), and a qPCR for *isg15* showed significant increase in both the *rnaseh2a* single mutant and the double mutant. There was no significant difference in expression between them (Figure 4.28C). Further, by western blotting, I observed an increase, in PARylation in the *rnaseh2a* single mutants, although it was not significant. I did not see this increase in the double mutant (Figure 4.28D and E). I also saw a significant increase in γH2AX in the single *rnaseh2a* and the double mutants. There was a slight reduction in γH2AX in the double mutant compared to the single *rnaseh2a* mutant, however, this was not significant (Figure 4.28F). Lastly, due to increased survival of the double mutants, and the potential reduced damage compared to the *rnaseh2a* single mutant, I wanted to look at apoptosis in the double mutants. By using acridine orange I looked at the level of apoptosis in the tails of the four lines and saw increased apoptosis in the *rnaseh2a* single mutant and the double mutant, however, there was no difference between the level of apoptosis between them (Figure 4.29).

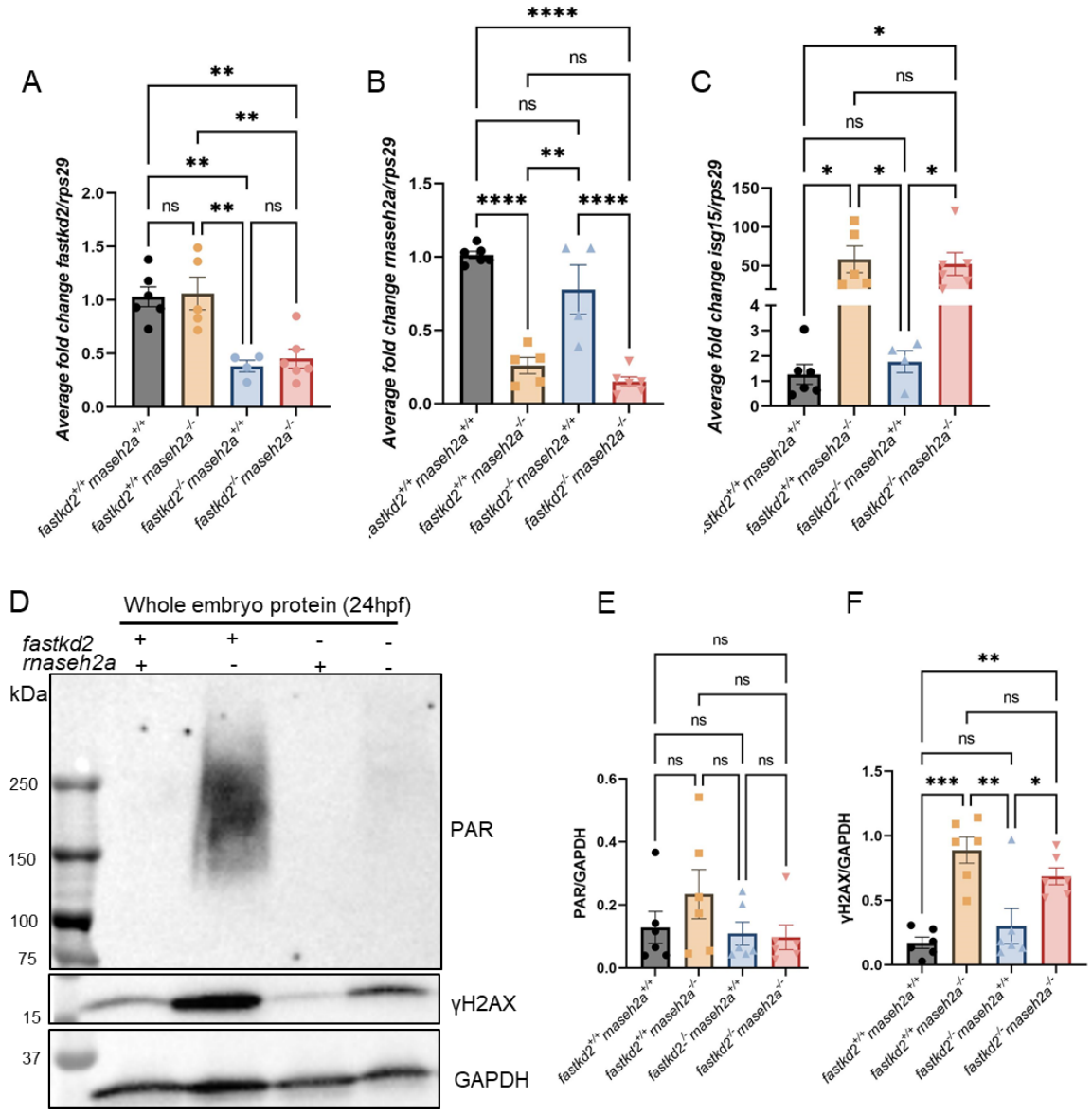

Figure 4.28: DNA damage response and inflammation in wild type, *rnaseh2a*, *fastkd2* and double mutant lines at 24hpf. A: Expression of *fastkd2*. B: Expression of *rnaseh2a*. C: Expression of *isg15*. D: Representative western blot for PAR, γH2AX and GAPDH. E: Quantification of PAR on western blot. F: Quantification of γH2AX on western blot. One-way ANOVA, n=6.

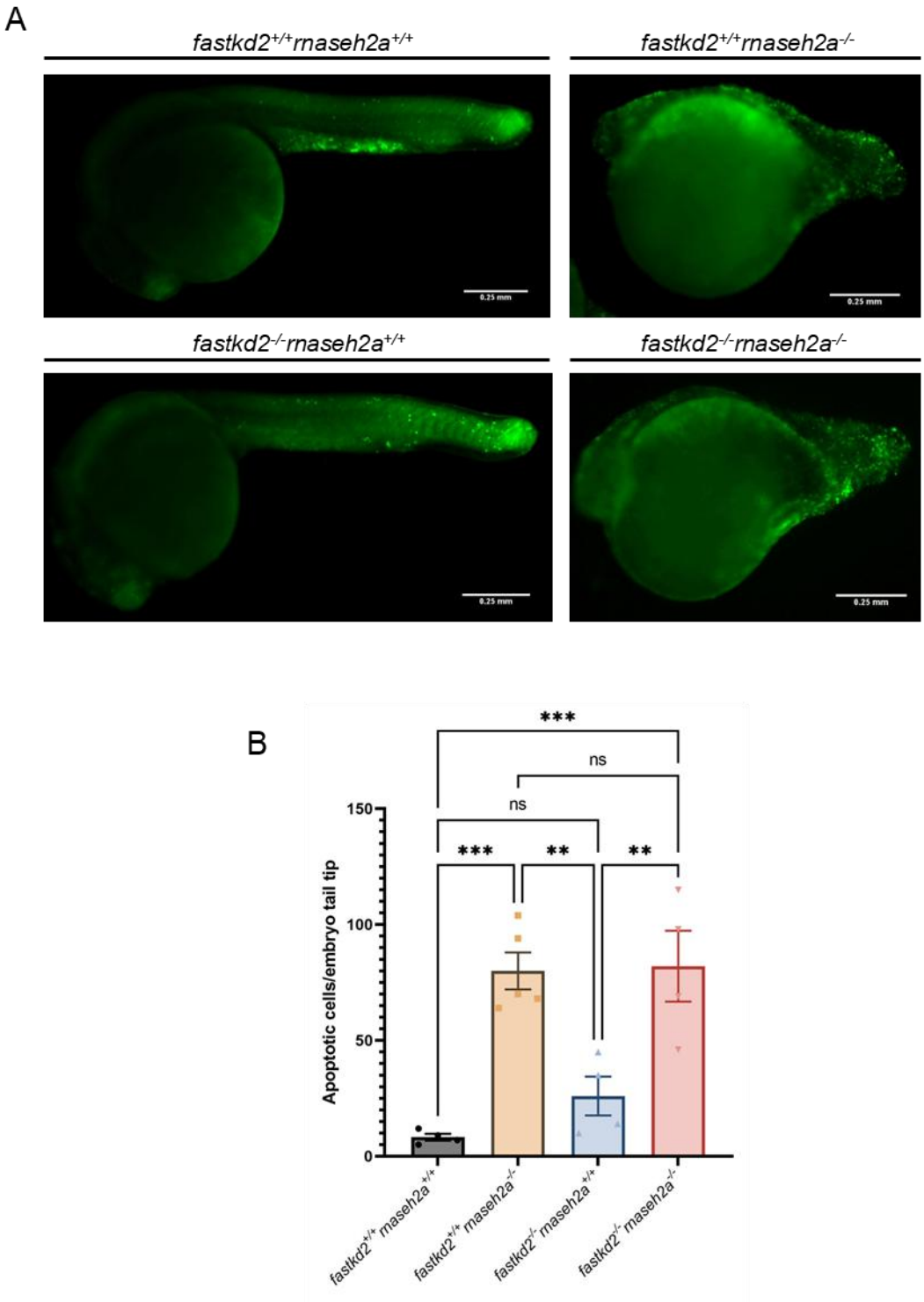

Figure 4.29: Apoptosis seen by acridine orange in the tail of wild type, *rnaseh2a*, *fastkd2* and double mutant lines at 24hpf. A: Pictures of acridine orange staining of 24hpf embryos. B: Quantification of apoptotic cells in the tail tip of embryos. Size measured was the size of the tail of the *rnaseh2a* single mutants. One-way ANOVA, n=4, n=5 for *rnaseh2a* single mutant.

4.2.15. *fastkd2* homozygous adults are not frailer than wild type siblings and do not have a ribonucleotide burden

Considering the *rnaseh2a* homozygous adults showed an increased frailty score (Chapter 3.2.7), I wondered whether a lack of FASTKD2 might cause the fish to become frailer too. However, at 29-months, using the frailty index from Chapter 3, the *fastkd2* homozygous fish were not significantly frailer than their wild type siblings. Both had majority pre-frail fish. They did not have a difference in BMI, width and length ratio, spinal height or cancer occurrence (Figure 4.30A-E). One difference observed at 23 months was that the homozygous fish had more ragged tales than the wild types. This was particularly evident amongst the male fish, although it was seen in both sexes (Figure 4.30F and G).

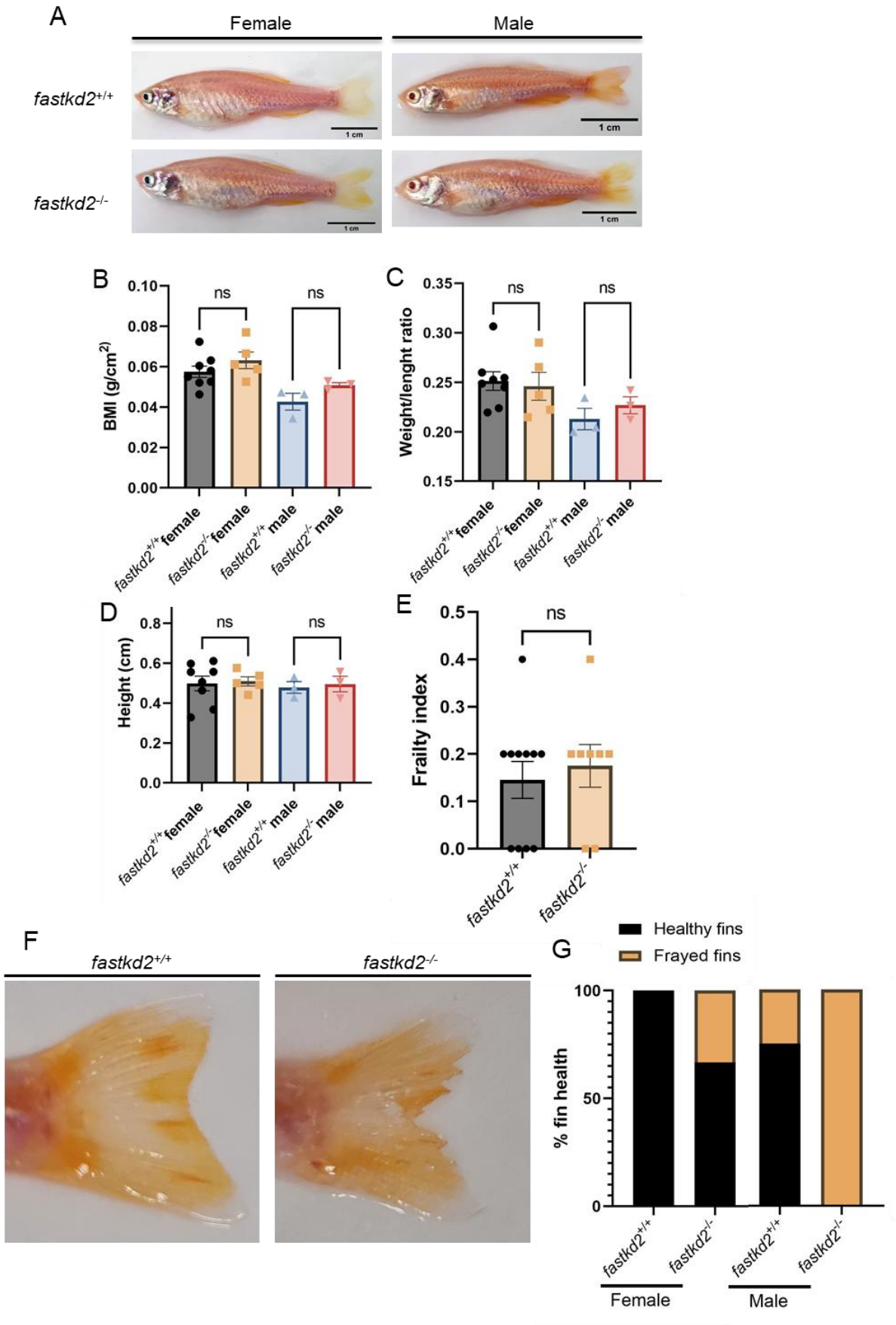
A
Female
Male
fastkd2+/+
fastkd2-/-
1 cm
B
BMI (g/cm2)
ns
C
Weight/lenght ratio
D
Height (cm)
E
Frailty index
fastkd2+/+ female
fastkd2-/- female
fastkd2+/+ male
fastkd2-/- male
F
G
Healthy fins
Frayed fins
% fin health
Female
Male

Figure 4.30: Frailty scoring of 29-month-old *fastkd2* 131bp wild type and homozygous zebrafish. A: Images of female and male wild type and homozygous 29-month-old adults. B: BMI of adults. C: Width/length ratio of adults. D: Spinal height of adults. E: Calculated frailty index of adults. Unpaired t-test, n=11 wild type and 8 homozygous. F: Pictures of tail fins from wild type and homozygous male adults showing ragged ends in homozygous fish. G: Percentage of fish in each tank with healthy and ragged tail fins at 23 months. Wild type female n = 8, Wild type male n = 7, Homozygous female n = 6, Homozygous male n = 6.

4.3. Discussion

FASTKD2, is part of the Fas-activated serine-threonine (FAST) family of proteins and is a nuclear expressed kinase that is transported into the mitochondria. In the mitochondria it is associated with rRNA and mRNA stability and maturation, however, a non-mitochondrial function of initiation of stress induced apoptosis has also been suggested. Loss of FASTKD2 results in encephalopathies in humans (Wu et al., 2022). Research from Professor Sherif El-Khamisy's lab suggests that FASTKD2 might also have a role in single rNMP removal from the mitochondrial DNA. One paper has reported that loss of *fastkd2* through morpholino injections into zebrafish embryos results in severe mitochondrial phenotypes and a full knockout would be lethal (Wei et al., 2020), and there is no whole organism model for loss of FASTKD2 function. In this project, I wanted to create a knockout model for *fastkd2* to investigate whether a loss of *fastkd2* in a whole organism rather than cells would result in reduced rNMP processing in particular in the mitochondria.

4.3.1. Knockout of *fastkd2* in zebrafish results in a weak mitochondrial phenotype that is non-lethal

To study the consequences of losing *fastkd2* function in a whole organism I made two zebrafish lines with frameshift mutations and early stop codons in *fastkd2* creating a truncated protein (Figure 4.3). One of the lines had a 132bp insertion and a 1bp deletion creating a 131bp difference from wild type. This insertion was found to be similar to parts of an intron found in the neighbouring gene *mdh1b*. The second line was a 5bp deletion. Most of the work in this thesis was performed on the 131bp insertion due to the low number of females in the 5bp deletion line and ease of genotyping. Whilst the homozygous embryos for both lines showed no external phenotype, the expression of *fastkd2* in both lines were significantly reduced (Figure 4.4) suggesting nonsense-mediated decay might be occurring (Lykke-

Andersen and Jensen, 2015). The observation that the *fastkd2* homozygous embryos were viable contradicts a paper published by Wei (2020). They performed morpholino injections into wild type zebrafish embryos targeting *fastkd2* and observed that with an increasing concentration of the morpholino they saw increased death compared to their control injections. Therefore, they concluded that *fastkd2* is indispensable for zebrafish development (Wei et al., 2020). However, there are several challenges with using morpholinos and they need to be used under caution. Phenotypes seen in morpholino injected embryos are often more severe than the mutated phenotypes. For example, morpholinos are often associated with off-target causing a naturally toxic phenotype that is p53 dependent. This phenotype is also dose dependent and occurs in 15-20% of all morpholines used. Further, knockout mutants may experience genetic compensation which is not seen in the morpholino injected animals (Bedell et al., 2011, Stainier et al., 2017). To investigate whether there was any compensation from any of the FASTK family members, I first looked at sequence homology and identified in a phylogenetic tree that *fastkd2* and *fastkd1* shared large similarities. Therefore, I looked at the expression levels of the FASTK members found in zebrafish, *fastk*, *fastkd1*, *fastkd3* and *fastkd4*, (I was not able to find *fastkd5*), and rather than seeing a compensation by the family members I saw a significant reduction in *fastkd1*, *fastkd3* and *fastkd4* in both *fastkd2* lines (Figure 4.5). This interdependence of the FASTKD members has also been observed before with FASTKD3 and FASTKD5, where a reduction in one lead to a reduction in others. This might suggest a close physical interaction between them all (Ohkubo et al., 2021).

To further compare my knockout line for *fastkd2* to the morpholino line created by Wei, I performed light induced larval movement analysis at 5dpf. They had seen no difference in speed at 48hpf (Wei et al., 2020), and equally I saw no difference in distance or time spent moving (Figure 4.6). Further, Wei reported a reduced response to touch at 48hpf, however, this was not observed in the knockout at 48hpf. I also looked at the time it took for a 5dpf larvae to stop moving after touch but saw no difference there either. Lastly, Wei reported a reduced heart rate in their 48hpf larvae, however, I saw no difference in heart rate at 5dpf (Figure 4.6). This difference could be due to the different methods of knockdown and knockout, where I might see compensatory mechanisms working, whilst Wei might see effects from injecting the morpholino.

One symptom seen in some patients with mutations in *fastkd2* are epileptic spasms (Wu et al., 2022). Therefore, I wanted to assess whether the *fastkd2* homozygous larvae at 4dpf were more susceptible to seizures when treated with the convulsant agent pentylenetetrazol (PTZ).

PTZ rapidly induces expression of synaptic-activity-regulated genes in the central nervous system, causing vigorous episodes of calcium flux in muscle cells and intense locomotor activity (Baxendale et al., 2012). Baxendale (2012) reported that PTZ could cause significant increase in swimming distance at 40, 20 and 10mM. However, I did not see any significant differences between wild type and homozygous *fastkd2* larvae when treated with PTZ (Figure 5.7). Between 20% and 60% of patients diagnosed with primary mitochondrial disease may develop seizures. The brain is a highly metabolic organ, which requires 20% of the body's oxygen supply to produce the ATP needed for normal function. Therefore, if the mitochondria are not able to produce the ATP for the high energy demand, it may result in changes in neuronal biogenetics and metabolism causing seizures (Moos et al., 2023).

By crossing the *fastkd2* mutants to a mitochondrial reporter line it appeared that the mutants had a decreased mitochondrial size. The shape or the number of the mitochondria was not changed (Figure 4.9). I also saw that the larvae had significantly more AMP and ADP than ATP. This might indicate that the cell's energy is compromised (Hardie, 2003) (Figure 4.10C and D). The larva also had a high NAD+ to NADH compared to wild types (Figure 4.10A). It is normal for a cell to have a more NAD+ than NADH, however, the increase seen in the homozygous larvae might suggest that they are not able to reduce the molecules efficiently which is required for ATP production (Anderson et al., 2017). In animal models, the NAD+/NADH ratio in muscle cells does increase with exercise (White and Schenk, 2012), which could reflect the mitochondrial disease seen in the *fastkd2* mutants. The larvae also had an increased NADP+ to NADPH ratio (Figure 4.10B), however, normally, cells have a higher NADPH pool than NADP+ (Merrill and Guynn, 1981). Similar to the *fastkd2* larvae, ND1 cells with human mitochondrial disease had a reduced NADPH to NADP ratio resulting in increased oxidative stress (Balsa et al., 2020), although I did not look at oxidative stress in the *fastkd2* mutant. However, there was no baseline DNA damage. The adults also had a trend towards an increase in ADP and AMP compared to ATP, however it was not significant. As I was only able to test 3 brains an increased sample number is warranted.

Further, I looked at the expression of several mitochondrial or mitochondrial related genes that have been reported to be changed in *fastkd2* patients including COX I and COX IV (Wu et al., 2022). I saw no change in any of these genes except for a reduction in *polg1* (Figure 4.11). POLG1 is the polymerase responsible for replication of the mtDNA. A reduction in *polg1* expression could indicate a reduction in replication in the mitochondria (Nava et al., 2020). Despite this, the expression of the mitochondrial genes did not change, making it unlikely to

be the case. Further, adult *fastkd2* homozygous brains and *fastkd2* homozygous 5dpf larvae, when looking at the protein levels did show a decrease in COX IV compared to the wild types, which could suggest a reason for the reduced mitochondrial function, however, this was not significant. These results taken together indicate that the *fastkd2* homozygous larvae do have a mitochondrial phenotype that causes a reduction in energy production which is viable.

It became obvious when working with the adult homozygous zebrafish that they exhibited one unusual behaviour. Once the tanks were disturbed, such as by moving them for pair mating, the fish would preferentially swim at the top of the tank (Figure 4.12A). This also led to them regularly jumping out of the tank if the water level was not low enough. Adult behaviour analysis of the fish revealed that the females would move significantly more in the top part of a single tank than their wild type siblings. This was not significant for the males (Figure 4.12B-F). A few theories were therefore explored. (1) The fish associate the top of the tank with where the food arrives. However, this seemed unlikely due to the behaviour mostly being observed after a disturbance. (2) The fish think they have a lack of oxygen due to not being able to produce enough energy. Therefore, they swim to the top to obtain more oxygen. Although, I did not observe the fish gulping at the water surface. I did observe a loss of swimming ability in the adult homozygous fish however, suggesting that the mitochondria are not able to produce enough energy (Figure 4.13D). (3) Dr Andy Griersons lab observed that fish with mutations in ALS genes also swam at the top of the tank. This they believed to be because they have lost the inhibition that suggests that swimming at the top is dangerous, as part of their dementia which they had observed (Oliveira et al., 2023). I did not observe a significant loss of cognitive memory in the *fastkd2* homozygous fish however (Figure 4.13A). (4) As it was only seen with one tank due to there only being one tank of *fastkd2* mutant with the 131bp mutation existing (the 5bp mutant line only had one female fish) it could have been due to the tank rather than the genotype. However, the fish were changed to different tanks every year and the behaviour persisted, suggesting this might not be the case. Therefore, I could not definitively conclude why the female fish have this preference, but due to the mitochondrial defects observed, I believe theory (2) is more likely with the fish thinking they require more oxygen. Further, female and male differences in behaviour have been reported in zebrafish. For examples, by using a T-maze test which assesses learnt behaviour, Yin and Horzmann saw that female and young fish entered the correct T-arm of the tank quicker than the males, and they entered the correct arm more often (Yin and Horzmann, 2024). It could be that the *fastkd2* females have learnt that they should be at the top of the tank in stressful situations to obtain more oxygen, however, the males have not.

4.3.2. FASTKD2 does not appear to remove single ribonucleotides in zebrafish

The reason I wanted to create a *fastkd2* knockout zebrafish model was to study the role of FASTKD2 in the ribonucleotide excision repair pathway. First, I wanted to identify if the lack of FASTKD2 resulted in any basal DNA damage, however, this was not observed (Figure 4.14). When 5dpf larvae were treated with Camptothecin (CPT), both wild type and homozygous larvae had increased DNA damage, but there was no difference in the damage between them except for more PARylation in the wild type CPT treated larvae (Figure 4.15). This could be a consequence of the energy imbalance seen in the homozygous larvae as PARP1 use NAD+ to function. However, the homozygous larvae did not have reduced NAD+ rather the opposite. Nevertheless, this imbalance might still affect enzyme function. Further, I saw no basal change in inflammation or senescence (Figure 4.17). Although, there was a potential decrease in senescence observed in the homozygous larvae after CPT treatment.

When I looked at the homozygous larvae and adult brains' ability to cleave single rNMPs, I observed no change when comparing them to the wild type. Further, the larvae did not have any changes in the rNMP levels in their genome (Figure 4.18). There was also no reduced rNMP cleavage activity in mitochondrial isolates (Figure 4.20). This could suggest that FASTKD2 might not be involved in the RER pathway in zebrafish. I did observe however, an increase in the catalytic subunit of RNaseH2 in the *fastkd2* homozygous larvae (Figure 4.19), which was not seen in a knockdown of *fastkd2* in human cells (Figure 4.21). This could suggest that RNaseH2 is compensating for the lack of FASKTD2 in zebrafish, however the knockdown in the cells is not sufficient to initiate a compensatory pathway. Further, I also saw a reduction in *rnaseh1* expression. This was only observed in one of the two *fastkd2* lines however and might therefore be a false result. Alternatively, RNaseH1 is vital in the mitochondria during replication (Nava et al., 2020). A lack of mtDNA replication could mean that RNaseH1 is not needed and therefore less is being produced, or the mRNA might be degraded. I had also seen an increase in *fastkd2* expression in the first generation *rnaseh2a* homozygous adults (Figure 3.14). I suggested that FASTKD2 and RNaseH2 could be compensating for one another once there is a lack of one of them in zebrafish. Therefore, the *fastkd2* knockout had no effect on rNMP cleavage.

Because of this observation, I created a double knockout mutant for *fastkd2* and *rnaseh2* to eliminate the possibility that RNaseH2 might be compensating in the *fastkd2* mutant. I predicted that I would see a worsening in the phenotype seen in *rnaseh2a* single mutants if FASTKD2 was compensating. First it is worth noting that both *rnaseh2a* and *fastkd2* are found

on chromosome 1, and therefore creating double mutants by crossing the two lines together would be extremely difficult. I had to make a new CRISPR line in the *fastkd2* homozygous background, and I created an 8bp deletion in *rnaseh2a* resulting in an early stop coding (Figure 4.22). First generation knockout mutants had no phenotype and were viable. Second generation mutants however had the same phenotype observed in the single *rnaseh2a* mutant. It is important to note that in my experiments the *rnaseh2a* single mutant and the double mutant are not related. The *rnaseh2a* single mutant is form the SH478 line, and the double mutant is from the *fastkd2* homozygous line. This could be the reason for the results that I was observing. The single *rnaseh2a* mutant generally had a more severe phenotype than the double mutant (Figure 4.23) and died earlier than the double mutants showing the opposite phenotype to what I would expect (Figure 4.24). When it came to their ability to remove rNMPs, there was no differences between the single and double mutant in whole lysate or in the mitochondrial lysate (Figure 4.25 and 4.26). It is interesting to observe that in the western blot showing the purity of the mitochondrial extraction from the 24hpf embryos (Figure 4.26A), there is a considerable amount of γH2AX in the mitochondrial lysate which is not expected as it is generally associated with nuclear DNA repair. However, studies have suggested that there is a mitochondrial function for H2AX which is separate from its DNA binding ability where it assists in import of mitochondrial proteins and can itself be transported into the mitochondria. A knockdown of H2AX also result in severe mitochondrial defects (Jeong et al., 2017, Weyemi et al., 2019). Although, the antibody is for phosphorylated H2AX, and I am not able to find any research about whether H2AX is phosphorylated in the mitochondria. I further observed that there could be less DNA damage in the double mutant than the single mutant, although this difference was not significant (Figure 4.27). This suggested that if FASTKD2 was removed from embryos lacking RNaseH2 function, there could be a slight rescue of the phenotype.

Interestingly, TOP1 has been identified to be able to cleave single rNMPs only in the absence of RNaseH2. Yeast colonies with a MetM644 to Gly substitution in DNA polymerase ε (pol2), causing an increase in rNMP insertions during replication as well as double knockout of both *rnaseh2* and *top1* show an increased survival after HU treatment compared to a pol2 and single *rnaseh2* knockout (Williams et al., 2013). Williams (2013) suggested that the rNMPs left in the genome in a *rnaseh2* knockout might cause R-loops during transcription which could be substrates for TOP1, therefore giving TOP1 more of a transcriptional role rather than a role in removing rNMPs specifically. However, in 2017, the detrimental effect of the *rnaseh2* only knockout in the mutated pol2 background was attributed to TOP1 causing an almost 12-times fold increase in mutations, in particular 2-5bp deletions (Williams et al., 2017). As mentioned,

Dr Chunyan Liao has shown evidence that FASTKD2 cleaves single rNMPs on the 3' side of the rNMP similar to how hydroxides cleave the rNMP (Manuscript in preparation). As I saw increased survival in my *fastkd2 rnaseh2a* double mutants, it is possible that FASTKD2 does cause a form of detrimental cleavage in the *rnaseh2a* single mutant which resembles a cut by hydroxide such as TOP1 does in the *rnaseh2a* knockout mouse model (Figure 4.31). However, when measuring the size of the cleavage bands from the activity assays from whole protein lysate from the wild type, single *rnaseh2a* and *fastkd2* and double mutants, I would have expected to see that the cleavage band by the *rnaseh2a* single mutant was the size of the cleavage product by hydroxide. However, this was not the case, and all the cleavage bands were significantly smaller than the band by hydroxide. Further, the cleavage bands by the *rnaseh2a* single mutant and the double mutant were about 1 bp smaller than the wild type and the *fastkd2* single mutant, which were mostly the same size as the RNaseH2 cleavage band. This was not significant however (Figure 4.26). This could indicate that the rNMP is not cleaved by FASTKD2, but rather TOP1, which causes a 2-5bp deletion.

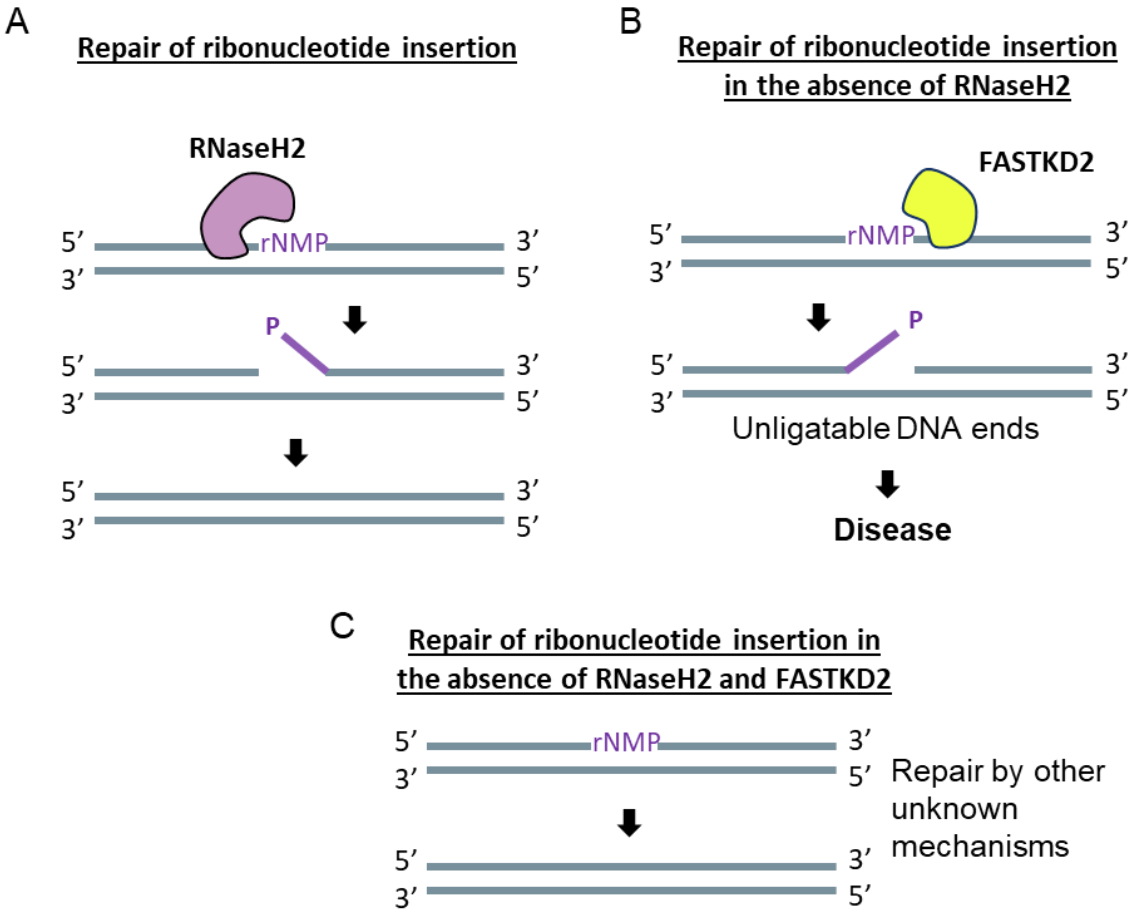

Figure 4.31: Hypothesised cleavage of rNMPs by FASTKD2. A: Cleavage of rNMP in the presence of RNaseH2. B: Cleavage of rNMP in the absence of RNaseH2. FASTKD2 cleaves

the rNMP at the 3' side, causing an unligatable nick similar to nicks by alkali conditions created by hydroxide. This causes genomic instability and disease. C: Repair of rNMPs in the absence of RNaseH2 and FASTKD2. The rNMP is removed and the nick repaired by another mechanism that causes damage, but not to the extent as FASTKD2.

Another factor could be the mitochondrial Topoisomerase IB (TOP1mt). It is encoded in the nucleus and exclusively localised to the mitochondria where it reduces topological stress during mtDNA replication and transcription. Knockout mice of TOP1mt are viable, however, TOP1mt has been associated with several cancers, and a lack of TOP1mt delays tumorigenesis (Baechler et al., 2019, Moreira et al., 2023). No current published research that I could identify implicates TOP1mt in ribonucleotide cleavage in the mtDNA.

4.3.3. FASTKD2 is required for apoptosis

A lack of FASTKD2 has shown to cause reduced nuclear fragmentation when apoptosis is induced through a mitochondrial mediated pathway in fibroblasts from patients with *fastkd2* mutations (Ghezzi et al., 2008). Further, knockdown of *fastkd2* prevents apoptosis in breast and prostate cancer cells and expression of *fastkd2* causes apoptosis in breast and non-breast cancer cells, which is independent of the mitochondrial localisation signal. Yeung et al (2011) showed that nuclear receptor interacting factor 3 (NRIF3) causes repression of interferon regulatory factor-2 binding protein 2 (IRF-2BP2) also known as DD1 interacting factor-1 (DIF-1) due to interacting with the death domain 1 (DD1) of NRIF3. Together with interferon regulatory factor-2 binding protein-1 (IRF-2BP1, or BP1) and enhanced at puberty 1 (EAP1) DIF-1 causes repression of *fastkd2* 150-300bp downstream of the transcription start site. DNA damage can initiate the p53 apoptosis pathway, causing either phosphorylation of NRIF3 which repress DIF-1, or p53 repress DIF-1 itself causing release of the DIF-1 complex and expression of *fastkd2*. This apoptosis is independent of the mitochondrial signal, and in 2014 Das speculated that an excess of FASTKD2 in the cytoplasm, reaches a threshold that further initiates apoptosis through the caspase-2 mediated pathway (Koeppel et al., 2009, Yeung et al., 2011, Das et al., 2014). Together, this suggests a strong role for FASTKD2 in apoptosis. Although, without overexpressing FASTKD2, knockdown of DIF-1 or expression of NRIF3 did not cause apoptosis in other cell types than breast and prostate cancer cells (Das et al., 2014).

Considering my results do not support a role for FASTKD2 in the RER pathway, I suggested that what I observed was the effect of apoptosis. I saw that when treating *fastkd2* homozygous

larvae with CPT to cause DNA damage, then looking for apoptosis, there was significantly less apoptosis after DNA damage in the homozygous compared to the wild type (Figure 4.16). Similarities are seen in mice defective in RNaseH2 which are not viable, and knockout of the apoptotic factor *p53* which causes partial rescue of the null phenotype (Reijns et al., 2012, Thomas et al., 2024). The *fastkd2 rnaseh2a* double mutant embryos have a lesser phenotype than the single *rnaseh2a* mutants do, possibly due to lack of apoptosis being initiated. I tested this hypothesis by looking at apoptosis in the single and double mutant, however I saw no differences in apoptosis (Figure 4.29). This could be due to the severity of the *rnaseh2a* mutant phenotype and the large amount of apoptosis happening. Alternatively, apoptosis through FASTKD2 is not happening in the *rnaseh2a* embryos. A major flaw with the apoptosis theory is that there is no increase in *fastkd2* expression in the *rnaseh2a* homozygous embryos (Figure 4.28). This suggests that the DIF-1 complex is not being released from *fastkd2* increasing its expression to cause apoptosis through the caspase-2 mediated pathway. Interestingly, Das et al (2014), suggested that it is the FAST_2 domain of FASTKD2 that is important for apoptosis (Das et al., 2014). The FAST_2 domain is not annotated in the zebrafish genome according to ensemble.org. Although this does not mean it is not there in zebrafish. A model for the potential apoptotic function of FASTKD2 in the *rnaseh2a* homozygous background can be seen in figure 4.32.

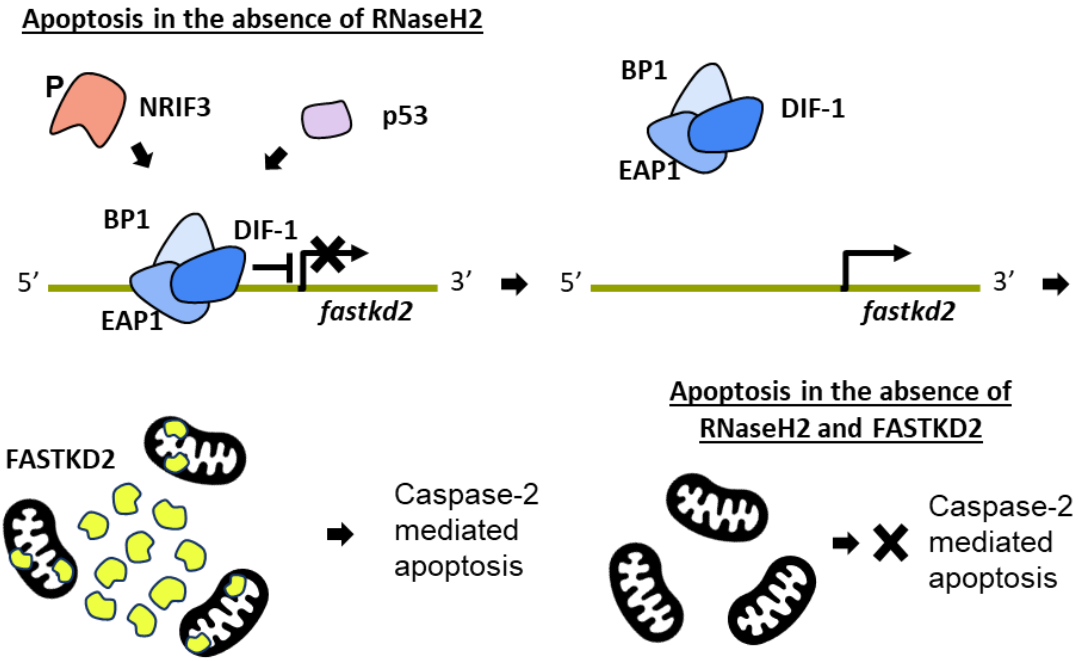

Figure 4.32: Model for apoptosis in *rnaseh2a* homozygous embryos mediated by FASTKD2. DNA breaks activate p53 or cause phosphorylation of NRIF3, which removes the DIF-1, BP1, EAP1 repression complex from the fastkd2, causing expression of fastkd2. An excessive

amount of nuclear FASTKD2 reaches a threshold causing apoptosis through a caspase-2 mediated pathway. With *fastkd2* mutated, there is no FASTKD2 to reach the apoptosis threshold and no apoptosis through the caspase-2 mediated pathway, causing less apoptosis and disease.

With this theory, the increase in *rnaseh2a* expression in the *fastkd2* mutants could be because of a general increase in oxidative damage due to the damaged mitochondria leading to an increase in rNMPs in the genome and therefore an increase in *rnaseh2a* expression. However, this does not explain the functional complementary assay in yeast initially performed where supplying FASTKD2 to an RNaseH1 and RNaseH2 deficient yeast. They saw that supplying FASTKD2 to the yeast caused increased growth compared to the mutants alone when grown on HU. With the apoptosis theory, I would expect to see decreased growth if FASTKD2 is supplied as it would increase apoptosis.

4.3.4. Adult *fastkd2* homozygous fish are no frailer than their wild type siblings

Lastly, seeing that a lack of RNaseH2 causes the adults to become frailer, I was interested in whether my adult *fastkd2* homozygous adults were frail. However, there was no difference in the wild type and homozygous BMI, width/length ratio, spinal height or tumour occurrence. The homozygous did have more damaged tail fins than the wild types suggesting they have lost their regenerative ability and suffer more fin damage. However, this was not enough to give them a higher frailty score than the wild types (Figure 4.30). Several studies have implicated the mitochondria as important in zebrafish fin regeneration. Sirt1 and UPR^{mt} are important for mitochondrial biogenesis, integrity and metabolic activity and shown by Lin (2021) to be required for fin regeneration (Lin et al., 2021). Further, knockout of mTOR causes inhibition of mitochondrial fission during fin regeneration (Xiao et al., 2024). Lastly, zebrafish with a knockout of *polg1* showed defective fin regeneration (Rahn et al., 2015). I have shown a significant decrease in *polg1* expression in the *fastkd2* homozygous larvae. This reduced *polg1* expression and the mitochondrial defects seen in the *fastkd2* homozygous mutants could be responsible for the reduced fin regeneration.

4.3.5. Conclusion

Here I have shown that a *fastkd2* homozygous knockout is viable and show no external phenotypes. They do have a mitochondrial defect resulting in less energy production. However, I have not shown that a loss of FASTKD2 result in any defects in the RER pathway

in whole cells or in the mitochondria. I show that double homozygous knockout mutants for *rnaseh2a* and *fastkd2* have increased survival compared to the *rnaseh2a* single homozygous knockout. This could be because FASTKD2 in a RNaseH2 null environment causes increased mutations as does TOP1. Alternatively, a loss of FASTKD2 might be improving the phenotype of *rnaseh2a* homozygous embryos due to a loss of an apoptosis pathway causing less cell death. However, neither of these two theories have much evidence towards them suggesting maybe another yet unknown mechanism in the process of rNMP repair.

Chapter 5 Creating an *aprataxin rnaseh2a* double mutant

5.1. Introduction

The protein APRATAXIN is encoded by the gene *aptx* and was identified separately by Moreira and Date in 2001 when studying patients with early-onset ataxia with ocular motor apraxia or ataxia-ocular apraxia 1 (AOA1). AOA1 is an autosomal recessive disease that develop in the first or second decade, and present with progressive ataxia, absence of tendon reflexes, distal loss of sense of position and vibration, pyramidal weakness of the leg, hypoalbuminemia, elevated total cholesterol and cerebellar atrophy. AOA1 presents very similarly to ataxia-telangiectasia (A-T) caused by mutations in *atm*. However, it lacks the immune deficiency, chromosomal instability and hypersensitivity to x-ray seen in A-T patients (Date et al., 2001, Moreira et al., 2001). 19 mutations in 40 families have been described to this date, and there is no current cure for the disease (Rana et al., 2013, Albaradie et al., 2022).

APRATAXIN is a member of the Histidine triad nucleotide-binding (Hint) branch of the histidine triad (HIT) superfamily of proteins, which consist of nucleotide hydrolases and transferases. Hint proteins operate as dimers. APRATAXIN contains four described domains, a central Hint-like histidine triad hydrolase domain (HIT), a C-terminal divergent zinc finger motif, and an N-terminal PNK-aprataxin amino-terminal (PANT), so named after being homologous to the terminal region of polynucleotide kinase (PNK). The PANT domain also has a forkhead-associated (FHA) motif which is a phospho-protein binding domain found in several DNA damage response proteins. There is also a predicted nuclear localisation domain between the PANT and the HIT domain (Figure 5.1) (Brenner, 2002, Clements et al., 2004, Rass et al., 2007, Moreira et al., 2001).

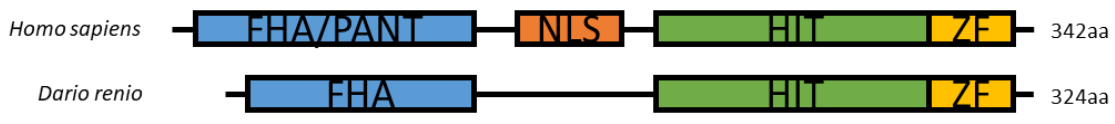

Figure 5.1: Diagram showing domains of human and zebrafish Aprataxin. The PANT and NLS domains have not been detected in zebrafish.

The function of APRATAXIN was for long unknown. *atpx* deficient cells had been described as sensitive to H_2O_2, a DNA damaging agent that causes single stranded breaks (SSB). A suggestion of an explanation for this is that the oxidative damage inflicted by H_2O_2 creates an improper 3'terminus causing abortive ligation to occur. However, consistent sensitivity to infrared radiation (IR) is not seen in AOA1 cells as is seen in A-T cells (Gueven et al., 2004, Harris et al., 2009, Imamura et al., 2023). It was also found that APRATAXIN interacted with XRCC1 and XRCC4 through the FHA domain, which interacts with DNA ligase III and IV suggesting a role in other forms of single and double stranded break repair (Clements et al., 2004, Tomkinson et al., 2006, Imamura et al., 2023). These observations made Ahel test whether APRATAXIN was involved in AMP-hydrolysis during abortive ligation of nicks (Ahel et al., 2006).

DNA ligation is a vital step in the maintenance of genomic integrity as it is involved in DNA replication, recombination and repair. It involves three chemical steps where at first an ATP molecule adenylates the active site lysine in the ligase releasing a pyrophosphate. The enzyme then binds the nick that is being sealed transferring an adenylyl to the 5'phosphate of the nick creating a 5'-5' phosphoanhydride intermediate. Lastly, the ligase ends by catalysing the 3' hydroxyl to seal the phosphodiester backbone and releasing an AMP (Tumbale et al., 2019) (Figure 5.2). If the nick has not been properly processed by other repair mechanisms before the ligase attempts to seal it, a Mg^{HiFi} site in the ligase will recognise the improper 3' end of the nick. APRATAXIN then access the nick by the ligase dissociating. APRATAXIN binds the nick via the C-terminal zinc finger domain, then catalytically removes the adenylyl from the 5'phosphate via the HIT domain, allowing for proper processing of the damage before the ligase can reattempt to seal the nick (Ahel et al., 2006, Rass et al., 2007, Tumbale et al., 2019) (Figure 5.2).

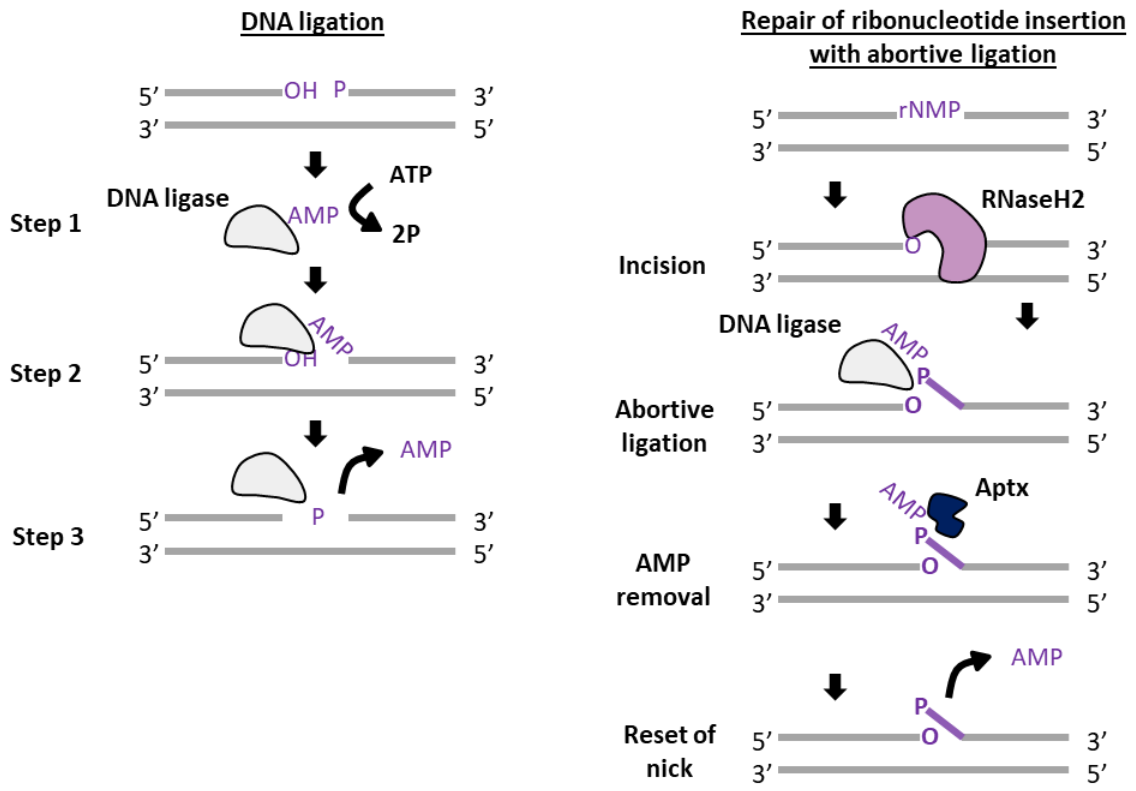

Figure 5.2: Schematic diagram of ligation and abortive ligation of a rNMP cleaved by RNaseH2, by APRATAXIN.

This process is proposed to be greatly challenged by RNA-DNA hybrids as was seen by Tumbale in 2014. Whilst 95% of nicked DNA substrates were ligated properly, if the 5' nucleotide of the nick was a ribonucleotide less than 1% of the substrates were ligated. They instead observed that 50% of the species created were 5'-adenylated products. This phenotype caused stunted or no growth in yeast deficient in APRATAXIN that had a mutation in *polg2* causing increased RNA incorporation in the DNA. These yeast cells also caused increased expression of the S-phase checkpoint marker *Rnr3*. However, if RNaseH2 activity was also removed from these yeast cells, the formation of these 5'RNA-AMP intermediates were not created to the same extent, and the checkpoint was not activated to the same exaggerated level (Tumbale et al., 2014).

Whilst APRATAXIN mostly localise in the nucleus, it has been observed that an isoform of APRATAXIN with an extra 14 amino acids on the N-terminal can localise to the mitochondria (Sykora et al., 2011). There is some evidence for APRATAXINs role in the mtDNA being more important for the stability of the mitochondrial genome than for the nuclear genome, possibly

because APRATAXIN works slower in the mtDNA than in the nucleus (Akbari et al., 2015). Cells with knockdown of *aptx* show increase in ROS, a reduced mtDNA copy number, increase in mtDNA lesion and a fragmented mitochondrial network. The loss of mitochondrial function could be a reason for the increased level of oxidative damage seen in patients with AOA1 (Harris et al., 2009, Sykora et al., 2011, Zheng et al., 2019).

APRATAXIN plays an important role in DNA damage repair, however, *aptx* knockout mice are viable with no morphological phenotype. Further, whilst knockout cells are less efficient at removing the 5'AMP, they have normal global rates of single stranded breaks (Ahel et al., 2006, El-Khamisy et al., 2009). As APRATAXIN is important for repair of abortive ligations after RNaseH2 cleavage of single rNMPs, I wondered whether making an *aptx rnaseh2a* double knockout in zebrafish could cause a phenotype in the zebrafish that could be used to study APRATAXIN function in a whole organism.

Hypothesis: *aptx* homozygous fish will show phenotypes similar to AOA1 patients such as decreased movement. Further, a *rnaseh2a aptx* double mutant will show an increase in ribonucleotide insertions, however, like yeast, no toxic rNMP ends will be created causing an improved phenotype compared to the *aptx* only.

Aims:

- Create a CRISPR/Cas9 knockout line for *aptx* in the SH478 *rnaseh2a* heterozygous zebrafish background
- Characterise *aptx* function in zebrafish larvae and assess any early phenotypes
- Characterise the *aptx rnaseh2a* double mutant zebrafish larvae

5.2. Results

5.2.1. Creating an *aptx* homozygous knockout in a *rnaseh2a* heterozygous background

Like humans, zebrafish have one version of the gene *aprataxin* (*aptx*). It is located on chromosome 1 and is 1303bp long forming a 342aa protein (ENSDART00000029252.7). It is 59.88% similar to the human APRATAXIN protein, which is 324aa encoded by a 1977bp long

gene on chromosome 9 (ENST00000379817.7) (Figure 5.3). Figure 5.3 also shows good sequence resemblance to mouse (ENSMUST00000030119.10), chicken (ENSGALT00010019417.1), tropical clawed frog (ENSXETT00000052107.4), coelacanth (ENSLACT00000003823.1) and spotted gar (ENSLOCT00000014226.1) showing good conservation. The gene for *rnaseh2a* was introduced in Chapter 3.2.7 and is also found on chromosome 1 of the zebrafish genome, only 932,993bp upstream of *aptx* (Figure 5.4A). As the mouse *aptx* mutant has no phenotype (El-Khamisy et al., 2009), when making a zebrafish *aptx* mutant I wanted to make it in the background of the *rnaseh2a* mutant in case it would cause a phenotype that could be used to study the function of APRATAXIN. As the *rnaseh2a* mutant is second generation lethal, I had to make the mutation in a *rnaseh2a* heterozygous cross. I made CRISPR/Cas9 guides using CHOPCHOP (https://chopchop.cbu.uib.no/) and created a line with a 40bp insertion in exon 4 with a stop codon 31bp into the insertion (Figure 5.4B). Due to the two genes being on the same chromosome, getting a double mutant should in theory be very difficult as the *rnaseh2a* mutations was in a heterozygous cross, not in a homozygous line like the *fastkd2* mutants in Chapter 4.2.11. In the F1 generation of the *aptx* heterozygous adults, seven fish were *aptx* heterozygous and one fish was *aptx* and *rnaseh2a* heterozygous. As both lines had the same 40bp mutation, I believe that a rare crossover event has happened in the one fish, where the 40bp *aptx* mutation, which was created on the opposite allele to the *rnaseh2a* mutation, crossed over to the allele with the *rnaseh2a* mutation. This way, when crossing the *aptx* only heterozygous and the *aptx rnaseh2a* heterozygous F1 fish, the F2 generation would be *aptx* homozygous *rnaseh2a* heterozygous.

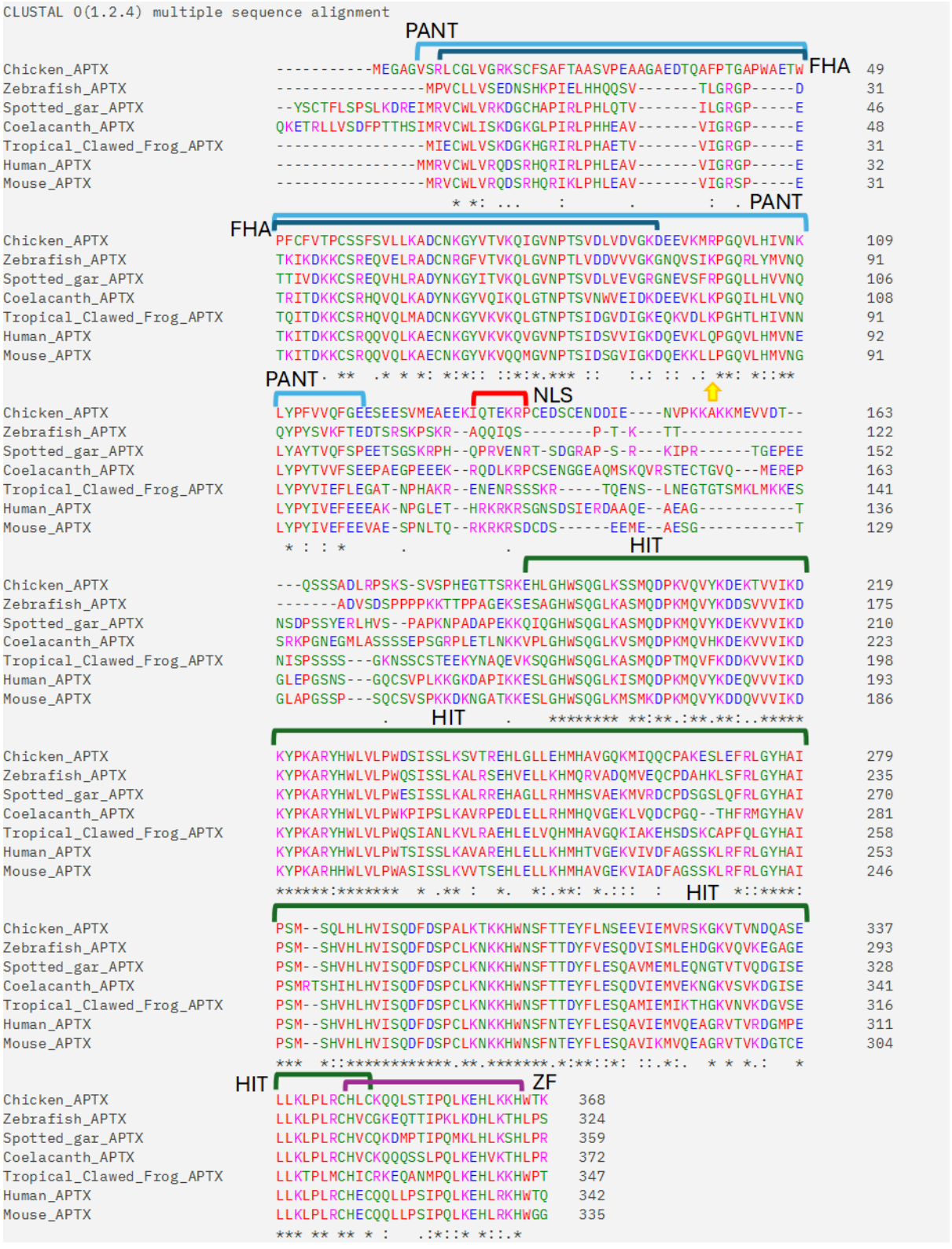

Figure 5.3: Comparison of human, mouse, chicken, tropical clawed frog, zebrafish, coelacanth and spotted gar APRATAXIN protein. Comparison performed using EMBL-EBI clustal omega multiple sequence alignment. Stars indicate same amino acid. Two dots and one dot indicate similar amino acids. Red amino are small hydrophobic amino acids, blue are acidic amino acids, magenta are basic amino acids and green are hydroxyls, sulfhydryl and amine amino

acids (Madeira et al., 2024). Yellow arrow indicates the site of the mutation in the zebrafish genome. Highlighted are the PANT domain in light blue and FHA domain in dark blue, the NLS in red, the HIT domain in green, and the Zinc finger (ZF) C-terminus in magenta. The mutation site in the zebrafish line is indicated by a yellow arrow.

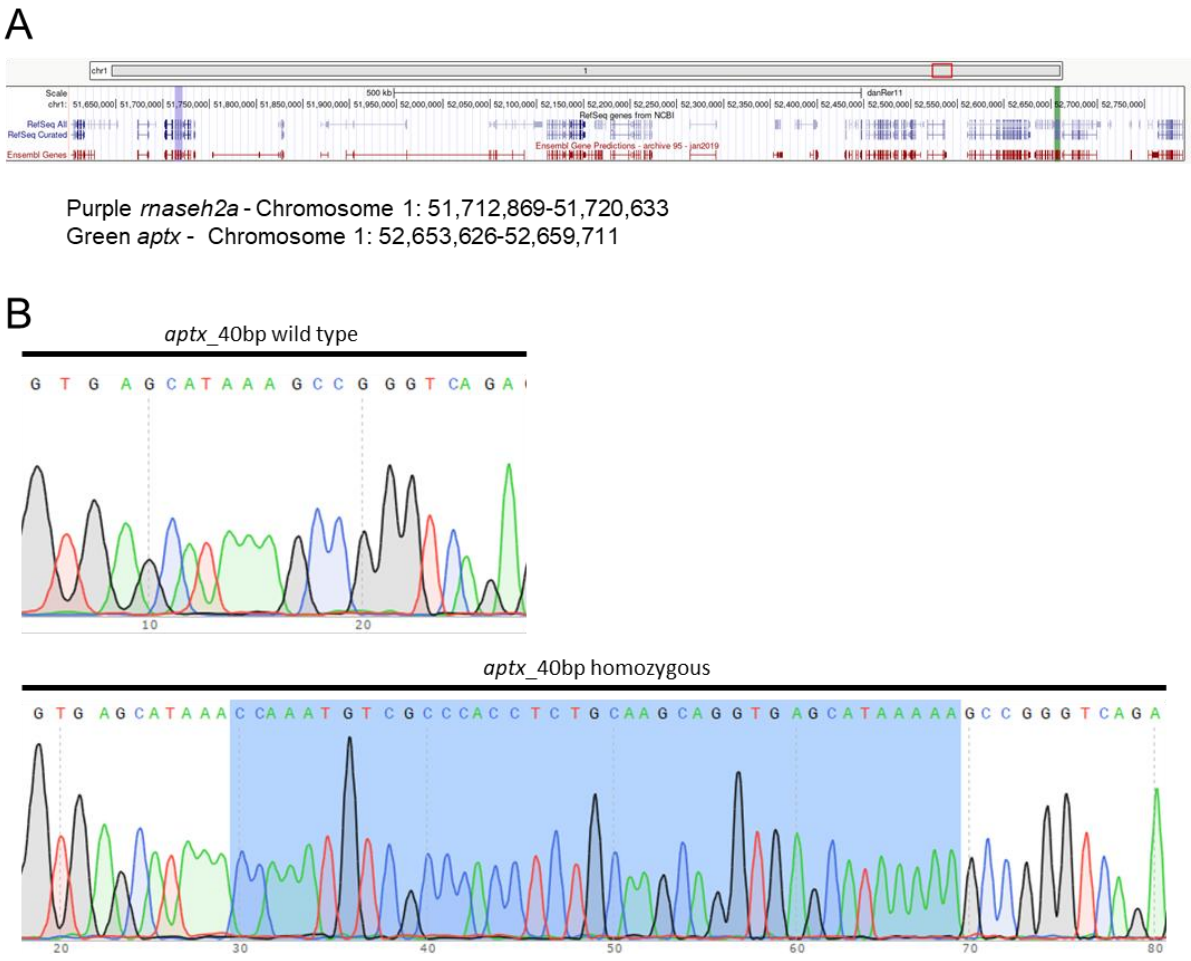

Figure 5.4: Sequence comparison between wild type and homozygous siblings *aptx* 5dpf larvae. A: Location of *aptx* compared to the *rnaseh2a* gene on chromosome 1 of the zebrafish genome. B: 40bp insertion comparison showing wild type sequence at the top and the 40bp insertion highlighted in blue in the homozygous at the bottom.

5.2.2. Phenotype of *aptx* homozygous and *aptx rnaseh2a* double homozygous larvae

As with the mice, the *aptx* homozygous zebrafish larvae are viable and show no morphological phenotype at 5dpf (Figure 5.5A). I also saw a significant reduction of *aptx* mRNA expression in the mutants, suggesting that there was likely nonsense-mediated decay of *aptx* occurring

(Figure 5.5B). Further, double homozygous larvae for *aptx* and *rnaseh2a* from *aptx* homozygous *rnaseh2a* heterozygous parents showed no phenotype (Figure 5.6A). There was also a significant decrease in *rnaseh2a* expression in the *aptx* homozygous larvae compared to wild type (Figure 5.6B). These samples were pool of *aptx* homozygous and *rnaseh2a* wild type, heterozygous and homozygous.

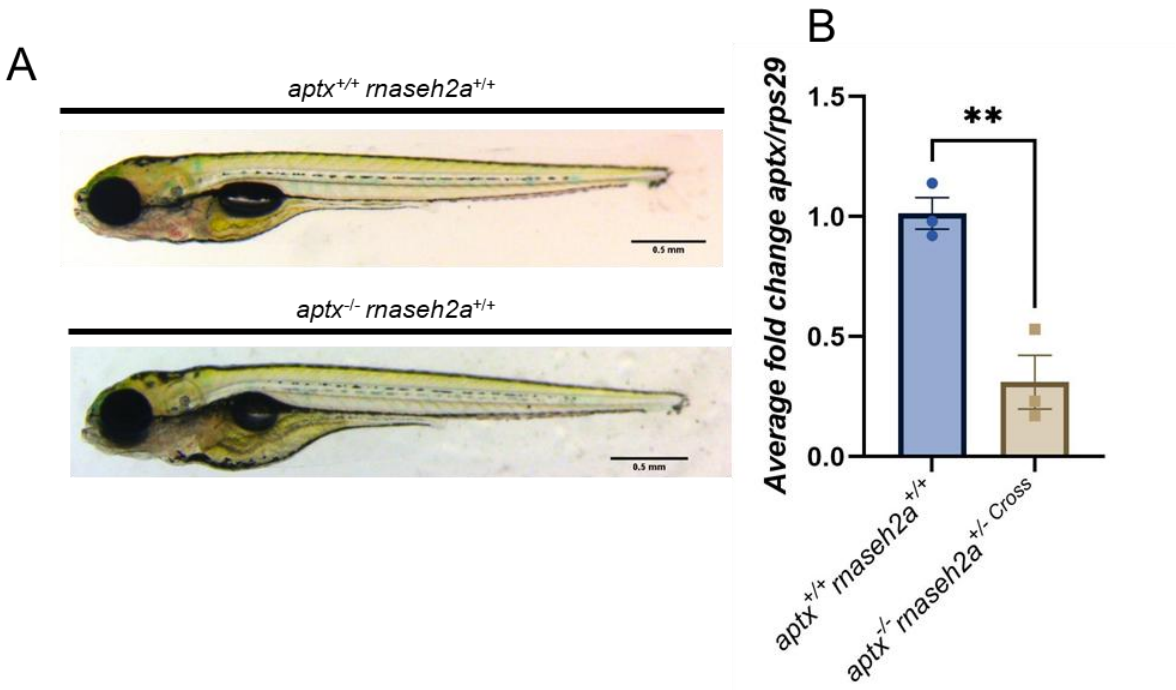

Figure 5.5: Phenotype of *aptx* wild type and homozygous 5dpf larvae. A: Bright field images of *aptx* wild type and homozygous cousins. B: Expression of *aptx* in *aptx* wild type and homozygous cousins. Unpaired t-test, n=3.

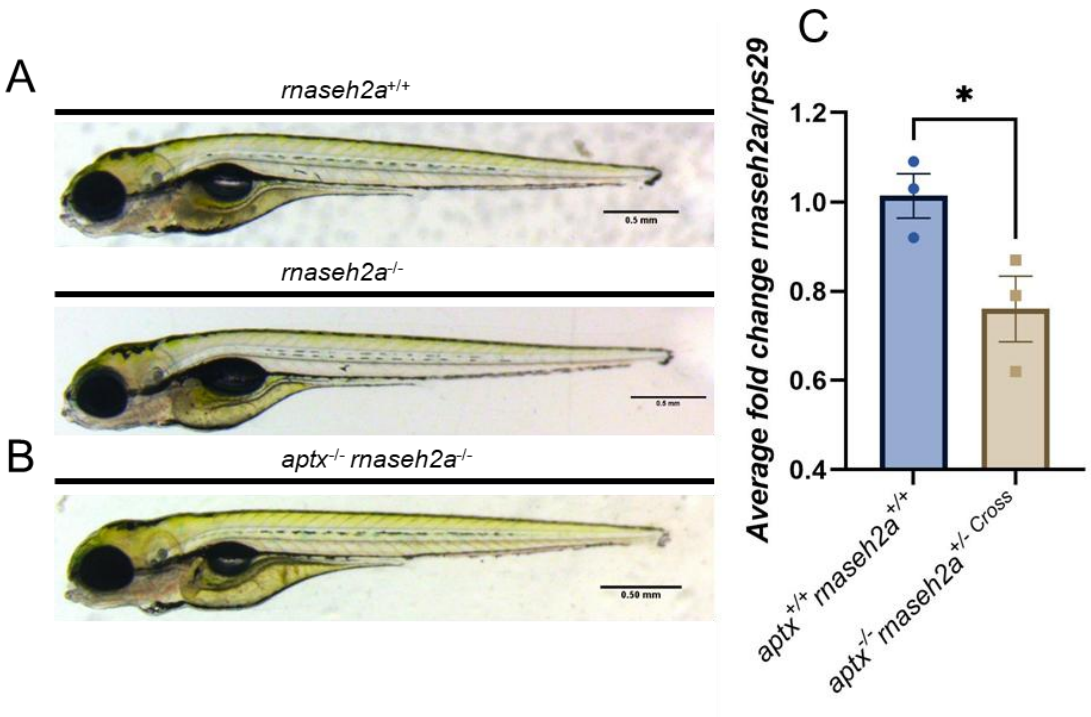

Figure 5.6: Phenotype of *aptx rnaseh2a* double homozygotes. A: Bright field image of *rnaseh2a* wild type and *rnashe2a* single homozygous from a heterozygous cross. Distantly related to the *aptx rnaseh2a* double mutant. B: Bright field image of *aptx rnaseh2a* double homozygous from a homozygous *aptx* heterozygous *rnaseh2a* cross. C: Expression of *rnaseh2a* in *aptx* wild type, and a pool of *aptx* homozygous *rnaseh2a* wild type, heterozygous and homozygous cousins at 5dpf from an *aptx* homozygous, *rnaseh2a* heterozygous cross. Unpaired t-test, n=3.

5.2.3. Behavioural analysis of *aprataxin* mutants

As introduced in the chapter introduction, individuals with AOA1 have motor disabilities (Pedroso et al., 2020). Therefore, I thought it would be interesting to investigate whether the *aptx* homozygous larvae at 5dpf had any movement disabilities. Larvae with inflated swim bladders were placed in a 96 well plate and filmed during a 30-minute light-dark cycle. I saw that the *aptx* homozygous fish moved significantly less and spent significantly less time moving than the wild types during the light and dark periods. They also spent significantly more time in inactivity than the wild type cousins too (Figure 5.7A-B and G). Whilst there was almost always at least a trend if not significance toward this pattern, the reduced movement was more pronounced at small movements than during large movements (Figure 5.7C-F). Representative images of the larvae movement during the first light period can be seen in figure 5.7H. As the homozygous *aptx* larvae in figure 5.7 were a mix of *rnaseh2a* wild type, heterozygous and homozygous larvae, I genotyped the larvae to see whether there were any

differences between the *aptx* single homozygous and the *aptx rnaseh2a* double homozygous larvae. However, I saw no difference between *aptx* wild type, *aptx* single homozygous or *aptx rnaseh2a* double homozygous when it came to the total time or the distance they moved or the time they spent moving (Figure 5.8A and B). However, there was still a trend where both *aptx* homozygous lines spent less time and moved less in the light. When looking at the small movements only, there was a significant difference in the time spent moving between wild types and *aptx rnaseh2a* double homozygous (Figure 5.8C). It was not significant for the *aptx* single mutant very likely due to the low numbers. Example images of the movement by the larvae can be seen in figure 5.8D.

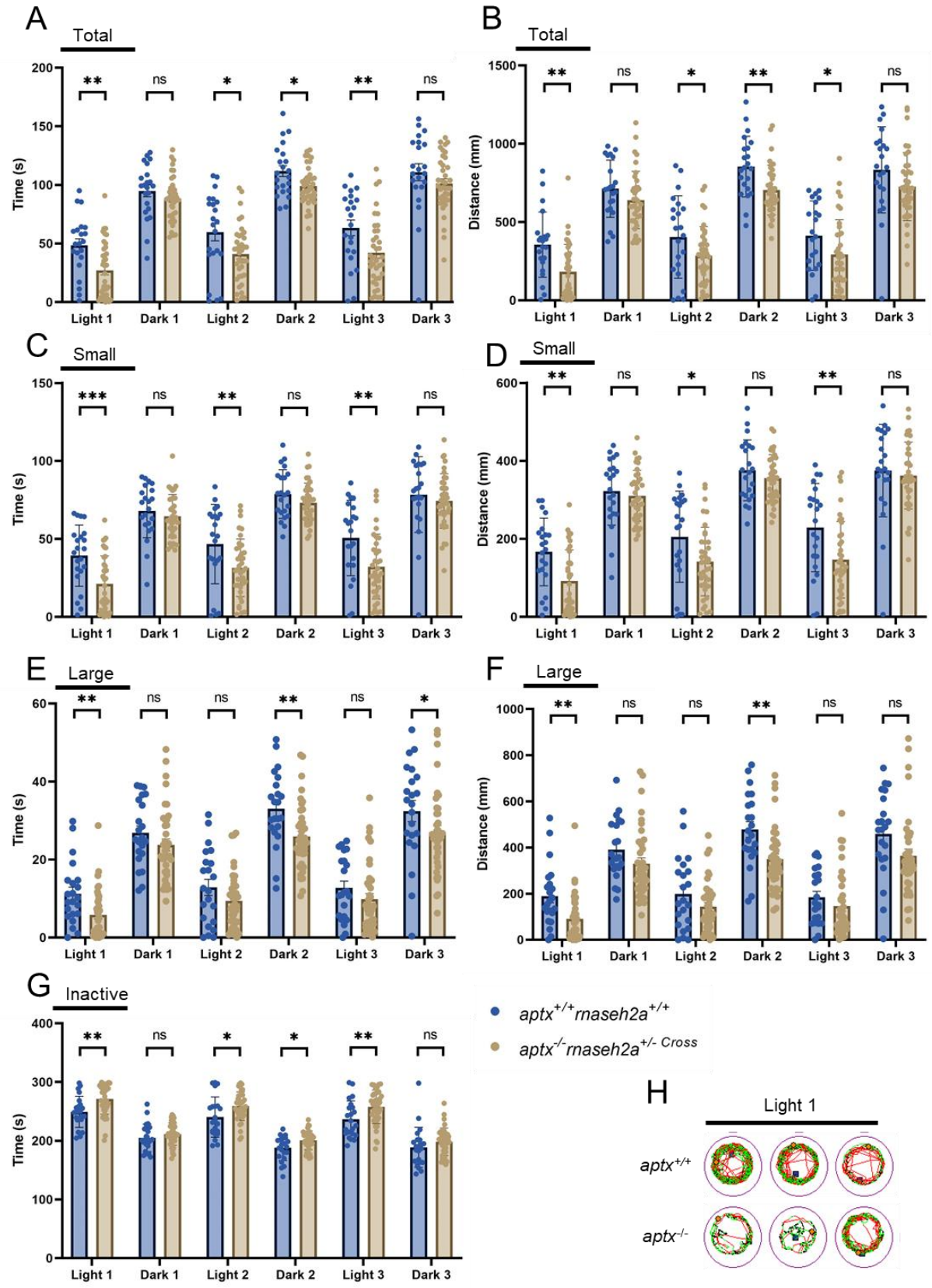

Figure 5.7: Movement analysis of *aptx* wild type and homozygous 5dpf larvae during a 30-minute light-dark cycle. A: Total time (s) spent moving. B: Total distance (mm) moved. C: Time (s) spent moving at small speed. D: Distance (mm) moved at small speed. E: Time (s) spent

moving at large speed. F: Distance (mm) moved at large speed. G: Time (s) spent inactive. F: Representative movement tracing from the light 1 period. Green = small movement, Red = large movement, Yellow circle = larvae. Unpaired t-test, wild type n= 22, homozygous n=38. Small speed refers to movement made between the thresholds 3 and 9 according to the Zebrabox Viewpoint system.

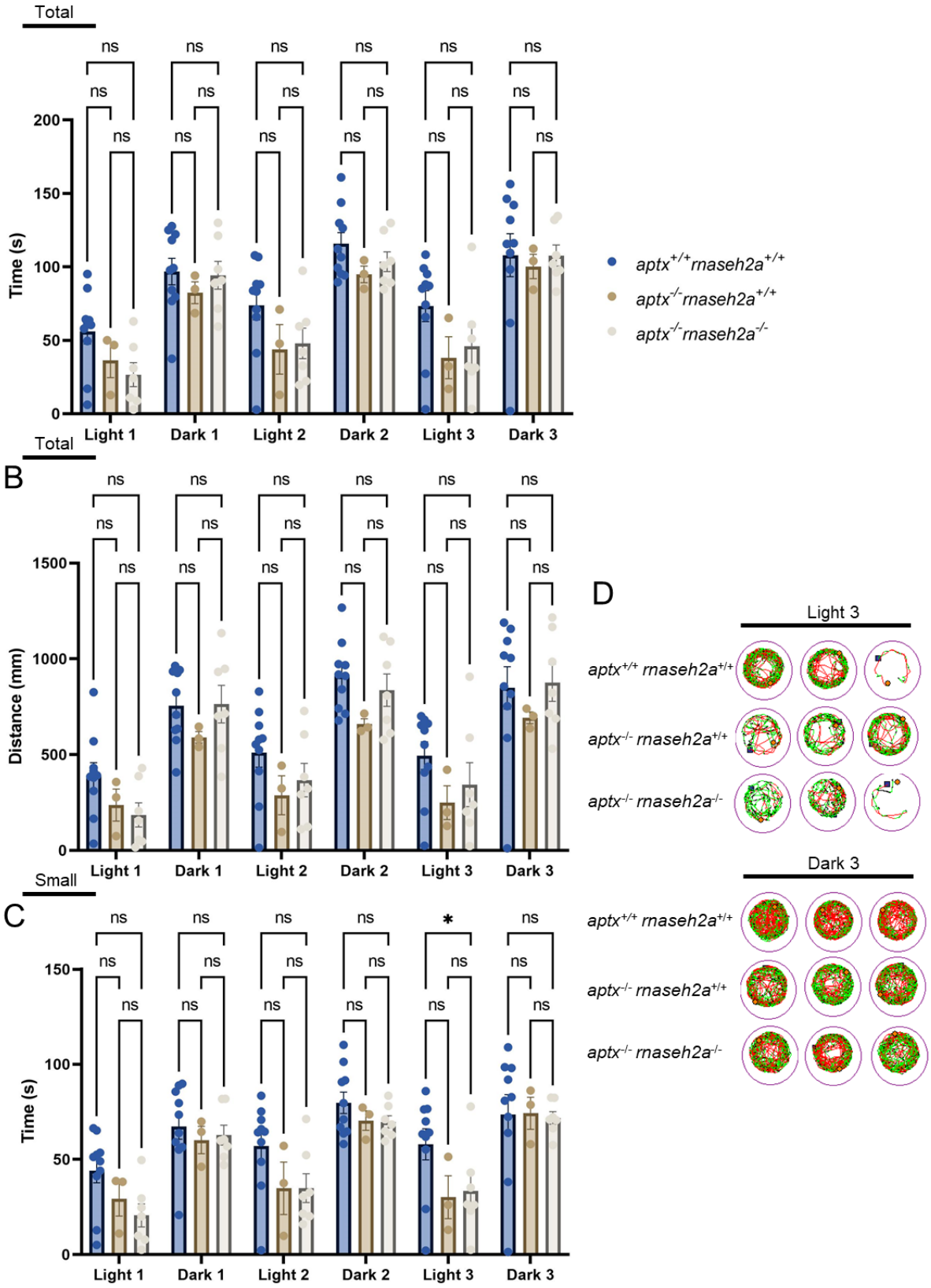

Figure 5.8: Movement analysis of *aptx_rnaseh2a* wild type, single *aptx* and double homozygous larvae at 5dpf during a 30-minute light-dark cycle. A: Total time (s) spent moving. B: Total distance (mm) moved. C: Time (s) spend moving at small speed. D:

Representative movement tracking at light and dark period 3 during the 30 minutes for wild type, single and double mutant larvae. Green = Small movement, Red = Large movement, Yellow circle = larvae. Two-Way ANOVA, wild type n= 10 (first 10 of assay), *aptx* homozygous n=3, *aptx rnaseh2a* homozygous n=7. Small speed refers to movement made between the thresholds 3 and 9 according to the Zebrabox Viewpoint system.

5.3. Discussion

Ligation is an important step in every DNA repair pathway. However, occasionally a DNA ligase might attempt to ligate a nick in the DNA prematurely by transferring an adenylyl to the 5'phosphate of the nicked base. This might happen after rNMP cleavage by RNaseH2, before the rNMP has been processed by other repair mechanisms. In this case, the abortive ligation can be corrected by APRATAXIN, where APRATAXIN cleaves of an adenylyl from the rNMP resetting the nick to be processed by the appropriate pathways (Ahel et al., 2006, Rass et al., 2007, Tumbale et al., 2014, Tumbale et al., 2019). However, this was shown by Tumbale in 2014 to not be very efficient, and if RNaseH2 cleaved a ribonucleotide and the ligase had to go through abortive ligation, there was only less than 1% chance of APRATAXIN to reset the nick for repair (Tumbale et al., 2014). Loss of APRATAXIN function in humans causes the disease Ataxia with Oculomotor Apraxia 1 (AOA1) where individuals display among others progressive ataxia, loss of tendon reflexes, distal loss of sense of position and vibration and weakness of the leg within the first or second decade (Date et al., 2001, Moreira et al., 2001). There are currently no treatments for AOA1, and single *aptx* homozygous mice show no phenotype (Ahel et al., 2006, El-Khamisy et al., 2009). Therefore, I hypothesised that by knocking out both *aptx* and *rnaseh2a* in zebrafish, I could create a model to study AOA1 in a whole organism.

Using CRISPR/Cas9 I created a 40bp insertion in exon 4 of *aptx*. This created a frameshift in the gene and an early stop codon causing a truncated gene that possibly went through non-sense mediated decay causing a loss of APRATAXIN (Figure 5.5B). However, the 5dpf larvae from a homozygous *aptx* cross did not show any morphological phenotype compared to their wild type cousins (Figure 5.5A). Further, this mutation was created in the background of a *rnaseh2a* heterozygous mutation to be able to create a double mutant. However, the double *aptx rnaseh2a* homozygous larvae did not show a phenotype either compared to the wild types or the distantly related *rnaseh2a* single mutant from a heterozygous cross (Figure 5.6). Further, due to the motor disabilities reported in AOA1 individuals (Pedroso et al., 2020), I decided to assess the movement abilities of the 5dpf larvae, and interestingly I saw that the

homozygous larvae, independent of the *rnaseh2a* mutation, moved significantly less than their wild type cousins (Figure 5.7 and 5.8). I used a light-dark cycle to invoke movement during filming. A transmission from light to dark is usually a stimulus for the larvae, causing increased movement (Basnet et al., 2019). Interestingly, a double mutant mouse for *aptx* and *atm* also shows ataxia and motor disorders. Single mutants for each gene however, did not as mentioned previously (Perez et al., 2021).

Once the *aptx* homozygous line was established, I unfortunately did not have enough time to assess its phenotype in detail, and there are several interesting studies that can be done in both larvae and adults. First, I would have liked to assess the ability of the larvae to process DNA breakages caused by CPT. Madson et al., (2023), showed that *aptx* knockout cells had a reduced cGAS-STING response upon activation, suggesting that APRATAXIN is important in the innate immune response (Madsen et al., 2023). CPT can activate the cGAS-STING response, and is a drug readily used in my lab to assess responses to DNA damage (Cao et al., 2022, Thomas et al., 2024). After CPT treatment, as well as assessing the immune response, I would like to assess the level of DNA damage by γH2AX immunofluorescence as well as western blot. In addition, APRATAXIN has been implicated in mitochondrial biology, and many AOA1 individuals present with peripheral neuropathy and ataxia which is also often seen in diseases associated with mitochondrial function such as mutations in *fastkd2* which was explored in Chapter 4. Cells with a loss of *aptx* show mitochondrial dysfunctions such as loss of mitochondria and mtDNA, as well as loss of ETC subunits such as coenzyme Q_{10} (CoQ_{10}) (Garcia-Diaz et al., 2015, Sykora et al., 2011). Further, as AOA1 is a disorder that manifests during the first or second decade of an individual's life, I would like to assess the *aptx* homozygous adult zebrafish in more detail. Perez et al., 2021, saw decreased weight with age in the *aptx atm* double knockout mice as well as decreased efficiency in the pole and gate tests at 400 days old (Perez et al., 2021). Therefore, to investigate if similar effects could be seen in the adult *aptx* mutant zebrafish, I would like to do tank behavioural analysis, swimtunnel assay and Y-maze behavioural tests on the adults. Kalueff (2013) presents several interesting adult behaviours for zebrafish that could be investigated with the methods mentioned that I would like to look into (Kalueff et al., 2013). Lastly, it would be interesting to observe second-generation *aptx rnaseh2a* homozygous embryos. In yeast, less 5'RNA-AMP products were created in double knockouts resulting in less checkpoint activation and disease (Tumbale et al., 2014). It would be interesting if a second-generation double knockout in zebrafish would change the phenotype seen in single *rnaseh2a* mutants (Thomas et al., 2024).

5.3.1. Conclusion

In this chapter, I have created an *aptx* homozygous *rnaseh2a* heterozygous zebrafish line which shows no morphological phenotype compared to their wild type cousins. However, like AOA1 individuals they have motor disability with reduced movement at 5dpf. This phenotype does not appear to be strongly influenced by an additional loss of *rnaseh2a*. As there is no other whole organism to study AOA1, it does seem that the *aptx* homozygous zebrafish might be a good model as there is a movement phenotype at 5dpf, which could be good to study drugs that might modulate the disease.

Chapter 6 Rescuing NuMA phenotype in *numa* knockout zebrafish embryos

6.1. Introduction

The Nuclear Mitotic Apparatus (NuMA) protein has several functions in nuclear structure (Kiyomitsu and Boerner, 2021). Recently it has also been linked to oxidative DNA damage at non-coding regions (promoters and enhancers) (Ray et al., 2022). During interphase NuMA is a nuclear protein, however during mitosis, it translocates to the cytoplasm to be involved in nuclear reformation and spindle formation (Merdes et al., 1996, Kiyomitsu and Boerner, 2021). It acts as a mitotic dynein adaptor, interacting with cytoplasmic dynein and dynactin to tether microtubules to spindle poles as shown by Merdes et al., (1996). When they immunodepleted NuMA from *Xenopus* eggs they failed to form normal mitotic spindles (Merdes et al., 1996). At the mitotic cell cortex NuMA interacts with leucine/glycine/asparagine-repeat-containing protein (LGN) to from a NuMA/LGN/Gαi complex to position the spindles correctly (Du and Macara, 2004, Kiyomitsu and Boerner, 2021).

Human NuMA is a large protein of 238kDa. Both the N-terminal and the C-terminal domains are globular domains, and the central part of the protein is a long coiled-coil domain. A schematic diagram of the domains of human NuMA can be seen in figure 6.1. Whereas the globular domains interact with other factors, the central domain is structural and has an intramolecular regulatory function (Compton et al., 1992, Yang et al., 1992, Kiyomitsu and Boerner, 2021). The globular N-terminus of NuMA performs the essential function of binding the dynein during spindle formation (Kotak et al., 2012). The globular C-terminus of NuMA, has several domains that are linked to both localisation and function. Two of its domains are for microtubule contact (Du et al., 2002, Gallini et al., 2016), as well as contact with LGN (Zhu et al., 2011, Seldin et al., 2013). It also has two domains for interactions with the plasma membrane (Kotak et al., 2014, Zheng et al., 2014). More important for this thesis is a DNA binding domain. A small C-terminal region from 2058-2115aa is required for DNA interactions *in vitro* and in cells, and it contains the critical amino acids for DNA interactions. Rajeevan et al., (2020), showed that cells lacking this region of NuMA had an improper chromosome recondensation during mitotic exit and the cells had an abnormal nuclear shape (Rajeevan et al., 2020). The C-terminus also contains a nuclear localisation signal (NLS) which can interact with importin-α and importin-β (Chang et al., 2017).

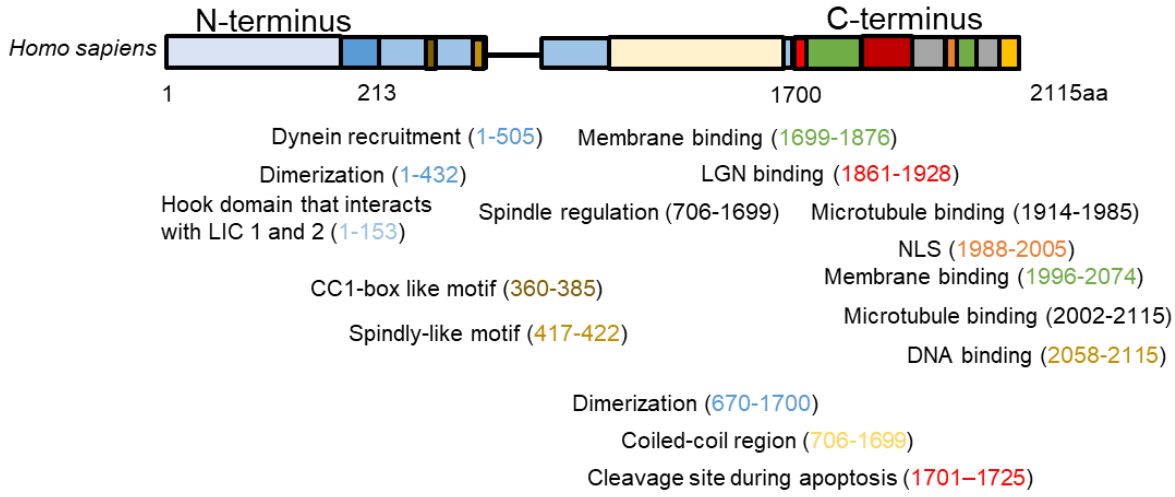

Figure 6.1: Diagram showing important domains of human NuMA. Adapted from Kiyomitus and Boerner (2021).

Recently, NuMA has been identified as a key player in oxidative DNA damage repair in non-coding promoter and enhancer regions. In 2019 Moreno identified that with a NuMA knockdown, in response to DNA damage, there was a decrease in 53BP1 and NuMA localisation and 53BP1 diffusion increased suggesting that 53BP1-mediated repair was negatively regulated by NuMA (Salvador Moreno et al., 2019). Further, in 2022, Rey showed that NuMA was a key player in protection against oxidative damage at promoter regions. By examining an existing RNA-seq dataset for the cerebellum on the GTEx portal, they identified high expression of NuMA along with other single stranded DNA repair proteins. When investigating other cell types, they identified that there was a delay in single stranded DNA repair caused by oxidative damage when there was a depletion of NuMA in each of these cell types. RNA-seq of NuMA deficient cells treated with H_2O_2 showed that several genes required for single stranded DNA repair, including *xrcc1*, *lig3, tdp1* and *parp1* were dependent on NuMA for their expression. However, double stranded DNA repair genes including *xrcc4*, *lig4*, *mer11* and *53bp1* were not. They also showed that through the PARylation of NuMA by PARP1, NuMA became an interactor of single stranded repair proteins such as XRCC1, PARP1 and TDP1, as well as the initiating form of DNA polymerase ε (Pol2). Furthermore, they identified that it was the globular C-terminal of NuMA that made these interactions, and the reintroduction of the globular C-terminal domain was sufficient to rescue DNA damage. NuMA is also required for retention of Pol2 at promoters, as NuMA depletion causes PARylation of Pol2 and release from the promoter. They believe this ensures rapid recovery of transcription after repair. They also observed an increase in oxidative damage in promoter regions

specifically in NuMA deficient cells. They concluded that NuMA is required to protect non-coding promoter regions from oxidative damage. Upon damage, single stranded repair proteins are recruited, and Pol2 is retained at the promoter for rapid recovery after repair (Ray et al., 2022, El-Khamisy, 2023).

Most of the research regarding NuMA function has been done *in vitro*, as NuMA is an essential protein for normal development in mice (Silk et al., 2009). Therefore, there is limited research on whole-organismal function of NuMA. To address this gap, Dr Ruth Thomas made a CRISPR/Cas9 knockout line of *numa* in zebrafish. *numa* mutant homozygous larvae are lethal at day 4, and they show a strong phenotype at 1dpf. In this project, I am asking the question whether the lethal phenotype of the *numa* mutant is due to its mitotic function, or its role in DNA repair. To answer this question, I wanted to incorporate different regions of *numa* into the *numa* homozygous background and look for a rescue of the phenotype. I started with attempting rescue of the phenotype with either full length *numa* or the C-terminus NuMA. The C-terminus region was chosen as it contains the DNA binding domains of NuMA, and if the phenotype observed in the larvae was due to the DNA repair function of NuMA, then the C-terminus only would cause a rescue.

Hypothesis: Incorporation of C-terminal NuMA (1700-2115aa) or full-length NuMA into the *numa*$^{-/-}$ zebrafish genome will rescue the phenotype seen in homozygous *numa* embryos. Further, re-introduction of different parts of *numa* will tell us what phenotype is associated with the DNA repair function of NuMA.

Aims:

- Make plasmids with C-terminal and full-length *numa*
- Inject plasmids into *numa* heterozygous crosses and raise viable *numa* siblings to create transgenics
- Observe a rescued *numa* phenotype

6.2. Results

6.2.1. *numa* homozygous zebrafish embryos are non-viable

Zebrafish have one copy of the *numa* gene, which is 7806bp long, with 22 coding exons and makes a 2450aa protein (ENSDART00000166209.2), whilst the human *numa* gene is 7198bp, making a 2115aa protein (ENST00000393695.8). The proteins share a 31% identity. A comparison of the human, zebrafish, mouse (ENSMUST00000084852.13), chicken (ENSGALT00010005604.1), tropical clawed frog (ENSXETT00000066916.2), coelacanth (ENSLACT00000012878.1) and spotted gar (ENSLOCT00000009578.1) proteins can be seen in Appendix 9.2. To study the involvement of NuMA in a whole organism, Dr Ruth Thomas made a heterozygous *numa* line with a 112bp insertion in exon 14 through CRISPR /Cas9 editing. The mutant had an early stop codon 5aa downstream of the insertion creating a truncated protein, completely removing the C-terminus of NuMA. Although the heterozygous adults survive until adulthood, their homozygous embryos showed a small head with small eyes, their heads were grey indicating necrosis, the embryos suffered from oedema of the heart and a curved tail causing them to only be able to swim in tight circles (Figure 6.2A). By day 4 their hearts stoped beating and the whole body started to go through necrosis to decompose. Figure 6.2B shows a decreased expression of *numa* in the homozygous compared to the siblings.

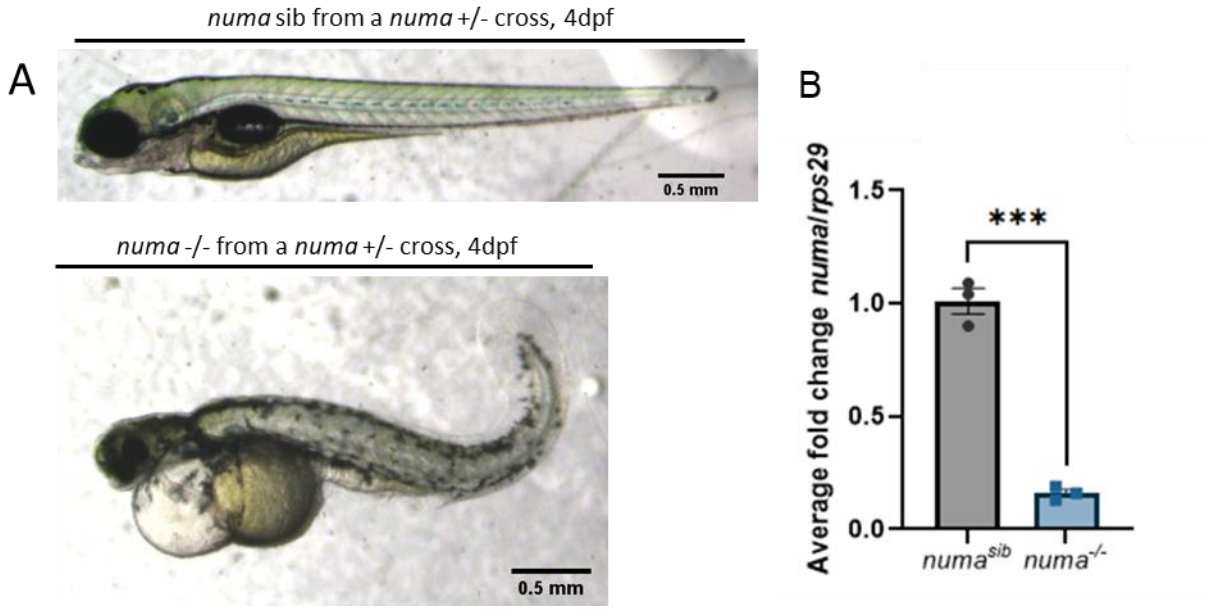

Figure 6.2: Phenotypes from a *numa* heterozygous cross. A: *numa* sibs show no phenotype at 4dpf whilst *numa* homozygous embryo at 4dpf presents with small head and eyes, necrosis in the head, oedema of the heart and a curved tail. B: Expression of *numa* in siblings and *numa* homozygous 24hpf embryos.

Attempts were made by Dr Ruth Thomas to rescue the phenotype of *numa* homozygous embryos. She had injected mRNA of both full length and C-terminus human *numa* into the one-cell stage zebrafish embryos, but the mRNA appeared to degrade causing no rescue of the phenotype. Therefore, in this thesis, I attempted to make plasmids containing full length or C-terminus human *numa* to integrate the DNA into the zebrafish genome using the Tol2 transposase system.

6.2.2. Generation of a pNuMA_1700-2117_ubi_CFP expression clone

To incorporate DNA into zebrafish genomes, I used the transposase Tol2. Tol2 originates from the medaka fish (*Oryzias latipes*) and the gene is 4.7kb in length and produces a transposase protein consisting of 4 exons. The transposase operates in a cut-and-paste fashion without rearranging the target sites. mRNA for Tol2 is injected together with a plasmid containing the DNA construct to be integrated into the genome of the zebrafish. The plasmid contains Tol2 recognition sites, where the transposase will cut and move the construct into an undefined open region of the zebrafish genome (Kawakami, 2007). The expression plasmids I would make for this project would contain the Tol2 sites. In between the Tol2 sites I would have *numa* full length or C-terminus with a GFP tag on the N-terminus. Expression would be by *ubiquitin* (*ubi*) promoter, which is a strong promoter with mostly ubiquitous expression in the embryo (Mosimann et al., 2011) (Figure 6.3).

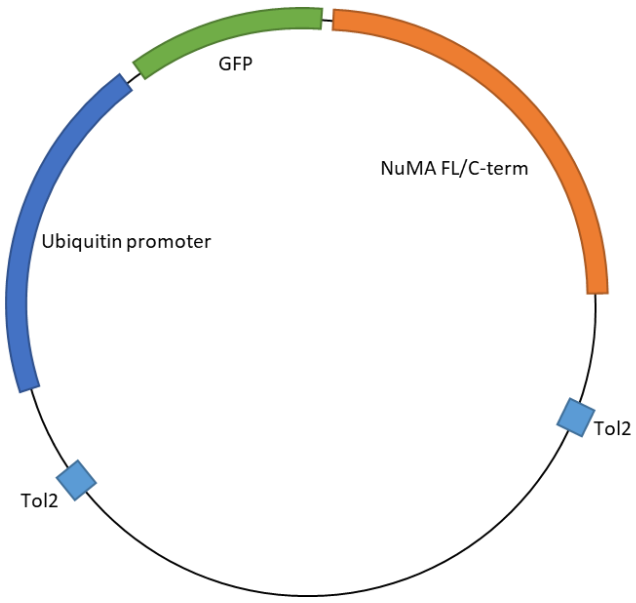

Figure 6.3: Schematic diagram of plasmid generated to rescue the *numa* phenotype seen in *numa* homozygous embryos. Within the two tol2 sites there is a *ubiquitin* promoter driving GFP attached to the N-terminus of the human *numa* full length (FL) or C-terminus gene.

Due to the large size of the NuMA protein, it was decided that it would be most appropriate to start making a plasmid containing the C-terminus of *numa*, between 1700-2115bp. It is the part of NuMA with the DNA binding domain, and it has been reported to be sufficient and indispensable for DNA repair. I used human *numa* because it was already available in a plasmid in Professor Sherif El-Khamisy's laboratory. However, as the plasmids were made for cell culture transfections, they did not contain the necessary segments for a LR reaction to be able insert the C-terminus of *numa* into a plasmid with the required Tol2 segments. Therefore, together with Dr Ruth Thomas, I attempted to PCR the C-terminus of *numa* from the plasmid using primers with overhanging attB1 and B2 sites for a following BP reaction. With PCR the C-terminus *numa* was successfully copied out of the plasmid (Figure 6.4A), however, the following BP reaction was not successful as shown in figure 6.4B, where the digestion of the BP product with XhoI, PvuI and BamHI shows that the plasmid was only containing the donor plasmid p221, and not the PCR product of 2044bp.

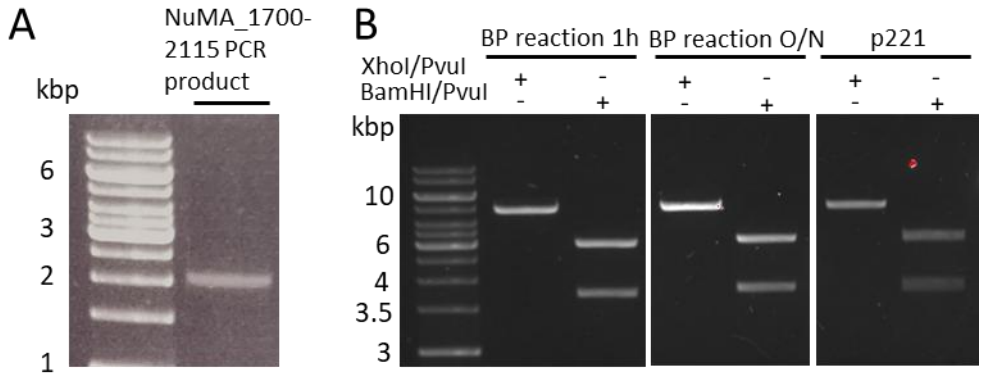

Figure 6.4: Attempted BP reaction for NuMA_1700-2115 into p221 vector. A: NuMA_1700-2115_GFP PCR product of 2044bp with attB1 and attB2 sites. B: Digestion with XhoI and PvuI and BamHI and PvuI for BP reactions with NuMA_1700-2115 PCR_GFP product and p221 donor vector, and same digestions for the p221 donor vector alone. Digestions were left for 1h as per manufacturer's instruction and overnight (O/N).

As the BP reaction was unsuccessful, I instead attempted restriction cloning into a plasmid that already contained the required LR reaction sites. The plasmid I chose to modify was an EGFP plasmid. By restriction digestions and gel purification, I isolated the C-terminus of *numa* bound to GFP on the N-terminus, and the backbone of the EGFP plasmid, removing the original GFP (Figure 6.5A). The two fragments were then ligated together (Figure 6.5B), before an LR reaction was performed to combine the pME_NuMA_1700-2115_GFP, with the ubi promoter, a polyadenylation signal in the 3'UTR for stabilisation and the Tol2 backbone (Figure 6.5C). The predicted plasmid (Snapgene) can be seen in figure 6.5D. The plasmid was injected into one-cell stage *numa* heterozygous crosses. *numa* sibling embryos showing GFP expression at 5dpf were chosen for raising (Figure 6.5E). However, none of the 15 embryos raised were transmitting GFP when outcrossed at 3 months. The plasmid itself did not cause a detectable rescue of the phenotype when injected into G0 as seen in figure 6.5F, where GFP-positive embryos still present with a small head with necrosis and small eyes, oedema of the heart and a curved tail, but this might be the result of mosaic inheritance of injected DNA.

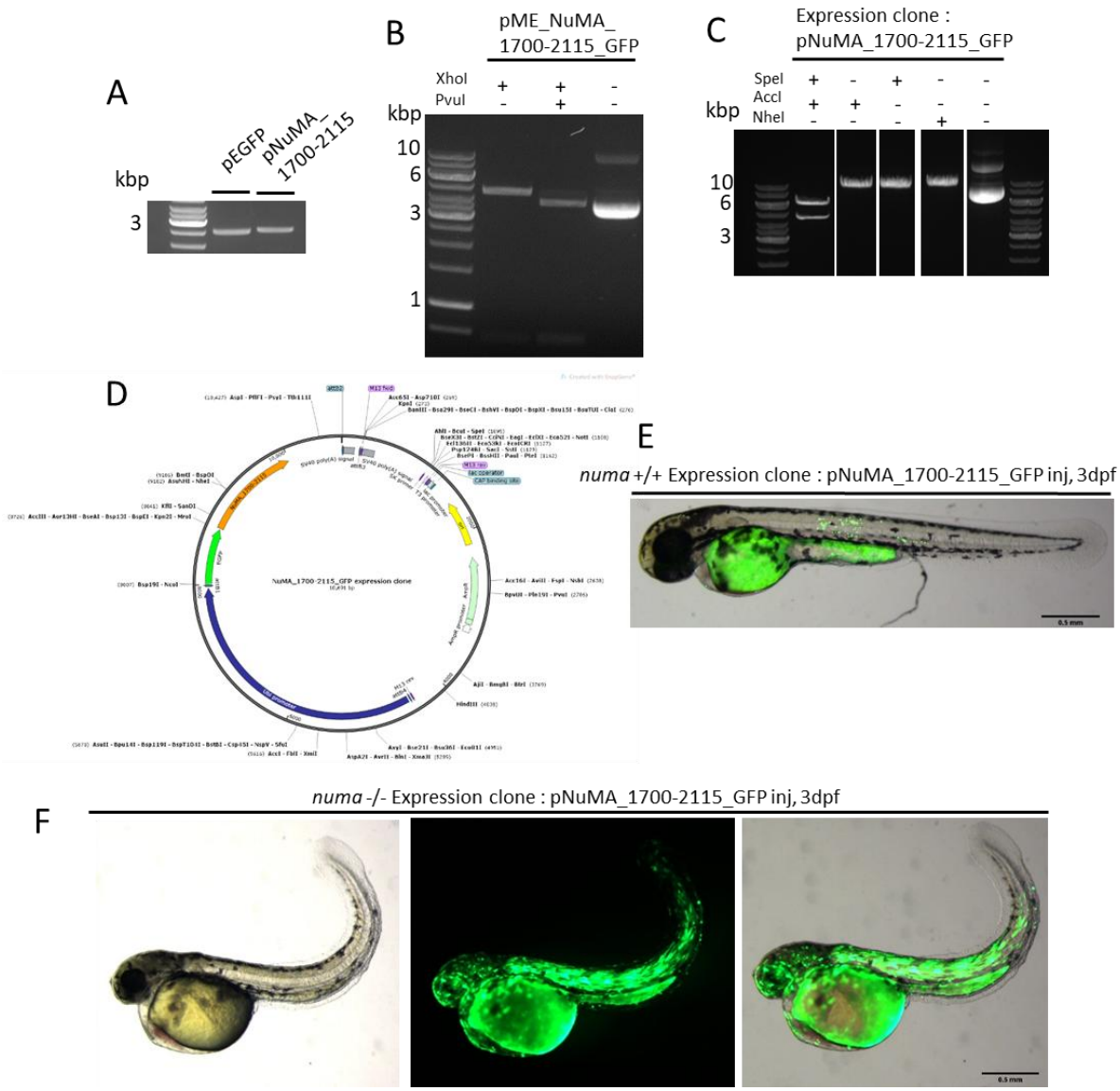

Figure 6.5: Digestion and ligations to produce a NuMA_1700-2115_GFP expression clone to be injected into *numa* heterozygous crosses. A: Gel extracted pEGFP vector without GFP (2591bp) and pNuMA_1700-2115_GFP (2641bp) after digestion with BtgI and EcoRI. B: Digestion with XhoI and PvuI after ligation of gel purified pEGFP and pNuMA_1700-2115_GFP (5232bp). C: Digestions with SpeI, AccI and NheI after LR reaction of pME_NuMA_1700-2115_GFP with ubi promoter, p3e-Sv40polyA, and empty vector tet2pA2 (10,691bp). D: Predicted plasmid map of NuMA_1700-2115_GFP expression clone. E and F: NuMA_1700-2115_GFP expression clone injected at one-cell stage into *numa* heterozygous cross embryos showing expression of the plasmid in wild type (E) and Homozygous (F), but no rescue of the *numa* phenotype (F) as the Homozygous embryo presents with small head and eye, necrosis in the head, oedema of the heart and a curved tail.

GFP needs to be expressed at a relatively high level to be visible (Amsterdam *et al.*, 1996). In the case that the GFP-NuMA was expressed, but the GFP was not visible, I modified the plasmid to contain a transgenesis marker: CFP controlled by a *cry* promoter. The *cry* promoter drives the expression the gene *crystallin* which is expressed in the lens, causing anything driven by the *cry* promoter to be expressed in the eye. Embryos with successful transmission of the plasmid would therefore have blue eyes. A new LR reaction was performed with a new Tol2 backbone containing the *cry*:CFP construct (Figure 6.6A). A predicted plasmid structure can be seen in figure 6.6B. The plasmid was injected into one-cell stage *numa* heterozygous crosses. Embryos with CFP fluorescent eyes and scattered GFP expression were raised to adulthood (Figure 6.6C). However, none of the 15 embryos raised were transmitting GFP or CFP expression eyes.

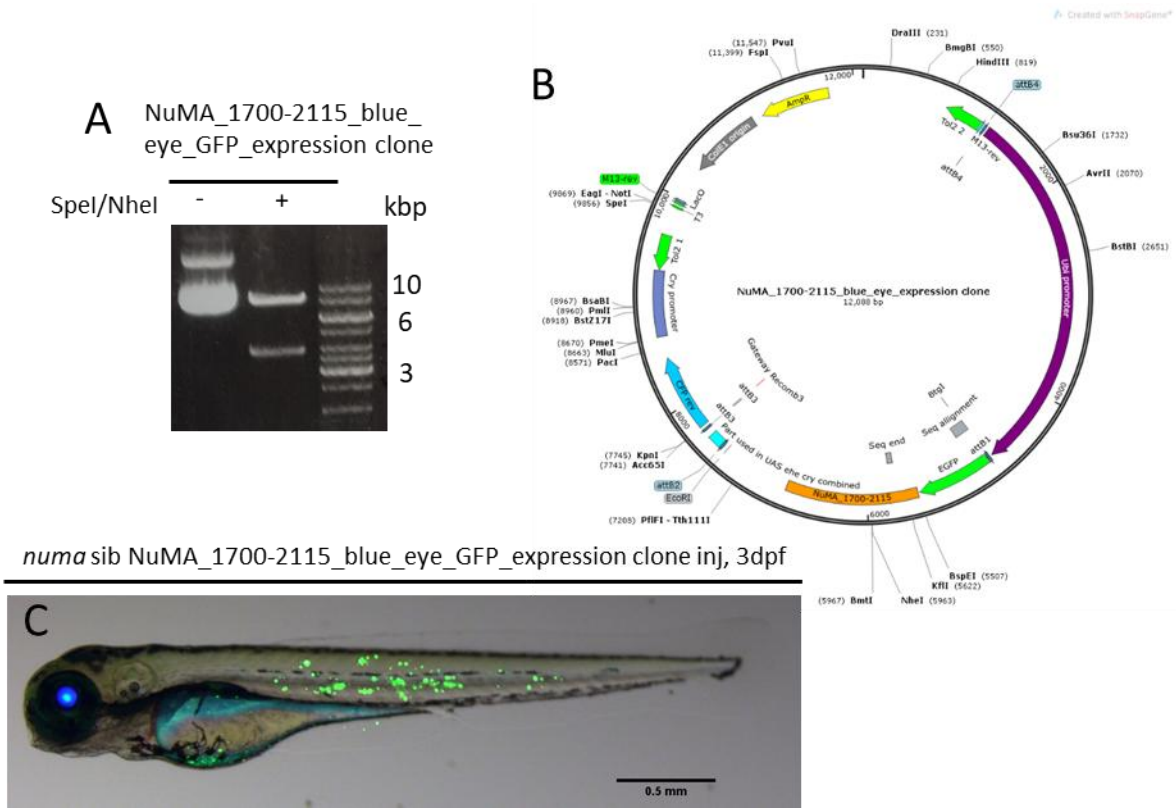

Figure 6.6: Confirmation of NuMA_1700-2115_GFP_blue_eye_expression clone to be injected into numa heterozygous crosses. A: Digest of NuMA_1700_2115_GFP_blue_eye expression clone after LR reaction with pME_NuMA_1700-2115_GFP, ubi promoter, p3e-Sv40polyA, and empty vector with CFP directed by a *cry* promoter (12,088bp) with SpeI and NheI. B: Predicted plasmid map of NuMA_1700-2115_GFP_blue_eyed_expression clone. C: NuMA_1700-2115_GFP_blue_eye_expression clone injected into one-cell stag *numa*

heterozygous cross embryos showing expression of the plasmid by blue eyes and GFP expression.

6.2.3. Generation of a pNuMA_FL_ubi_CFP expression clone

To compare the ability of the C-terminus of NuMA to rescue the phenotype of homozygous *numa*, I also made a full-length NuMA plasmid to assess its ability to rescue the phenotype. Using the same pEGFP plasmid I digested out 8bp, keeping the GFP in the plasmid. Full-length NuMA was digested out of its plasmid without GFP (Figure 6.7A). The fragments were ligated together, transformed and purified (Figure 6.7B), and an LR reaction was performed combining pNuMA_FL_GFP with the *ubi* promoter, a 3'UTR for stabilisation and the Tol2 backbone (Figure 6.7C). The predicted plasmid can be seen in figure 6.6D. The plasmid was injected into one-cell stage *numa* heterozygous crosses. *numa* sibs with GFP expression were chosen for raising (Figure 6.7E), however, none of the 15 embryos raised transmitted any GFP. The plasmid did not cause any rescue by injection either, as GFP positive homozygous embryos presented with a small necrotic head with small eyes, heart oedema, and a curved tail (Figure 6.7F).

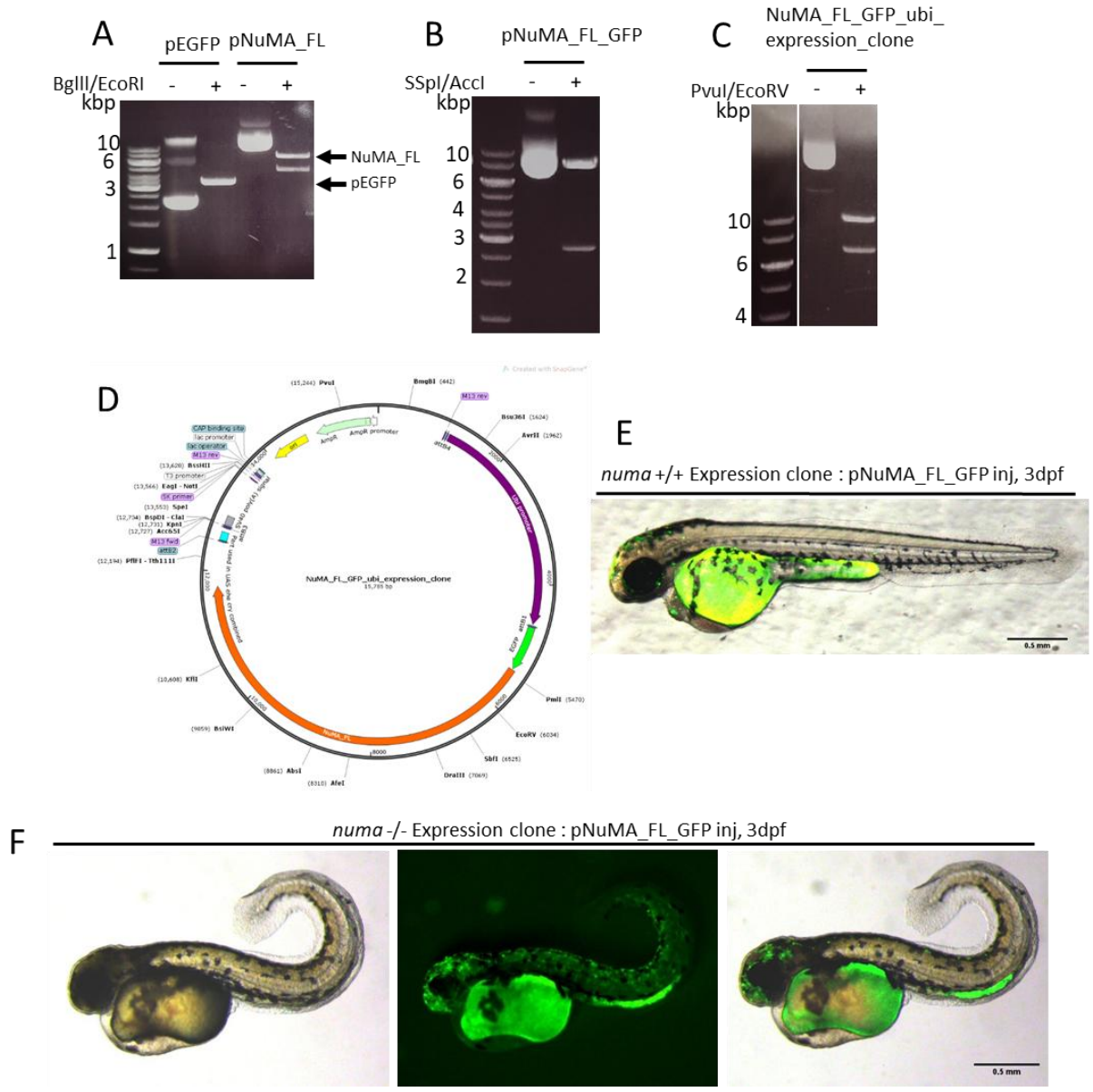

Figure 6.7: Digestion and ligation to produce a NuMA_FL_GFP_ubi_expression clone to be injected into numa heterozygous crosses. A: Digestion of pNuMA_FL (7608bp) and pEGFP with GFP (2718bp) with BglII and EcoRI. B: Digestion with SSpI and AccI after ligation of gel purified pNuMA_FL and pEGFP (10,326bp). C: Digestions with PvuI and EcoRV after LR reaction of pNuMA_FL_GFP with ubi promoter, p3e-Sv40polyA, and empty vector tet2pA2 (15,785bp). D: Predicted plasmid map of NuMA_FL_GFP_ubi_expression _clone. E and F: NuMA_FL_GFP_ubi_expression clone injected at one-cell stage into *numa* heterozygous cross embryos showing expression of the plasmid in wild type (E) and Homozygous (F), but no rescue of the *numa* phenotype (F) as the Homozygous embryo presents with small head and eye, necrosis in the head, oedema of the heart and a curved tail.

As with the C-terminal *numa* plasmid, it was considered that the FL plasmid might be incorporated into the genome, however, the GFP-*numa* might not be expressed highly enough to be visible. Therefore, as with the C-terminus *numa* plasmid, a new LR reaction was done with a backbone containing CFP controlled by a *cry* promoter (Figure 6.8A). A predicted plasmid structure can be seen in Figure 6.8B. The plasmid was injected into one-cell stage eggs from *numa* heterozygous incrosses. Embryos with CFP fluorescent eyes and scattered GFP expression were raised to adulthood (Figure 6.8C). One of the 15 fish raised transmitted blue eyes, but no GFP (Figure 6.8D and E). There was however, no rescue of the phenotype as seen by the homozygous offspring in figure 6.8E. The embryos presented with a small necrotic head with small eyes, heart oedema, and a curved tail. Furthermore, the embryos did not express any NuMA or GFP-tagged NuMA as seen in the western blot in figure 6.8F. There was an increase in GFP at 25kDa in the blue eye positive embryos; however, due to the similarity in protein structure of GFP and CFP, this was believed to be CFP. Further, a PCR of critical parts of the plasmid; CFP-*cry* promoter border, ubiquitin promoter-GFP border and C-terminal *numa*, showed, that the full plasmid was present in the embryos with blue eyes, but not in the embryos without blue eyes, even though the GFP and *numa* were not expressed (Figure 6.8G). A PCR of the *cry* promoter showed that all the samples contained endogenous DNA (Figure 6.8G).

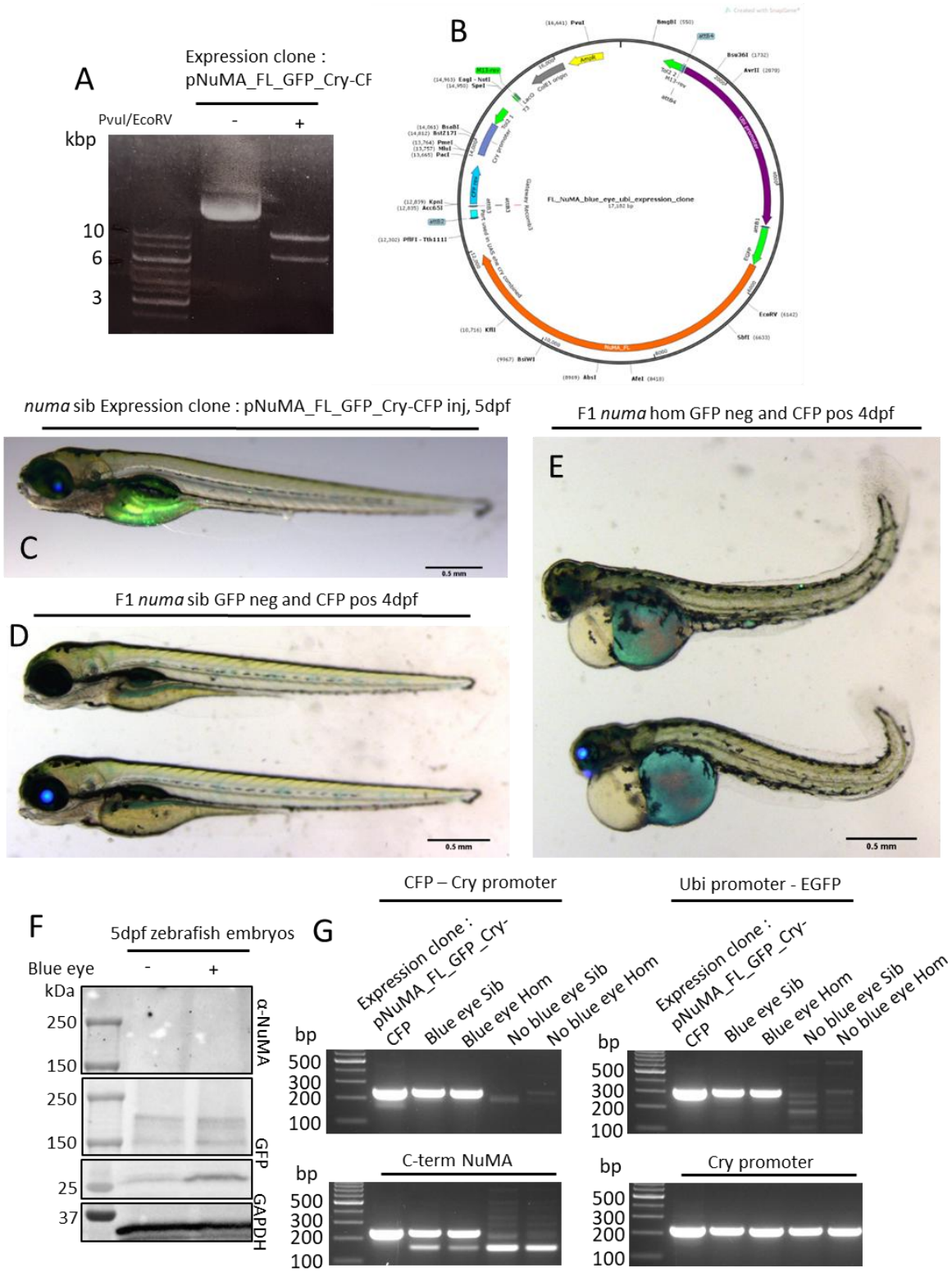

Figure 6.8: Confirmation of FL_NuMA_GFP_blue_eye_ubi_expression clone to be injected into numa heterozygous crosses. A: Digest of FL_NuMA_GFP_blue_eye_ubi_expression clone after LR reaction with pNuMA_FL_GFP, ubi promoter, p3e-Sv40polyA, and empty vector with CFP directed by a *cry* promoter (17,182bp) with PvuI and EcoRV. C: FL_NuMA_blue_eye_ubi_expression clone injected into one-cell stag *numa* heterozygous

cross embryos showing expression of the plasmid by blue eyes and GFP expression. D and E: Transmission of the plasmid from G0 to F1 seen by blue eyes but no GFP in sibs (D) and Homozygotes (E). Top embryo does not have the transmitted plasmid; bottom embryo has the transmitted plasmid based on blue eye expression. No rescue of the NuMA phenotype (E) seen by small head and eyes, necrosis in the head, oedema of the heart and a curved tail. F: Western blot confirming that there was no human NuMA expression or GFP tagged human NuMA in the embryos that transmit the plasmid. G: PCRs of the CFP-*cry* promoter junction, Ubi promoter-EGFP junction, C-terminal NuMA (1700-2115bp) and the *cry* promoter, showing that the full plasmid was present in embryos with blue eyes, however, NuMA was not being expressed. *cry* promoter was used as a control for the PCR of the embryos with no blue eyes.

6.2.4. NuMA and ribonucleotide incorporation

Research by Matthew Dawson in Professor Sherif El-Khamisy's laboratory suggests that when there is a lack of NuMA, there is an increase in R-loops in the genome. Therefore, I looked at whether a potential increase in R-loops could cause an increase in R-loop resolving factors. I looked at the expression of the catalytic RNaseH2 subunit, *rnaseh2a*, as well as *rnaseh1* as whilst RNaseH1 is believed to be the primary resolver of R-loops, RNaseH2 has been shown to be able to resolve R-loops too (Lockhart et al., 2019). However, in *numa* homozygous zebrafish embryos, there was no change in the expression of any of the genes. I also looked at the expression of *fastkd2* as a potential other resolver of single ribonucleotides but saw no significant change in its expression either (Figure 6.9).

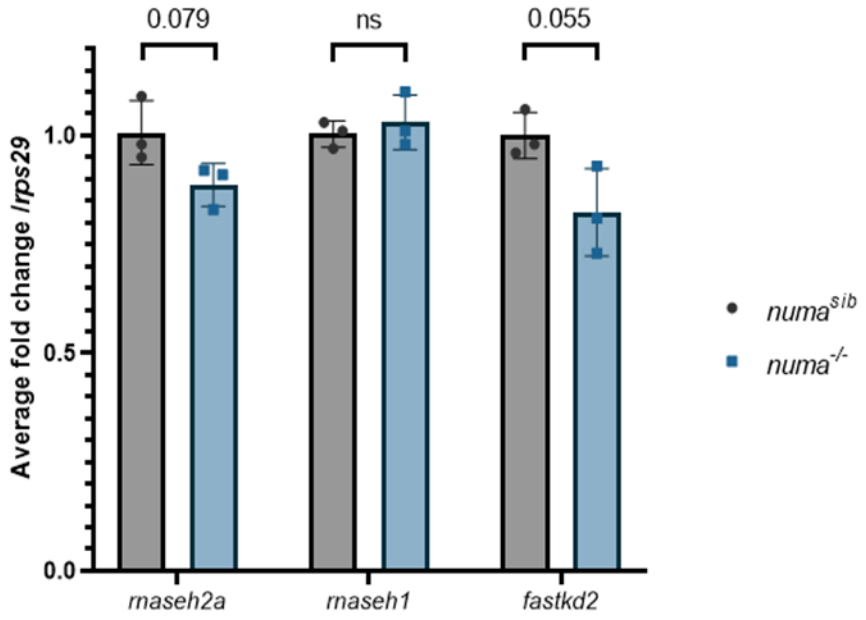

Figure 6.9: Expression of *rnaseh2a*, *rnaseh1* and *fastkd2* in siblings and *numa* knockout. Unpaired t-test, n=3.

6.2.5. Aged heterozygous *numa* adults do not show a frailty phenotype

Many ageing diseases are related to DNA damage repair proteins. Therefore, I wanted to investigate whether NuMA may be linked to accelerated or poor ageing. *numa* homozygous zebrafish do not survive past 4dpf. Therefore, I was only able to look at *numa* heterozygous adults and their wild type siblings. At 3 years, the *numa* heterozygous adults did not show an increased frailty phenotype compared to their wild type siblings. Criteria for frailty used were as for chapter 3, width/length ratio, BMI, spinal height, cancer occurrence and fin damage. Figure 6.9 shows images of 3-year-old *numa* wild type and heterozygous siblings as well as the frailty index score given to wild type and heterozygous adults following the index proposed in chapter 3, showing no difference in the scores.

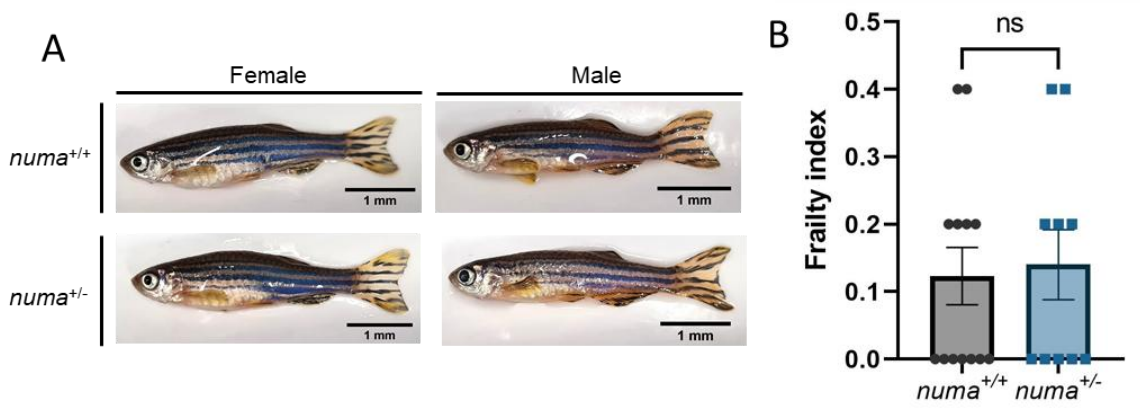

Figure 6.10: Frailty index score given to aged (3 years) wild type and heterozygous *numa* adults. A: Images of 3-year-old female and male *numa* wild type and homozygous adutls. B: Index score given to wild type and adult *numa* wild type and heterozygous fish. Index considers width/length ratio, BMI, spinal height, cancer occurrence and fin condition. Unpaired t-test, wild type n= 13, heterozygous n= 10.

6.3. Discussion

NuMA is a protein with several functions. Both as a key player in mitotic spindle formation and as a protector of oxidative damage at non-transcribed regulatory regions such as promoters and enhancers. Most of NuMAs function has been established through *in vitro* work, as mice models are embryonic lethal due to NuMAs vital role in development. Therefore, to study NuMAs role at a whole-organismal level, I took advantage of the zebrafish's external fertilisation and Dr Ruth Thomas made a CRISPR/Cas9 knockout line for *numa* in zebrafish. The zebrafish are lethal at 4dpf with a strong phenotype at 24hpf. I wanted to assess which part of NuMA is responsible for the lethality of the whole organism by attempting to rescue the phenotype. I compared the rescue of full-length versus the C-terminus of NuMA as the C-terminus contains the DNA binding and DNA repair domains.

6.3.1. Creating a NuMA rescue zebrafish line

I made several plasmids containing either full length or C-terminus human *numa* that were injected into one-cell stage *numa* heterozygous crosses. However, I was mostly unsuccessful in integrating the plasmid into the genome of the embryos, and once I got integration, GFP and NuMA were not expressed.

Firstly, the BP clonase reaction was unsuccessful (Figure 6.4). There is no definitive reason for this to be the case. However, due to there being several bands in the PCR reaction, I did a gel extraction to obtain the PCR product of the correct size. Some components of the gel might then inhibit the BP clonase reaction (Research gate chat forum). Further, the BP clonase enzyme is an unstable enzyme, and needs to be stored at -80˚C. It is possible that the enzyme used in the reaction was freeze-thawed too many times and lost its catalytic ability. Due to the difficulty with the BP clonase reaction, I opted to do digestion and ligations instead to make the middle entry clone needed for the final LR clonase reaction. By following this method, I managed to make two expression clones for C-terminus *numa*. One without and one with a blue eye selection marker. As well as two expression clones for full-length *numa*, one without and one with a blue eye selection marker (Figure 6.5-6.8). Initially I made the plasmids without the blue eye marker, as the expression of the GFP tagged *numa* would be ubiquitously expressed in the embryos due to the ubiquitin promoter. Once the embryos were injected, the GFP was visible under a fluorescent microscope, and selection for raising was simple (Figure 6.5 and 6.7). However, when I could not observe any GFP in the F1 generation I considered the possibility that either, the GFP is not expressed, or the *numa* is expressed in such a small amount, that I could not pick up the GFP expression. For this reason, I decided to use a blue eye marker in the plasmid to select for transmission (Figure 6.6 and 6.8). I could not find any F1 fish with the blue eyes for the C-terminus *numa*. One F1 fish for full-length *numa* did express blue eyes and no GFP (Figure 6.8), suggesting the plasmid had been integrated into the genome. However, the homozygous embryos showed no rescue of the phenotype. Further, there was no GFP expression to indicate that *numa* was expressed. A western blot confirmed that no human NuMA was expressed in the embryos (Figure 6.8F), however a PCR did confirm that the full plasmid was integrated into the genome (Figure 6.8G).

The *ubiquitin* promoter from zebrafish was reported as a useful ubiquitous promoter by Mosimann et al, (2011). They made it because the current promoters available for zebrafish, such as *h2afx*, *tbp*, some versions of *β-actin* control element and the *Xenopus laevis*-derived *elongation factor 1a* (*XlEef1a1*) were unreliable at different developmental stages, and had an occurrence to stop expressing in certain tissues of the adult zebrafish. They took inspiration form *Drosophila* where the most common promoter was from the 5' region of the *ubiquitin* gene. When using it with EGFP they saw expression in all tissues, although the level of expression in each tissue was not ubiquitously equal (Mosimann et al., 2011). I propose that the *ubi* promoter may be the reason for the lack of expression of GFP or NuMA in the F1 that transmitted blue eyes. Although, it is worth noting that the *ubi* promoter worked well for making the mitochondrial reporter line in Chapter 4. The GFP expression I saw in the G0 embryos

may have been because the construct had been inserted after another promoter driving the expression, rather than *ubi* driving the expression, or it might have become silenced. This is possible as Tol2 transposases randomly integrates the construct into the genome, although they do in human cells prefer regions that are not transcriptionally repressed (Grabundzija et al., 2010). It is also possible that the construct was inserted into a silenced area of the genome; however, this is unlikely due to the nature of Tol2 and the observation of blue eyes still being expressed. Another possibility is that GFP and *numa* C-terminus or full-length is too long for the *ubi* promoter. The *ubi* promoter is able to drive a high expression of GFP alone, however GFP is only 717bp. GFP and the C-terminus of *numa* is 1986bp and GFP and full-length *numa* is 7080bp. Lastly, both the C-terminal and full-length *numa* start with an ATG site which could confuse transcription when I wanted it to start with the ATG at the GFP on the N-terminal end of *numa*.

Further, the transmission rate of the integrated plasmid was very low. Only one full-length injected fish passed the plasmid onto the F1 generation, and none of the C-terminus injected fish passed on the plasmid after a total of 60 larvae being raised and tested for transmission. For the full-length *numa*, this could be understood by the large size of the construct. Between the Tol2 sites of the full-length plasmid, there is 13,919bp to transpose. Good efficiency with Tol2 is up to 11kbp (Kawakami, 2007). However, for smaller constructs such as the C-terminus *numa* plasmid, which is 8825bp there should be a transmission rate of 50% to 70% to the F1 generation using the Tol2 method (Kawakami, 2007). I also saw no rescue of the NuMA phenotype in the G0 generation. This is not unexpected however, as the integration of the plasmid was mosaic. With the NuMA phenotype being so lethal, expression of *numa* in all cells is likely to be needed for a viable rescue.

When continuing with this research, I suggest attempting a new LR reaction with a different promoter. Common promoters used in zebrafish are the *XlEef1a1* and the *h2afx.* However, they have been reported to be silenced in certain tissues such as the blood vessels, gills, swim bladder, the central nervous system, retina and caudal fin (Thummel et al., 2006). Burket et al, (2008), also reported on four new promoters, *the TATA box binding protein (tbp)*, the *taube nuss-like (tbnl),* the *eukaryotic elongation factor 1-gamma (eef1g*) and the *beta-actin-1 (bactin1)*. They reported that they show similar patterns to the *XlEef1a1* and *h2afx* in the adult, although they do express in the central nervous system and fin as well (Mosimann et al., 2011). Further, it is worth attempting the rescue using the zebrafish *numa* gene rather than the human gene. The zebrafish genome has 70% sequence identity with the human genome, so it is

plausible that using a human gene in Zebrafish should be feasible (Howe et al., 2013). In this project, I used the human gene due to its availability in the lab, and no zebrafish *numa* cDNA was available. However, it is possible that there are differences between the human and zebrafish gene that means it cannot be expressed in zebrafish.

6.3.2. NuMA and genomic instability

Matthew Dawson in Professor Sherif El-Khamisy's lab recently identified that a depletion of NuMA causes an increase in R-loops (not published). R-loops are three stranded DNA structures that can be commonly found at promoter sites where the nascent RNA strand during transcription re-anneals to the complementary strand in the double stranded helix, pushing the transcribing strand out causing a loop (Dumelie and Jaffrey, 2017). Due to this discovery, I wanted to know whether there was an increase in the expression of R-loop resolving proteins in the *numa* homozygous zebrafish embryos. However, I saw no significant changes in the levels of the catalytic unit of RNaseH2, *rnaseh2a*, or the R-loop resolver *rnaserh1*. There is a trend of a reduction in *rnaseh2a* which is almost significant (Figure 6.9). However, RNaseH2 is mainly associated with the removal of single ribonucleotides rather than a stretch of ribonucleotides such as R-loops. Although, I have not investigated whether there is an increase in R-loops in the zebrafish model. Therefore, I do not know if I would expect an increase in the resolving factors. This could be investigated by using an s9.6 antibody in a zebrafish IF which detects RNA:DNA hybrids within nuclei or a new DRIP-seq method, ULI-ssDRIP-seq(Weinreb et al., 2021). I further saw a reduction in *fastkd2*, although not significant (Figure 6.9). Whilst I do not have any firm evidence that FASTKD2 does resolve ribonucleotide misincorporations or R-loops, FASTKD2 has been associated with apoptosis. Other non-published data from Professor El-Khamisy's lab by Dr Sarah Antar suggest that NuMA knockout cells have a greater survival rate than wild type cells when treated with CPT. The reduction of *fastkd2* expression in the NuMA knockout cells might reflect the protection against apoptosis that the NuMA knockout cells possess.

As explored in Chapter 1.2.1, several age-related diseases are related to the ageing hallmark genomic instability. NuMA depletion causes increased genomic instability and is embryonic lethal. However, even with functioning NuMA at the embryonic stage, it is unlikely that the repair capability of NuMA stays intact with age (El-Khamisy, 2023). Further, increased oxidative damage in aged brains were seen in 2004 together with a decrease in transcription (Lu et al., 2004). Therefore, I explored whether the aged heterozygous *numa* adult zebrafish at 3 years of age had any frailty phenotypes compared to their wild type siblings. Using the

frailty index described in chapter 3, I saw however no differences in the frailty of the fish (Figure 6.10). Thus, a potential decrease in the levels of functional NuMA due to heterozygosity, is not sufficient to cause a clear ageing phenotype in zebrafish.

6.3.3. Conclusion

In this Chapter, I created two expression clones for C-terminal *numa* and two for full-length *numa.* I saw no rescue of the *numa* phenotype, and they were unsuccessful in expressing GFP-tagged NuMA. I have no definitive answer for why there was no expression. However, I believe it could be due to the *ubi* promoter, and I suggest trying other promoters going forwards with the project. Further, I saw no increase in R-loop resolving factors in *numa* homozygous fish even though NuMA cells show an increase in R-loops at promoter regions. I saw a trend of decrease in *fastkd2* suggesting there might be protection against apoptosis in the *numa* homozygous larvae, however, this was not significant. Lastly, I did not see any increased frailty in heterozygous *numa* adults, suggesting that one *numa* gene is enough to maintain healthy ageing.

Chapter 7 General discussion

7.1. Overview

The human population is living longer than it has ever before due to interventions into diseases that previously caused death at older ages. However, many people are living these extra years in ill health costing themselves and the society a lot of time and money. These people might live with multimorbidity, having two or more diseases at the same time or be frail, where minor illness might have a major impact on a person's life and ultimately lead to death. To improve the lives of the older generation it is important that we understand why some people age poorly and become frail and others not (World Health Organisation, 2024, Office for Health Improvement and Disparities, 2023, Office for National Statistics, 2024). In 2013, the ageing community came together to write the hallmarks of ageing which were later updated in 2023 to include a total of 12 hallmarks (Figure 1.2). They included, primary, antagonistic and integrative hallmarks, which all occur with normal ageing and can speed up ageing or reduce ageing if modified (Lopez-Otin et al., 2023, Lopez-Otin et al., 2013).

Among these hallmarks is genomic instability, which includes damage to the DNA. There are about 10^4-10^5 breaks in the DNA in every cell every day. Breaks in the DNA can lead to paused transcription or replication, mutations to the DNA or ultimately cell death if it cannot be repaired (Marteijn et al., 2014, Yousefzadeh et al., 2021, Lopez-Otin et al., 2023). One of the most common forms of DNA damage is the incorporation of ribonucleotides (rNTPs/rNMPs) into the DNA. rNTP incorporation can be a part of the normal cell function as part of DNA repair or as primer during DNA replication. However, whilst the DNA polymerases have an intrinsic ability to separate deoxyribonucleotides (dNTPs) from rNTPs within the nucleus, it is believed that in humans there might be as many as 3 million rNTPs incorporated into the genome by among others the DNA polymerases (Nick McElhinny et al., 2010b, Brown and Suo, 2011, Clausen et al., 2013, Kellner and Luke, 2020). If these rNMPs are not removed by the correct mechanisms they can cause DNA deletions, or spontaneous cleavage of the C'2 hydroxyl on the rNMP, causing unligatable DNA nicks, as well as change the shape of the DNA (Figure 1.3) (DeRose et al., 2012, Meroni et al., 2017, Kellner and Luke, 2020). The common way to remove single rNMPs from the genome is via the trimeric enzyme RNaseH2. RNaseH2 recognises the rNMP in the DNA, and its catalytic subunit RNaseH2A cleaves at the 5' end of the rNMP. The rNMP is further cleaved by FEN1 at the 3' end. The gap is filled by DNA polymerase δ and ligated by DNA ligase 1 (Figurer 1.6) (Reijns et al., 2012, Sparks et al., 2012).

If DNA ligase attempts to ligate the nick after RNaseH2 cleavage or spontaneous cleavage of the rNMP, an adenylated 5'-RNA-DNA junction is created, and the nick cannot be ligated. These nicks may go through abortive ligation by APRATAXIN where APRATAXIN removes the AMP attached to the rNMP and resets the nick for the ribonucleotide excision repair (RER) or other repair processes to occur. However, research has shown that APRATAXIN is not very efficient at resetting nick caused by RNaseH2 (Tumbale et al., 2014). Loss of APRATAXIN function causes the disease Ataxia-oculomotor apraxia type 1 (AOA1) (Ahel et al., 2006, Tumbale et al., 2014). Further, if RNaseH2 is non-functional it causes the human neurological disease Aicardi-Goutières Syndrome (AGS). Loss of RNaseH2 is lethal in mice and second-generation lethal in zebrafish (Aicardi and Goutieres, 1984, Reijns et al., 2012, Thomas et al., 2024). This lethality in mice is associated with Topoisomerase 1 (TOP1) cleaving the rNMP in the absence of RNaseH2 causing a 2-5bp deletion (Huang et al., 2017, Pommier et al., 2022, Reijns et al., 2022). Fragments of DNA leak into the cytoplasm, which activates the cGAS-STING inflammatory pathway triggering the transcription of several inflammatory genes including *il-1b* and *tnfα* (Mackenzie et al., 2016).

As well as the cleavage of the rNMP by TOP1 in the absence of RNaseH2, FASTKD2 has been proposed to be able to cleave single rNMPs. FASTKD2 is a nuclear protein that has a mitochondrial targeting signal. In the mitochondria, FASTKD2 is important for rRNA and mitochondrial mRNA processing and stability, and a loss of FASTKD2 function is associated with encephalopathies in humans (Popow et al., 2015, Wu et al., 2022). FASTKD2 also has a non-mitochondrial function in apoptosis via the caspase-2 mediated pathway (Das et al., 2014, Yeung et al., 2011). The mitochondria do not have any RNaseH2 to remove single rNMPs from the mitochondrial DNA (mtDNA). It does have RNaseH1 to remove primers in the mtDNA, however, RNaseH1 is not able to remove single rNMPs. Therefore, it is suspected that there might be as many as 30-60 rNMPs in the mtDNA at any time (Nava et al., 2020). FASTKD2 was identified in a genetic functional complementation study in yeast homozygous for RNaseH1 and RNaseH2 as able to rescue reduced growth on hydroxyurea (HU), prompting the possibility that FASTKD2 is able to cleave single rNMPs in the mtDNA.

In this thesis, I aimed to investigate the role of the RER pathway in robust versus frail ageing in zebrafish. I further aimed to investigate an alternative enzyme in the RER pathway, FASTKD2, and as its role had not been fully characterised in zebrafish, I first investigated what a lack of FASTKD2 would do to the fish. I then aimed to create a model to study AOA1, by

knocking out *aprataxin* and *rnaseh2a* in the same zebrafish model. Lastly, I aimed to rescue the severe phenotype seen in NuMA homozygous larvae by incorporating the NuMA cDNA into the NuMA homozygous background to attempt to identify what function of NuMA causes the severe phenotype discussed in chapter 6.

7.2. Ribonucleotide excision repair in ageing

In Chapter 3 I explored whether a loss in ribonucleotide excision from the DNA correlated with increasing age. I saw that rather than correlating with age, it correlated with the status of the aged fish. Whether the fish of the same age were robust or frail. To do this I created a quick and easy frailty index for zebrafish. A frailty scoring system for zebrafish has not been published yet and could have great implications zebrafish researchers. Zebrafish are increasingly being used in ageing research, and there needs to be a unified way to talk about their ageing. I am not trying to argue that my way of defining frailty in zebrafish is the correct way, but I want to start a discussion as to how we will look at frailty in zebrafish.

By using the frailty index, I saw that the brains from robust old fish cleaved single ribonucleotides significantly better than frail old brains, and this was in particular seen in female fish (Figure 3.7). Similar ideas were explored by Storci et al (2019) when they saw that centenarian fibroblasts had significantly less DNA damage than old fibroblasts, and that they had significantly more of all the three subunits of RNaseH2 (Storci et al., 2019). As well as having a significantly decreased ability to remove single ribonucleotides, female frail brains also had more ribonucleotides in the genome, although not significant, and more single stranded DNA damage, but not double stranded DNA damage (Figure 3.8 and 3.9). The lack of double stranded DNA damage might be the reason why the frail fish did not experience an increase in inflammation or senescence in the brain (Figure 3.10). This was not the case for the more replicative tail fin tissue, where the old frail females did not have a reduced ability to cleave ribonucleotides, however they did have significantly more expression of the RNA of the subunits of RNaseH2, and other repair enzymes associated with RER (Figure 3.11). This idea was further emphasised by the *rnaseh2a* homozygous adults experiencing significantly more frailty at 3 years of age than their wild type siblings (Figure 3.13). These observations are interesting as only Storci has published research that suggest that RNaseH2 has an implication in ageing. Considering the number of rNMPs in the genome, and my results, it would be reasonable to assume an involvement of the RER pathway in ageing, and the more we can understand about ageing, the better for society and the individual.

When further exploring the ageing of other “DNA damage-gene” mutant fish, I saw that the *fastkd2* mutants were no frailer than their wild type siblings were at 29 months. However, whilst the wild types scored more than the homozygous on increased spinal height, the homozygous adults had more damaged tail fins than the wild types (Figure 4.30). As for the *numa* heterozygous adults, they did not have an increased frailty compared to the wild types either. However, this could be due to one copy of *numa* being enough for normal ageing (Figure 6.10). I was not able to study the aged *aprataxin* homozygous mutants as they were only 5 months old when finishing the thesis. However, as the *rnaseh2a* homozygous adults were frailer than their siblings, it would be very interesting to see whether this frailty would be rescued or worsened in a double *aprataxin rnaseh2a* mutant.

7.2.1. Further work on ribonucleotide excision repair in ageing

There are several experiments I would have liked to perform to continuing this research. For example, I would like to investigate whether there are any 2-5bp deletions in the aged robust and frail brains associated with TOP1 cleavage. This can be done by whole genome sequencing, which was attempted by Dr Ruth Thomas, however, she did not see any 2-5bp deletion signatures in the *rnaseh2a* homozygous embryos with a n-number of one (Thomas et al., 2024). However, in this thesis, I did show that in the *rnashe2a* second generation mutant embryos, there appears to be a mutation signature similar to TOP1 in the cleavage assay (Figure 4.26), which could suggest that in the mutants, TOP1 does cleave single ribonucleotides. I also think that doing TOP1-CC analysis on robust and frail brains. This would tell me whether there is any TOP1 bound to the DNA, and if there were more, this could be linked to the reduced RNaseH2 activity. Although TOP1 has other rolls in the cell, this could prompt further investigations (Hidmi et al., 2024).

Further to this, I would like to perform RNA-seq on robust and frail brains to investigate what other genes might be down- or upregulated, and whether any of them may be associated with ribonucleotide damage. Similar was done with 35 frail and robust human leukocyte samples to look at circular RNA as biomarkers, where they identified several differences between the two groups (Iparraguirre et al., 2023). An interesting paper also came out in 2018 by Aramillo Irizar et al., where they sequenced the transcriptome of young, middle aged and old, humans, mice, zebrafish and the short-lived killifish *Nothobranchius furzeri.* Here they saw that old individuals had a transcriptional signature that went away from a cancer signature and towards a degenerative diseases and inflammatory signature. They hypothesised that this is because, the individuals that have avoided cancer, have done so because of the immune system is a

barrier to cancer development, however, a causation to degenerative disease (Aramillo Irizar et al., 2018). This concept is interesting as AGS is an inflammatory degenerative disease, and although I see no increased inflammation in frail brains, there is in the frail fin clips and in the *rnaseh2a* homozygous adult brains, although not significant (Figure 3.14). Further, whilst cancer occurrences were rare in the old fish scored by the experts, if they were present, they were not commonly seen in the fish that were scoring the frailest by the experts (Figure 3.6). RNA-seq has also been done on prematurely ageing *telomerase* deficient zebrafish brains comparing them to young and old zebrafish (Martins et al., 2024). However, no RNA-seq to this date has looked at normal robust and frail ageing.

Late in my PhD, I started investigating the fin tissue to compare to the brain tissue. These are two very different tissues in that one is more replicative than the other is. To further this research, looking at other tissues would be interesting, such as muscles, heart and the kidney. One paper reported that there was no inflammation in the brains of mice with mutations in *rnaseh2b*, however there was in the heart and the kidney (Mackenzie et al., 2016). In addition, individuals with mutations in *rnaseh2b* commonly have chronic kidney disease (He et al., 2021). Lastly, an advantage of zebrafish is that they can be maintained under similar conditions, which is impossible to achieve with humans. However, after 3 years of living there is still going to be a remarkable difference between the fish as well. Therefore, a number of three fish for some of the experiments is not sufficient to determine significance, in particular for the alkaline cleavage assay. A higher number of fish for several of the experiments would therefore be advised, and the appropriate number of fish to use could have been obtained through a power calculation. Power calculations can take into account the standard deviation from previous or similar studies to assess an appropriate number of replicates for a significant result. Websites such as G*Power (http://www.gpower.hhu.de) can be used to calculate the power number (Serdar et al., 2021).

7.3. FASTKD2 and APRATAXIN in ribonucleotide excision repair in zebrafish

In Chapter 4, I introduced FASTKD2 as a potential protein that can cleave single ribonucleotides from the mitochondrial genome. Knockouts of *fastkd2* were viable but had a reduced mitochondrial volume and energy production (Figure 4.9 and 4.10). The mutant did not have any basal DNA damage (Figure 4.14), however, when exposed to the DNA damaging agent CPT, the larvae had potentially less PARylation, and a significant reduction in apoptosis compared to wild type larvae (Figure 4.15 and 4.16). DNA damage has not been reported in

any people with FASKTD2 mutation, although a reduction in mtDNA was noted (Shah and Balasubramaniam, 2021). FASTKD2 knockout cells have also been associated with a loss of apoptosis (Yeung et al., 2011). Further, when investigating the mutant in relation to ribonucleotide excision, I saw no change in cleavage or ribonucleotide incorporation in the nuclear or the mitochondrial genome (Figure 4.18 and 4.10). This could indicate that FASTKD2 does not cleave single ribonucleotides in the mitochondria, or that there was contamination by RNaseH2 in the mitochondrial lysate.

Alternatively, for the nucleus, it could mean that if FASTKD2 cleave ribonucleotides in the nuclear genome, it does not do so if RNaseH2 is active similar to how TOP1 function (Williams et al., 2017, Williams et al., 2013). Therefore, I made a double mutant for *fastkd2* and *rnaseh2a* to investigate the ribonucleotide cleavage potential with neither of the enzymes. What I saw was that the double mutant was potentially healthier than the *rnaseh2a* single mutant was, and had potentially less single stranded DNA breaks, but not double stranded breaks (Figure 4.24 and 4.28). However, there was no difference in the cleavage capacity of the single *rnaseh2a* mutant and double mutant in the nuclear or the mitochondrial genome (Figure 4.25 and 4.27). I came up with two theories for what I was seeing:

1) Like TOP1, FASTKD2 only cleaves ribonucleotides when RNaseH2 is not functional. When this is the case FASTKD2 cleaves at the 3'end of the ribonucleotide creating an unrepairable nick further causing double stranded breaks and disease. When neither RNaseH2 or FASTKD2 are functional, these nicks do not occur, and the ribonucleotide is repaired by other, less detrimental methods. However, I compared the cleavage band size from the ribonucleotide cleavage assay from the wild type, *rnaseh2a* single homozygous, *fastkd2* single homozygous and *fastkd2 rnashe2a* double mutant lines to the cleavage band by RNaseH2 and potassium hydroxide (KOH) which cleaves at the 3' end of the rNMP. I saw that all the bands were significantly different from the KOH band. Further, the band by the *rnaseh2a* single mutant and the double mutants appeared to potentially be 1 bp smaller than the band by purified RNaseH2 (Figure 4.26). This could suggest that the rNMP is not cleaved by FASTKD2, but rather TOP1 causing a 2-5bp deletion.

2) FASTKD2 is not involved in ribonucleotide excision repair. What I see is similar to when p53 is knockout in *rnaseh2a* mutants (Reijns et al., 2012, Thomas et al., 2024). When knocking out *fastkd2* in the *rnaseh2* mutant background I removed apoptosis via the caspase-2 mediated pathway, resulting in less apoptosis and increased survival. Although, I did see less

apoptosis when treating the *fastkd2* homozygous larvae with CPT (Figure 4.16), this theory also seems unlikely. There is no increase in *fastkd2* expression in the *rnaseh2a* single mutant (Figure 5.28), suggesting DIF-1 is not regulating *fastkd2* expression in response to DNA damage by rNMPs. Therefore, the apoptotic pathway is not activated. Further, there is no difference in apoptosis between the *rnaseh2a* single mutant and the double mutant (Figure 4.29).

However, even though the *fastkd2* mutant did not replicate the ribonucleotide cleavage disability seen in human cells, this is still the first knockout mutant of *fastkd2*. The mutant does have a mitochondrial phenotype similar to patients with *fastkd2* mutations and could therefore be used in further research when studying the diseases and FASTKD2 function.

In Chapter 5, I introduced APRATAXIN. As there is no model of AOA1, I wanted to see if I could create a model for AOA1 by knocking out both *rnaseh2a* and *aprataxin* in zebrafish larvae. Whilst the larvae had no external phenotypes (Figure 5.5 and 5.6), they did show a significant reduction in movement when exposed to light and dark (Figure 5.7). This is also seen in humans with AOA1 and in mice with knockout of both *aprataxin* and *atm* (Perez et al., 2021). This phenotype did not appear to be modified by the *rnaseh2a* mutation (Figure 5.8). Even though I did not have time to fully investigate this mutant line, the evidence does suggest that this could be the first model organism showing any AOA1 disease, and it could therefore be used to further understand the disease and to develop treatments.

7.3.1. Further work on FASTKD2 and APRATAXIN in ribonucleotide excision repair in zebrafish

There are several experiments that could be started to further the research into FASTKD2 and APRATAXIN. One major issue with Chapter 4 is that the *rnaseh2a* single mutants and the *fastkd2 rnaseh2a* double mutant is not related. Therefore, the differences in survival I see could be due to other genetic factors. One improvement to this project is to compare the two lines in the same background. This was not initially done due to the time remaining in the PhD. I would also like to investigate the apoptosis function of FASTKD2 in further detail. It is a function that has not been explored in detail, and by further investigating the caspase-2 mediated apoptosis pathway before and after CPT treatment, I think more of FASTKD2's function could be eluded. Assays such as TUNEL could be attempted on this line after induction of stress by CPT (Kyrylkova et al., 2012). Lastly, investigating the energy production

in the old *fastkd2* wild type and homozygous brains by mass spectrometry would be of interest to assess whether this is something that is worsening with age. Another potential caveat in thesis research is that human and zebrafish FASTKD2 only hare 35% sequence homology at a protein level, and there is very poor homology at the human mitochondrial targeting signal. Even though zebrafish FASTKD2 is predicted to locate to the mitochondria, one important experiment to perform would be to identify if it does in fact locate to the mitochondria. One way I could have done this is to create a fusion protein between FASTKD2 and a fluorophore and then study its localisation against mitotracker. Zebrafish are radially used to track protein localisation and there are protocols available for mitotracker use in zebrafish larvae (Wrighton et al., 2021, Choe et al., 2021). Further, as there are no available antibody that can recognise zebrafish FASTKD2, it would be possible to raise a zebrafish specific antibody that could be used in IFs or on western blots on mitochondrial isolates (Staudt et al., 2015).

For the *aprataxin* homozygous line, there are several experiments that need to be completed, as this line was only sexually mature with one month left of research in this PhD. Several suggestions for future work can be seen in Chapter 5.3, however, briefly, *aprataxin* is associated with mitochondrial defects (Sykora et al., 2011, Garcia-Diaz et al., 2015), and therefore, investigating the mitochondrial function would be of great interest. Further, loss of aprataxin causes loss of inflammatory signalling which would also be important to investigate (Madsen et al., 2023). I would also like to do movement analysis on the adult fish, as Perez et al., (2021) saw a worsening phenotype of their mice with age (Perez et al., 2021).

7.4. Summary

In summary, this thesis has explored the role of ribonucleotide excision repair in ageing as well as new forms of ribonucleotide excision repair. I have shown that in zebrafish, the excision of ribonucleotides from the brain genome is less efficient if the fish is frail, but this is not the case in other tissues such as the replicative fin tissue. Further, whilst removing the function of FASTKD2 in fish does not appear to affect frailty, or ability to remove ribonucleotide in the nuclear or mitochondrial genome, it does cause a viable mitochondrial phenotype where they are not able to produce enough energy. Lastly, by removing the function of APRATAXIN, the larvae show similar movement disabilities to patients with AOA1.

Chapter 8 References

ABBOTTS, R. & WILSON, D. M., 3RD 2017. Coordination of DNA single strand break repair. *Free Radic Biol Med,* 107**,** 228-244.

ABOU-DAHECH, M. S. & WILLIAMS, F. E. 2024. Aging, Age-Related Diseases, and the Zebrafish Model. *Journal of Dementia and Alzheimer's Disease* [Online], 1.

AHEL, I., RASS, U., EL-KHAMISY, S. F., KATYAL, S., CLEMENTS, P. M., MCKINNON, P. J., CALDECOTT, K. W. & WEST, S. C. 2006. The neurodegenerative disease protein aprataxin resolves abortive DNA ligation intermediates. *Nature,* 443**,** 713-6.

AICARDI, J., BARBOSA, C., ANDERMANN, E., ANDERMANN, F., MORCOS, R., GHANEM, Q., FUKUYAMA, Y., AWAYA, Y. & MOE, P. 1988. Ataxia-ocular motor apraxia: a syndrome mimicking ataxia-telangiectasia. *Ann Neurol,* 24**,** 497-502.

AICARDI, J. & GOUTIERES, F. 1984. A progressive familial encephalopathy in infancy with calcifications of the basal ganglia and chronic cerebrospinal fluid lymphocytosis. *Ann Neurol,* 15**,** 49-54.

AKBARI, M., SYKORA, P. & BOHR, V. A. 2015. Slow mitochondrial repair of 5'-AMP renders mtDNA susceptible to damage in APTX deficient cells. *Sci Rep,* 5**,** 12876.

ALBARADIE, R., ALHARBI, A., ALSAFFAR, G., ALHAMAD, B. & BASHIR, S. 2022. Ataxia with oculomotor apraxia type 1 associated with mutation in the APTX gene: A case study and literature review. *Exp Ther Med,* 24**,** 709.

ALMAGRO ARMENTEROS, J. J., SALVATORE, M., EMANUELSSON, O., WINTHER, O., VON HEIJNE, G., ELOFSSON, A. & NIELSEN, H. 2019. Detecting sequence signals in targeting peptides using deep learning. *Life Sci Alliance,* 2**,** e201900429.

AMORIM, J. A., COPPOTELLI, G., ROLO, A. P., PALMEIRA, C. M., ROSS, J. M. & SINCLAIR, D. A. 2022. Mitochondrial and metabolic dysfunction in ageing and age-related diseases. *Nat Rev Endocrinol,* 18**,** 243-258.

ANCHELIN, M., ALCARAZ-PEREZ, F., MARTINEZ, C. M., BERNABE-GARCIA, M., MULERO, V. & CAYUELA, M. L. 2013. Premature aging in telomerase-deficient zebrafish. *Dis Model Mech,* 6**,** 1101-12.

ANDERSON, K. A., MADSEN, A. S., OLSEN, C. A. & HIRSCHEY, M. D. 2017. Metabolic control by sirtuins and other enzymes that sense NAD(+), NADH, or their ratio. *Biochim Biophys Acta Bioenerg,* 1858**,** 991-998.

ANTONICKA, H. & SHOUBRIDGE, E. A. 2015. Mitochondrial RNA Granules Are Centers for Posttranscriptional RNA Processing and Ribosome Biogenesis. *Cell Rep,* 10**,** 920-932.

ARAMILLO IRIZAR, P., SCHÄUBLE, S., ESSER, D., GROTH, M., FRAHM, C., PRIEBE, S., BAUMGART, M., HARTMANN, N., MARTHANDAN, S., MENZEL, U., MÜLLER, J., SCHMIDT, S., AST, V., CALIEBE, A., KÖNIG, R., KRAWCZAK, M., RISTOW, M., SCHUSTER, S., CELLERINO, A., DIEKMANN, S., ENGLERT, C., HEMMERICH, P., SÜHNEL, J., GUTHKE, R., WITTE, O. W., PLATZER, M., RUPPIN, E. & KALETA, C. 2018. Transcriptomic alterations during ageing reflect the shift from cancer to degenerative diseases in the elderly. *Nature Communications,* 9**,** 327.

ARTUSO, L., ROMANO, A., VERRI, T., DOMENICHINI, A., ARGENTON, F., SANTORELLI, F. M. & PETRUZZELLA, V. 2012. Mitochondrial DNA metabolism in early development of zebrafish (Danio rerio). *Biochim Biophys Acta,* 1817**,** 1002-11.

ARUDCHANDRAN, A., CERRITELLI, S., NARIMATSU, S., ITAYA, M., SHIN, D. Y., SHIMADA, Y. & CROUCH, R. J. 2000. The absence of ribonuclease H1 or H2 alters the sensitivity of Saccharomyces cerevisiae to hydroxyurea, caffeine and ethyl methanesulphonate: implications for roles of RNases H in DNA replication and repair. *Genes Cells,* 5**,** 789-802.

BAECHLER, S. A., FACTOR, V. M., DALLA ROSA, I., RAVJI, A., BECKER, D., KHIATI, S., MILLER JENKINS, L. M., LANG, M., SOURBIER, C., MICHAELS, S. A., NECKERS, L. M., ZHANG, H. L., SPINAZZOLA, A., HUANG, S. N., MARQUARDT, J. U. & POMMIER, Y. 2019. The mitochondrial type IB topoisomerase drives mitochondrial translation and carcinogenesis. *Nature Communications,* 10**,** 83.

BALASUBRAMANIAN, B., POGOZELSKI, W. K. & TULLIUS, T. D. 1998. DNA strand breaking by the hydroxyl radical is governed by the accessible surface areas of the hydrogen atoms of the DNA backbone. *Proceedings of the National Academy of Sciences,* 95**,** 9738-9743.

BALSA, E., PERRY, E. A., BENNETT, C. F., JEDRYCHOWSKI, M., GYGI, S. P., DOENCH, J. G. & PUIGSERVER, P. 2020. Defective NADPH production in mitochondrial disease complex I causes inflammation and cell death. *Nat Commun,* 11**,** 2714.

BARTSCH, K., KNITTLER, K., BOROWSKI, C., RUDNIK, S., DAMME, M., ADEN, K., SPEHLMANN, M. E., FREY, N., SAFTIG, P., CHALARIS, A. & RABE, B. 2017. Absence of RNase H2 triggers generation of immunogenic micronuclei removed by autophagy. *Hum Mol Genet,* 26**,** 3960-3972.

BASNET, R. M., ZIZIOLI, D., TAWEEDET, S., FINAZZI, D. & MEMO, M. 2019. Zebrafish Larvae as a Behavioral Model in Neuropharmacology. *Biomedicines,* 7.

BAXENDALE, S., HOLDSWORTH, C. J., MEZA SANTOSCOY, P. L., HARRISON, M. R., FOX, J., PARKIN, C. A., INGHAM, P. W. & CUNLIFFE, V. T. 2012. Identification of compounds with anti-convulsant properties in a zebrafish model of epileptic seizures. *Dis Model Mech,* 5**,** 773-84.

BEDELL, V. M., WESTCOT, S. E. & EKKER, S. C. 2011. Lessons from morpholino-based screening in zebrafish. *Brief Funct Genomics,* 10**,** 181-8.

BOHGAKI, T., BOHGAKI, M. & HAKEM, R. 2010. DNA double-strand break signaling and human disorders. *Genome Integr,* 1**,** 15.

BOWER, N. I., VOGRIN, A. J., LE GUEN, L., CHEN, H., STACKER, S. A., ACHEN, M. G. & HOGAN, B. M. 2017. Vegfd modulates both angiogenesis and lymphangiogenesis during zebrafish embryonic development. *Development,* 144**,** 507-518.

BREM, R. & HALL, J. 2005. XRCC1 is required for DNA single-strand break repair in human cells. *Nucleic Acids Res,* 33**,** 2512-20.

BRENNER, C. 2002. Hint, Fhit, and GalT: function, structure, evolution, and mechanism of three branches of the histidine triad superfamily of nucleotide hydrolases and transferases. *Biochemistry,* 41**,** 9003-14.

BROWN, J. A. & SUO, Z. 2011. Unlocking the sugar "steric gate" of DNA polymerases. *Biochemistry,* 50**,** 1135-42.

BROWN, L., HEAVEN, A., QUINN, C., GOODWIN, V., CHEW-GRAHAM, C., MAHMOOD, F., HALLAS, S., JACOB, I., BRUNDLE, C., BEST, K., DAFFU-O'REILLY, A., SPILSBURY, K., YOUNG, T. A., HAWKINS, R., HANRATTY, B., TEALE, E. & CLEGG, A. 2021. Community Ageing Research 75+ (CARE75+) REMOTE study: a remote model of recruitment and assessment of the health, well-being and social circumstances of older people. *BMJ Open,* 11**,** e048524.

CALDECOTT, K. W. 2022. DNA single-strand break repair and human genetic disease. *Trends Cell Biol,* 32**,** 733-745.

CALDECOTT, K. W. 2024. Causes and consequences of DNA single-strand breaks. *Trends Biochem Sci,* 49**,** 68-78.

CANNAN, W. J. & PEDERSON, D. S. 2016. Mechanisms and Consequences of Double-Strand DNA Break Formation in Chromatin. *J Cell Physiol,* 231**,** 3-14.

CAO, L., TIAN, H., FANG, M., XU, Z., TANG, D., CHEN, J., YIN, J., XIAO, H., SHANG, K., HAN, H. & LI, X. 2022. Activating cGAS-STING pathway with ROS-responsive nanoparticles delivering a hybrid prodrug for enhanced chemo-immunotherapy. *Biomaterials,* 290**,** 121856.

CAYUELA, M. L., CLAES, K. B. M., FERREIRA, M. G., HENRIQUES, C. M., VAN EEDEN, F., VARGA, M., VIERSTRAETE, J. & MIONE, M. C. 2018. The Zebrafish as an Emerging Model to Study DNA Damage in Aging, Cancer and Other Diseases. *Front Cell Dev Biol,* 6**,** 178.

CERRITELLI, S. M. & CROUCH, R. J. 2019. RNase H2-RED carpets the path to eukaryotic RNase H2 functions. *DNA Repair (Amst),* 84**,** 102736.

CHANG, C. C., HUANG, T. L., SHIMAMOTO, Y., TSAI, S. Y. & HSIA, K. C. 2017. Regulation of mitotic spindle assembly factor NuMA by Importin-beta. *J Cell Biol,* 216**,** 3453-3462.

CHATTERJEE, N. & WALKER, G. C. 2017. Mechanisms of DNA damage, repair, and mutagenesis. *Environ Mol Mutagen,* 58**,** 235-263.

CHAVALI, L. N. M., YDDAL, I., BIFULCO, E., MANNSÅKER, S., RØISE, D., LAW, J. O., FRØYSET, A. K., GRELLSCHEID, S. N. & FLADMARK, K. E. 2023. Progressive Motor and Non-Motor Symptoms in Park7 Knockout Zebrafish. *Int J Mol Sci,* 24.

CHEN, W., ZHAO, H. & LI, Y. 2023. Mitochondrial dynamics in health and disease: mechanisms and potential targets. *Signal Transduct Target Ther,* 8**,** 333.

CHEN, X., ERRANGI, B., LI, L., GLASSER, M. F., WESTLYE, L. T., FJELL, A. M., WALHOVD, K. B., HU, X., HERNDON, J. G., PREUSS, T. M. & RILLING, J. K. 2013. Brain aging in humans, chimpanzees (Pan troglodytes), and rhesus macaques (Macaca mulatta): magnetic resonance imaging studies of macro- and microstructural changes. *Neurobiol Aging,* 34**,** 2248-60.

CHOE, C. P., CHOI, S.-Y., KEE, Y., KIM, M. J., KIM, S.-H., LEE, Y., PARK, H.-C. & RO, H. 2021. Transgenic fluorescent zebrafish lines that have revolutionized biomedical research. *Laboratory Animal Research,* 37**,** 26.

CHOI, T. Y., CHOI, T. I., LEE, Y. R., CHOE, S. K. & KIM, C. H. 2021. Zebrafish as an animal model for biomedical research. *Exp Mol Med,* 53**,** 310-317.

CHON, H., SPARKS, J. L., RYCHLIK, M., NOWOTNY, M., BURGERS, P. M., CROUCH, R. J. & CERRITELLI, S. M. 2013. RNase H2 roles in genome integrity revealed by unlinking its activities. *Nucleic Acids Res,* 41**,** 3130-43.

CHON, H., VASSILEV, A., DEPAMPHILIS, M. L., ZHAO, Y., ZHANG, J., BURGERS, P. M., CROUCH, R. J. & CERRITELLI, S. M. 2009. Contributions of the two accessory subunits, RNASEH2B and RNASEH2C, to the activity and properties of the human RNase H2 complex. *Nucleic Acids Res,* 37**,** 96-110.

CLAUSEN, A. R., ZHANG, S., BURGERS, P. M., LEE, M. Y. & KUNKEL, T. A. 2013. Ribonucleotide incorporation, proofreading and bypass by human DNA polymerase delta. *DNA Repair (Amst),* 12**,** 121-7.

CLEAL, M., FONTANA, B. D., RANSON, D. C., MCBRIDE, S. D., SWINNY, J. D., REDHEAD, E. S. & PARKER, M. O. 2021. The Free-movement pattern Y-maze: A cross-species measure of working memory and executive function. *Behav Res Methods,* 53**,** 536-557.

CLEMENTS, P. M., BRESLIN, C., DEEKS, E. D., BYRD, P. J., JU, L., BIEGANOWSKI, P., BRENNER, C., MOREIRA, M. C., TAYLOR, A. M. & CALDECOTT, K. W. 2004. The ataxia-oculomotor apraxia 1 gene product has a role distinct from ATM and interacts with the DNA strand break repair proteins XRCC1 and XRCC4. *DNA Repair (Amst),* 3**,** 1493-502.

COLMAN, R. J. 2018. Non-human primates as a model for aging. *Biochim Biophys Acta Mol Basis Dis,* 1864**,** 2733-2741.

COLMAN, R. J., KEMNITZ, J. W., LANE, M. A., ABBOTT, D. H. & BINKLEY, N. 1999a. Skeletal effects of aging and menopausal status in female rhesus macaques. *J Clin Endocrinol Metab,* 84**,** 4144-8.

COLMAN, R. J., LANE, M. A., BINKLEY, N., WEGNER, F. H. & KEMNITZ, J. W. 1999b. Skeletal effects of aging in male rhesus monkeys. *Bone,* 24**,** 17-23.

COLMAN, R. J., MCKIERNAN, S. H., AIKEN, J. M. & WEINDRUCH, R. 2005. Muscle mass loss in Rhesus monkeys: age of onset. *Exp Gerontol,* 40**,** 573-81.

COMPTON, D. A., SZILAK, I. & CLEVELAND, D. W. 1992. Primary structure of NuMA, an intranuclear protein that defines a novel pathway for segregation of proteins at mitosis. *J Cell Biol,* 116**,** 1395-408.

COOKE, M. S., EVANS, M. D., DIZDAROGLU, M. & LUNEC, J. 2003. Oxidative DNA damage: mechanisms, mutation, and disease. *FASEB J,* 17**,** 1195-214.

CRISTINI, A., TELLIER, M., CONSTANTINESCU, F., ACCALAI, C., ALBULESCU, L. O., HEIRINGHOFF, R., BERY, N., SORDET, O., MURPHY, S. & GROMAK, N. 2022. RNase H2, mutated in Aicardi-Goutieres syndrome, resolves co-transcriptional R-loops to prevent DNA breaks and inflammation. *Nat Commun,* 13**,** 2961.

CROSSLEY, M. P., BOCEK, M. & CIMPRICH, K. A. 2019. R-Loops as Cellular Regulators and Genomic Threats. *Mol Cell,* 73**,** 398-411.

CROW, R. S., PETERSEN, C. L., COOK, S. B., STEVENS, C. J., TITUS, A. J., MACKENZIE, T. A. & BATSIS, J. A. 2020. Reported Weight Change in Older Adults and Presence of Frailty. *J Frailty Aging,* 9**,** 74-81.

DAS, S., YEUNG, K. T., MAHAJAN, M. A. & SAMUELS, H. H. 2014. Fas Activated Serine-Threonine Kinase Domains 2 (FASTKD2) mediates apoptosis of breast and prostate cancer cells through its novel FAST2 domain. *BMC Cancer,* 14**,** 852.

DATE, H., ONODERA, O., TANAKA, H., IWABUCHI, K., UEKAWA, K., IGARASHI, S., KOIKE, R., HIROI, T., YUASA, T., AWAYA, Y., SAKAI, T., TAKAHASHI, T., NAGATOMO, H., SEKIJIMA, Y., KAWACHI, I., TAKIYAMA, Y., NISHIZAWA, M., FUKUHARA, N., SAITO, K., SUGANO, S. & TSUJI, S. 2001. Early-onset ataxia with ocular motor apraxia and hypoalbuminemia is caused by mutations in a new HIT superfamily gene. *Nat Genet,* 29**,** 184-8.

DECOUT, A., KATZ, J. D., VENKATRAMAN, S. & ABLASSER, A. 2021. The cGAS-STING pathway as a therapeutic target in inflammatory diseases. *Nat Rev Immunol,* 21**,** 548-569.

DEROSE, E. F., PERERA, L., MURRAY, M. S., KUNKEL, T. A. & LONDON, R. E. 2012. Solution structure of the Dickerson DNA dodecamer containing a single ribonucleotide. *Biochemistry,* 51**,** 2407-16.

DEY, A., FLAJSHANS, M., PSENICKA, M. & GAZO, I. 2023. DNA repair genes play a variety of roles in the development of fish embryos. *Front Cell Dev Biol,* 11**,** 1119229.

DI MICCO, R., KRIZHANOVSKY, V., BAKER, D. & D'ADDA DI FAGAGNA, F. 2021. Cellular senescence in ageing: from mechanisms to therapeutic opportunities. *Nat Rev Mol Cell Biol,* 22**,** 75-95.

DORSEMANS, A. C., SOULE, S., WEGER, M., BOURDON, E., LEFEBVRE D'HELLENCOURT, C., MEILHAC, O. & DIOTEL, N. 2017. Impaired constitutive and regenerative neurogenesis in adult hyperglycemic zebrafish. *J Comp Neurol,* 525**,** 442-458.

DU, Q. & MACARA, I. G. 2004. Mammalian Pins is a conformational switch that links NuMA to heterotrimeric G proteins. *Cell,* 119**,** 503-16.

DU, Q., TAYLOR, L., COMPTON, D. A. & MACARA, I. G. 2002. LGN blocks the ability of NuMA to bind and stabilize microtubules. A mechanism for mitotic spindle assembly regulation. *Curr Biol,* 12**,** 1928-33.

DUMELIE, J. G. & JAFFREY, S. R. 2017. Defining the location of promoter-associated R-loops at near-nucleotide resolution using bisDRIP-seq. *Elife,* 6.

DUNCAN, A. E., COLMAN, R. J. & KRAMER, P. A. 2011. Longitudinal study of radiographic spinal osteoarthritis in a macaque model. *J Orthop Res,* 29**,** 1152-60.

EDWARDS, K. A., HALLIGAN, B. D., DAVIS, J. L., NIVERA, N. L. & LIU, L. F. 1982. Recognition sites of eukaryotic DNA topoisomerase I: DNA nucleotide sequencing analysis of topo I cleavage sites on SV40 DNA. *Nucleic Acids Res,* 10**,** 2565-76.

EL-KHAMISY, S. F. 2023. Oxidative DNA damage and repair at non-coding regulatory regions. *Trends Cell Biol,* 33**,** 939-949.

EL-KHAMISY, S. F., KATYAL, S., PATEL, P., JU, L., MCKINNON, P. J. & CALDECOTT, K. W. 2009. Synergistic decrease of DNA single-strand break repair rates in mouse neural cells lacking both Tdp1 and aprataxin. *DNA Repair (Amst),* 8**,** 760-6.

FERNANDEZ-VIZARRA, E., ENRIQUEZ, J. A., PEREZ-MARTOS, A., MONTOYA, J. & FERNANDEZ-SILVA, P. 2011. Tissue-specific differences in mitochondrial activity and biogenesis. *Mitochondrion,* 11**,** 207-13.

FRADE, J. M. & OVEJERO-BENITO, M. C. 2015. Neuronal cell cycle: the neuron itself and its circumstances. *Cell Cycle,* 14**,** 712-20.

FRIED, L. P., TANGEN, C. M., WALSTON, J., NEWMAN, A. B., HIRSCH, C., GOTTDIENER, J., SEEMAN, T., TRACY, R., KOP, W. J., BURKE, G., MCBURNIE, M. A. & CARDIOVASCULAR HEALTH STUDY COLLABORATIVE RESEARCH, G. 2001. Frailty in older adults: evidence for a phenotype. *J Gerontol A Biol Sci Med Sci,* 56**,** M146-56.

FRIEDMAN, D. B. & JOHNSON, T. E. 1988. A mutation in the age-1 gene in Caenorhabditis elegans lengthens life and reduces hermaphrodite fertility. *Genetics,* 118**,** 75-86.

FU, I., SMITH, D. J. & BROYDE, S. 2019. Rotational and translational positions determine the structural and dynamic impact of a single ribonucleotide incorporated in the nucleosome. *DNA Repair (Amst),* 73**,** 155-163.

GALLINI, S., CARMINATI, M., DE MATTIA, F., PIROVANO, L., MARTINI, E., OLDANI, A., ASTERITI, I. A., GUARGUAGLINI, G. & MAPELLI, M. 2016. NuMA Phosphorylation by Aurora-A Orchestrates Spindle Orientation. *Curr Biol,* 26**,** 458-69.

GARCIA-DIAZ, B., BARCA, E., BALREIRA, A., LOPEZ, L. C., TADESSE, S., KRISHNA, S., NAINI, A., MARIOTTI, C., CASTELLOTTI, B. & QUINZII, C. M. 2015. Lack of

aprataxin impairs mitochondrial functions via downregulation of the APE1/NRF1/NRF2 pathway. *Hum Mol Genet,* 24**,** 4516-29.

GERHARD, G. S. & CHENG, K. C. 2002. A call to fins! Zebrafish as a gerontological model. *Aging Cell,* 1**,** 104-11.

GHEZZI, D., SAADA, A., D'ADAMO, P., FERNANDEZ-VIZARRA, E., GASPARINI, P., TIRANTI, V., ELPELEG, O. & ZEVIANI, M. 2008. FASTKD2 nonsense mutation in an infantile mitochondrial encephalomyopathy associated with cytochrome c oxidase deficiency. *Am J Hum Genet,* 83**,** 415-23.

GILBERT, M. J., ZERULLA, T. C. & TIERNEY, K. B. 2014. Zebrafish (Danio rerio) as a model for the study of aging and exercise: physical ability and trainability decrease with age. *Exp Gerontol,* 50**,** 106-13.

GONZALO, S. & KREIENKAMP, R. 2015. DNA repair defects and genome instability in Hutchinson-Gilford Progeria Syndrome. *Curr Opin Cell Biol,* 34**,** 75-83.

GORDON, E. H. & HUBBARD, R. E. 2020. Differences in frailty in older men and women. *Med J Aust,* 212**,** 183-188.

GORDON, E. H. & HUBBARD, R. E. 2022. Frailty: understanding the difference between age and ageing. *Age Ageing,* 51.

GRABUNDZIJA, I., IRGANG, M., MATES, L., BELAY, E., MATRAI, J., GOGOL-DORING, A., KAWAKAMI, K., CHEN, W., RUIZ, P., CHUAH, M. K., VANDENDRIESSCHE, T., IZSVAK, Z. & IVICS, Z. 2010. Comparative analysis of transposable element vector systems in human cells. *Mol Ther,* 18**,** 1200-9.

GRAF, M., BONETTI, D., LOCKHART, A., SERHAL, K., KELLNER, V., MAICHER, A., JOLIVET, P., TEIXEIRA, M. T. & LUKE, B. 2017. Telomere Length Determines TERRA and R-Loop Regulation through the Cell Cycle. *Cell,* 170**,** 72-85 e14.

GUEVEN, N., BECHEREL, O. J., KIJAS, A. W., CHEN, P., HOWE, O., RUDOLPH, J. H., GATTI, R., DATE, H., ONODERA, O., TAUCHER-SCHOLZ, G. & LAVIN, M. F. 2004. Aprataxin, a novel protein that protects against genotoxic stress. *Hum Mol Genet,* 13**,** 1081-93.

GUO, C., SUN, L., CHEN, X. & ZHANG, D. 2013. Oxidative stress, mitochondrial damage and neurodegenerative diseases. *Neural Regen Res,* 8**,** 2003-14.

HALLIWELL, B., ADHIKARY, A., DINGFELDER, M. & DIZDAROGLU, M. 2021. Hydroxyl radical is a significant player in oxidative DNA damage in vivo. *Chem Soc Rev,* 50**,** 8355-8360.

HAMILTON, N., RUTHERFORD, H. A., PETTS, J. J., ISLES, H. M., WEBER, T., HENNEKE, M., GARTNER, J., DUNNING, M. J. & RENSHAW, S. A. 2020. The failure of microglia to digest developmental apoptotic cells contributes to the pathology of RNASET2-deficient leukoencephalopathy. *Glia,* 68**,** 1531-1545.

HARDIE, D. G. 2003. Minireview: the AMP-activated protein kinase cascade: the key sensor of cellular energy status. *Endocrinology,* 144**,** 5179-83.

HARMAN, D. 1956. Aging: a theory based on free radical and radiation chemistry. *J Gerontol,* 11**,** 298-300.

HARRIS, J. L., JAKOB, B., TAUCHER-SCHOLZ, G., DIANOV, G. L., BECHEREL, O. J. & LAVIN, M. F. 2009. Aprataxin, poly-ADP ribose polymerase 1 (PARP-1) and apurinic endonuclease 1 (APE1) function together to protect the genome against oxidative damage. *Hum Mol Genet,* 18**,** 4102-17.

HAYES, A. J., REYNOLDS, S., NOWELL, M. A., MEAKIN, L. B., HABICHER, J., LEDIN, J., BASHFORD, A., CATERSON, B. & HAMMOND, C. L. 2013. Spinal deformity in aged

zebrafish is accompanied by degenerative changes to their vertebrae that resemble osteoarthritis. *PLoS One,* 8**,** e75787.

HE, T., XIA, Y. & YANG, J. 2021. Systemic inflammation and chronic kidney disease in a patient due to the RNASEH2B defect. *Pediatr Rheumatol Online J,* 19**,** 9.

HEAVEN, A., BROWN, L., YOUNG, J., TEALE, E., HAWKINS, R., SPILSBURY, K., MOUNTAIN, G., YOUNG, T., GOODWIN, V., HANRATTY, B., CHEW-GRAHAM, C., BRUNDLE, C., MAHMOOD, F., JACOB, I., DAFFU-O'REILLY, A. & CLEGG, A. 2019. Community ageing research 75+ study (CARE75+): an experimental ageing and frailty research cohort. *BMJ Open,* 9**,** e026744.

HEGDE, M. L., HAZRA, T. K. & MITRA, S. 2008. Early steps in the DNA base excision/single-strand interruption repair pathway in mammalian cells. *Cell Res,* 18**,** 27-47.

HENRIQUES, C. M., CARNEIRO, M. C., TENENTE, I. M., JACINTO, A. & FERREIRA, M. G. 2013. Telomerase is required for zebrafish lifespan. *PLoS Genet,* 9**,** e1003214.

HERNANDEZ-SEGURA, A., NEHME, J. & DEMARIA, M. 2018. Hallmarks of Cellular Senescence. *Trends Cell Biol,* 28**,** 436-453.

HIDMI, O., OSTER, S., MONIN, J. & AQEILAN, R. I. 2024. TOP1 and R-loops facilitate transcriptional DSBs at hypertranscribed cancer driver genes. *iScience,* 27**,** 109082.

HONJO, Y. & ICHINOHE, T. 2019. Cellular responses to ionizing radiation change quickly over time during early development in zebrafish. *Cell Biol Int,* 43**,** 516-527.

HOWE, K., CLARK, M. D., TORROJA, C. F., TORRANCE, J., BERTHELOT, C., MUFFATO, M., COLLINS, J. E., HUMPHRAY, S., MCLAREN, K., MATTHEWS, L., MCLAREN, S., SEALY, I., CACCAMO, M., CHURCHER, C., SCOTT, C., BARRETT, J. C., KOCH, R., RAUCH, G. J., WHITE, S., CHOW, W., KILIAN, B., QUINTAIS, L. T., GUERRA-ASSUNCAO, J. A., ZHOU, Y., GU, Y., YEN, J., VOGEL, J. H., EYRE, T., REDMOND, S., BANERJEE, R., CHI, J., FU, B., LANGLEY, E., MAGUIRE, S. F., LAIRD, G. K., LLOYD, D., KENYON, E., DONALDSON, S., SEHRA, H., ALMEIDA-KING, J., LOVELAND, J., TREVANION, S., JONES, M., QUAIL, M., WILLEY, D., HUNT, A., BURTON, J., SIMS, S., MCLAY, K., PLUMB, B., DAVIS, J., CLEE, C., OLIVER, K., CLARK, R., RIDDLE, C., ELLIOT, D., THREADGOLD, G., HARDEN, G., WARE, D., BEGUM, S., MORTIMORE, B., KERRY, G., HEATH, P., PHILLIMORE, B., TRACEY, A., CORBY, N., DUNN, M., JOHNSON, C., WOOD, J., CLARK, S., PELAN, S., GRIFFITHS, G., SMITH, M., GLITHERO, R., HOWDEN, P., BARKER, N., LLOYD, C., STEVENS, C., HARLEY, J., HOLT, K., PANAGIOTIDIS, G., LOVELL, J., BEASLEY, H., HENDERSON, C., GORDON, D., AUGER, K., WRIGHT, D., COLLINS, J., RAISEN, C., DYER, L., LEUNG, K., ROBERTSON, L., AMBRIDGE, K., LEONGAMORNLERT, D., MCGUIRE, S., GILDERTHORP, R., GRIFFITHS, C., MANTHRAVADI, D., NICHOL, S., BARKER, G., et al. 2013. The zebrafish reference genome sequence and its relationship to the human genome. *Nature,* 496**,** 498-503.

HOWLETT, S. E., RUTENBERG, A. D. & ROCKWOOD, K. 2021. The degree of frailty as a translational measure of health in aging. *Nat Aging,* 1**,** 651-665.

HUANG, S. N., WILLIAMS, J. S., ARANA, M. E., KUNKEL, T. A. & POMMIER, Y. 2017. Topoisomerase I-mediated cleavage at unrepaired ribonucleotides generates DNA double-strand breaks. *EMBO J,* 36**,** 361-373.

HUANG, Z., SUN, S., LEE, M., MASLOV, A. Y., SHI, M., WALDMAN, S., MARSH, A., SIDDIQUI, T., DONG, X., PETER, Y., SADOUGHI, A., SHAH, C., YE, K., SPIVACK, S. D. & VIJG, J. 2022. Single-cell analysis of somatic mutations in human bronchial epithelial cells in relation to aging and smoking. *Nat Genet,* 54**,** 492-498.

HWANG, J. & PARK, S. 2022. Gender-Specific Risk Factors and Prevalence for Sarcopenia among Community-Dwelling Young-Old Adults. *Int J Environ Res Public Health,* 19**,** 7232.

IMAMURA, R., SAITO, M., SHIMADA, M., KOBAYASHI, J., ISHIAI, M. & MATSUMOTO, Y. 2023. APTX acts in DNA double-strand break repair in a manner distinct from XRCC4. *J Radiat Res,* 64**,** 485-495.

IPARRAGUIRRE, L., ALBERRO, A., IÑIGUEZ, S. G., MUÑOZ-CULLA, M., VERGARA, I., MATHEU, A. & OTAEGUI, D. 2023. Blood RNA-Seq profiling reveals a set of circular RNAs differentially expressed in frail individuals. *Immun Ageing,* 20**,** 33.

JARVIS, R. B. & KNOWLES, J. F. 2003. DNA damage in zebrafish larvae induced by exposure to low-dose rate γ-radiation: detection by the alkaline comet assay. *Mutation Research/Genetic Toxicology and Environmental Mutagenesis,* 541**,** 63-69.

JEONG, J. H., CHEOL KANG, Y., PIAO, Y., KANG, S. & PAK, Y. K. 2017. miR-24-mediated knockdown of H2AX damages mitochondria and the insulin signaling pathway. *Exp Mol Med,* 49**,** e313.

JOURDAIN, A. A., POPOW, J., DE LA FUENTE, M. A., MARTINOU, J. C., ANDERSON, P. & SIMARRO, M. 2017. The FASTK family of proteins: emerging regulators of mitochondrial RNA biology. *Nucleic Acids Res,* 45**,** 10941-10947.

KALUEFF, A. V., GEBHARDT, M., STEWART, A. M., CACHAT, J. M., BRIMMER, M., CHAWLA, J. S., CRADDOCK, C., KYZAR, E. J., ROTH, A., LANDSMAN, S., GAIKWAD, S., ROBINSON, K., BAATRUP, E., TIERNEY, K., SHAMCHUK, A., NORTON, W., MILLER, N., NICOLSON, T., BRAUBACH, O., GILMAN, C. P., PITTMAN, J., ROSEMBERG, D. B., GERLAI, R., ECHEVARRIA, D., LAMB, E., NEUHAUSS, S. C., WENG, W., BALLY-CUIF, L. & SCHNEIDER, H. 2013. Towards a comprehensive catalog of zebrafish behavior 1.0 and beyond. *Zebrafish,* 10**,** 70-86.

KANE, A. E. & HOWLETT, S. E. 2021. Sex differences in frailty: Comparisons between humans and preclinical models. *Mech Ageing Dev,* 198**,** 111546.

KAPAHI, P., CHEN, D., ROGERS, A. N., KATEWA, S. D., LI, P. W., THOMAS, E. L. & KOCKEL, L. 2010. With TOR, less is more: a key role for the conserved nutrient-sensing TOR pathway in aging. *Cell Metab,* 11**,** 453-65.

KASE, Y., SHIMAZAKI, T. & OKANO, H. 2020. Current understanding of adult neurogenesis in the mammalian brain: how does adult neurogenesis decrease with age? *Inflamm Regen,* 40**,** 10.

KAUFMANN, T., STRASSER, A. & JOST, P. J. 2012. Fas death receptor signalling: roles of Bid and XIAP. *Cell Death Differ,* 19**,** 42-50.

KAWAKAMI, K. 2007. Tol2: a versatile gene transfer vector in vertebrates. *Genome Biol,* 8 Suppl 1**,** S7.

KELLNER, V. & LUKE, B. 2020. Molecular and physiological consequences of faulty eukaryotic ribonucleotide excision repair. *EMBO J,* 39**,** e102309.

KENNEDY, S. R., SALK, J. J., SCHMITT, M. W. & LOEB, L. A. 2013. Ultra-sensitive sequencing reveals an age-related increase in somatic mitochondrial mutations that are inconsistent with oxidative damage. *PLoS Genet,* 9**,** e1003794.

KENYON, C., CHANG, J., GENSCH, E., RUDNER, A. & TABTIANG, R. 1993. A C. elegans mutant that lives twice as long as wild type. *Nature,* 366**,** 461-464.

KHANDAGALE, P., THAKUR, S. & ACHARYA, N. 2020. Identification of PCNA-interacting protein motifs in human DNA polymerase delta. *Biosci Rep,* 40.

KHOR, E. S., NOOR, S. M. & WONG, P. F. 2019. Understanding the Role of ztor in Aging-related Diseases Using the Zebrafish Model. *In Vivo,* 33**,** 1713-1720.

KIM, M., MAHMOOD, M., REZNIK, E. & GAMMAGE, P. A. 2022. Mitochondrial DNA is a major source of driver mutations in cancer. *Trends Cancer,* 8**,** 1046-1059.

KIMMEL, C. B., BALLARD, W. W., KIMMEL, S. R., ULLMANN, B. & SCHILLING, T. F. 1995. Stages of embryonic development of the zebrafish. *Dev Dyn,* 203**,** 253-310.

KIMURA, K. D., TISSENBAUM, H. A., LIU, Y. & RUVKUN, G. 1997. daf-2, an insulin receptor-like gene that regulates longevity and diapause in Caenorhabditis elegans. *Science,* 277**,** 942-6.

KISHI, S. 2004. Functional aging and gradual senescence in zebrafish. *Ann N Y Acad Sci,* 1019**,** 521-6.

KISHI, S., BAYLISS, P. E., UCHIYAMA, J., KOSHIMIZU, E., QI, J., NANJAPPA, P., IMAMURA, S., ISLAM, A., NEUBERG, D., AMSTERDAM, A. & ROBERTS, T. M. 2008. The identification of zebrafish mutants showing alterations in senescence-associated biomarkers. *PLoS Genet,* 4**,** e1000152.

KISHI, S., SLACK, B. E., UCHIYAMA, J. & ZHDANOVA, I. V. 2009. Zebrafish as a genetic model in biological and behavioral gerontology: where development meets aging in vertebrates--a mini-review. *Gerontology,* 55**,** 430-41.

KISHI, S., UCHIYAMA, J., BAUGHMAN, A. M., GOTO, T., LIN, M. C. & TSAI, S. B. 2003. The zebrafish as a vertebrate model of functional aging and very gradual senescence. *Exp Gerontol,* 38**,** 777-86.

KIYOMITSU, T. & BOERNER, S. 2021. The Nuclear Mitotic Apparatus (NuMA) Protein: A Key Player for Nuclear Formation, Spindle Assembly, and Spindle Positioning. *Front Cell Dev Biol,* 9**,** 653801.

KLUG, W. S., CUMMINGS, M. R., SPENDER, C. A. & PALLADION, M. A. 2016. *Concepts of Genetics*, Pearson.

KOEPPEL, M., VAN HEERINGEN, S. J., SMEENK, L., NAVIS, A. C., JANSSEN-MEGENS, E. M. & LOHRUM, M. 2009. The novel p53 target gene IRF2BP2 participates in cell survival during the p53 stress response. *Nucleic Acids Res,* 37**,** 322-35.

KONDRATOV, R. V. 2007. A role of the circadian system and circadian proteins in aging. *Ageing Res Rev,* 6**,** 12-27.

KOTAK, S., BUSSO, C. & GONCZY, P. 2012. Cortical dynein is critical for proper spindle positioning in human cells. *J Cell Biol,* 199**,** 97-110.

KOTAK, S., BUSSO, C. & GONCZY, P. 2014. NuMA interacts with phosphoinositides and links the mitotic spindle with the plasma membrane. *EMBO J,* 33**,** 1815-30.

KRANZUSCH, P. J., LEE, A. S., BERGER, J. M. & DOUDNA, J. A. 2013. Structure of human cGAS reveals a conserved family of second-messenger enzymes in innate immunity. *Cell Rep,* 3**,** 1362-8.

KROKAN, H. E. & BJORAS, M. 2013. Base excision repair. *Cold Spring Harb Perspect Biol,* 5**,** a012583.

KURO-O, M. 2010. Klotho. *Pflügers Archiv - European Journal of Physiology,* 459**,** 333-343.

KURO-O, M., MATSUMURA, Y., AIZAWA, H., KAWAGUCHI, H., SUGA, T., UTSUGI, T., OHYAMA, Y., KURABAYASHI, M., KANAME, T., KUME, E., IWASAKI, H., IIDA, A., SHIRAKI-IIDA, T., NISHIKAWA, S., NAGAI, R. & NABESHIMA, Y. I. 1997. Mutation of the mouse klotho gene leads to a syndrome resembling ageing. *Nature,* 390**,** 45-51.

KUSAKABE, M., ONISHI, Y., TADA, H., KURIHARA, F., KUSAO, K., FURUKAWA, M., IWAI, S., YOKOI, M., SAKAI, W. & SUGASAWA, K. 2019. Mechanism and regulation of DNA damage recognition in nucleotide excision repair. *Genes Environ,* 41**,** 2.

KYRYLKOVA, K., KYRYACHENKO, S., LEID, M. & KIOUSSI, C. 2012. Detection of apoptosis by TUNEL assay. *Methods Mol Biol,* 887**,** 41-7.

LACONI, E., MARONGIU, F. & DEGREGORI, J. 2020. Cancer as a disease of old age: changing mutational and microenvironmental landscapes. *Br J Cancer,* 122**,** 943-952.

LAGOUGE, M. & LARSSON, N. G. 2013. The role of mitochondrial DNA mutations and free radicals in disease and ageing. *J Intern Med,* 273**,** 529-43.

LAM, I. & KEENEY, S. 2014. Mechanism and regulation of meiotic recombination initiation. *Cold Spring Harb Perspect Biol,* 7**,** a016634.

LANGELIER, M. F., EISEMANN, T., RICCIO, A. A. & PASCAL, J. M. 2018. PARP family enzymes: regulation and catalysis of the poly(ADP-ribose) posttranslational modification. *Curr Opin Struct Biol,* 53**,** 187-198.

LAPIERRE, L. R. & HANSEN, M. 2012. Lessons from C. elegans: signaling pathways for longevity. *Trends Endocrinol Metab,* 23**,** 637-44.

LEE, H. W., BLASCO, M. A., GOTTLIEB, G. J., HORNER, J. W., 2ND, GREIDER, C. W. & DEPINHO, R. A. 1998. Essential role of mouse telomerase in highly proliferative organs. *Nature,* 392**,** 569-74.

LEES, H., WALTERS, H. & COX, L. S. 2016. Animal and human models to understand ageing. *Maturitas,* 93**,** 18-27.

LI, M. & LIU, Y. 2016. Topoisomerase I in Human Disease Pathogenesis and Treatments. *Genomics Proteomics Bioinformatics,* 14**,** 166-171.

LI, T. & CHEN, Z. J. 2018. The cGAS-cGAMP-STING pathway connects DNA damage to inflammation, senescence, and cancer. *J Exp Med,* 215**,** 1287-1299.

LI, W., SIMARRO, M., KEDERSHA, N. & ANDERSON, P. 2004. FAST is a survival protein that senses mitochondrial stress and modulates TIA-1-regulated changes in protein expression. *Mol Cell Biol,* 24**,** 10718-32.

LI, X., LI, C., ZHANG, W., WANG, Y., QIAN, P. & HUANG, H. 2023. Inflammation and aging: signaling pathways and intervention therapies. *Signal Transduct Target Ther,* 8**,** 239.

LI, Y. & BREAKER, R. R. 1999. Kinetics of RNA Degradation by Specific Base Catalysis of Transesterification Involving the 2'-Hydroxyl Group. *Journal of the American Chemical Society,* 121**,** 5364-5372.

LIN, Y. F., SAM, J. & EVANS, T. 2021. Sirt1 promotes tissue regeneration in zebrafish through regulating the mitochondrial unfolded protein response. *iScience,* 24**,** 103118.

LIU, A. & YING, S. 2023. Aicardi-Goutieres syndrome: A monogenic type I interferonopathy. *Scand J Immunol,* 98**,** e13314.

LIU, B., WANG, J., CHAN, K. M., TJIA, W. M., DENG, W., GUAN, X., HUANG, J. D., LI, K. M., CHAU, P. Y., CHEN, D. J., PEI, D., PENDAS, A. M., CADINANOS, J., LOPEZ-OTIN, C., TSE, H. F., HUTCHISON, C., CHEN, J., CAO, Y., CHEAH, K. S., TRYGGVASON, K. & ZHOU, Z. 2005. Genomic instability in laminopathy-based premature aging. *Nat Med,* 11**,** 780-5.

LOCKHART, A., PIRES, V. B., BENTO, F., KELLNER, V., LUKE-GLASER, S., YAKOUB, G., ULRICH, H. D. & LUKE, B. 2019. RNase H1 and H2 Are Differentially Regulated to Process RNA-DNA Hybrids. *Cell Rep,* 29**,** 2890-2900 e5.

LOPEZ-LLUCH, G. & NAVAS, P. 2016. Calorie restriction as an intervention in ageing. *J Physiol,* 594**,** 2043-60.

LOPEZ-OTIN, C., BLASCO, M. A., PARTRIDGE, L., SERRANO, M. & KROEMER, G. 2013. The hallmarks of aging. *Cell,* 153**,** 1194-217.

LOPEZ-OTIN, C., BLASCO, M. A., PARTRIDGE, L., SERRANO, M. & KROEMER, G. 2023. Hallmarks of aging: An expanding universe. *Cell,* 186**,** 243-278.

LU, T., PAN, Y., KAO, S. Y., LI, C., KOHANE, I., CHAN, J. & YANKNER, B. A. 2004. Gene regulation and DNA damage in the ageing human brain. *Nature,* 429**,** 883-91.

LUJAN, S. A., WILLIAMS, J. S., CLAUSEN, A. R., CLARK, A. B. & KUNKEL, T. A. 2013. Ribonucleotides are signals for mismatch repair of leading-strand replication errors. *Mol Cell,* 50**,** 437-43.

LYKKE-ANDERSEN, S. & JENSEN, T. H. 2015. Nonsense-mediated mRNA decay: an intricate machinery that shapes transcriptomes. *Nat Rev Mol Cell Biol,* 16**,** 665-77.

MACKENZIE, K. J., CARROLL, P., LETTICE, L., TARNAUSKAITE, Z., REDDY, K., DIX, F., REVUELTA, A., ABBONDATI, E., RIGBY, R. E., RABE, B., KILANOWSKI, F., GRIMES, G., FLUTEAU, A., DEVENNEY, P. S., HILL, R. E., REIJNS, M. A. & JACKSON, A. P. 2016. Ribonuclease H2 mutations induce a cGAS/STING-dependent innate immune response. *EMBO J,* 35**,** 831-44.

MACKENZIE, K. J., CARROLL, P., MARTIN, C. A., MURINA, O., FLUTEAU, A., SIMPSON, D. J., OLOVA, N., SUTCLIFFE, H., RAINGER, J. K., LEITCH, A., OSBORN, R. T., WHEELER, A. P., NOWOTNY, M., GILBERT, N., CHANDRA, T., REIJNS, M. A. M. & JACKSON, A. P. 2017. cGAS surveillance of micronuclei links genome instability to innate immunity. *Nature,* 548**,** 461-465.

MADEIRA, F., MADHUSOODANAN, N., LEE, J., EUSEBI, A., NIEWIELSKA, A., TIVEY, A. R. N., LOPEZ, R. & BUTCHER, S. 2024. The EMBL-EBI Job Dispatcher sequence analysis tools framework in 2024. *Nucleic acids research,* 52**,** W521-W525.

MADSEN, H. B., PEASE, L. I., SCANLAN, R. L., AKBARI, M., RASMUSSEN, L. J., SHANLEY, D. P. & BOHR, V. A. 2023. The DNA repair enzyme, aprataxin, plays a role in innate immune signaling. *Front Aging Neurosci,* 15**,** 1290681.

MARCOZZI, S., BIGOSSI, G., GIULIANI, M. E., GIACCONI, R., PIACENZA, F., CARDELLI, M., BRUNETTI, D., SEGALA, A., VALERIO, A., NISOLI, E., LATTANZIO, F., PROVINCIALI, M. & MALAVOLTA, M. 2023. Cellular senescence and frailty: a comprehensive insight into the causal links. *Geroscience,* 45**,** 3267-3305.

MARTEIJN, J. A., LANS, H., VERMEULEN, W. & HOEIJMAKERS, J. H. 2014. Understanding nucleotide excision repair and its roles in cancer and ageing. *Nat Rev Mol Cell Biol,* 15**,** 465-81.

MARTINS, R. R., BESSE, S., ELLIS, P. S., HARTOPP, N., MUGHAL, N., EVANS, O., WAHIB, M. H., YAZIGAN, Z., MORTIBOYS, H., RERA, M. & HENRIQUES, C. M. 2024. Telomerase-Dependent Ageing In The Zebrafish Brain. *bioRxiv***,** 2022.05.24.493215.

MATSUNAMI, K. 2018. Frailty and Caenorhabditis elegans as a Benchtop Animal Model for Screening Drugs Including Natural Herbs. *Front Nutr,* 5**,** 111.

MEHTA, A. & HABER, J. E. 2014. Sources of DNA double-strand breaks and models of recombinational DNA repair. *Cold Spring Harb Perspect Biol,* 6**,** a016428.

MERDES, A., RAMYAR, K., VECHIO, J. D. & CLEVELAND, D. W. 1996. A complex of NuMA and cytoplasmic dynein is essential for mitotic spindle assembly. *Cell,* 87**,** 447-58.

MERONI, A., MENTEGARI, E., CRESPAN, E., MUZI-FALCONI, M., LAZZARO, F. & PODESTA, A. 2017. The Incorporation of Ribonucleotides Induces Structural and Conformational Changes in DNA. *Biophys J,* 113**,** 1373-1382.

MERRILL, D. K. & GUYNN, R. W. 1981. The calculation of the cytoplasmic free [NADP+]/[NADPH] ratio in brain: effect of electroconvulsive seizure. *Brain Res,* 221**,** 307-18.

MILLER, A. J., ROMAN, B. & NORSTROM, E. 2016. A method for easily customizable gradient gel electrophoresis. *Analytical Biochemistry,* 509**,** 12-14.

MOOS, W. H., FALLER, D. V., GLAVAS, I. P., KANARA, I., KODUKULA, K., PERNOKAS, J., PERNOKAS, M., PINKERT, C. A., POWERS, W. R., SAMPANI, K., STELIOU, K. & VAVVAS, D. G. 2023. Epilepsy: Mitochondrial connections to the 'Sacred' disease. *Mitochondrion,* 72**,** 84-101.

MOREIRA, F., ARENAS, M., VIDEIRA, A. & PEREIRA, F. 2023. Evolution of TOP1 and TOP1MT Topoisomerases in Chordata. *J Mol Evol,* 91**,** 192-203.

MOREIRA, M. C., BARBOT, C., TACHI, N., KOZUKA, N., UCHIDA, E., GIBSON, T., MENDONCA, P., COSTA, M., BARROS, J., YANAGISAWA, T., WATANABE, M., IKEDA, Y., AOKI, M., NAGATA, T., COUTINHO, P., SEQUEIROS, J. & KOENIG, M. 2001. The gene mutated in ataxia-ocular apraxia 1 encodes the new HIT/Zn-finger protein aprataxin. *Nat Genet,* 29**,** 189-93.

MORHAM, S. G., KLUCKMAN, K. D., VOULOMANOS, N. & SMITHIES, O. 1996. Targeted disruption of the mouse topoisomerase I gene by camptothecin selection. *Mol Cell Biol,* 16**,** 6804-9.

MORSLI, S., HENRIQUES, C. M., ELLIS, P. S., MORTIBOYS, H., BAXENDALE, S., LOYNES, C. A., RENSHAW, S. A. & BELLANTUONO, I. 2023. A p21-GFP zebrafish model of senescence for rapid testing of senolytics in vivo. *Aging Cell,* 22**,** e13835.

MOSIMANN, C., KAUFMAN, C. K., LI, P., PUGACH, E. K., TAMPLIN, O. J. & ZON, L. I. 2011. Ubiquitous transgene expression and Cre-based recombination driven by the ubiquitin promoter in zebrafish. *Development,* 138**,** 169-77.

NÄSSEL, D. R. & BROECK, J. V. 2016. Insulin/IGF signaling in Drosophila and other insects: factors that regulate production, release and post-release action of the insulin-like peptides. *Cellular and Molecular Life Sciences,* 73**,** 271-290.

NAVA, G. M., GRASSO, L., SERTIC, S., PELLICIOLI, A., MUZI FALCONI, M. & LAZZARO, F. 2020. One, No One, and One Hundred Thousand: The Many Forms of Ribonucleotides in DNA. *Int J Mol Sci,* 21**,** 1706.

NICK MCELHINNY, S. A., GORDENIN, D. A., STITH, C. M., BURGERS, P. M. & KUNKEL, T. A. 2008. Division of labor at the eukaryotic replication fork. *Mol Cell,* 30**,** 137-44.

NICK MCELHINNY, S. A., KUMAR, D., CLARK, A. B., WATT, D. L., WATTS, B. E., LUNDSTROM, E. B., JOHANSSON, E., CHABES, A. & KUNKEL, T. A. 2010a. Genome instability due to ribonucleotide incorporation into DNA. *Nat Chem Biol,* 6**,** 774-81.

NICK MCELHINNY, S. A., WATTS, B. E., KUMAR, D., WATT, D. L., LUNDSTROM, E. B., BURGERS, P. M., JOHANSSON, E., CHABES, A. & KUNKEL, T. A. 2010b. Abundant ribonucleotide incorporation into DNA by yeast replicative polymerases. *Proc Natl Acad Sci U S A,* 107**,** 4949-54.

NIEDERNHOFER, L. J., GARINIS, G. A., RAAMS, A., LALAI, A. S., ROBINSON, A. R., APPELDOORN, E., ODIJK, H., OOSTENDORP, R., AHMAD, A., VAN LEEUWEN, W., THEIL, A. F., VERMEULEN, W., VAN DER HORST, G. T., MEINECKE, P., KLEIJER, W. J., VIJG, J., JASPERS, N. G. & HOEIJMAKERS, J. H. 2006. A new

progeroid syndrome reveals that genotoxic stress suppresses the somatotroph axis. *Nature,* 444**,** 1038-43.

O'CAOIMH, R., SEZGIN, D., O'DONOVAN, M. R., MOLLOY, D. W., CLEGG, A., ROCKWOOD, K. & LIEW, A. 2021. Prevalence of frailty in 62 countries across the world: a systematic review and meta-analysis of population-level studies. *Age Ageing,* 50**,** 96-104.

O'DRISCOLL, M. 2012. Diseases associated with defective responses to DNA damage. *Cold Spring Harb Perspect Biol,* 4**,** a012773-a012773.

OFFICE FOR HEALTH IMPROVEMENT AND DISPARITIES 2023. A consensus on healthy ageing.

OFFICE FOR NATIONAL STATISTICS 2024. Estimates of the very old, including centenarians, England and Wales: 2002 to 2022. *In:* STOREY, A. (ed.).

OFFICE FOR NATIONAL STATISTICS (ONS) 2019. Estimates of the very old, including centenarians, UK: 2002 to 2018. *In:* PATEL, V. (ed.).

OGURA, Y., KANEKO, R., UJIBE, K., WAKAMATSU, Y. & HIRATA, H. 2021. Loss of alphaklotho causes reduced motor ability and short lifespan in zebrafish. *Sci Rep,* 11**,** 15090.

OHKUBO, A., VAN HAUTE, L., RUDLER, D. L., STENTENBACH, M., STEINER, F. A., RACKHAM, O., MINCZUK, M., FILIPOVSKA, A. & MARTINOU, J. C. 2021. The FASTK family proteins fine-tune mitochondrial RNA processing. *PLoS Genet,* 17**,** e1009873.

OKA, T., NISHIMURA, Y., ZANG, L., HIRANO, M., SHIMADA, Y., WANG, Z., UMEMOTO, N., KUROYANAGI, J., NISHIMURA, N. & TANAKA, T. 2010. Diet-induced obesity in zebrafish shares common pathophysiological pathways with mammalian obesity. *BMC Physiol,* 10**,** 21.

OLIVEIRA, N. A. S., PINHO, B. R. & OLIVEIRA, J. M. A. 2023. Swimming against ALS: How to model disease in zebrafish for pathophysiological and behavioral studies. *Neurosci Biobehav Rev,* 148**,** 105138.

PAN, J., FEI, C. J., HU, Y., WU, X. Y., NIE, L. & CHEN, J. 2023. Current understanding of the cGAS-STING signaling pathway: Structure, regulatory mechanisms, and related diseases. *Zool Res,* 44**,** 183-218.

PANDEY, N. & BLACK, B. E. 2021. Rapid Detection and Signaling of DNA Damage by PARP-1. *Trends Biochem Sci,* 46**,** 744-757.

PAYNE, B. A., WILSON, I. J., HATELEY, C. A., HORVATH, R., SANTIBANEZ-KOREF, M., SAMUELS, D. C., PRICE, D. A. & CHINNERY, P. F. 2011. Mitochondrial aging is accelerated by anti-retroviral therapy through the clonal expansion of mtDNA mutations. *Nat Genet,* 43**,** 806-10.

PEDROSO, J. L., VALE, T. C., DA COSTA, S. C. G., SANTOS, M., ALONSO, I. & BARSOTTINI, O. G. P. 2020. Complex Movement Disorders in Ataxia with Oculomotor Apraxia Type 1: Beyond the Cerebellar Syndrome. *Tremor Other Hyperkinet Mov (N Y),* 10**,** 39.

PEREZ, H., ABDALLAH, M. F., CHAVIRA, J. I., NORRIS, A. S., EGELAND, M. T., VO, K. L., BUECHSENSCHUETZ, C. L., SANGHEZ, V., KIM, J. L., PIND, M., NAKAMURA, K., HICKS, G. G., GATTI, R. A., MADRENAS, J., IACOVINO, M., MCKINNON, P. J. & MATHEWS, P. J. 2021. A novel, ataxic mouse model of ataxia telangiectasia caused by a clinically relevant nonsense mutation. *Elife,* 10.

PETERMANN, E., LAN, L. & ZOU, L. 2022. Sources, resolution and physiological relevance of R-loops and RNA-DNA hybrids. *Nat Rev Mol Cell Biol,* 23**,** 521-540.

PETRUSEVA, I. O., EVDOKIMOV, A. N. & LAVRIK, O. I. 2014. Molecular mechanism of global genome nucleotide excision repair. *Acta Naturae,* 6**,** 23-34.

PIPER, M. D. W. & PARTRIDGE, L. 2018. Drosophila as a model for ageing. *Biochimica et Biophysica Acta (BBA) - Molecular Basis of Disease,* 1864**,** 2707-2717.

PIZZINO, G., IRRERA, N., CUCINOTTA, M., PALLIO, G., MANNINO, F., ARCORACI, V., SQUADRITO, F., ALTAVILLA, D. & BITTO, A. 2017. Oxidative Stress: Harms and Benefits for Human Health. *Oxid Med Cell Longev,* 2017**,** 8416763.

POMMIER, Y., NUSSENZWEIG, A., TAKEDA, S. & AUSTIN, C. 2022. Human topoisomerases and their roles in genome stability and organization. *Nat Rev Mol Cell Biol,* 23**,** 407-427.

POPOW, J., ALLEAUME, A. M., CURK, T., SCHWARZL, T., SAUER, S. & HENTZE, M. W. 2015. FASTKD2 is an RNA-binding protein required for mitochondrial RNA processing and translation. *RNA,* 21**,** 1873-84.

PURSELL, Z. F., ISOZ, I., LUNDSTROM, E. B., JOHANSSON, E. & KUNKEL, T. A. 2007. Yeast DNA polymerase epsilon participates in leading-strand DNA replication. *Science,* 317**,** 127-30.

PUTS, M. T., VISSER, M., TWISK, J. W., DEEG, D. J. & LIPS, P. 2005. Endocrine and inflammatory markers as predictors of frailty. *Clin Endocrinol (Oxf),* 63**,** 403-11.

RAGU, S., MATOS-RODRIGUES, G. & LOPEZ, B. S. 2020. Replication Stress, DNA Damage, Inflammatory Cytokines and Innate Immune Response. *Genes (Basel),* 11**,** 409.

RAHN, J. J., BESTMAN, J. E., STACKLEY, K. D. & CHAN, S. S. 2015. Zebrafish lacking functional DNA polymerase gamma survive to juvenile stage, despite rapid and sustained mitochondrial DNA depletion, altered energetics and growth. *Nucleic Acids Res,* 43**,** 10338-52.

RAJEEVAN, A., KESHRI, R., KAPOOR, S. & KOTAK, S. 2020. NuMA interaction with chromatin is vital for proper chromosome decondensation at the mitotic exit. *Mol Biol Cell,* 31**,** 2437-2451.

RANA, A. Q., KHAN, O. A. & AKTHAR, R. 2013. Progressive ataxia associated with ocular apraxia type 1 (AOA1) with a presence of a novel mutation on the aprataxin gene. *Ann Indian Acad Neurol,* 16**,** 269-71.

RASS, U., AHEL, I. & WEST, S. C. 2007. Actions of aprataxin in multiple DNA repair pathways. *J Biol Chem,* 282**,** 9469-9474.

RAY, S., ABUGABLE, A. A., PARKER, J., LIVERSIDGE, K., PALMINHA, N. M., LIAO, C., ACOSTA-MARTIN, A. E., SOUZA, C. D. S., JURGA, M., SUDBERY, I. & EL-KHAMISY, S. F. 2022. A mechanism for oxidative damage repair at gene regulatory elements. *Nature,* 609**,** 1038-1047.

REECE-HOYES, J. S. & WALHOUT, A. J. M. 2018. Gateway Recombinational Cloning. *Cold Spring Harb Protoc,* 2018**,** pdb.top094912.

REIJNS, M. A., BUBECK, D., GIBSON, L. C., GRAHAM, S. C., BAILLIE, G. S., JONES, E. Y. & JACKSON, A. P. 2011. The structure of the human RNase H2 complex defines key interaction interfaces relevant to enzyme function and human disease. *J Biol Chem,* 286**,** 10530-9.

REIJNS, M. A., RABE, B., RIGBY, R. E., MILL, P., ASTELL, K. R., LETTICE, L. A., BOYLE, S., LEITCH, A., KEIGHREN, M., KILANOWSKI, F., DEVENNEY, P. S., SEXTON, D., GRIMES, G., HOLT, I. J., HILL, R. E., TAYLOR, M. S., LAWSON, K. A., DORIN, J. R. & JACKSON, A. P. 2012. Enzymatic removal of ribonucleotides from DNA is essential for mammalian genome integrity and development. *Cell,* 149**,** 1008-22.

REIJNS, M. A. M., PARRY, D. A., WILLIAMS, T. C., NADEU, F., HINDSHAW, R. L., RIOS SZWED, D. O., NICHOLSON, M. D., CARROLL, P., BOYLE, S., ROYO, R., CORNISH, A. J., XIANG, H., RIDOUT, K., GENOMICS ENGLAND RESEARCH, C., COLORECTAL CANCER DOMAIN UK, G. P., SCHUH, A., ADEN, K., PALLES, C., CAMPO, E., STANKOVIC, T., TAYLOR, M. S. & JACKSON, A. P. 2022. Signatures of TOP1 transcription-associated mutagenesis in cancer and germline. *Nature,* 602**,** 623-631.

RICE, G., PATRICK, T., PARMAR, R., TAYLOR, C. F., AEBY, A., AICARDI, J., ARTUCH, R., MONTALTO, S. A., BACINO, C. A., BARROSO, B., BAXTER, P., BENKO, W. S., BERGMANN, C., BERTINI, E., BIANCHERI, R., BLAIR, E. M., BLAU, N., BONTHRON, D. T., BRIGGS, T., BRUETON, L. A., BRUNNER, H. G., BURKE, C. J., CARR, I. M., CARVALHO, D. R., CHANDLER, K. E., CHRISTEN, H. J., CORRY, P. C., COWAN, F. M., COX, H., D'ARRIGO, S., DEAN, J., DE LAET, C., DE PRAETER, C., DERY, C., FERRIE, C. D., FLINTOFF, K., FRINTS, S. G., GARCIA-CAZORLA, A., GENER, B., GOIZET, C., GOUTIERES, F., GREEN, A. J., GUET, A., HAMEL, B. C., HAYWARD, B. E., HEIBERG, A., HENNEKAM, R. C., HUSSON, M., JACKSON, A. P., JAYATUNGA, R., JIANG, Y. H., KANT, S. G., KAO, A., KING, M. D., KINGSTON, H. M., KLEPPER, J., VAN DER KNAAP, M. S., KORNBERG, A. J., KOTZOT, D., KRATZER, W., LACOMBE, D., LAGAE, L., LANDRIEU, P. G., LANZI, G., LEITCH, A., LIM, M. J., LIVINGSTON, J. H., LOURENCO, C. M., LYALL, E. G., LYNCH, S. A., LYONS, M. J., MAROM, D., MCCLURE, J. P., MCWILLIAM, R., MELANCON, S. B., MEWASINGH, L. D., MOUTARD, M. L., NISCHAL, K. K., OSTERGAARD, J. R., PRENDIVILLE, J., RASMUSSEN, M., ROGERS, R. C., ROLAND, D., ROSSER, E. M., ROSTASY, K., ROUBERTIE, A., SANCHIS, A., SCHIFFMANN, R., SCHOLL-BURGI, S., SEAL, S., SHALEV, S. A., CORCOLES, C. S., SINHA, G. P., SOLER, D., SPIEGEL, R., STEPHENSON, J. B., TACKE, U., TAN, T. Y., TILL, M., TOLMIE, J. L., et al. 2007. Clinical and molecular phenotype of Aicardi-Goutieres syndrome. *Am J Hum Genet,* 81**,** 713-25.

ROCKWOOD, K., FOX, R. A., STOLEE, P., ROBERTSON, D. & BEATTIE, B. L. 1994. Frailty in elderly people: an evolving concept. *CMAJ,* 150**,** 489-95.

ROCKWOOD, K., HOGAN, D. B. & MACKNIGHT, C. 2000. Conceptualisation and measurement of frailty in elderly people. *Drugs Aging,* 17**,** 295-302.

RYDBERG, B. & GAME, J. 2002. Excision of misincorporated ribonucleotides in DNA by RNase H (type 2) and FEN-1 in cell-free extracts. *Proc Natl Acad Sci U S A,* 99**,** 16654-9.

SAFARI, R., HOSEINIFAR, S. H. & KAVANDI, M. 2016. Modulation of antioxidant defense and immune response in zebra fish (Danio rerio) using dietary sodium propionate. *Fish Physiol Biochem,* 42**,** 1733-1739.

SAHIN, E. & DEPINHO, R. A. 2010. Linking functional decline of telomeres, mitochondria and stem cells during ageing. *Nature,* 464**,** 520-8.

SALVADOR MORENO, N., LIU, J., HAAS, K. M., PARKER, L. L., CHAKRABORTY, C., KRON, S. J., HODGES, K., MILLER, L. D., LANGEFELD, C., ROBINSON, P. J., LELIEVRE, S. A. & VIDI, P. A. 2019. The nuclear structural protein NuMA is a negative regulator of 53BP1 in DNA double-strand break repair. *Nucleic Acids Res,* 47**,** 2703-2715.

SANCHEZ-CONTRERAS, M. & KENNEDY, S. R. 2022. The Complicated Nature of Somatic mtDNA Mutations in Aging. *Front Aging,* 2.

SANTHAKUMAR, K., JUDSON, E. C., ELKS, P. M., MCKEE, S., ELWORTHY, S., VAN ROOIJEN, E., WALMSLEY, S. S., RENSHAW, S. A., CROSS, S. S. & VAN EEDEN,

F. J. M. 2012. A Zebrafish Model to Study and Therapeutically Manipulate Hypoxia Signaling in Tumorigenesis. *Cancer Research,* 72**,** 4017-4027.

SASSA, A., YASUI, M. & HONMA, M. 2019. Current perspectives on mechanisms of ribonucleotide incorporation and processing in mammalian DNA. *Genes Environ,* 41**,** 3.

SCHARER, O. D. 2013. Nucleotide excision repair in eukaryotes. *Cold Spring Harb Perspect Biol,* 5**,** a012609.

SCIALO, F., SRIRAM, A., FERNANDEZ-AYALA, D., GUBINA, N., LOHMUS, M., NELSON, G., LOGAN, A., COOPER, H. M., NAVAS, P., ENRIQUEZ, J. A., MURPHY, M. P. & SANZ, A. 2016. Mitochondrial ROS Produced via Reverse Electron Transport Extend Animal Lifespan. *Cell Metab,* 23**,** 725-34.

SELDIN, L., POULSON, N. D., FOOTE, H. P. & LECHLER, T. 2013. NuMA localization, stability, and function in spindle orientation involve 4.1 and Cdk1 interactions. *Mol Biol Cell,* 24**,** 3651-62.

SERDAR, C. C., CIHAN, M., YÜCEL, D. & SERDAR, M. A. 2021. Sample size, power and effect size revisited: simplified and practical approaches in pre-clinical, clinical and laboratory studies. *Biochem Med (Zagreb),* 31**,** 010502.

SHAH, R. & BALASUBRAMANIAM, S. 2021. Clinical Phenotype of FASTKD2 Mutation. *J Pediatr Neurosci,* 16**,** 319-322.

SHEN, R., LIU, D., WANG, X., GUO, Z., SUN, H., SONG, Y. & WANG, D. 2021. DNA Damage and Activation of cGAS/STING Pathway Induce Tumor Microenvironment Remodeling. *Front Cell Dev Biol,* 9**,** 828657.

SILK, A. D., HOLLAND, A. J. & CLEVELAND, D. W. 2009. Requirements for NuMA in maintenance and establishment of mammalian spindle poles. *J Cell Biol,* 184**,** 677-90.

SIMARRO, M., GIMENEZ-CASSINA, A., KEDERSHA, N., LAZARO, J. B., ADELMANT, G. O., MARTO, J. A., RHEE, K., TISDALE, S., DANIAL, N., BENARAFA, C., ORDUNA, A. & ANDERSON, P. 2010. Fast kinase domain-containing protein 3 is a mitochondrial protein essential for cellular respiration. *Biochem Biophys Res Commun,* 401**,** 440-6.

SINGH, A. P., SOSA, M. X., FANG, J., SHANMUKHAPPA, S. K., HUBAUD, A., FAWCETT, C. H., MOLIND, G. J., TSAI, T., CAPODIECI, P., WETZEL, K., SANCHEZ, E., WANG, G., COBLE, M., TANG, W., CADENA, S. M., FISHMAN, M. C. & GLASS, D. J. 2019. αKlotho Regulates Age-Associated Vascular Calcification and Lifespan in Zebrafish. *Cell Reports,* 28**,** 2767-2776.e5.

SMITH, J. T., NOREN HOOTEN, N., MODE, N. A., ZONDERMAN, A. B., EZIKE, N., KAUSHAL, S. & EVANS, M. K. 2023. Frailty, sex, and poverty are associated with DNA damage and repair in frail, middle-aged urban adults. *DNA Repair (Amst),* 129**,** 103530.

SMOLIŃSKA, K., SOBCZYŃSKI, J., SZOPA, A., WNOROWSKI, A., TOMASZEWSKA, E., MUSZYŃSKI, S., WINIARSKA-MIECZAN, A., CZERNECKI, T., BIELAK, A., DOBROWOLSKA, K., SMOLIŃSKI, K., KLEBANIUK, R. & DOBROWOLSKI, P. 2024. Innovative high fat diet establishes a novel zebrafish model for the study of visceral obesity. *Scientific Reports,* 14**,** 3012.

SPARKS, J. L., CHON, H., CERRITELLI, S. M., KUNKEL, T. A., JOHANSSON, E., CROUCH, R. J. & BURGERS, P. M. 2012. RNase H2-initiated ribonucleotide excision repair. *Mol Cell,* 47**,** 980-6.

STAINIER, D. Y. R., RAZ, E., LAWSON, N. D., EKKER, S. C., BURDINE, R. D., EISEN, J. S., INGHAM, P. W., SCHULTE-MERKER, S., YELON, D., WEINSTEIN, B. M., MULLINS, M. C., WILSON, S. W., RAMAKRISHNAN, L., AMACHER, S. L., NEUHAUSS, S. C. F., MENG, A., MOCHIZUKI, N., PANULA, P. & MOENS, C. B. 2017. Guidelines for morpholino use in zebrafish. *PLoS Genet,* 13**,** e1007000.

STAUDT, N., MÜLLER-SIENERTH, N., FANE-DREMUCHEVA, A., YUSAF, S. P., MILLRINE, D. & WRIGHT, G. J. 2015. A panel of recombinant monoclonal antibodies against zebrafish neural receptors and secreted proteins suitable for wholemount immunostaining. *Biochem Biophys Res Commun,* 456**,** 527-33.

STORCI, G., DE CAROLIS, S., PAPI, A., BACALINI, M. G., GENSOUS, N., MARASCO, E., TESEI, A., FABBRI, F., ARIENTI, C., ZANONI, M., SARNELLI, A., SANTI, S., OLIVIERI, F., MENSA, E., LATINI, S., FERRACIN, M., SALVIOLI, S., GARAGNANI, P., FRANCESCHI, C. & BONAFE, M. 2019. Genomic stability, anti-inflammatory phenotype, and up-regulation of the RNAseH2 in cells from centenarians. *Cell Death Differ,* 26**,** 1845-1858.

SUGAWARA, S., OKADA, R., LOO, T. M., TANAKA, H., MIYATA, K., CHIBA, M., KAWASAKI, H., KATOH, K., KAJI, S., MAEZAWA, Y., YOKOTE, K., NAKAYAMA, M., OSHIMA, M., NAGAO, K., OBUSE, C., NAGAYAMA, S., TAKUBO, K., NAKANISHI, A., KANEMAKI, M. T., HARA, E. & TAKAHASHI, A. 2022. RNaseH2A downregulation drives inflammatory gene expression via genomic DNA fragmentation in senescent and cancer cells. *Commun Biol,* 5**,** 1420.

SYKORA, P., CROTEAU, D. L., BOHR, V. A. & WILSON, D. M., 3RD 2011. Aprataxin localizes to mitochondria and preserves mitochondrial function. *Proc Natl Acad Sci U S A,* 108**,** 7437-42.

TAKANOHASHI, A., PRUST, M., WANG, J., GORDISH-DRESSMAN, H., BLOOM, M., RICE, G. I., SCHMIDT, J. L., CROW, Y. J., LEBON, P., KUIJPERS, T. W., NAGARAJU, K. & VANDERVER, A. 2013. Elevation of proinflammatory cytokines in patients with Aicardi-Goutieres syndrome. *Neurology,* 80**,** 997-1002.

THOMAS, R. C., ZAKSAUSKAITE, R., AL-KANDARI, N. Y., HYDE, A. C., ABUGABLE, A. A., EL-KHAMISY, S. F. & VAN EEDEN, F. J. 2024. Second generation lethality in RNAseH2a knockout zebrafish. *Nucleic Acids Res,* 52**,** 11014-11028.

THUMMEL, R., BURKET, C. T. & HYDE, D. R. 2006. Two different transgenes to study gene silencing and re-expression during zebrafish caudal fin and retinal regeneration. *ScientificWorldJournal,* 6 Suppl 1**,** 65-81.

THYME, S. B. & SCHIER, A. F. 2016. Polq-Mediated End Joining Is Essential for Surviving DNA Double-Strand Breaks during Early Zebrafish Development. *Cell Rep,* 15**,** 707-714.

TIAN, Q., TAUPIN, J., ELLEDGE, S., ROBERTSON, M. & ANDERSON, P. 1995. Fas-activated serine/threonine kinase (FAST) phosphorylates TIA-1 during Fas-mediated apoptosis. *J Exp Med,* 182**,** 865-74.

TOMKINSON, A. E., VIJAYAKUMAR, S., PASCAL, J. M. & ELLENBERGER, T. 2006. DNA ligases: structure, reaction mechanism, and function. *Chem Rev,* 106**,** 687-99.

TRIFUNOVIC, A., WREDENBERG, A., FALKENBERG, M., SPELBRINK, J. N., ROVIO, A. T., BRUDER, C. E., BOHLOOLY, Y. M., GIDLOF, S., OLDFORS, A., WIBOM, R., TORNELL, J., JACOBS, H. T. & LARSSON, N. G. 2004. Premature ageing in mice expressing defective mitochondrial DNA polymerase. *Nature,* 429**,** 417-23.

TSAI, S. B., TUCCI, V., UCHIYAMA, J., FABIAN, N. J., LIN, M. C., BAYLISS, P. E., NEUBERG, D. S., ZHDANOVA, I. V. & KISHI, S. 2007. Differential effects of

genotoxic stress on both concurrent body growth and gradual senescence in the adult zebrafish. *Aging Cell,* 6**,** 209-24.

TUMBALE, P., WILLIAMS, J. S., SCHELLENBERG, M. J., KUNKEL, T. A. & WILLIAMS, R. S. 2014. Aprataxin resolves adenylated RNA-DNA junctions to maintain genome integrity. *Nature,* 506**,** 111-5.

TUMBALE, P. P., JURKIW, T. J., SCHELLENBERG, M. J., RICCIO, A. A., O'BRIEN, P. J. & WILLIAMS, R. S. 2019. Two-tiered enforcement of high-fidelity DNA ligation. *Nat Commun,* 10**,** 5431.

UEHARA, R., CERRITELLI, S. M., HASIN, N., SAKHUJA, K., LONDON, M., IRANZO, J., CHON, H., GRINBERG, A. & CROUCH, R. J. 2018. Two RNase H2 Mutants with Differential rNMP Processing Activity Reveal a Threshold of Ribonucleotide Tolerance for Embryonic Development. *Cell Rep,* 25**,** 1135-1145 e5.

VALDIGLESIAS, V., SANCHEZ-FLORES, M., MARCOS-PEREZ, D., LORENZO-LOPEZ, L., MASEDA, A., MILLAN-CALENTI, J. C., PASARO, E. & LAFFON, B. 2019. Exploring Genetic Outcomes as Frailty Biomarkers. *J Gerontol A Biol Sci Med Sci,* 74**,** 168-175.

VELDMAN, M. B. & LIN, S. 2008. Zebrafish as a developmental model organism for pediatric research. *Pediatr Res,* 64**,** 470-6.

WANG, W., MANI, A. M. & WU, Z. H. 2017. DNA damage-induced nuclear factor-kappa B activation and its roles in cancer progression. *J Cancer Metastasis Treat,* 3**,** 45-59.

WATT, D. L., JOHANSSON, E., BURGERS, P. M. & KUNKEL, T. A. 2011. Replication of ribonucleotide-containing DNA templates by yeast replicative polymerases. *DNA Repair (Amst),* 10**,** 897-902.

WEI, H. & YU, X. 2016. Functions of PARylation in DNA Damage Repair Pathways. *Genomics Proteomics Bioinformatics,* 14**,** 131-139.

WEI, X., DU, M., LI, D., WEN, S., XIE, J., LI, Y., CHEN, A., ZHANG, K., XU, P., JIA, M., WEN, C., ZHOU, H., LYU, J., YANG, Y. & FANG, H. 2020. Mutations in FASTKD2 are associated with mitochondrial disease with multi-OXPHOS deficiency. *Hum Mutat,* 41**,** 961-972.

WEINREB, J. T., GHAZALE, N., PRADHAN, K., GUPTA, V., POTTS, K. S., TRICOMI, B., DANIELS, N. J., PADGETT, R. A., DE OLIVEIRA, S., VERMA, A. & BOWMAN, T. V. 2021. Excessive R-loops trigger an inflammatory cascade leading to increased HSPC production. *Dev Cell,* 56**,** 627-640 e5.

WEYEMI, U., PAUL, B. D., BHATTACHARYA, D., MALLA, A. P., BOUFRAQECH, M., HARRAZ, M. M., BONNER, W. M. & SNYDER, S. H. 2019. Histone H2AX promotes neuronal health by controlling mitochondrial homeostasis. *Proc Natl Acad Sci U S A,* 116**,** 7471-7476.

WHITE, A. T. & SCHENK, S. 2012. NAD(+)/NADH and skeletal muscle mitochondrial adaptations to exercise. *Am J Physiol Endocrinol Metab,* 303**,** E308-21.

WILLIAMS, J. S., CLAUSEN, A. R., NICK MCELHINNY, S. A., WATTS, B. E., JOHANSSON, E. & KUNKEL, T. A. 2012. Proofreading of ribonucleotides inserted into DNA by yeast DNA polymerase varepsilon. *DNA Repair (Amst),* 11**,** 649-56.

WILLIAMS, J. S., GEHLE, D. B. & KUNKEL, T. A. 2017. The role of RNase H2 in processing ribonucleotides incorporated during DNA replication. *DNA Repair (Amst),* 53**,** 52-58.

WILLIAMS, J. S. & KUNKEL, T. A. 2014. Ribonucleotides in DNA: origins, repair and consequences. *DNA Repair (Amst),* 19**,** 27-37.

WILLIAMS, J. S., LUJAN, S. A. & KUNKEL, T. A. 2016. Processing ribonucleotides incorporated during eukaryotic DNA replication. *Nat Rev Mol Cell Biol,* 17**,** 350-63.

WILLIAMS, J. S., SMITH, D. J., MARJAVAARA, L., LUJAN, S. A., CHABES, A. & KUNKEL, T. A. 2013. Topoisomerase 1-mediated removal of ribonucleotides from nascent leading-strand DNA. *Mol Cell,* 49**,** 1010-5.

WORLD HEALTH ORGANISATION. 2024. *Ageing and health* [Online]. Available: https://www.who.int/news-room/fact-sheets/detail/ageing-and-health [Accessed].

WRIGHTON, P. J., SHWARTZ, A., HEO, J. M., QUENZER, E. D., LABELLA, K. A., HARPER, J. W. & GOESSLING, W. 2021. Quantitative intravital imaging in zebrafish reveals in vivo dynamics of physiological-stress-induced mitophagy. *J Cell Sci,* 134.

WU, T., MAO, L., CHEN, C., YIN, F. & PENG, J. 2022. A novel homozygous missense mutation in the FASTKD2 gene leads to Lennox-Gastaut syndrome. *J Hum Genet,* 67**,** 589-594.

XIAO, G., LI, X., YANG, H., ZHANG, R., HUANG, J., TIAN, Y., NIE, M. & SUN, X. 2024. mTOR mutation disrupts larval zebrafish tail fin regeneration via regulating proliferation of blastema cells and mitochondrial functions. *J Orthop Surg Res,* 19**,** 321.

YANG, C. H., LAMBIE, E. J. & SNYDER, M. 1992. NuMA: an unusually long coiled-coil related protein in the mammalian nucleus. *J Cell Biol,* 116**,** 1303-17.

YANG, W. & HEKIMI, S. 2010. A Mitochondrial Superoxide Signal Triggers Increased Longevity in Caenorhabditis elegans. *PLOS Biology,* 8**,** e1000556.

YEUNG, K. T., DAS, S., ZHANG, J., LOMNICZI, A., OJEDA, S. R., XU, C. F., NEUBERT, T. A. & SAMUELS, H. H. 2011. A novel transcription complex that selectively modulates apoptosis of breast cancer cells through regulation of FASTKD2. *Mol Cell Biol,* 31**,** 2287-98.

YIN, J.-H. & HORZMANN, K. A. 2024. The influence of sex and age differences in an adult zebrafish () T-maze model of cognition. *Journal of Fish Biology,* n/a.

YOUSEFZADEH, M., HENPITA, C., VYAS, R., SOTO-PALMA, C., ROBBINS, P. & NIEDERNHOFER, L. 2021. DNA damage-how and why we age? *Elife,* 10.

YOUSEFZADEH, M. J., ZHAO, J., BUKATA, C., WADE, E. A., MCGOWAN, S. J., ANGELINI, L. A., BANK, M. P., GURKAR, A. U., MCGUCKIAN, C. A., CALUBAG, M. F., KATO, J. I., BURD, C. E., ROBBINS, P. D. & NIEDERNHOFER, L. J. 2020. Tissue specificity of senescent cell accumulation during physiologic and accelerated aging of mice. *Aging Cell,* 19**,** e13094.

YU, L., TUCCI, V., KISHI, S. & ZHDANOVA, I. V. 2006. Cognitive aging in zebrafish. *PLoS One,* 1**,** e14.

YUAN, R., PETERS, L. L. & PAIGEN, B. 2011. Mice as a mammalian model for research on the genetics of aging. *Ilar j,* 52**,** 4-15.

ZAKSAUSKAITE, R., THOMAS, R. C., VAN EEDEN, F. & EL-KHAMISY, S. F. 2021. Tdp1 protects from topoisomerase 1-mediated chromosomal breaks in adult zebrafish but is dispensable during larval development. *Sci Adv,* 7.

ZHANG, L., CHEN, C., FU, J., LILLEY, B., BERLINICKE, C., HANSEN, B., DING, D., WANG, G., WANG, T., SHOU, D., YE, Y., MULLIGAN, T., EMMERICH, K., SAXENA, M. T., HALL, K. R., SHARROCK, A. V., BRANDON, C., PARK, H., KAM, T. I., DAWSON, V. L., DAWSON, T. M., SHIM, J. S., HANES, J., JI, H., LIU, J. O., QIAN, J., ACKERLEY, D. F., ROHRER, B., ZACK, D. J. & MUMM, J. S. 2021. Large-scale phenotypic drug screen identifies neuroprotectants in zebrafish and mouse models of retinitis pigmentosa. *Elife,* 10.

ZHDANOVA, I. V., YU, L., LOPEZ-PATINO, M., SHANG, E., KISHI, S. & GUELIN, E. 2008. Aging of the circadian system in zebrafish and the effects of melatonin on sleep and cognitive performance. *Brain Res Bull,* 75**,** 433-41.

ZHENG, J., CROTEAU, D. L., BOHR, V. A. & AKBARI, M. 2019. Diminished OPA1 expression and impaired mitochondrial morphology and homeostasis in Aprataxin-deficient cells. *Nucleic Acids Res,* 47**,** 4086-4110.

ZHENG, L. & SHEN, B. 2011. Okazaki fragment maturation: nucleases take centre stage. *J Mol Cell Biol,* 3**,** 23-30.

ZHENG, Z., WAN, Q., MEIXIONG, G. & DU, Q. 2014. Cell cycle-regulated membrane binding of NuMA contributes to efficient anaphase chromosome separation. *Mol Biol Cell,* 25**,** 606-19.

ZHU, J., WEN, W., ZHENG, Z., SHANG, Y., WEI, Z., XIAO, Z., PAN, Z., DU, Q., WANG, W. & ZHANG, M. 2011. LGN/mInsc and LGN/NuMA complex structures suggest distinct functions in asymmetric cell division for the Par3/mInsc/LGN and Galphai/LGN/NuMA pathways. *Mol Cell,* 43**,** 418-31.

ZIADA, A. S., SMITH, M. R. & COTE, H. C. F. 2020. Updating the Free Radical Theory of Aging. *Front Cell Dev Biol,* 8**,** 575645.

ZIMMERMANN, M., MURINA, O., REIJNS, M. A. M., AGATHANGGELOU, A., CHALLIS, R., TARNAUSKAITE, Z., MUIR, M., FLUTEAU, A., AREGGER, M., MCEWAN, A., YUAN, W., CLARKE, M., LAMBROS, M. B., PANEESHA, S., MOSS, P., CHANDRASHEKHAR, M., ANGERS, S., MOFFAT, J., BRUNTON, V. G., HART, T., DE BONO, J., STANKOVIC, T., JACKSON, A. P. & DUROCHER, D. 2018. CRISPR screens identify genomic ribonucleotides as a source of PARP-trapping lesions. *Nature,* 559**,** 285-289.

Chapter 9 Appendix

Appendix 9.1: Scripts for alkaline gel plot

Python script for ladder size

```
import pandas as pd

ladder3 = pd.read_excel(r"file name.xlsx", sheet_name = "Ladder")

ladder4 = ladder3.values.tolist()

#print(ladder4)

ladder_list = []

for sublist in ladder4:
    for item in sublist:
        ladder_list.append(item)

#print(ladder_list)

# Identifying the index nr of the peak numbers.

list_of_peak_index = []
list_index = -1 # start at -1 becasue the if statement is for the number after the peak
```

```
zero_switch = 0
temp = 0

for nr in ladder_list:
    if nr > temp or (nr < 21000 and nr < temp): # Change the nr according to what your
    #lowest peak is that is higher than the baseline
        zero_switch = 0
    if nr > 21000 and nr < temp and zero_switch == 0: # This number is the same as above
        list_of_peak_index.append(list_index)
        zero_switch = 1
    temp = nr
    list_index = list_index + 1

#print(list_of_peak_index)

# If two of your peaks are very close, it might mean that there are two peak intensities
# close together. Go your your list, find the highest value. Delete the other.

#del list_of_peak_index[0]

print(list_of_peak_index)
```

R script for plotting

```
library(tidyverse)
library(ggpubr)
library(cowplot)
library(readxl)
library(XLConnect)

## Data import ----

gel_val <- read_excel("file name.xlsx", sheet = "Dat2")
blank <- read_excel("file name.xlsx", sheet = "Blank")

## Looking at data ----

str(gel_val)
str(blank)

## Plotting the data ----

ggplot(gel_val, aes(x = Distance, y = Value, colour = Type))+
  geom_point()+
  theme_bw()

## Calculating blank ----

mean_blank <- mean(blank$Value)
```

```
mean_blank


## Subtracting blank from data ----


gel_val$Blanked <- apply(gel_val[c("Value")], 1, function(x))


str(gel_val)


## Summarizing data ----


sumData <- gel_val %>%
  group_by(Distance, Treatment, Type) %>%
  summarise(
    mean_Value = mean(Value, na.rm = TRUE),
    sd_Value = sd(Value, na.rm = TRUE),
    se_Value = sd(Value, na.rm = TRUE)/sqrt(sum(!is.na(Value))),
    mean_Blanked = mean(Blanked, na.rm = TRUE),
    sd_Blanked = sd(Blanked, na.rm = TRUE),
    se_Blanked = sd(Blanked, na.rm = TRUE)/sqrt(sum(!is.na(Blanked)))
  )


sumData


## PLOTTING DATA ----


## Plotting summery data with blanking ----
# Y axis removed for final figure
```

```
f1 <- ggplot(sumData[(sumData$mean_Blanked>0),], aes(x = Distance, y = mean_Blanked, colour = Type))+
  geom_smooth(aes(group = Type), span = 0.1, size = 1.1, se = FALSE)+
  facet_wrap(Treatment ~., scales = "free_y", nrow = 2)+
  ylab("Intensity")+
  xlab("Size (bp)")+
  scale_x_continuous(limits=c(0, 460),
                     breaks = c(85, 119, 175, 213, 266, 301, 343, 390, 452, 527), # Your python list. Need to be same
                     #number of numbers as ladder labels
                     labels = c("10k", "8k", "6k", "5k", "4k", "3k", "3k", "2k", "1.5k", "1k"))+ # Thermo scientific ladder
                     scale_colour_manual(values = c("type1" = "colour1",
                                                    "type2" = "colour2"))+
                      theme_minimal()+
                      theme(legend.position = "bottom")+
                      theme(strip.text.x = element_text(size = 12, colour = "black", face = "bold"))+
                      theme(panel.grid.major.x = element_blank())+
                      theme(panel.grid.minor.x = element_blank())+
                      theme(panel.grid.major.y = element_blank())+
                      theme(panel.grid.minor.y = element_line())


                     f1
```

Appendix 9.2: Human and zebrafish NuMA protein comparison.

Comparison of human, mouse, chicken, tropical clawed frog, zebrafish, coelacanth and spotted gar NuMA protein. Comparison performed using EMBL-EBI clustal omega multiple sequence alignment. Stars indicate same amino acid. Two dots and one dot indicate similar amino acids. Red amino are small hydrophobic amino acids, blue are acidic amino acids, magenta are basic amino acids and green are hydroxyls, sulfhydryl and amine amino acids (Madeira et al., 2024). N-terminus and C-terminus marked with blue and orange.

```
CLUSTAL O(1.2.4) multiple sequence alignment


Zebrafish_NuMA                  ------------------------------------------------------------       0
Spotted_gar_NuMA                ------------------------------------------------------------       0
Chicken_NuMA                    MLGPPSPIAERRLLLPGDSKVPGAGRWLLQEGRGDGWWGRKGAAPHGQQPRVAPALPSLR       60
Human_NuMA                      ------------------------------------------------------------       0
Mouse_NuMA                      ------------------------------------------------------------       0
Tropical_Clawed_Frog_NuMA       ------------------------------------------------------------       0
Coelacanth_NuMA                 ------------------------------------------------------------       0


Zebrafish_NuMA                  ------------------------------------------------------------       0
Spotted_gar_NuMA                ------------------------------------------------------------       0
Chicken_NuMA                    RAVPDVGLLKQQGKEGGGGGESWGVPWPCEGQTPPDGPPGFGSSWGRSPLLAVPGGKDGD       120
Human_NuMA                      ------------------------------------------------------------       0
Mouse_NuMA                      ------------------------------------------------------------       0
Tropical_Clawed_Frog_NuMA       ------------------------------------------------------------       0
Coelacanth_NuMA                 ------------------------------------------------------------       0


Zebrafish_NuMA                  ------------------------------------------------------------       0
Spotted_gar_NuMA                ------------------------------------------------------------       0
Chicken_NuMA                    LVRTARRPGTAALGSVSPLLPPSPRECRSPNYNRCSVPCAAGRAVPPWGWERRAVGTGGH       180
Human_NuMA                      ------------------------------------------------------------       0
Mouse_NuMA                      ------------------------------------------------------------       0
Tropical_Clawed_Frog_NuMA       ------------------------------------------------------------       0
Coelacanth_NuMA                 ------------------------------------------------------------       0
                                                                                  N-term

Zebrafish_NuMA                  ---------------------------------MKFNKNKAGPLLTWMNSVF-PENQIW       25
Spotted_gar_NuMA                ------------------------------------------------------------       0
Chicken_NuMA                    PPPSPSTPPGFSLPQNEDVGCSPRSGCYPGSLAEMPLHTTRAAALLAWVNSTKACAEPLG       240
Human_NuMA                      ---------------------------------MTLHATRGAALLSWVNSLH-VADPVE       25
Mouse_NuMA                      ---------------------------------MTLHATRAATLLSWVNSLH-VADPVE       25
Tropical_Clawed_Frog_NuMA       ---------------------------------MAAHSGKMEALLCWVNSLK-VGEPIE       25
Coelacanth_NuMA                 --------------------------YNQEKKMSLNTTKATALIAWVNSLH-VAEPIV       31


Zebrafish_NuMA                  EFGHMRDGFRLLEICFKLKGREDVE-AYKTLSLYNKLEIIFNDLHDDF-HLTDRQRFLIL       83
Spotted_gar_NuMA                ------------------------------------------------------------       0
Chicken_NuMA                    DLSQLQDCRVFIQIINKIHRT-EEGESVLEQSLAERAAFICGFLQKLCKHKSATENLVSA       299
Human_NuMA                      AVLQLQDCSIFIKIIDRIHGT-EEGQQILKQPVSERLDFVCSFLQKNRKHPSSPECLVSA       84
Mouse_NuMA                      TVLQLQDCSIFIKIINTIHDT-KEGQQILQQPLPERLDFVCSFLQKNRKHPSSTQCLVSV       84
Tropical_Clawed_Frog_NuMA       RFSQLQDLGILLKVVGILSGNSEETALVLQQIPEERLNFLCAFLQRYCRPGSSAENLVQW       85
Coelacanth_NuMA                 KLTQLQDCTIFIKIIGKVNRNESIGSDVLEASLQEKLQFLSNFLQFKCRYNPASGGLVSW       91


Zebrafish_NuMA                  GKISEGLDLELQLAKVALLLCYCSFKKT-N---PVALNSRTESDITFMFRFVRDDASGLC       139
Spotted_gar_NuMA                --------------------------MCTSLQGFENLNYKTQAELASVLRFVLDNEDSLS       34
Chicken_NuMA                    QKLLEGEEL--ELAKVAVLLLYHSSMSSKSPRDWNEFDYQIQVELATILKFVLDHEESLS       357
Human_NuMA                      QKVLEGSEL--ELAKMTMLLLYHSTMSSKSPRDWEQFEYKIQAELAVILKFVLDHEDGLN       142
Mouse_NuMA                      QKVIEGSEM--ELAKMIMLFLYQSTMSSRNLRDWEQFEYGVQAELAVILKFMLDHEESLN       142
Tropical_Clawed_Frog_NuMA       QKILQGENLEVELSKAIVLLFYYSTMSSKNPKKSEDFDHKTQTELASILRFVLDNEDALC       145
Coelacanth_NuMA                 QNILQGENLEIELSKVTVLLLYLSTISYCQLKECEGLEYNTQTELASILRFVLDNENELC       151
                                                          .      ::   : ::: :::*: *. . *


Zebrafish_NuMA                  LDEGLDQFLDQDSVMNLANSSSGSSCSSPFYIDEESPMFGRFQRPPRVQFQELCTVASSS       199
Spotted_gar_NuMA                LNDNLENFLKRKVKFALSSVSSLSSIS-----DEDSPVF-TRKRKPEVQFVDLQTVASSS       88
Chicken_NuMA                    --ENLEVFLQRRAPLSSPGT-SSSSSE-----E--RSP---GLSHPQVRFLELQKIASSS       404
Human_NuMA                      LNEDLENFLQKAP-VPSTCS-ST-FPE-----E--LSPP-SHQAKREIRFLELQKVASSS       191
```

```
Mouse_NuMA                    LTEDLESFLEKVP-Y--THA-ST-LSE-----E--LSPP-SHQTKRKIRFLEIQRIASSS      189
Tropical_Clawed_Frog_NuMA     LDDKLINFLQRKARFPSLGD-DTSSCS-----DAASPNV-SHRRKSEVRFLELHRVASSS      198
Coelacanth_NuMA               LSN-LEQFLQKQGVFSSTSS-I---IS-----EEG--SP-VFRRKPIVRFLDLHRIASNS      198
                                : *  **.:              .     :             ::* ::  :**.*

Zebrafish_NuMA                ----------DSSPMQDLMSTPHFQLKKLRKELAHEGDVRDELEKELADHISIISEKEG      248
Spotted_gar_NuMA              ----------VSSPIQDILKTPQFQLRKLRKQLAEERNMRDELELELANSNKIITERET      137
Chicken_NuMA                  SSMNNML-PGTPASPVGDVLQTPQFQLRRLKKQLAIERENRDELEMELAENRKLITEKEA      463
Human_NuMA                    -SGNNFL-SGSPASPMGDILQTPQFQMRRLKKQLADERSNRDELELELAENRKLLTEKDA      249
Mouse_NuMA                    -SENNFL-SGSPSSPMGDILQTPQFQMRRLKKQLADERSNRDDLELELSESLKLLTEKDA      247
Tropical_Clawed_Frog_NuMA     -TMKSLS-ADPPSSPMIEVLHTPQFQMRRLKKQLSEVRDCRDELEVELAENRKHLAEKEA      256
Coelacanth_NuMA               -SMNNYLPSPSPSSPIRDVLQTPQFQMRRLRKQLADERALRDELDQELAENRRLLAEKDT      257
                                          :**: ::: **:**:::*:*:*:     **:*: **::    ::*::

Zebrafish_NuMA                LISQLQHRVERMLREQGEL--EKDHKAALLELQEKNESLLHRVHEVLKQCQDLKTDNSQK      306
Spotted_gar_NuMA              QLSLLQQRVQRLMRQSNEQ---SQESNELEDLRIKNESLLKRLQDILKQCQDLKTNKGQM      194
Chicken_NuMA                  QITMMQHRIDRLALLNEKQAADQLEPREMEELRERNESLLVRLHEALKQCQDLKTEKGQM      523
Human_NuMA                    QIAMMQQRIDRLALLNEKQAASPLEPKELEELRDKNESLTMRLHETLKQCQDLKTEKSQM      309
Mouse_NuMA                    QIAMMQQRIDHLALLNEKQAASSQEPSELEELRGKNESLTVRLHETLKQCQNLKTEKSQM      307
Tropical_Clawed_Frog_NuMA     QISLLQQQIEHLRILRENQA-ELQEPKELEELREKNESLMIRLRDTLKQCQDMKTDKKQL      315
Coelacanth_NuMA               QILEMQQRIGRLVILSEKQA-NQVELKELEELQNKNESLSAKLHSTLKQCQDLKTSQTQM      316
                               :  :*::: ::     :      .   : :*: :****  :::. *****::**.: *

Zebrafish_NuMA                EKKIDELTEENGTLSAQLRNVFSQLARAEQEVAKLTVVHESAQTEWKNRKELLEKELNEA      366
Spotted_gar_NuMA              ERKIDQLTEENGNLSFQMRDVLDRLTKAQAAVDKLSDEQEISVKEWESRRVSLESELNQA      254
Chicken_NuMA                  DRKINQLSEENGDLSFKLREIASHLVQLQDALNELSEEHNSALMQSQAKQAQLEGELRAV      583
Human_NuMA                    DRKINQLSEENGDLSFKLREFASHLQQLQDALNELTEEHSKATQEWLEKQAQLEKELSAA      369
Mouse_NuMA                    DRKISQLSEENGDLSFKVREFANHLQQLQGAFNDLIEEHSKASQEWAEKQARLENELSTA      367
Tropical_Clawed_Frog_NuMA     ERKNDQLAEENGELSYKVRDLSNRLAQLQEALYETTEEHELSLSNWEQKQSQLESELSGA      375
Coelacanth_NuMA               QRKIDTLTEENGELSLKERDFASRLKQSEKDLKELTEEYREILRDWESKEAQLNAEVNAS      376
                              ::* . *:**** ** : *:. .:* : :  . .          :   :.  *: *:

Zebrafish_NuMA                VTHKECLSEQVLILQGKISVLEDELKKAQS---QERGEVLGPIMEWEKLKQELADLTLQL      423
Spotted_gar_NuMA              IANKEDLSEQILILQGKISLLEDQLSKAQSQ-HREEGEVMGDVLKMESLRQEVADLAVKV      313
Chicken_NuMA                  LQEKKCLEEKVEILQGKISLLEDQLVKLGDCSTQEKGEVMGDVLKLEELKQEVSSLTTKG      643
Human_NuMA                    LQDKKCLEEKNEILQGKLSQLEEHLSQLQDNPPQEKGEVLGDVLQLETLKQEAATLAANN      429
Mouse_NuMA                    LQDKKCLEEKNEILQGKLSQLEDQATRLQESPAPEKGEVLGDALQLDTLKQEAAKLATDN      427
Tropical_Clawed_Frog_NuMA     VGEKKYLEEHHLILQGKISMLEDQLKKMGEREVEEKGDCMGDILKLEDLKQEVTALSTQC      435
Coelacanth_NuMA               LSAKKCLEEKIQILEGKISVLEDQLEKAREA-SPVKGEVMGDILQLEALKHEVAELAIKV      435
                              :  *: *.*:  **:**:* **:.  :  .     .*: :*  :: : *::* : *: .

Zebrafish_NuMA                AQLQESISHLEKKKAEVEALLAEERCSFEKETARLQLVVFDLEKSINSIRLERETLQEAL      483
Spotted_gar_NuMA              SQLEDVIARLEEEKSQTQMELNTERIKFENEKSHLDGVISGLQQTLSDLKCEKETLERTS      373
Chicken_NuMA                  IELQASVLRLEEEKSQRDAALQAERNRFEMEKLQLGTHISNLQSSVSELHLAKEKLEQEL      703
Human_NuMA                    TQLQARVEMLETERGQQEAKLLAERGHFEEEKQQLSSLITDLQSSISNLSQAKEELEQAS      489
Mouse_NuMA                    TQLQTRVETLECERGKQEAQLLAERSRFEDEKQQLASLIADLQSSVSNLSQAKEELEQAS      487
Tropical_Clawed_Frog_NuMA     LSLTEQIHQLEEEKSTTEIDMEAQRSRFESEKSQLQEIVTNLQTSLSEITFQKERQDNEA      495
Coelacanth_NuMA               NELQSVIKQLEEEKASLQTELDTERAKFAAEHSQATNLIASLQASISEINSQKRSLEQAA      495
                               .*   :  ** ::.  :  :  :*  *  *  :    : .*: ::..:   :.  :.

Zebrafish_NuMA                KTQKEMLSAQISALERDVSRLQQVEVQLTAEIKISADLRQQREELEGKVASL----DRMV      539
Spotted_gar_NuMA              RERQEQLTNQIETLNMEIAKLSDIVHQRELEVKEM---EK-----------------QE      412
Chicken_NuMA                  RAQEARLTAQADALTAEVGKLSGFLQQQEKEAAEL---RMQAEQERAQAEELRH----RD      756
Human_NuMA                    QAHGARLTAQVASLTSELTTLNATIQQQDQELAGL---KQQAKEKQAQLAQTLQ------      540
Mouse_NuMA                    QAQGAQLTAQLTSM----TGLNATLQQRDQELASL---KEQAKKEQAQMLQTMQ------      534
Tropical_Clawed_Frog_NuMA     RAQQEHLTCQITTLKLEISKLKSSLVHKEEELKGI---HHQVEEEKREKNQLLENFKILE      552
Coelacanth_NuMA               RAQEEQLTAQIATLHSEISKLNAFLVQKDHELVNL---QHKAEEEKKHKTQLTEDLQTQE      552
                              : :   *: *  ::      *.    :   *       .

Zebrafish_NuMA                HSLHAEIQGLEVERASQQDAINSLISDLQIARA----TVQEYEKKL-----------EEH      584
Spotted_gar_NuMA              QAARETIDGLNKQVD-------DLGDALRLKEEEAVSNAQQWNLERQESSRRENSLQEAS      465
Chicken_NuMA                  MASQEALGELSRRVE-------QLGASLKHSEEELVRVTQEAEGKA-------RQLGAEH      802
Human_NuMA                    -QQEQASQGLRHQVE-------QLSSSLKQKEQQLKEVAEKQEATRQDHAQQLATAAEER      592
Mouse_NuMA                    -EQEQAAQGLRQQVE-------QLSSSLKLKEQQLEEAAKEQEATRQDHAQQLAIVAEAR      586
Tropical_Clawed_Frog_NuMA     ESSKQNIQELVNQVE-------QISSSLKVSEGNLVGLTQQLESK----AKEVDYLREEQ      601
Coelacanth_NuMA               LSARKTIQDLKFQVE-------ELDTALKHKDDSLSQFKQELEAERENEARQIAALKDAR      605
                                 .     *  .          .:   *:          :: :

Zebrafish_NuMA                QKVVAENNSLKN-----------EACTMQQELNNHLKAIGDLQAEVNELRFEKTEEENKV      633
Spotted_gar_NuMA              VTAARERDAALAEYHHFQKAKEEEIEQLGQQILTLEDHQRTHQSLISELREEKQVLEVKV      525
Chicken_NuMA                  EKAVQERDAALQQLQHLQQAKEKQLAALSSQLQSLEAAS---KASSMEMQQEKAELNQKV      859
Human_NuMA                    EASLRERDAALKQLEALEKEKAAKLEILQQQLQVANEARDSAQTSVTQAQREKAELSRKV      652
Mouse_NuMA                    EASLRERDTARQQLETVEKEKDAKLESLQQQLQAANDARDNAQTSVTQAQQEKAELSQKI      646
Tropical_Clawed_Frog_NuMA     QKVACERDSTLSTFNEYKCKKDEEFSVLNMTMKTLEQDHQASLSVIEELKREKAELASKL      661
Coelacanth_NuMA               ETAVGERDSISLQYAEFKKENERLFCALNQKIQTLEETRVAEQAATTELRNEKDELITKV      665
                                   *.::                 :   :          :   : : **     *:
```

```
Zebrafish_NuMA                SEALVKIESLQTEILHLCEKISLKDEEIRNLTKEYESVDNELKLVKEQNVEINAMIKSNR      693
Spotted_gar_NuMA              AALEAAV----TELRSKCQSLEFENEA-------------------------------ER      550
Chicken_NuMA                  QELQARV----LELSAQCQQSSA-----------------------------------      878
Human_NuMA                    EELQACV----ETAR-------------------------------------------      663
Mouse_NuMA                    GELHACI----EASH-------------------------------------------      657
Tropical_Clawed_Frog_NuMA     QELDATI----LDLLAKCQNLDSENAS-------------------------------QS      686
Coelacanth_NuMA               QELNDAI----LELSS--------NKK-------------------------------QD      682
                                    :

Zebrafish_NuMA                KEHEETVEKLQQELHCAASAASEKQEQMLVLSAEVTSLKEQICRYSENEAQKQQELSILE      753
Spotted_gar_NuMA              SSHIQTVESLTTRL---------------------QDTERTLHDYKG----KLAHQSSIA      585
Chicken_NuMA                  --QAGSAETLRAQL---------------------RELEGKLKDSQQ----KLADKEKVA      911
Human_NuMA                    ----QEQHEAQAQV---------------------AELELQLRSEQQ----KATEKERVA      694
Mouse_NuMA                    ----QEQRQVQARV---------------------TELEAQLKAEQQ----KTTEREKVV      688
Tropical_Clawed_Frog_NuMA     KSHAAAVESLKAQL---------------------SEQESQLKIYQK----KVSSCELVS      721
Coelacanth_NuMA               LAHLQVVEIMKREL---------------------QESEEKLKQYEQ----KLVDLNVVN      717
                                    .    .:                      . :  :   .     *    . :

Zebrafish_NuMA                AQHNVLKENLTSLQNQLAEATTSASQKESEFILLQQELSHQETLREQTQELEKIKREELE      813
Spotted_gar_NuMA              EENNKLHHQLAALEE--------------------------TVVNLRAELEAERKRFEE      618
Chicken_NuMA                  KENTRLQERLLFLEE--------------------------SVRNTEGILEDEKRRAAE      944
Human_NuMA                    QEKDQLQEQLQALKE--------------------------SLKVTKGSLEEEKRRAAD      727
Mouse_NuMA                    QEKAQLQEQLRALEE--------------------------SLKITKGSLEEEKRRAAD      721
Tropical_Clawed_Frog_NuMA     EENSQLKEQLLSMDE--------------------------SLRHLREHLEKEKMKFAA      754
Coelacanth_NuMA               QENMGLKEQLSAMEQ--------------------------QIRKLQGTLDVEKRRFLE      750
                               ::  *:..*  :.:                          :      *:  : .

Zebrafish_NuMA                GIVSELQAKIIEVSSIASEREACVSSLQYEMKDQLSKAK---------------------      852
Spotted_gar_NuMA              TRVTD--------------LQRISQMGEEVQDLASKNQRMSAELELVQKELLKEKQGKL      663
Chicken_NuMA                  SLEGN--------------LARIAELEAEKQQLVQRGEQAL-------QQHSEELARRQ      982
Human_NuMA                    ALEEQ--------------QRCISELKAETRSLVEQHKRER-------KELEEERAGRK      765
Mouse_NuMA                    ALKEQ--------------QCRATEMEAESRSLMEQREREQ-------KELEQEKAGRK      759
Tropical_Clawed_Frog_NuMA     SLDSD--------------GKRISHLEEEMKKLSESRDAAL-------SNLAEERAAGQ      792
Coelacanth_NuMA               THEET--------------NKKIAHMEEEIKKQVELKDKAL-------LDFKREADNWA      788
                                                 : :  * :.  .  .

Zebrafish_NuMA                QCEA---DLRNEMKEKVGNLQELLDAANHGIAEKEHHLESLNQSLKQMELLYCQKEEEII      909
Spotted_gar_NuMA              TAESSLENLREEGIVVTTKLTTERDQAYFVIKEKEQAIQKLNSEVGALEGKLALTEETKI      723
Chicken_NuMA                  ALETRLQQVAEERREETAALQRQLAEVAKGEEGERGRLEKRLQE----------------      1026
Human_NuMA                    GLEARLQQLGEAHQAETEVLRRELAEAMAAQHTAESECEQLVKEVAAWRERYEDSQQEEA      825
Mouse_NuMA                    GLEARIQQLEEAHQAETEALRHELAEATASQHRAESECERLIREVESRQKRFEARQQEEA      819
Tropical_Clawed_Frog_NuMA     KIESQLKHLQEEYHTANETLQAKMAESSAAIKQREAERDELSKVVDIWKAKYEESQQKIV      852
Coelacanth_NuMA               QLEGQLKQLAEENLHKFQKLQCELSSAVSAIKEKEEEREKLCGEIALWKQQYEAVHSSED      848
                                *    .: :        *              .   :

Zebrafish_NuMA                AS-QQAKQQLENNIAEQKQQLDEIQQNREILRNERDHLS---------------------      947
Spotted_gar_NuMA              QELAAKKEEIERLISKTEQSLLELETVKKAKENADVHLQSTIEEHQNQLSTLSQELNDVR      783
Chicken_NuMA                  -----------LSREHGQACQRLQAEQERVAELEARVARMASEQQEQLAALQDQLARAK      1074
Human_NuMA                    QYGAMFQEQLMTLKEECEKARQELQEAKEKVAGIESHSELQISRQQNELAELHANLARAL      885
Mouse_NuMA                    RYGAMFQEQLMALKGEKTGQ--EVQ-----EEAVEIHSEGQPGQQQSQLAQLHASLAKAI      872
Tropical_Clawed_Frog_NuMA     QNSCQMEEQIQHLKKAHTDVCQQLEGEKSKVLMLEAKIKETNSSQLEQINRLECELSEAY      912
Coelacanth_NuMA               KKCSQMEAVICKLKEDHEVVSGQLQAKCKKLAEVEAEMKQHTISHQEKTSALQNDLSSVL      908
                                             .::           .

Zebrafish_NuMA                --------------TRVSSLQEEIHRSQQDFSDLQTDHNVLKEKLVNLQDQVEQAMITAS      993
Spotted_gar_NuMA              ATLKQKESKLEALQAELLLKQEELKTQQECILHLQKESLVLGELKKRLADEVQGTLIYKQ      843
Chicken_NuMA                  EK----EGKE----------QEKL-A---------------------------------      1085
Human_NuMA                    QQVQEKEVRAQKLADDLSTLQEKMAA---------------------------------      911
Mouse_NuMA                    QQVQEKEVRAQKLVDDLSALQEKMAA---------------------------------      898
Tropical_Clawed_Frog_NuMA     SRIKEREAEEKKLLSALHSSEEKFQIAHQ-------------------------------      941
Coelacanth_NuMA               AQMKEKESEELRLQAEVASMKEKFEMVQC-------------------------------      937
                                           :*::

Zebrafish_NuMA                QKESELLLLQQELSHQETLRE-----------------KALELEAIKREEFEKKVKELQ      1035
Spotted_gar_NuMA              EAED----KEKEVVHLKALLTAKENEIKSFLQSIQTGEERSSAIQALL-EKREEEIKSLQ      898
Chicken_NuMA                  --------SAERVGKLEAE---------------------------V-RKASEALE---      1105
Human_NuMA                    --------TSKEVARLETL---------------------------V-RKAGEQQE---      931
Mouse_NuMA                    --------TNKEVACLKTL---------------------------V-LKAGEQQE---      918
Tropical_Clawed_Frog_NuMA     ---G----ESERLSHLETA---------------------------L-SNAKSELD---      962
Coelacanth_NuMA               ---E----KANQVSAAETK---------------------------S-RKLGEELS---      958
                                       :.:   ::                               :  .  .

Zebrafish_NuMA                DRILEVS-----------------------------------TLASQREAQVISLENEM      1059
Spotted_gar_NuMA              SRVLELEQACAEQKQHISALEKELAEAQRLVVEKTSAFEAQTSQLLDQHQDRVVSLEQCL      958
Chicken_NuMA                  ------------------AVSKELSEERL-------------------------------      1116
```

```
Human_NuMA                  ------------------TASRELVKEPA----RAGDRQ--PEWLEEQQGR-------QF       960
Mouse_NuMA                  ------------------TASLELLKEPP----RAANRA--SDQLGEQQGR-------PF       947
Tropical_Clawed_Frog_NuMA   ------------------CLVREVSDEKH----KKEELEALVKELKEQKSERIQSLESEV      1000
Coelacanth_NuMA             ------------------QVSKEFSEMQT----AKAELELKIKQLNDDQREKIVALELEL       996


Zebrafish_NuMA              RDQQLSANQSKDNLCREWQEKLGILKGELDVVSRDAADKDH-QLESLDQKLKEMEMVVLQ      1118
Spotted_gar_NuMA            ESS--------ESICSEQKRQVDKLSKELEEVRSLFEIRETALKEER--TSLQLEIEKQK      1008
Chicken_NuMA                -------------KSKELEAVATQEASEVARLSAALEEAAREHGQEL--ARREEEAKRLQ      1161
Human_NuMA                  CST--------QAALQAMEREAEQMGNELERLRAALMESQGQQQEER--GQQERE VARLT      1010
Mouse_NuMA                  SST--------HAAVKAMEREAEQMGGELERLRAALIKSQGQQQEER--GQQEREVARLT      997
Tropical_Clawed_Frog_NuMA   KTS--------LAAVKERESETAKLSEEVKDLNRQLEEIGQKHKEEL--AQKNTEIEQLI      1050
Coelacanth_NuMA             SKT--------LKAANEKEATIDKLTSEAGVLQAKIEETEQHNTQEL--VLKEEQIESLI      1046
                                           :        *   :            :.      : :


Zebrafish_NuMA              KEKDVMETHQAKEDLEKRIAELEECKQKLEIMRNERDHLSTEVASLKEEIHSYQDTQMQK      1178
Spotted_gar_NuMA            RELD-------------------------------------VLKLEEQ----------QERDCL      1025
Chicken_NuMA                KELE---------------------------------DAKADCAAEKA---RKVELEVQL      1185
Human_NuMA                  QERG---------------------------------RAQADLALEKA---ARAELEMRL      1034
Mouse_NuMA                  QERG---------------------------------QAQADLAQEKA---AKAELEMRL      1021
Tropical_Clawed_Frog_NuMA   EAKE---------------------------------KAALDLASKT-------EMGAQL      1070
Coelacanth_NuMA             DEKD---------------------------------QISAELAAEKE---SKSQVEIQL      1070
                                                                   :           :

Zebrafish_NuMA              QQTISVLEVENNALKENMAALEKQLAEEITTASQKNSELQNKLHQQESLHEKAQELEIGR      1238
Spotted_gar_NuMA            KNQV-------VATVEELQKLQAESLVASSLISEKDNELEDLKKELQDVNGKLQVLQYRD      1078
Chicken_NuMA                QNSI-------NEQRVERSAHQQELARSLELIEEKEGELDELRLKNVSRGEE--------      1230
Human_NuMA                  QNAL-------NEQRVEFATLQEALAHALTEKEGKDQELAKLRGLEAAQIKE--------      1079
Mouse_NuMA                  QNTL-------NEQRVEFAALQEALAHALTEKEGTDQELAKLRGQEAAQRTE--------      1066
Tropical_Clawed_Frog_NuMA   QKLL-------DTHKGELSALQNELSRSLDLISQKESEVERLHKEAAVTQEE--------      1115
Coelacanth_NuMA             QQSL-------CEHQKREAALQTELSSALEVIQKKEENLTR--------QEE--------      1107
                            :: :            .    :          . .: ::           :

Zebrafish_NuMA              -------------HEEFERRVRELQAKVQEVSTLASEKEAVAYSLQEELTGHLKAKVSED      1285
Spotted_gar_NuMA            DERTKLTDAKEIQSKELENTIEQLRGDVLAAS---S-------------------------      1111
Chicken_NuMA                -------------LRDLQKTVSKLKGELASVE---AVK-ERASKMDSELQGFLEAARSRD      1273
Human_NuMA                  -------------LEELRQTVKQLKEQLAKKE---KEH-A---------SG---------      1104
Mouse_NuMA                  -------------LKELQQTLEQLKIQLVKKE---KEH-PAGGASGEDASG---------      1100
Tropical_Clawed_Frog_NuMA   -------------IRKQQQTMGKLTEELTALV---ALK-EQAALQEKEIAQHVRATKGAE      1158
Coelacanth_NuMA             -------------LHNQQEIIHKLQAEVSAVE--------------------------      1126
                                        .. .. : :*  .:

Zebrafish_NuMA              ----DLRRVLEEK---VETLQREIETASCDATSKDGL-------LQTLD-QKLRQMEMLC      1330
Spotted_gar_NuMA            --------LASEKQGTMESLEKELNSLKQDIE--------KQRERELLSCQAVAAEESKC      1155
Chicken_NuMA                AEMDSIKAVYAK-EASLKNLEEKIRHREQESGSSQDLYQEKLKEAQMLSV-EVERLEQKC      1331
Human_NuMA                  -----------------SGAQSEA------AG----RTEPTGPKLEALRA-EVSKLEQQC      1136
Mouse_NuMA                  -----------------PGTQSET------AG----KTDAPGPELQALRA-EISKLEQQC      1132
Tropical_Clawed_Frog_NuMA   AEMANLKAIISEKTKNIESLEHDIKNQKGDLACIQEQYRSKQEEARGLQG-QIVDLEREC      1217
Coelacanth_NuMA             ----DLKTIIANKEKEIEESHRKLESGDQEKIAFQSLHQEKLQEAECLQS-KVVQLEQRC      1181
                                         . .                      . *    :   *  *

Zebrafish_NuMA              QQKEDAVFEIQNSKEDLQKEMNELVSKNQELEGCLQHLEMVKKEKDLLSNEVTSLKEQIN      1390
Spotted_gar_NuMA            RQLEATISQLRSEVNAASSLVSERE---LELTSLQEEIKKLKEQEDLRSQEAAKVKAQQ-      1211
Chicken_NuMA                REQQDTIAGLEKAVAEGSQQ-------------QQAELEASQR---------EAVRH---      1366
Human_NuMA                  QKQQEQADSLERS-----------------------------------------------      1149
Mouse_NuMA                  QQQQQQVEGLTHS-----------------------------------------------      1145
Tropical_Clawed_Frog_NuMA   KEQKELICQAQKQAAEAETLASEKV---STSERQLEGIQALEG---------EIHKE---      1262
Coelacanth_NuMA             TEQEENNRT---------------------------------------------------      1190
                             : :

Zebrafish_NuMA              DQSLRAKQSEADLCIVFEEKIETLQGQLESSSCDVSDKEKHLQTLHQ-------------      1437
Spotted_gar_NuMA            --------------KELQGTIERLQTEVQVATSCAAEKEQLARTLQNKIDALQQEMGEKD      1257
Chicken_NuMA                ----------------RETAAELQRLLDASRSAQALQDGTVESLRK-------------      1396
Human_NuMA                  --------------------------LEAERASRAERDSALETLQG-------------      1169
Mouse_NuMA                  --------------------------LKSERACRAEQDKALETLQG-------------      1165
Tropical_Clawed_Frog_NuMA   ----------------RQKTCDLLKQLEASQAAQADKETELQALKK-------------      1292
Coelacanth_NuMA             --------------------SDLEQQLQASRSVQAQQQSAIEALKI-------------      1216
                                              :.   .  : ::   .:*:

Zebrafish_NuMA              -------------------------KVSQMDLLCQQKE---NAVLEMQNAKEDLQKK--      1466
Spotted_gar_NuMA            ILRCRAVSEEESCRRVLEDKVTQLEAQVLKASSLASERELKLNALLSEIKEKDNLRSQAI      1317
Chicken_NuMA                --------------ELQDKSKELAQS--KTAVAAAEKE--VASLRAAAQEKGHLEEG--      1435
Human_NuMA                  --------------QLEEKAQELGHS--QSALASAQRE--LAAFRTKVQDHSKAEDE--      1208
Mouse_NuMA                  --------------QLEEKARELGHN--QAASASAQRE--LQALRAKAQDHSKAEEE--      1204
Tropical_Clawed_Frog_NuMA   --------------ELFHKVQELEQS--QKSSTESSRE--LSSMLSAAQERQRALTE--      1331
Coelacanth_NuMA             --------------EASEKSDVIEHK--QQSLAATENE--LSAVRSLLNEKEKFEET--      1255
```

```
                                          .  :      ..*    :.    : :

Zebrafish_NuMA                ---IDELVSEKQQLEGCLQNLEMV-------KSERDLLSTEVTSLKDQ---LND-----Q       1508
Spotted_gar_NuMA              STEEAQQNALEEKIEKLQSELLAATSLASEGQSAVAQLQAELKALKDTHVQLIEK----D       1373
Chicken_NuMA                  ---------WKEQLSQCIQELERK-------NSLLGSLEHEVSILH---RQLTEKEGESK       1476
Human_NuMA                    ---------WKAQVARGRQEAERK-------NSLISSLEEEVSILN---RQVLEKEGESK       1249
Mouse_NuMA                    ---------WKAQVARGQQEAERK-------SSLISSLEEEVSILN---RQVLEKEGESK       1245
Tropical_Clawed_Frog_NuMA     ---------AKQQAEQYQKEIEMK-------SKEVGSLHAEVKSLS---SKVEV----SA       1368
Coelacanth_NuMA               ---------LKKQVSDYLKEIESH-------KSKVNASEQELSSLQ---LQCRERKEENE       1296
                                       : :     .:           ..       *:. *

Zebrafish_NuMA                DLK--AKQSEDDLRKVLEEKIKNLQGQLETASRDVSEKDQLLQTLDQKVTQMDQLCKQKE       1566
Spotted_gar_NuMA              ELRSKASACEEHEREQLRENIDKLQAEVLAASALAAEREQRADTFQKKLDALQQENEERD       1433
Chicken_NuMA                  ELKR-LIMAESEKSKKLEERLRVLQTEMATAASRAAERCS---LMKVEVQRCQEEMEKQR       1532
Human_NuMA                    ELKR-LVMAESEKSQKLEERLRLLQAETASNSARAAERSS---ALREEVQSLREEAEKQR       1305
Mouse_NuMA                    ELKR-LVVAESEKSQKLEERLRLLQVETASNSARAAERSS---ALREEVQSLREEVEKQR       1301
Tropical_Clawed_Frog_NuMA     EFEQ-RLLKETNRSTKLEEKLKKLHGDVEASSKELLEKNRAMDSLKTEAQTCRQEADKQR       1427
Coelacanth_NuMA               SLKC-NISAEVEKCQQLQTLIETLQAELASASTQVEQKDGVVQTLENQIQSFRGEAEKHE       1355
                              .:.     * .    *.  :  *: :  : :    ::      :  :        .::

Zebrafish_NuMA                KYALDLLQVKENLEKRIGEITVEKQQLEGCQQNLETVSKDKDNLLNELTFLKVEIQSYQE       1626
Spotted_gar_NuMA              FLRCRAIAAEEAQRKELEE------TIVNLKNEMLSASSP--SFQLENEKLVTEKEALRK       1485
Chicken_NuMA                  M-----------------------TIEALKRDRH-------CQSEREEELRQEVKVCQD       1561
Human_NuMA                    V-----------------------ASENLRQELT-------SQAERAEELGQELKAWQE       1334
Mouse_NuMA                    V-----------------------VSENSRQELA-------SQAERAEELGQELKAWQE       1330
Tropical_Clawed_Frog_NuMA     M-----------------------AVEGLQQSLS-------SQAETNDRLQQEIRSWQG       1456
Coelacanth_NuMA               M-----------------------VLKELHEELT-------SEKKTKEDLHTEMKSWEE       1384
                                                        :..                * * .  .

Zebrafish_NuMA                KEVQMKHELSVLENEHNILQENLDTLQKQVVELTASASQKESELQNEVCKQ-EKLQEKAQ       1685
Spotted_gar_NuMA              ELSKAEAELSDVRLELTKAQT-------LIAELL-PAKRKCQQQQAELCLAQAKHQEELE       1537
Chicken_NuMA                  KFFQKEQLLSSLQQELGSAQA-------LAGEVV-PLKHLCQQLQAERASLESKHREDLE       1613
Human_NuMA                    KFFQKEQALSTLQLEHTSTQA-------LVSELL-PAKHLCQQLQAEQAAAEKRHREELE       1386
Mouse_NuMA                    KFFQKEQALSALQLEHTSTQA-------LVSELL-PAKHLCQQLQAEQAAAEKRFREELE       1382
Tropical_Clawed_Frog_NuMA     NCAEKEQQISSLQQNLSSNQS-------LLEEFA-SLKRSYQEIIAEREVMQEKHQEELL       1508
Coelacanth_NuMA               KYRHKEMEIADLHKQLTDTQS-------LTGELM-PLKQQCQQQQNDLRLAETKHKEELE       1436
                              :  . :  :: :. :    *           *.    .:  .:   :      : :*.

Zebrafish_NuMA                KLEKDAGDLQAKILE----IST------LASEREAQISSLKDEINS--------------       1721
Spotted_gar_NuMA              QRERAVAALEDDLQQVKEELSTLRPLREMTSEQDRAIQKLQEENAAHKGQVCKLQQINSQ       1597
Chicken_NuMA                  QRAKATTALQAELARARVEVAELPALRDRAAEQERALQRLQKETASSSERLAALQAANSR       1673
Human_NuMA                    QSKQAAGGLRAELLRAQRELGELIPLRQKVAEQERTAQQLRAEKASYAEQLSMLKKAHGL       1446
Mouse_NuMA                    QSKQAAGGLQAELMRAQRELGELGSLRQKIVEQERAAQQLRAEKASYAEQLSMLKKAHGL       1442
Tropical_Clawed_Frog_NuMA     GQKKLTERFQAELQKTKEDMAEMVLLKEKVHNQELRLQKLHSENDDHLSQIAHLQQLNSR       1568
Coelacanth_NuMA               KMQKLVSNLQSELEKVQSELAENIPLKELCSAQEGAIERLEKENCSYRDQVCKLQQTNSL       1496
                                 : .  :. .: .    :.           ::   . *. *

Zebrafish_NuMA                ---QHLKAKQSEDDLLRVFEEKIENLQ----GQLEIARLDVS----DKDQLLQTLNQKLK       1770
Spotted_gar_NuMA              LTSENLEICSESSLGARRFDAELAVERESHSFALEKVRTEYQKQIAALKEDVLEGKKRQD       1657
Chicken_NuMA                  LAEENRALSESVSRGQQRLDAELGQAREKHTRELECVRLEAEKAMASSRQEAEEAARKLE       1733
Human_NuMA                    LAEENRGLGERANLGRQFLEVELDQAREKYVQELAAVRADAETRLAEVQREAQSTARELE       1506
Mouse_NuMA                    LAEENRGLGERANLGRQFLEVELDQAREKYVQELAAVRTDAETHLAEMRQEAQSTSRELE       1502
Tropical_Clawed_Frog_NuMA     LVGENQSLSQASDQGAKKLESEVSNLKEQHEEQLKSLRLQHEKTLREGNERVQDLSQKLE       1628
Coelacanth_NuMA               LVGQNLE----SSQGQKKFEDELAKVKETHAEALQCVHSDFK--------------QQLT       1538
                                 ::       .   : :: ::   :      *   : : .              :.

Zebrafish_NuMA                QMEELCKQKETCVLEMHQTKEDLEKKTVELQADKSQQNQQNLEML-RQEKDHLKSLNQTI       1829
Spotted_gar_NuMA              VLTEKYESIKKKVLSDRQKFQDERQKLV-IQV-------EDMQKFLDSETSKVDELMDRL       1709
Chicken_NuMA                  AMSNKYENTKVKVLEERQKFQEERQKLM-AQV-------EQLEVFQKEQAKQVEELNKKL       1785
Human_NuMA                    VMTAKYEGAKVKVLEERQRFQEERQKLT-AQV-------EQLEVFQREQTKQVEELSKKL       1558
Mouse_NuMA                    VMTAKYEGAKVKVLEERQRFQEERQKLT-AQV----------------------EELSKKL       1540
Tropical_Clawed_Frog_NuMA     TATGKYEHVKTRVVDDWKAFQEEKQRLL-LQV-------QELEAAKKEQSEQVQELNKQL       1680
Coelacanth_NuMA               ALTKKCDAAERSVLEEREKFQEERQKLN-TRV-------LFKEIFCIEQLETVEECAKKK       1590
                                    .  :  *:.  :  :: .::    :.                      ..  .
                                                                          C-term
Zebrafish_NuMA                RRECEASRKIRAELELNVEEQTASILALKKASQQWEEQNQELLEQLKAKTEAVEHYKAQV       1889
Spotted_gar_NuMA              ATAKS-----------------EQNNVKEQNEELQKQTSELQEQLTHKDGALEHYKAQV       1751
Chicken_NuMA                  VQHEKATR-SQQQRVK---VL---EGELQSEATRQQERVAELEEQLAQKEQAAEHYKAQM       1838
Human_NuMA                    ADSDQASK-VQQQKLK---AVQAQGGESQQEAQRLQAQLNELQAQLSQKEQAAEHYKLQM       1614
Mouse_NuMA                    TEHDQASK-VQQQKLK---AFQAQRGESQQEVQRLQTQLNELQAQLSQKEQAAEHYKLQM       1596
Tropical_Clawed_Frog_NuMA     SQQEKALR-SQQ---H---KLKQQEGETHEEAEKAQKRVVELESQVEQQTQAVEHYKAQM       1733
Coelacanth_NuMA               KLNEHNSK-IQDELVL---KMRGCLLKLQEEVQEQQKELSEVQAQLSQKEQAVEHYKGQM       1646
                                                    :.   . : .  *:  *:  :  * **** *:

Zebrafish_NuMA                EKAMNHYNGKKQLLLEAQELNKTLEQSLEVSKREAKAL-------ETELTLARMELNQAN       1942
Spotted_gar_NuMA              EKAKTHYGAKKQQLQEATEQIQALEKKLEGSQQENNTLKAEQKQLVTELQQAQL------       1805
```

```
Chicken_NuMA                EKAKTHYDAKKQQNQDLAEKLKA----MEQLQKENAELRTESERLAKELQQSVLQAKEAE      1894
Human_NuMA                  EKAKTHYDAKKQQNQELQEQLRS----LEQLQKENKELRAEAERLGHELQQAGLKTKEAE      1670
Mouse_NuMA                  EKAKTHYDAKKQQNQKLQEQLQD----LEELQKENKELRSEAERLGRELQQAGLKTKEAE      1652
Tropical_Clawed_Frog_NuMA   EKAKLYYDAKKKQNQELSEELQSHIREQEHLRKENVDLKAESEQLSKELQHSLLQNKEAE      1793
Coelacanth_NuMA             EKAKAHYDAKKSQNQELVVKLQSVEEKVESAHKENTGLRSEVDRLNRELQHSLLQSVEAE      1706
                            ***  :*..**.   .     :      *  ::*   *         **  : :

Zebrafish_NuMA              DKEKSLAAKVKTLEAQVDFADRQLREKRRIADDGEDLRQKENLYF-RVPEKQQDTSADSL      2001
Spotted_gar_NuMA            -SIKKLSSKVSSLQAQVDLADRQLREQ-KFQAGSNTTKNHVSECSD-VPEKTQETSKDSL      1862
Chicken_NuMA                LSCRELSGQVRSLETQLEFADQQLRELGKFPAPKATLKEPESFRQN-----PSDLSTDSL      1949
Human_NuMA                  QTCRHLTAQVRSLEAQVAHADQQLRDLGKFQVATDALKSREPQAKP-----QLDLSIDSL      1725
Mouse_NuMA                  QTCRHLTAQVRSLEAQVAHADQQLRDLGKFQVATDALKSREPQVKP-----QLDLSIDSL      1707
Tropical_Clawed_Frog_NuMA   QNCKNLSNRVRSLEAQVEYADRQLRDLGKFQLATDSMKSRETFGAPRVTRSHADVSIDSL      1853
Coelacanth_NuMA             KSNKSLLAQVQSLEAQVEYADRQLRELGKFQLPSDALKRRGSTCIPQSVETPGNISGDSL      1766
                             . : *  :* :*::*:  **:***:  ::       :               : * ***

Zebrafish_NuMA              EFELNDS--LNTTCRSAVPGESSTPLVR-----SSERLAAKRRALGAESLETLYFTPMGK      2054
Spotted_gar_NuMA            DLSLDDS--LNSTRKPSTSTDKTTPPVRS-----SERLAAKRRLLSGESLETLYFTPMMV      1915
Chicken_NuMA                DLSLDEGQPLNSTRKATRS-----HSDGSAAPGGTEPRASQRLPRKVESLESLYFTPIAS      2004
Human_NuMA                  DLSCEEGTPLSITSKLPRT-----QPDGTSVPGEPASPISQRLPPKVESLESLYFTPIPA      1780
Mouse_NuMA                  DLSLEEGTPCSVASKLPRT-----QPDGTSVPGEPASPISQRLPPKVESLESLYFTPTPA      1762
Tropical_Clawed_Frog_NuMA   DLSFEDDQLLNSTSKNGRCNE--EPATSSVHASSMESPTTGQLPKKVESLESLYFTPIPT      1911
Coelacanth_NuMA             NLSGEDLQPLSPTRKVLA-----SPPFPFSYRKHVQENANQRLPPKVESLESLYFTPIHN      1821
                            ::. ::    . : :                          :     ****:*****

Zebrafish_NuMA              QGYKRKVDHNDGFERKLESSITSIGDLVVDSAKKLTASARRRRTTQVINITLAKKAQG-S      2113
Spotted_gar_NuMA            RA-----------ESKLESSIASLGELTLDSAKKSR--SARRRTTQIINITLTKKTP-GA      1961
Chicken_NuMA                RT-----------QPKLESSAGSLADVSLESGCRTR--SGRRRTTQIINITMTKKETT-T      2050
Human_NuMA                  RS-----------QAPLESSLDSLGDVFLDSGRKTR--SARRRTTQIINITMTKKLDV--      1825
Mouse_NuMA                  RG-----------QAPLETSLDSLGDAFPDSGRKTR--SARRRTTQIINITMTKKLEL--      1807
Tropical_Clawed_Frog_NuMA   RA-----------QSKLESSLGSIGDLSLDSSKKTR--SARRRTTQIINITMTKKTK-EE      1957
Coelacanth_NuMA             RV-----------QSKMDSSISSLGDLSLDSGRKTR--SARRRTTQLMSSTMAKEQLVEE      1868
                            :            :  :::*  *:.:   :*. :    : ******::. *::*:

Zebrafish_NuMA              ---SESEESFSSLHSARSHPNLAVHQ----SRPISID-------FS--------EDGPAT      2151
Spotted_gar_NuMA            PEPESVNSSFYSLQSAQSHPNLFTQTQ--KSRPVSMA------SLSSR--LNASQEFLDN      2011
Chicken_NuMA                EEPGGADASFSSILSEQPQKAAPARARLRSAR--------SLASFPSQDSLSKLDTSSPQ      2102
Human_NuMA                  EEPDSANSSFYSTRSAPAS-----QASLRAT--------------SSTQSLARLG----S      1862
Mouse_NuMA                  EEPDSANSSFYSTQSAPAS-----QANLRAT--------------SSTQSLARLG----S      1844
Tropical_Clawed_Frog_NuMA   PEAESANTSFYSLRSAPSYQSLHQQKPRRPGRPQAAVSAPALASLPSQESLAKTEQF-SD      2016
Coelacanth_NuMA             DESDNANASFFSVQSAKSQPDLLMQS-LKSGRPRSM------------------ALV-GS      1908
                                  : ** *  *         :

Zebrafish_NuMA              TLSKADTLQNLPGYRRSTVHSVG----------PPRATSTFCIGAENEPEHAADDWMRIA      2201
Spotted_gar_NuMA            EISASESLFNLPGYRPGAASTVTAR----------RSTNAFVAGAQNEPEH-TEDWMRIA      2060
Chicken_NuMA                EPSGHAALLSLPGYRPATRSSLRRSQAGSSS--SLGRSSIYLGTCQDEPEQ-LDDWNRIA      2159
Human_NuMA                  PDYGNSALLSLPGYRPTTRSSARRSQAGVSSGAPPGRNSFYMGTCQDEPEQ-LDDWNRIA      1921
Mouse_NuMA                  PDDGNSALLSLPGYRPTTRSSARRSQARMSSGAPQGRNSFYMGTCQDEPEQ-LDDWNRIA      1903
Tropical_Clawed_Frog_NuMA   DSFNNSVLMNLPGYRPPTRRSARLSQTG-------GRSSFYMSTCQDEPDP-QEDWNRIA      2068
Coelacanth_NuMA             NNLDSSAVFKLPGYRPSTRSSTRRSLIGDGATASDAMSTFHLHSCQNEPDQ-LEDWNRIA      1967
                                   : .*****  :  :                .. .   .::**:   :** ***

Zebrafish_NuMA              ELQSRNKACLPHLKSSYPLESRPSL-GPSFTVTDEDLRLGDPSETIRRASMMPGQILESL      2260
Spotted_gar_NuMA            ELQTRNKSCLPHLKSSYPLENRPSINIPSFCISDDDVKLGDPDETIRRASMLPGQLNETL      2120
Chicken_NuMA                ELQQRNRACPPHLKTCYPLESRPSDVL--GTITDEEMKTGDPTETLRRASMQPSQIAEGA      2217
Human_NuMA                  ELQQRNRVCPPHLKTCYPLESRPSLSL--GTITDEEMKTGDPQETLRRASMQPIQIAEGT      1979
Mouse_NuMA                  ELQQRNRVCPPHLKTCYPLESRPTLSL--ATITDEEMKTGDPRETLRRASMQPAQIAEGV      1961
Tropical_Clawed_Frog_NuMA   ELQARNKACPPHLKTSYPLESRPSLLS--STITDEEVKLGDPKETLRRATMLPSQIQEST      2126
Coelacanth_NuMA             ELQQRNRICPPHLKTSYPLESRPSL-G--MPITDEDLKTGDPRETLRRATMIPSQIKKM-      2023
                            *** **: * ****:.****.**:       ::*:::: *** **:***:* * *: :

Zebrafish_NuMA              NSRRFSLAPETSSSQAPARSHPQRATMLPCQIQSSTAAHRASQLTKTSSRSHTSENKRS-      2319
Spotted_gar_NuMA            ASHRMSMLPGQ--------IPAHRMTMLPGQISEGLSSHRASMLPQPSTQYSWRATGD-V      2171
Chicken_NuMA                AARRGMLGG-----------------------------------------GWAHGGITT      2235
Human_NuMA                  ------------------------------------------------------GITT      1983
Mouse_NuMA                  ------------------------------------------------------GITT      1965
Tropical_Clawed_Frog_NuMA   GSTRRMSLA-------------------------------------ASEHMRGPSIST      2147
Coelacanth_NuMA             ---------------------------------------------QDSGVTT      2030

Zebrafish_NuMA              -PLAPKRPASQLQGPDTPEAKKLA-SCFPRPMTPKGRFGNS--------Q----NRPPVS      2365
Spotted_gar_NuMA            SQQLKRCSNVPQEGGDTPESKKMMTACFPRPMTPKDKNDRRFTVQNA--QN----RPPSC      2225
Chicken_NuMA                RQQRKRLSDESHQGPDTPESKKPV-SCFPRPQTPRERRSSHLSRR-----SE--QQAPSK      2287
Human_NuMA                  RQQRKRVSLEPHQGPGTPESKKAT-SCFPRPMTPRDRHEGRKQSTTEAQKKA--APASTK      2040
Mouse_NuMA                  RQQRKRVSSETHQGPGTPESKKAT-SCFPRPMTPRDRHEGRKQSSTADTQKK--AAPVLK      2022
Tropical_Clawed_Frog_NuMA   RQQMKRVSEESHLGPDTPEAKKSA-TCFPRPMTPKDKHDARRLSTVESKGNS----SHQA      2202
```

```
Coelacanth_NuMA              RRHKKRLSEEGHQGADTPESKKSM-TCFPRPMTPKDKNDGKRQATLEANRKRDLASRTPK      2089
                                  :       * .***:**   :***** **: :

Zebrafish_NuMA               PAERRQSVMFTVVNTPKNSARGDSRL---------------------------------      2391
Spotted_gar_NuMA             QDGRRESVMFSVANTPKKKGGSLLQRSMSKIRNSTRKSPGFA-----------------      2267
Chicken_NuMA                 QPERRQSMAFSILNTPKKLGNSLLRRAANRKTTPK-NSP--RGTA---------------      2329
Human_NuMA                   QADRRQSMAFSILNTPKKLGNSLLRRGASKKALSK-ASPNTRSGT---------------      2084
Mouse_NuMA                   QADRRQSMAFSILNTPKKLGNSLLRRGASKKTPAK-VSPNPRSGT---------------      2066
Tropical_Clawed_Frog_NuMA    QPTRRQSTAFSIFNTPRKLGNSLLKRGLNKKTTPK-NSPRGRGASGSAGSTSGKSPHRSL      2261
Coelacanth_NuMA              QADRRQSMAFSILNTPKKIGSSLLNRVTRKKVTPR-KSPRLSASKLPQVQDASK------      2142
                                ***:*  *:: ***:: . .  .

Zebrafish_NuMA               -------------------------------------------  2391
Spotted_gar_NuMA             -SKTPRRSPRISSSKSPKNAASIKKMSRKPMKNMK---I----  2302
Chicken_NuMA                 -----RRSPRIASTKSPKGKAGR-RALKD-------TKF----  2355
Human_NuMA                   -----RRSPRIATTTASAATAAA-IGATPRAKGK--AKH----  2115
Mouse_NuMA                   -----RRSPRIATTTTGTA---T-VATTPRAKGK--VKH----  2094
Tropical_Clawed_Frog_NuMA    RKSPSRRSPRASTAKSPKASTKVGIGMGGRSAVMCSSAWAELH  2304
Coelacanth_NuMA              -KVKGRRSLRNV-----------KI------------------  2155
```